IL
NUOVO CIMENTO
ORGANO DELLA SOCIETÀ ITALIANA DI FISICA
SOTTO GLI AUSPICI DEL CONSIGLIO NAZIONALE DELLE RICERCHE

VOL. I, N. 4 *Serie decima* 1° Aprile 1955

Determination of the Ultrasonic Absorption Coefficient of Benzol with Thermal Method.

E. GROSSETTI

Istituto di Fisica dell'Università - Napoli

(ricevuto il 24 Dicembre 1954)

Summary. — Measures effected with the thermal method for the frequency 1.8 MHz to determinate the ultrasonic absorption coefficient in benzol are reported. The value obtained for α is much higher than the theoretical one. This anomaly could be ascribed to the high value of the second volume viscosity coefficient, according with Liebermann's measures.

In a preceding paper [1] we have given some measurement of the u.s. absorption coefficient effected with the thermal method, that is, founding on the heat quantity generated in a calorimeter by u.s. waves passed through various layers of liquids; we have found that for increasing frequencies, also the values obtained by this method result higher than the theoretical ones, but slightly lower than those determined by mechanical methods. It is well known that benzol differs from all other liquids for its very high value of the u.s. absorption coefficient. On the other hand LIEBERMANN's measurements of the second viscosity coefficient have effectively demonstrated that this coefficient is remarkably higher for benzol; this fact induces to assume that the discrepancy in the ultrasonic field originates from this extremely high value of the volume viscosity coefficient which before was not taken in due account. Because of the importance of the question we have measured with this thermal method the absorption coefficient for benzol, as this method is apt to give a more reliable

[1] E. GROSSETTI: *Nuovo Cimento*, **11**, 250 (1954).

result than the other ones. If with the thermal method we would also have obtained such a high value, the thesis ascribing the anomaly of benzol to its high value of the volume viscosity coefficient would have been confirmed.

We made only some few changements to the apparatus used and described in a preceding paper [1].

The perspex' calorimeter A was substituted with a double wall calorimeter made with thin brass sheet and the tube L was reduced to about 30 cm. Instead of the cellophane leaf we placed a thin alluminium leaf. We worked at 1.8 MHz, that is on the third harmonic of the emitting quartz crystal. We measured the temperature increase of the benzol in the calorimeter due to the heat generated with the arriving ultrasonic waves. We measured the increase of temperature for the quartz at 8, 12, 16 cm, from the plate. The duration of the ultrasonics was 5 min and the increase of the temperature was obtained from the galvanometer deflections which we red every 30 seconds during 5 minutes before and after the arrival of the ultrasonics.

In Fig. 1 we give the pattern of one of these measurements, the position of the quartz being 16 cm from plate R. The increase of temperature is measured by AB. The measurements effected on benzol with the thermal method at 1.8 MHz have given the value of the absorption coefficient $\alpha = 2.72 \cdot 10^{-2} \pm 0.17 \cdot 10^{-2}$, which is a value 100 times higher than the classical one, and very close to the one obtained by other authors with mechanical and optical methods. In conclusion, the absorption coefficient of benzol obtained with the thermal method is anomalous, at least at the frequency used which is nearly the same as the one used for the measurement of the second viscosity coefficient; the observed anomaly could be explained assuming a high value for the volume viscosity coefficient.

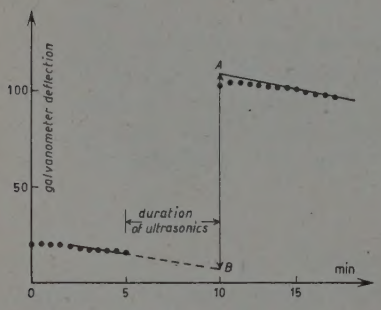

Fig. 1.

Further measurements will be effected with other frequencies.

I am much indebted to Prof. Antonio Carrelli for the material assistance provided and for the valuable suggestions given.

RIASSUNTO

Si riferiscono misure effettuate col metodo termico alla frequenza di 1,8 MHz per determinare il coefficiente d'assorbimento ultracustico in benzolo. Il valore ottenuto per α è molto maggiore del teorico, anomalia che potrebbe essere ascritta all'elevato valore del secondo coefficiente di viscosità di volume secondo la misura di Liebermann.

IL NUOVO CIMENTO Vol. I, N. 4 1° Aprile 1955

Ultrasonic Grating Remaning After Stopping the Supersonic Waves (V).

A. Carrelli and F. Porreca

Istituto di Fisica Sperimentale dell'Università - Napoli

(ricevuto il 28 Dicembre 1954)

Summary. — Continuing the examination of the diffracted line persistence, after stopping the ultrasonics, the dependence of the effect on the frequency is showed. Moreover, the duration t_p in the suspensions containing particles with different mass, separated by centrifugation, shows clearly that the effect is bigger in the suspensions with particles of lesser mass, at the same concentration. Then, the line persistence increases with increasing contact surface particle-liquid.

Continuing our experimental investigations on the diffraction phenomena persisting in some liquid suspensions after stopping the ultrasonics ([1-4]), we have studied in which way the time of persistence t_p of the diffracted lines varies as a function of the ultrasonic frequency ν.

In a preceding note (3) we fixed the laws of dependence of the duration of the lines as a function both of the ultrasonic duration t_u for a power w and of the ultrasonic power for a constant t_u; the graphs were obtained at different frequencies, thus bringing to view the deciding importance for the duration t_p of this third parameter besides the other two, namely duration t_u and power w of the ultrasonics.

1. – In order to illustrate this dependence on the frequency we report (fig. 1) the maximum values of persistence of the diffracted lines for a constant power and a duration t_u of the ultrasonics which gives the highest t_p.

(1) A. Carrelli e F. Porreca: *Nuovo Cimento*, **9**, 90 (1952).
(2) A. Carrelli e F. Porreca: *Nuovo Cimento*, **10**, 98 (1953).
(3) A. Carrelli e F. Porreca: *Nuovo Cimento*, **10**, 883 (1953).
(4) A. Carrelli e F. Porreca: *Nuovo Cimento*, **10**, 1406 (1953).

We have made some other experiments to define better the pattern of the graphs; beside the frequencies employed in the preceding work — 0.590 MHz, 1.770 MHz, 2.910 MHz, 4.130 MHz — we used also the frequencies 0.35 MHz and 0.625 MHz employing an other piezoelectric quartz.

The graphs of Fig. 1 refer to that ultrasonic power at which we have the diffracted lines until the 4-th order. They show a maximum of t_p for the

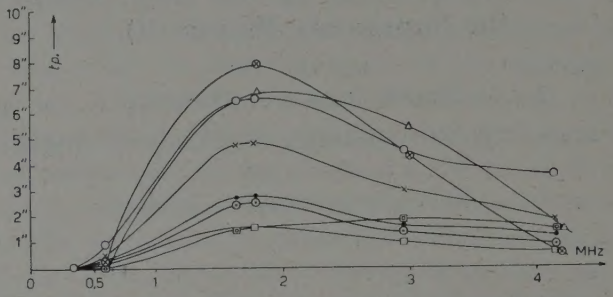

Fig. 1. – Ultrasonics with diffracted lines up to the IV order.

⊗ HgCl in water
△ $BaSO_4$ in water
x Starch in ethyl alcohol
● Starch in methyl alcohol
O Starch in water
□ Polyvynil alchool in methyl alcohol
⊙ Polyvynil alcohol in ethyl alcohol
⧈ Polyvynil alcohol in amyl alcohol

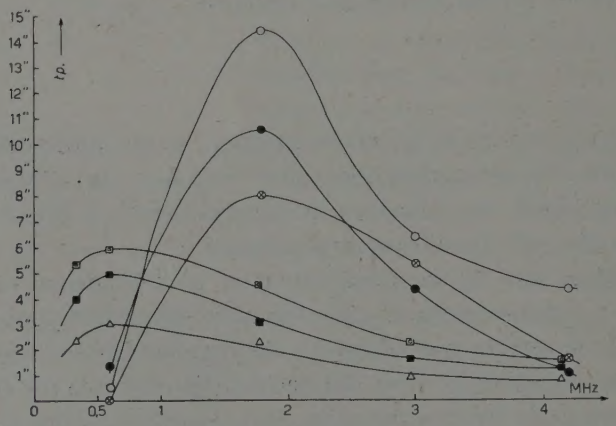

Fig. 2. – Ultrasonics with diffracted lines up to the VIII order.

○ Starch in water
● HgCl in water
⊗ $BaSO_4$ in water
⧈ Polyvynil alcohol in amyl alcohol
■ Polyvynil alcohol in aethyl alcohol
△ Polyvynil alcohol in methyl alcohol

frequency 1.7 MHz $\pm$ 0.3, excepting polyvinyl alcohol in amyl alcohol which diagram shows a not very clear maximum at a frequency (which is therefore not easy to fix) comprised between 2.0 and 4.0 MHz, a clearly higher value than the one relative to the other substances.

It is also necessary to remark that the frequency giving the highest t_p varies notably with the ultrasonic power.

Fig. 2 shows similar graphs obtained with ultrasonics of such a power to give eight orders of diffracted lines. We deduce therefore that the examined substances show the maximum of t_p at different frequencies, that is for polyvinyl alcohol in methyl, ethyl and amyl alcohol t_p is maximum at the frequency of 0.6 MHz $\pm$ 0.2; for $BaSO_4$, HgCl and starch in water t_p is maximum for 1.9 MHz $\pm$ 0.2.

2. – We wanted to determine the dimensions of the grains of those substances which give the effect. We obtained a limit value sifting the powders through a series of filters having different thickness. The radius of the grains resulted to be less than 10^{-3} cm.

In order to obtain more exact values we referred to the rate of falling of the particles in suspension (given in note (4)), assuming the law of Stokes

TABLE I.

	V cm/hour	$r \cdot 10^4$ (cm) of the suspended particles
Starch in water	2.4 $\pm$ 1.2	1.9 $\pm$ 0.5
Starch in ethyl alcohol	8.0 $\pm$ 2.2	2.9 $\pm$ 0.9
Starch in methyl alcohol	10.0 $\pm$ 4.5	3.1 $\pm$ 1.2
HgCl in water	10.0 $\pm$ 4.0	3.8 $\pm$ 1.5
$BaSO_4$ in water	5.2 $\pm$ 1.5	2.7 $\pm$ 1.2
Polyvynil alcohol in ethyl alcohol	27.0 $\pm$ 8.5	6.1 $\pm$ 2.0

to be verified (*). It is thus possible to obtain the values (listed in Table I) for the radius of the grains which we assume to be spherical.

We have also investigated about the dependence of the t_p on the different mass of grains in suspension, all the other parameters remaining constant.

It is clear that suspensions of the same concentration formed by particles with a smaller mass must contain a higher number of grains.

(*) It is convenient to specify that in this note the speed values listed in Table II can be derived from Figs. 5 and 6 only by admitting that the diffracted lines disappear when the particles in suspension deposit on the bottom of the batch containing the liquid.

With stationary waves the presence of a higher number of grains accumulating on the nodal planes must produce a higher variation of the refracting index, and therefore a longer duration of the diffracted lines, because of the higher number of grains which have part in the phenomenon at the stopping of the ultrasonics. To resolve this problem we centrifugated some suspensions having initially the same concentration and containing grains of different sizes. Operating at high speed (1 200 turns per minute) it has been easy to separate a suspension containing smaller grains (sol. A) from the remaining substance which deposited on the bottom.

After this first separation the remaining suspension has been stirred again and subjected to a centrifugation at smaller speed (750 turns per minute). We could thus separate from the substance deposited on the bottom a second suspension containing bigger grains (sol. B).

It is not easy to establish if the two portions thus selected have the same concentration. There is no doubt however that the higher quantity of substance deposits on the bottom when we operate at the highest number of turns per minute: therefore sol. A must be less concentrated than sol. B.

Besides, the light transmitting power of sol. B is lesser than the one of sol. A, and that also points to the fact that sol. B is more concentrated than sol. A.

We then measured in these solutions the duration t_p of the persistence of the diffracted lines at the stopping of the ultrasonics in function of their duration t_u. These measurements refer to values of t_u between 0 and 10 s for which the time of persistence t_p is practically maximum.

All these experimental determinations have been carried out at the same ultrasonic power which has been chosen very high to have a big effect, as it results using the data of reference ([3]). We saw that the maximum t_p obtained with 8-10 orders does not vary for small fluctuations of the ultrasonic power.

Notwithstanding the minor concentration, the four suspensions with particles of smaller mass (sol. A) have given the results which are reported in Figs. 3*a* and 3*b*, (water-starch

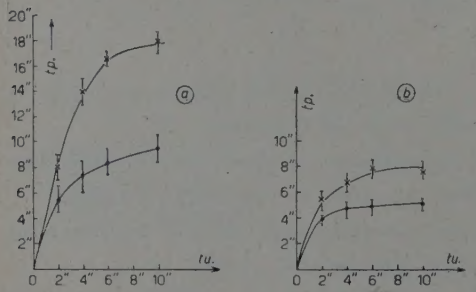

Fig. 3*a*. – Starch in water.
ν=1,8 MHz. x Solution A ● Solution B.

Fig. 3*b*. – Starch in water.
ν=3.0 MHz. x Solution A ● Solution B.

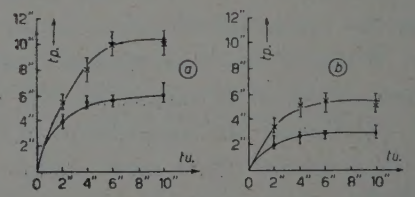

Fig. 4*a*. – $BaSO_4$ in water.
ν=1.8 MHz. x Solution A ● Solution B.

Fig. 4*b*. – $BaSO_4$ in water.
ν=3.0 MHz. x Solution A ● Solution B.

for $\nu = 1.770$ MHz and $\nu = 2.910$ MHz) and in Figs. 4*a* and 4*b*, ($BaSO_4$ in water at the same frequencies). They show a clearly higher t_p than the one relative to the particles of bigger mass (sol. B), exactly as it was to be expected on the basis of what we have just said. The effect is so big that the t_p of the solutions B, notwithstanding their higher concentration ([5]), is decisely lesser than the one measured in the solutions A which contain grains of lesser mass and which have certainly a minor concentration. It is therefore possible to conclude that the t_p depends more on the number of grains per cm^3 than on the total mass of grains per cm^3 and the persistence effect increases as the surface of the particles in suspension increases.

([5]) A. Carrelli e F. Porreca: loc. cit. ([2]), p. 99.

RIASSUNTO

Continuando lo studio sulla persistenza delle righe di diffrazione, al cessare degli ultrasuoni, si mostra la dipendenza dell'effetto dalla frequenza. Inoltre, i tempi di persistenza t_p in sospensioni con granuli più piccoli, selezionati mediante centrifugazione, mostrano chiaramente che l'effetto è maggiore per le sostanze con granuli di minore massa, a parità di concentrazione. Quindi esso aumenta con la superficie di contatto liquido-granuli.

Behaviour of Suspensions Crossed by a Small Light Beam Modulated by Ultrasonics.

F. Fanti and F. Porreca

Istituto di Fisica Sperimentale dell'Università - Napoli

(ricevuto il 28 Dicembre 1954)

Summary. — In this paper we continue to study the change of the light intensity along the diffracted image of the slit, caused by the passage trough liquids subjected to ultrasonics, of a monochromatic light beam, the thickness of which equals the supersonics, wave-length. The distribution in the liquid suspensions, in which the diffracted lines persist after stopping the ultrasonics, is unlike the one in the substances not showing this effect. Moreover, the first suspensions, show two different diffraction patterns by displacing the supersonic grating of $\lambda_{u.s.}/4$, at right angles with the light direction. A similar experiment has been made by coupling two model phase gratings (parallel slits cut in a plexiglas plate) and we obtained results like the one in the suspensions which show the persistence effect. This supports the assumption that such an effect is due to the building of a second phase grating, formed by the suspended particles accumulated in the nodal planes of the supersonic phase grating.

1. – Continuing previous researches [1] we report some observations made on the optical behaviour of suspensions subjected to stationary ultrasonic waves, crossed by a monochromatic light beam having an amplitude nearly equal to the ultrasonic wavelength λ in the liquid.

We used the same experimental arrangement previously described (Fig. 1). The amplitude of the luminous beam can be reduced by means of a slit F_2, which can be made equal to the value of the ultrasonic λ in the liquid. In these conditions one observes, as it is known, a single widened line in the

[1] F. Porreca: *Nuovo Cimento*, **9**, 274 (1952).

focal plane F. The broadening ([2]) depends on the u.s. intensity and on the depth of the u.s. beam. We have already shown ([3]) that, if we keep these two parameters constant, different liquids show great and definite differences with the same u.s. power. These differences must be ascribed — after having accounted for experimental errors — to a not perfectly sinusoidal distribution of the refractive index, contrary to the actual assumption made in theoretical calculations. We therefore thought it interesting to extend these researches to the suspensions which present the permanence effect ([4]).

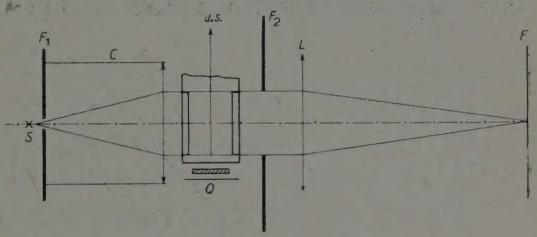

Fig. 1.

As we are of opinion that the suspended particles which accumulation for a time in the nodal planes produce the persistence and modify the value of the refraction index relatively to the pure liquid, we have made some experiments to confirm this assumption.

From microphotograms of the diffraction patterns we obtained graphs of the luminous intensity of the diffracted slit image. The determinations have

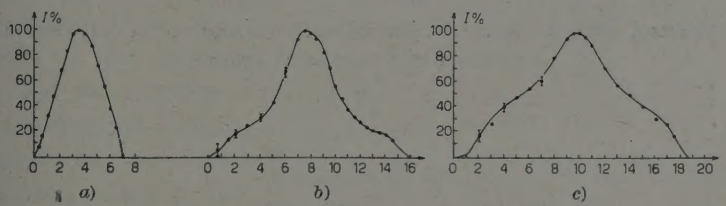

Fig. 2. – *a*) H_2O without u.s.; *b*) H_2O with u.s. up to the III order; *c*) H_2O with u.s. up to the V order.

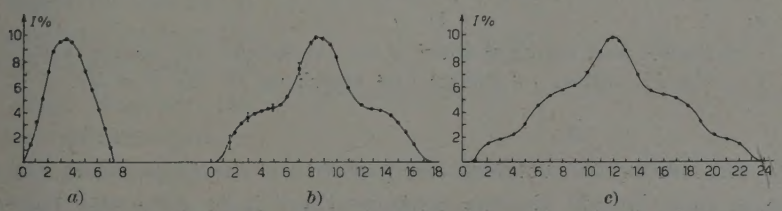

Fig. 3. – *a*) Starch and H_2O without u.s.; *b*) Starch and H_2O with u.s. up to the III order; *c*) Starch and H_2O with u.s. up to the V order.

([2]) R. Lucas and P. Biquard: *Journ. de Phys.*, **7**, 474 (1932).

([3]) F. Porreca: *Nuovo Cimento*, **9**, 280 (1952).

([4]) A. Carrelli and F. Porreca: *Nuovo Cimento*, **10**, 1406 (1953) and notes in the bibliography.

been made at two different u.s. powers corresponding to the appearance of the diffraction fringes of 3-rd and 5-th order, counted when the slit F_2 is much larger than λ. Figs. 2, 3 and 4 show respectively the intensity pattern in pure water, in a suspension of starch in water, and in a suspension of $BaSO_4$ in water. There

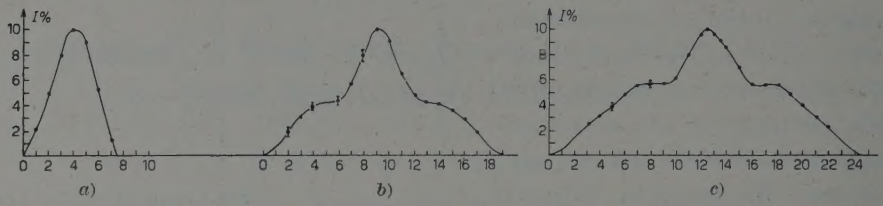

Fig. 4. – *a*) H_2O and $BaSO_4$ without u.s.; *b*) H_2O and $BaSO_4$ with u.s. up to the III order; *c*) H_2O and $BaSO_4$ with u.s. up to the V order.

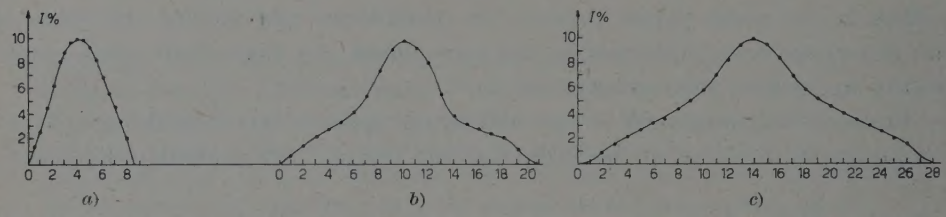

Fig. 5. – *a*) Benzol without u.s.; *b*) Benzol with u.s. up to the III order; *c*) Benzol with u.s. up to the V order.

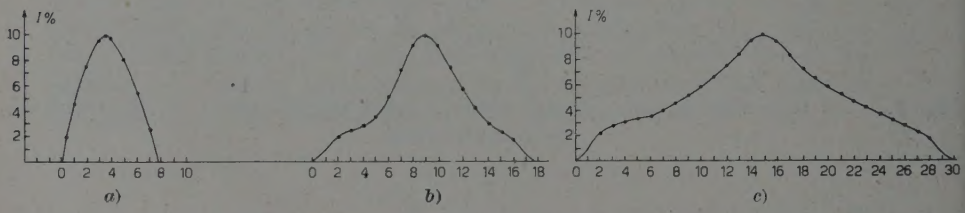

Fig. 6. – *a*) Benzol and starch without u.s.; *b*) Benzol and starch with u.s. up to the III order; *c*) Benzol and starch up to the V order.

is a very clear difference between the pattern for the suspensions and the one obtained in pure liquid. On the contrary there is no difference between suspensions, which do not show the permanence effect, and the pure liquid. Compare for instance Fig. 6 referring to starch in benzol and Fig. 5 referring to pure benzol.

We have further been able to show that with those substances which give the permanence, a deplacement of F_2, at right angles to the light beam direction, causes a periodic variation of the diffraction pattern with the period $\lambda/4$, a phenomenon which does not take place with the pure solvent.

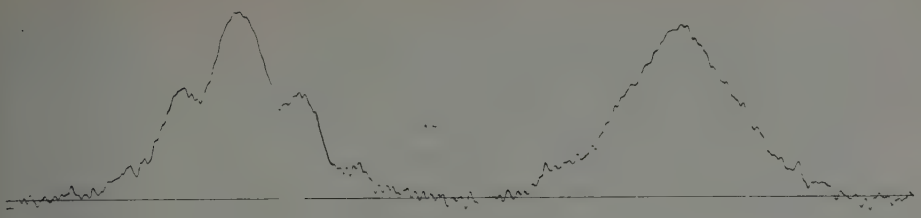

a) *b*)

Microphotograph n. 1. – Starch in water.

a) Vertical abscissa of $F_2 = x$; *b*) Vertical abscissa of $F_2 = x \pm \lambda/4$.

Microphotograph 1 shows the diffraction pattern for a suspension of starch in water, for two positions of F_2 differing by $\lambda/4$.

2. – Conclusively, these experimental results seem to prove that the suspensions giving the permanence of the diffraction fringes of the even orders. produce a pattern differing from the other ones.

In the case of the pair benzol-starch the intensity has the same distribution as for pure benzol, and this means that the presence of the suspended particles accumulated in the nodal planes of the waves does not alter the distribution of the refraction index of the liquid; on the contrary this distribution is modified in the other class of suspensions ($BaSO_4$ in water and starch in water). It is to this alteration that the persistence of the diffracted orders after stopping the ultrasonic perturbation is due; that is, a second phase grating is built with the constant $\lambda/2$, which diffracts the light and coexists with the other phase grating due to the pure liquid.

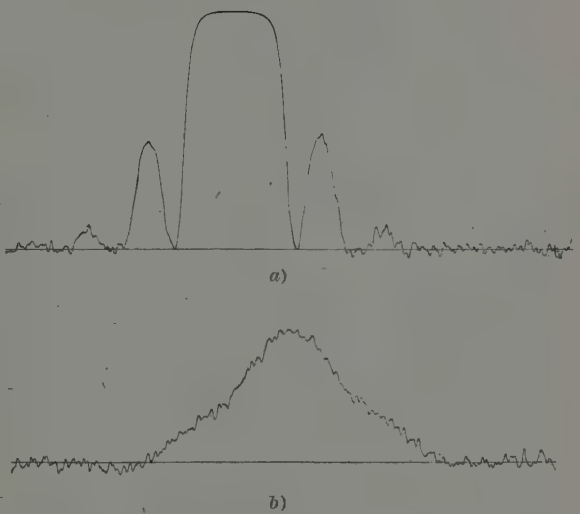

a)

b)

Microphotograph n. 2. – Phase gratings.

a) Vertical abscissa of $F_2 = x$; *b*) Vertical abscissa $F_2 = x \pm \lambda/4$.

We obtained a direct experimental proof for the co-existence of the two gratings by superposing two artificial gratings obtained from plexiglas plates ruled in such a way as to have the one with a constant double than the other; in the microphotograph (2) we used these two artificial phase gratings instead

of the batch, with slit F_2 having a width equal to the larger of the two constants. Also in this case we obtained the same diffraction pattern, and displacing the gratings relatively to F_2 we observed the same variations of pattern as we have observed for the suspension water-starch.

In microphotograph 2 we show the results obtained for a displacement of $\lambda^*/4$. Microphotograph 1 is less blurred owing to the sharper discontinuity of the artificial gratings as compared to the ultrasonic ones.

It is therefore clearly proved that in the suspensions presenting the permanence effect two phase gratings exist, one of them being due to the gathering of the suspended particles in the nodal planes.

We wish to thank here Prof. Antonio Carrelli to whom we feel greatly indebted for assistance given and valuable suggestions and guidance.

RIASSUNTO

In questo lavoro si continua lo studio della distribuzione della intensità luminosa della figura di diffrazione, che si ottiene facendo attraversare un mezzo liquido sottoposto agli ultrasuoni da un sottile fascio luminoso di larghezza uguale alla lunghezza d'onda ultrasonora. La distribuzione ottenuta nel caso delle sospensioni che presentano l'effetto di persistenza delle righe diffratte al cessare degli ultrasuoni, è diversa da quella presentata dalle sostanze che non presentano tale effetto. Inoltre, per le prime, spostando il reticolo ultrasonoro di $\lambda_{u.s.}/4$, si ottiene l'alternarsi di due caratteristiche figure di diffrazione. Analoga esperienza è stata compiuta sovrapponendo due reticoli modello di fase, ottenuti con fenditure equidistanti incise su lamine di plexiglas, con risultati identici a quelli avuti con le sospensioni che danno l'effetto di persistenza della figura di diffrazione al cessare degli ultrasuoni. Questa costituisce una prova indiretta che tale effetto è dovuto alla formazione di un secondo reticolo di fase, costituito dalle particelle sospese accumulate nei piani nodali del reticolo di fase ultrasonoro.

IL NUOVO CIMENTO Vol. I, N. 4 1° Aprile 1955

Singular Potentials in Relativistic Equations of Motion.

J. WERLE

Physical Institute P.A.N. - Warsaw (Poland)

(ricevuto il 28 Dicembre 1954)

Summary. — It is shown that in relativistic equations of motion for a particle moving in external potentials some additional forces of purely relativistic origin appear. These forces are repulsive for scalar and pseudoscalar potentials thus preventing the particle from coming too near to the singularity of the potential in spite of its apparently attractive character. An adiabatic approximation to the interaction potential for two nucleons interacting through the pseudoscalar field is obtained. An interesting feature of this potential is a strong repulsive term acting at short distances between nucleons.

One of the most interesting problems in the recent theory of nuclear forces is the problem of repulsive forces acting between nucleons at short distances apart. The existence of a repulsive core postulated on purely phenomenological grounds by R. JASTROW (1) has been supported by M. LEVY (2) in his non-adiabatic theory of two-nucleon systems. Regarding the problem of the repulsive core the question arises whether it is necessary to have an evidently repulsive potential in relativistic equations of motion. If so, the repulsive core would be connected with higher order in the coupling constant processes. But there also exists another possibility: that the effect does not depend on the sign of the potential and is hidden in the relativistic form of the equations of motion. In this second case the existence of the repulsive core could be independent of the higher order terms in g^2.

(1) R. JASTROW: *Phys. Rev.*, **81**, 165 (1951).
(2) M. LEVY: *Phys. Rev.*, **88**, 725 (1952).

The aim of this paper is to show that rather this second alternative is true. It can be shown that all relativistic equations of motion of a particle in an external potential contain in a hidden form some additional forces of purely relativistic origin. These forces are especially important near the singularities of the potential. The sign of these additional forces is independent of the sign of the potential and depends solely on the transformation properties of the potential. The forces are attractive, when the potential is the fourth component of a vector (e.g. Coulomb potential), but they are repulsive for scalar and pseudoscalar potentials.

The existence of additional forces of the above mentioned character can be shown in various ways. The simplest method consists in transition from the relativistic equations of motion to the approximate non-relativistic equations. This transition is to be done in such a manner as to get rid of all restrictions of the type $v \ll c$, or $g\Phi \ll mc^2$, etc., which are untenable in the vicinity of the singularity. An expansion of the relativistic equations can be given, which in the first approximation leads to non-relativistic equations satisfying these requirements. As an illustration let us take Klein-Gordon equation describing the motion of the particle in a scalar Φ and a vector potential $A_\mu = (A_1, A_2, A_3, A_4 = i\varphi)$:

$$\left\{ -\left(-i\hbar \frac{\partial}{\partial t} + e\varphi \right)^2 + c^2 \left(-i\hbar \nabla - \frac{e}{c} \boldsymbol{A} \right)^2 + c^2 \left(mc + \frac{g\Phi}{c} \right)^2 \right\} \Psi = 0 . \tag{1}$$

We set

$$\Psi = \exp\left[-\frac{imc^2 t}{\hbar} \right] \psi, \qquad \psi = \psi_0 + \lambda' \psi_1 + \lambda'^2 \psi_2 + \ldots \tag{2}$$

and assume that the operation $(i\hbar/mc^2)\,\partial/\partial t$ raises the order of the expression by one, i.e. is equivalent to a multiplication by $\lambda' \ll 1$. Comparing the terms of the same order in λ' we get an infinite set of equations. In the lowest order approximation we thus obtain non-relativistic Schrödinger equation

$$i\hbar \frac{\partial \psi_0}{\partial t} = \left\{ \frac{1}{2m} \left(-i\hbar \nabla - \frac{e}{c} \boldsymbol{A} \right)^2 + V_e + V_m \right\} \psi_0, \tag{3}$$

but with modified potentials

$$V_e = e\varphi - \frac{e^2 \varphi^2}{2mc^2}, \qquad V_m = g\Phi + \frac{g^2 \Phi^2}{2mc^2} . \tag{4}$$

We call potentials (4) « equivalent » because inserted in a non-relativistic Schrö-

dinger equation they describe very well all relativistic effects inherent in (1). The approximation is very good provided that the condition $(i\hbar/mc^2)\,\partial\psi/\partial t \ll 1$ is satisfied. This has a simple physical meaning in the case of static potentials and stationary solutions. Then it reduces to the condition $|\varepsilon| = |E - mc^2| \ll mc^2$, where E denotes the total energy, mc^2 the rest energy of the particle. The non-relativistic equation (3) also describes all relativistic effects in the vicinity of the singularity, if and only if $\varepsilon \ll mc^2$. From the form of equivalent potentials (4) we see that the additional force is attractive if $\varphi = -iA_4$ is the fourth component of a vector but it is repulsive for a scalar potential Φ. The differences between solutions of (1) and of approximate equation (3) vanish in the limit $\lambda = \varepsilon/mc^2 \to 0$. The same results can be obtained by means of a similar expansion method in classical theory ([3]).

The whole effect is of course independent of the approximation method used. The existence of repulsive or attractive forces can be shown in a more straightforward manner by examining the behaviour of the wave function Ψ near the singularity. For instance in the case of attractive central potential $\varphi = \varphi(r)$, $A_k = \Phi = 0$ the additional attractive force raises the probability density of finding the particle near the singularity. That is the reason why even for a Coulomb potential $e\varphi = -Ze^2/r$ no stationary solutions of (1) exist for $Z > 137/2$ and $l = 0$. If φ contains a still higher attractive singularity of the type $e\varphi = -a^2/r^n$ $(n > 1)$ then no stationary solutions exist at all, because the asymptotic form of Ψ contains a superposition of two highly oscillating terms ([4])

$$\Psi \sim c_1(E) \exp\left[+ i \frac{A}{r^{n-1}}\right] + c_2(E) \exp\left[- i \frac{A}{r^{n-1}}\right]. \tag{5}$$

Therefore the eigenvalue problem in the physical meaning of this word does not exist if the singular potential φ is the fourth component of a vector. For a scalar potential Φ with the same atrractive singularity $g\Phi = -a^2/r^n$ we find the following factor in the asymptotic form of Ψ:

$$\Psi \sim c_1(E) \exp\left[+ \frac{A}{r^{n-1}}\right] + c_2(E) \exp\left[- \frac{A}{r^{n-1}}\right]; \qquad A > 0\,. \tag{6}$$

In order to get quadratically integrable solutions we must put $c_1 = 0$. The eigenvalue problem is now well defined. Strong repulsive relativistic force diminishes enormously the probability density of finding the particle near the singularity: $|\Psi|^2 \sim \exp[-2A/r^{n-1}]$.

([3]) J. WERLE: *Bull. Ac. Pol. Sc.*, **1**, 281 (1953).
([4]) K. M. CASE: *Phys. Rev.*, **80**, 797 (1950).

Let us now briefly discuss Dirac equations with singular potentials φ, Φ of the same kind. Of course a transition to the approximate non-relativistic Pauli equation can be made. One finds in this way the same equivalent potentials V_e and V_m but with additional spin dependent terms, which have the same structure but opposite signs for both cases. However the relativistic force can be investigated more directly by examining the asymptotic behaviour of the solutions of the Dirac equations in the vicinity of a static central attractive singular potential. After separation of the angular dependence we obtain for the radial part of the Dirac function two equations ([4])

$$\frac{\mathrm{d}u}{\mathrm{d}r} - \varkappa \frac{u}{r} = \left(-\lambda - \frac{a^2}{r^n}\right) w\,, \tag{7}$$

$$\frac{\mathrm{d}w}{\mathrm{d}r} + \varkappa \frac{w}{r} = \left(2 + \lambda \pm \frac{a^2}{r^n}\right) u\,, \tag{8}$$

where we set $\hbar = c = m = 1$, $\varkappa = \pm (j + \frac{1}{2})$, $\lambda = \varepsilon/mc^2$. The upper sign in (8) refers to the vector potential $\varphi = (1/i)A_4$ and the lower to the scalar potential Φ, both containing an attractive singularity of the same type. Different signs in (8) cause quite different asymptotic behaviour of Ψ. In the first case solutions of Dirac equations contain a superposition of the same oscillating functions as in (5). In the second case we again have a factor containing (6). Thus we see that in Dirac equations also, the eigenvalue problem for the scalar potential always exists, because at small distances the attractive orce changes into a strong repulsive force. This relativistic force prevents the particle from coming near the singularity. The probability density of finding the particle near the singularity falls again very rapidly: $|\Psi|^2 \sim \sim \exp[-2A/r^{n-1}]$.

Now let us consider Dirac equations with pseudoscalar potential Φ':

$$\left\{-i\hbar \frac{\partial}{\partial t} - i\hbar c \boldsymbol{\alpha} \nabla + \varrho_3 mc^2 + g\varrho_2 \Phi'\right\} \Psi = 0\,. \tag{9}$$

Setting

$$\left\{\begin{array}{l} \Psi = \begin{pmatrix} \psi_1 \\ \psi_2 \\ \psi_3 \\ \psi_4 \end{pmatrix} = (\chi_1 + \varrho_1 \chi_2) \exp\left[-\frac{imc^2 t}{\hbar}\right], \\ \chi_1 = \begin{pmatrix} \psi_1 \\ \psi_2 \\ 0 \\ 0 \end{pmatrix} \exp\left[\frac{imc^2 t}{\hbar}\right], \qquad \chi_2 = \begin{pmatrix} \psi_3 \\ \psi_4 \\ 0 \\ 0 \end{pmatrix} \exp\left[\frac{imc^2 t}{\hbar}\right], \end{array}\right. \tag{10}$$

we can write (9) in the form

$$(11) \qquad i\hbar \frac{\partial}{\partial t} \chi_1 = -i\hbar c \boldsymbol{\sigma} \nabla \chi_2 - ig\Phi' \chi_2 ,$$

$$(12) \qquad \left(i\hbar \frac{\partial}{\partial t} + 2mc^2 \right) \chi_2 = -i\hbar c \boldsymbol{\sigma} \nabla \chi_1 + ig\Phi' \chi_1 ,$$

where σ_i denote the usual Pauli matrices. Eliminating χ_2 we obtain a strict equation for stationary solutions in a static potential Φ':

$$(13) \qquad \left\{ -\frac{\hbar^2}{2m} \Delta + \frac{\hbar g}{2mc} \boldsymbol{\sigma} \nabla \Phi' + \frac{g^2}{2mc^2} \Phi'^2 \right\} \chi_1 = \varepsilon (1 + \lambda/2) \chi_1 .$$

The equivalent potential now has the form

$$(14) \qquad V'_m = \frac{\hbar g}{2mc} \boldsymbol{\sigma} \nabla \Phi' + \frac{g^2}{2mc^2} \Phi'^2 .$$

It again contains a strong repulsive force acting at short distances.

It is obvious that Φ' can be in general interpreted as an operator, which contains the coordinates and Pauli matrices of another particle, which we denote by number 2. Using the equivalence theorem [5] for pseudovector and pseudoscalar coupling we can set in the first (really static) approximation:

$$(15) \qquad \Phi' = \frac{\hbar g}{2mc} \boldsymbol{\sigma}_{(2)} \nabla_{(2)} \frac{\exp[-\mu r_{12}]}{r_{12}} .$$

Then the equivalent potential (14) has the form

$$(16) \qquad V'_m = -\left(\frac{\hbar g}{2mc} \right)^2 (\boldsymbol{\sigma}_{(1)} \cdot \nabla_{(1)})(\boldsymbol{\sigma}_{(2)} \cdot \nabla_{(2)}) \frac{\exp[-\mu r_{12}]}{r_{12}} - \\ + \frac{\hbar^2 g^4}{8 m^3 c^4} \left(\mu + \frac{1}{r_{12}} \right)^2 \frac{\exp[-2\mu r_{12}]}{r_{12}} .$$

Apart from the usual non-central term containing a $1/r^3$ singularity we see a central repulsive term with a singularity as high as $1/r^4$.

All cases considered here are good illustrations of the statement that at short distances between particles there exist some forces of purely relativistic

(5) F. J. DYSON: *Phys. Rev.*, **73**, 929 (1948); K. M. CASE: *Phys. Rev.*, **75**, 1306 (1949).

origin. Their sign is independent of the sign of the interaction potential but depends on the transformation properties of the potential. These forces are very small in the theory of atom, because their range is then 10^4 times smaller than atomic radius. But they are probably very important in the nuclei because the range of the repulsive force is almost of the same order of magnitude as the range of attractive nuclear forces ([3]). There are some indications that the same holds true quite generally for relativistic equations of two body problem.

A full report of this paper will be published in *Acta Physica Polonica*.

The author wishes to express his gratitude to Prof. L. INFELD for many valuable suggestions concerning the problem of singular potentials.

RIASSUNTO (*)

Si dimostra che nelle equazioni relativistiche del moto di una particella in potenziali esterni appaiono delle forze addizionali di origine puramente relativistica. Queste forze sono repulsive per potenziali scalari e pseudoscalari, impedendo in tal modo alla particella di avvicinarsi troppo alla singolarità del potenziale ad onta del suo carattere apparentemente attrattivo. Si ottiene un'approssimazione adiabatica al potenziale di interazione di due nucleoni interagenti tramite il campo pseudoscalare. Una particolarità interessante di questo potenziale è un termine fortemente repulsivo che agisce fra i nucleoni a distanza ravvicinata.

(*) *Traduzione a cura della Redazione.*

IL NUOVO CIMENTO Vol. I, N. 4 1° Aprile 1955

Vortex Motions of the Madelung Fluid.

M. Schönberg

Faculdade de Filosofia, Ciencias e Letras da Universidade de São Paulo, Brasil

(ricevuto il 3 Gennaio 1955)

Summary. — The general motions of the continuous medium (Madelung fluid), whose irrotational motions are described by the Schrödinger equation, are discussed. It is shown that many of the basic theorems of the vortex motions of the inviscid barotropic fluids are also valid for the Madelung fluid. A detailed discussion of the Clebsch parameters is given. It is shown that there is a special type of steady motions, similar to the Beltrami motions in which the streamlines coincide with the vortex-lines, which corresponds to a close generalization of the ordinary stationary states. The quantization of the vortex-tubes is discussed. Examples of Beltrami and discontinuous motions of the Madelung fluid are given. It is shown that the general motions of the Madelung fluid can also be physically interpreted in terms of the ordinary quantal states of a particle.

1. – Introduction.

Madelung [1] showed that the Schrödinger equation for a particle is equivalent to a set of equations that describe a flow in space. Let us denote by Ψ the wave function of a particle of mass m and charge e moving in the electromagnetic field described by the potentials A_0, $\boldsymbol{A}$. It follows from the Schrödinger equation

$$i\hbar \frac{\partial \Psi}{\partial t} = \left\{ \frac{1}{2m} \left(\frac{\hbar}{i} \frac{\partial}{\partial \boldsymbol{x}} - \frac{e}{c} \boldsymbol{A} \right)^2 + eA_0 \right\} \Psi , \tag{1}$$

[1] E. Madelung: *Zeits. f. Phys.*, **40**, 332 (1926).

that the amplitude R and the phase $S/\hbar$ of Ψ satisfy the equations

$$\frac{\partial S}{\partial t} + \frac{1}{2m}\left(\frac{\partial S}{\partial \boldsymbol{x}} - \frac{e}{c}\boldsymbol{A}\right)^2 + eA_0 - \frac{\hbar^2}{2m}\frac{\Delta R}{R} = 0\,, \tag{2}$$

$$\frac{\partial R^2}{\partial t} + \operatorname{div}\left\{\frac{R^2}{m}\left(\frac{\partial S}{\partial \boldsymbol{x}} - \frac{e}{c}\boldsymbol{A}\right)\right\} = 0\,, \tag{3}$$

$$\Psi = R\exp\left[\frac{i}{\hbar}S\right]. \tag{4}$$

Let us introduce the velocity $\boldsymbol{v}$ and the mass density $m\varrho$

$$\boldsymbol{v} = \frac{1}{m}\left(\frac{\partial S}{\partial \boldsymbol{x}} - \frac{e}{c}\boldsymbol{A}\right), \qquad \varrho = R^2. \tag{5}$$

It follows from (2) and (3) that

$$m\left(\frac{\partial}{\partial t} + \boldsymbol{v}\cdot\frac{\partial}{\partial \boldsymbol{x}}\right)\boldsymbol{v} = e\left(\boldsymbol{E} + \frac{\boldsymbol{v}}{c}\wedge\boldsymbol{H}\right) + \frac{\hbar^2}{2m}\frac{\partial}{\partial \boldsymbol{x}}\frac{\Delta R}{R}\,, \tag{6}$$

($\boldsymbol{E}$ = electric field; $\boldsymbol{H}$ = magnetic field)

$$\frac{\partial \varrho}{\partial t} + \operatorname{div}(\varrho\boldsymbol{v}) = 0\,. \tag{7}$$

Equation (6) has the form of the Euler equation of motion of a special kind of charged fluid medium of charge density $e\varrho$, the velocity being $\boldsymbol{v}$ and the spatial components of the stress tensor having the values

$$T_{ab} = m\varrho v_a v_b + \frac{\hbar^2}{m}\frac{\partial R}{\partial x_a}\frac{\partial R}{\partial x_b} - \delta_{ab}\frac{\hbar^2}{4m}\Delta\varrho\,. \tag{8}$$

Indeed, since the density of mechanical momentum is

$$\boldsymbol{G} = m\varrho\boldsymbol{v} \tag{9}$$

the equation (6) is equivalent to the following

$$\frac{\partial \boldsymbol{G}}{\partial t} + \operatorname{div} T = e\varrho\left(\boldsymbol{E} + \frac{\boldsymbol{v}}{c}\wedge\boldsymbol{H}\right), \tag{10}$$

div T denoting the divergence of the three-dimensional tensor defined by (8). Equation (7) is the continuity equation of the Madelung fluid.

It follows from the first equation (5) that the vorticity ζ of the motion of the Madelung fluid associated to the Schrödinger equation (1) satisfies the condition

$$\zeta = \operatorname{rot} \boldsymbol{v} = -\frac{e}{mc}\boldsymbol{H}. \tag{11}$$

In the absence of magnetic fields $\zeta = 0$ and the motions associated to the equation (1) are irrotational. We shall call the motions satisfying the condition (11) quasi-irrotational. TAKABAYASHI ([2]) called the attention to the fact that the equations (6) and (7), in the absence of magnetic fields, are valid both for the rotational and irrotational motions of the Madelung fluid and may be regarded as a generalization of the Schrödinger equation (1). Independently, we remarked that (6) and (7) generalize the Schrödinger equation (1) and introduced also the distinction between quasi-irrotational and general motions of the Madelung fluid. *The presence or absence of vorticity is not the fundamental fact, since the Schrödinger equation may be applicable even when there is vorticity, provided the motion be quasi-irrotational. This is shown even clearer by the extension of the Madelung hydrodynamical model to particles with spin* ([3]): *in the case of a particle with spin there is vorticity, even in the absence of magnetic fields.*

We have shown ([4]) that it is possible to generalize the wave equations of the quantum mechanics by a suitable modification of the usual variational principles. We started from a generalized form of the classical Hamilton-Jacobi theory and from a new kind of classical variational principle associated to that generalization. In the particular case of the non relativistic wave equation for a spinless particle, our generalization can also be derived from the analysis of the general motions of the Madelung fluid, as will be shown in section 3. The theory of reference ([4]) was further extended ([5]) to all the field formalisms admitting the gauge-invariance of the first kind. We showed in that paper that the generalization procedure amounts to replace certain integrable field quantities by non integrable quantities, whose differences of values at infinitesimally close points in space-time are definite. In the particular case of the non relativistic Schrödinger equation, the phase S becomes a non integrable quantity in the general vortex motion of the Madelung fluid.

We showed in reference ([5]) that the general theorems on the vortex motions

([2]) T. TAKABAYASHI: *Prog. Theor. Phys.*, **9**, 187 (1953).

([3]) M. SCHÖNBERG: *Nuovo Cimento*, **12**, 103 (1954); D. BOHM, R. SCHILLER and J. TIOMNO: *Suppl. Nuovo Cimento*, **1**, 48 (1955).

([4]) M. SCHÖNBERG: *Nuovo Cimento*, **11**, 674 (1954).

([5]) M. SCHÖNBERG: *Nuovo Cimento*, **12**, 649 (1954).

of the inviscid barotropic fluids under the action of conservative forces have their analogues in the generalization of the ordinary gauge-invariant field formalisms, by the introduction of non integrable quantities, the vorticity being replaced by a non-integrability vector $\boldsymbol{\eta}$. The lines of force of the $\boldsymbol{\eta}$-field play the part of the vortex-lines of the ordinary hydrodynamics. The η-tubes formed by those η-lines have a time independent strength, the strength being defined as the flux of the vector $\boldsymbol{\eta}$ through any section of the tube. In the case of the vortex motions of the Madelung fluid we have

$$\boldsymbol{\eta} = \operatorname{rot} \boldsymbol{u}\,, \qquad \boldsymbol{u} = m\boldsymbol{v} + \frac{e}{c}\boldsymbol{A}\,. \tag{12}$$

There is a circulation theorem for the vector $\boldsymbol{u}$

$$\int_C \boldsymbol{u}\cdot\delta\boldsymbol{x} = \int_{C_0} \boldsymbol{u}_0\cdot\delta\boldsymbol{x}_0\,, \tag{13}$$

C being a closed fluid line formed, at the time t, by the fluid elements lying at the time 0 on the closed curve C_0; $\boldsymbol{x}_0$ and $\boldsymbol{u}_0$ being the position and $\boldsymbol{u}$-vectors at the time 0. We shall extend the ordinary hydrodynamical vortex theorems to the Madelung fluid in section **2**.

The importance of the Clebsch parameters for the generalization of the gauge-invariant field theories was shown in references ([4]) and ([5]). The properties of the Clebsch parameters will be discussed in detail in section **3**. The first equation (5) is replaced by

$$\boldsymbol{v} = \frac{1}{m}\left(\frac{\partial S}{\partial \boldsymbol{x}} + \lambda\frac{\partial \mu}{\partial \boldsymbol{x}} - \frac{e}{c}\boldsymbol{A}\right), \tag{14}$$

in the case of a general motion. S, λ and μ are the Clebsch parameters. It will be shown in section **4** that the same distribution of velocities is also described by the parameters S', λ' and μ' defined by the equations

$$\begin{cases} \lambda\dfrac{\partial \mu}{\partial \boldsymbol{x}} - \lambda'\dfrac{\partial \mu'}{\partial \boldsymbol{x}} = \dfrac{\partial}{\partial \boldsymbol{x}}\Gamma(t, \mu, \mu')\,, \\ S' = S + \Gamma + F(t)\,. \end{cases} \tag{15}$$

Γ being an arbitrary function of t, μ, μ' and F an arbitrary function of t. The equations of motion in terms of the Clebsch parameters are

$$\begin{cases} \dfrac{\partial \mu}{\partial t} + \boldsymbol{v}\cdot\dfrac{\partial \mu}{\partial \boldsymbol{x}} = \dfrac{\partial K}{\partial \lambda}\,, \qquad \dfrac{\partial \lambda}{\partial t} + \boldsymbol{v}\cdot\dfrac{\partial \lambda}{\partial \boldsymbol{x}} = -\dfrac{\partial K}{\partial \mu}\,, \\ \dfrac{\partial S}{\partial t} + \lambda\dfrac{\partial \mu}{\partial t} + \dfrac{1}{2m}\left(\dfrac{\partial S}{\partial \boldsymbol{x}} + \lambda\dfrac{\partial \mu}{\partial \boldsymbol{x}} - \dfrac{e}{c}\boldsymbol{A}\right)^2 + eA_0 - \dfrac{\hbar^2}{2m}\dfrac{\Delta R}{R} = K\,, \end{cases} \tag{16}$$

$$(K = \text{function of } t,\ \lambda,\ \mu)\,.$$

$K(t, \lambda, \mu)$ being an arbitrary function. The simplest choice $K = 0$ renders the parameters λ and μ constants of the motion. We shall always assume that λ and μ are chosen as constants of the motion and $K = 0$. We shall extend the equation (4) to the case of the general motions of the fluid. Thus we get the generalized Schrödinger equation

$$(17)\qquad \begin{cases} i\hbar\dfrac{\partial\Psi}{\partial t} = \dfrac{1}{2m}\left(\dfrac{\hbar}{i}\dfrac{\partial}{\partial \boldsymbol{x}} - \dfrac{e}{c}\boldsymbol{A} + \lambda\dfrac{\partial\mu}{\partial \boldsymbol{x}}\right)^2\Psi + \left(eA_0 + \lambda\dfrac{\partial\mu}{\partial t}\right)\Psi\,, \\ \dfrac{\partial\lambda}{\partial t} + \boldsymbol{v}\cdot\dfrac{\partial\lambda}{\partial \boldsymbol{x}} = 0\,, \qquad \dfrac{\partial\mu}{\partial t} + \boldsymbol{v}\cdot\dfrac{\partial\mu}{\partial \boldsymbol{x}} = 0\,. \end{cases}$$

When λ and μ are taken as constants of the motion, the function Γ in the transformation (15) is to be taken also as time independent. It will be shown in section **6** that

$$(18)\qquad \lambda'\frac{\partial\mu'}{\partial t} = \lambda\frac{\partial\mu}{\partial t} - \frac{\partial\Gamma}{\partial t}\,, \qquad \left(\frac{\partial\Gamma}{\partial t} = \frac{\lambda\Gamma}{\partial\lambda}\frac{\partial\lambda}{\partial t} + \frac{\partial\Gamma}{\partial\mu}\frac{\partial\mu}{\partial t}\right).$$

It is convenient to take $F = 0$ in the second equation (15) in order to have

$$(19)\qquad \Psi' = \Psi\exp\left[\frac{i}{\hbar}\Gamma\right].$$

The form of the first equation (17) shows taht $-(c/e)\lambda(\partial\mu/\partial \boldsymbol{x})$ and $(1/e)\lambda(\partial\mu/\partial t)$ may be regarded as the potentials of a field. This point of view allows us to consider the change of the Clebsch parameters as a change of the gauge of those potentials. Equations (15), (18) and (19) correspond precisely to a change of the gauge of the potentials such that the new potentials be also expressible in terms of Clebsch parameters λ', μ'. This point will be discussed in more detail in section **6**.

At any instant of time t the Madelung fluid will have a quasi-irrotational part occupying a region Ω_t and a region where $\boldsymbol{\eta} \neq 0$, if the two parts do exist at a given instant of time t_0. In the region Ω_t, λ and μ can be taken as nil, but the function S will not be single-valued in general, unless Ω_t is simply connected. The circulation of the vector $\boldsymbol{u}$ along a closed path C within Ω_t is a linear combination with integer coefficients p_l of the cyclic constants K_l

$$(20)\qquad \int_C \boldsymbol{u}\cdot\delta\boldsymbol{x} = \sum_{l=1}^{n} p_l K_l\,,$$

$n - 1$ being the order of connectivity of Ω_t. The order of connectivity and the cyclic constants are invariants of the motion, as a consequence of the circulation theorem (13). *In order that the wave function Ψ be single-valued the*

strengthes of the η-tubes must be integral multiples of h. This point will be discussed in section **5**.

The generalized Schrödinger equation is discussed in section **6**. It is shown that it can be obtained from a variational principle of the same type as that for the ordinary Schrödinger equation. The new principle is obtained from the ordinary one by introducing the extra potentials $-(e/e)\lambda(\partial\mu/\partial \boldsymbol{x})$ and $(1/e)\lambda(\partial\mu/\partial t)$, λ and μ being variated as independent quantities. It is shown that, besides the gauge-transformations corresponding to the different possible choices of the Clebsch parameters, the equations (17) admit also the transformation

$$\Psi' = C\Psi, \quad \lambda' = \lambda, \quad \mu' = \mu \quad (C = \text{arbitrary constant}). \tag{21}$$

This invariance results from the fact that the quantum potential is invariant for the substitution of R by CR.

The steady motions of the Madelung fluid are discussed in section **7**. In those motions

$$W = \frac{m\boldsymbol{v}^2}{2} + eA_0 - \frac{\hbar^2}{2m}\frac{\Delta R}{R}, \tag{22}$$

is a constant of the motion of the elements of the fluid (Bernoulli theorem for the Madelung fluid). The value of W is not the same for all the streamlines, unless

$$\boldsymbol{v} \wedge \boldsymbol{\eta} = 0 \qquad \text{(everywhere)}. \tag{23}$$

The steady motions satisfying the condition (23) correspond to those discussed by BELTRAMI [6] and STEKLOFF [7] in hydrodinamics. In those motions the energy per unit mass of the fluid is everywhere the same. It is proven in section **7** that (23) is a necessary and sufficient condition in order that it be possible to choose λ and μ as time independent constants of the motion, in a steady motion of the Madelung fluid. *The steady motions satisfying the condition* (23) *may be considered as the generalization of the ordinary stationary states for the generalized Schrödinger equation. The ordinary stationary states correspond to the steady Beltrami motions of the Madelung fluid in which* $\boldsymbol{\eta} = 0$. *Therefore the condition* $\boldsymbol{\eta} = 0$ *plays a fundamental part in the quantization of the values of the energy.*

A simple case of steady motion in which $\boldsymbol{v} \wedge \boldsymbol{\eta} = 0$ is discussed in section **8**. The trajectories of the elements of fluid within a circular cylinder are helices. The motion is irrotational outside the cylinder, where the trajectories are

(6) E. BELTRAMI: *Nuovo Cimento*, **25**, 212 (1889).
(7) W. STEKLOFF: *An. Fac. Sci. Univ. Toulouse*, **10**, 271 (1908).

circles lying on planes perpendicular to the axis of the cylinder. The azimuthal component of the vorticity on the cylinder limiting the vortex is infinite. This Beltrami motion is closely related to the two dimensional vortex motion discussed in reference ([8]). The method used to derive the former motion from the latter consists in impressing to the elements of fluid velocities perpendicular to the plane of the motion and constant along each trajectory of the two-dimensional motion, in such a way that W be constant through the mass of the fluid. Thus the circular trajectories are replaced be helices within the cylinder. In the outer region no extra-velocity was impressed, because W was already constant in that region. This method can be applied to derive Beltrami motions from a large class of two-dimensional vortex motions in which the trajectories are circles centred at the origin and described in uniform motion.

Motions in which the velocity is discontinuous across a surface Σ are discussed in section 9. The discontinuity of the tangential component of the velocity is associated with the existence of a vortex sheet on Σ. A method is given to obtain simple discontinuous motions from stationary two-dimensional solutions of the ordinary Schrödinger equation. It is shown that with an R satisfying the condition

$$\frac{\partial R}{\partial n}\,\frac{\partial R}{\partial \boldsymbol{x}} \wedge \boldsymbol{n} = 0\,, \tag{24}$$

$\boldsymbol{n}$ denoting the unit vector on the normal to a surface Σ, the stresses on Σ are normal, as in the case of the inviscid ordinary fluids. There is an essential difference between the discontinuous motions of the Madelung fluid and those of the inviscid ordinary fluids, arising from the fact that the effect of the pressure in the latter case is replaced by that of the quantum potential which depends on second order derivatives of the density.

The physical interpretation of the general motions of the Madelung fluid is not yet entirely clear. *It is however remarkable that any motion of the fluid corresponds to a quantal state of motion of a particle, because the first equation* (17) *may be regarded as an ordinary Schrödinger equation for a particle moving in an electromagnetic field described by the potentials* $A_0 + A_{0,\mathrm{in}}$, $\boldsymbol{A} + \boldsymbol{A}_{\mathrm{in}}$

$$A_{0,\mathrm{in}} = \frac{\lambda}{e}\,\frac{\partial \mu}{\partial t}\,, \qquad \boldsymbol{A}_{\mathrm{in}} = -\frac{c\lambda}{e}\,\frac{\partial \mu}{\partial \boldsymbol{x}}\,. \tag{25}$$

The « inner » electromagnetic field described by the $A_{0,\mathrm{in}}$, $\boldsymbol{A}_{\mathrm{in}}$ is

$$\boldsymbol{H}_{\mathrm{in}} = -\frac{c}{e}\boldsymbol{\eta}\,, \qquad \boldsymbol{E}_{\mathrm{in}} = -\frac{\boldsymbol{v}}{c} \wedge \boldsymbol{H}_{\mathrm{in}}\,. \tag{26}$$

The Lorentz force due to the « inner » field vanishes: $\boldsymbol{E}_{\mathrm{in}} + \boldsymbol{v}/c \wedge \boldsymbol{H}_{\mathrm{in}} = 0$.

([8]) M. Schönberg: *Nuovo Cimento*, **12**, 300 (1954).

It will be shown in section 6 that the system (17) may be replaced by the following

$$(27)\qquad \begin{cases} i\hbar\,\dfrac{\partial\Psi}{\partial t} = \dfrac{1}{2m}\left(\dfrac{\hbar}{i}\,\dfrac{\partial}{\partial \boldsymbol{x}} - \dfrac{e}{c}(\boldsymbol{A}+\boldsymbol{A}_{\text{in}})\right)^2\Psi + e(A_0 + A_{0,\text{in}})\Psi, \\ \dfrac{\mathrm{d}}{\mathrm{d}t}\begin{pmatrix}\boldsymbol{H}_{\text{in}}\\ \varrho\end{pmatrix} - \begin{pmatrix}\boldsymbol{H}_{\text{in}}\\ \varrho\end{pmatrix}\cdot\dfrac{\partial}{\partial \boldsymbol{x}}\,\boldsymbol{v} = 0\,, \qquad \boldsymbol{E}_{\text{in}} + \dfrac{\boldsymbol{v}}{c}\wedge\boldsymbol{H} = 0\,, \\ \boldsymbol{H}_{\text{in}} = \operatorname{rot}\boldsymbol{A}_{\text{in}}\,, \qquad \boldsymbol{E}_{\text{in}} = -\dfrac{\partial}{\partial \boldsymbol{x}}\,A_{0,\text{in}} - \dfrac{1}{c}\,\dfrac{\partial}{\partial t}\,\boldsymbol{A}_{\text{in}}\,. \end{cases}$$

The second equation (27) gives the variation of η with time.

2. – Extension of the Helmholtz and Cauchy Vortex Theorems to the Madelung Fluid.

By solving equations (6) and (7) of section 1 we get $\boldsymbol{v}(t, \boldsymbol{x})$ and $\varrho(t, \boldsymbol{x})$. The trajectories of the elements of the fluid are determined by the differential equation

$$(1)\qquad \frac{\mathrm{d}\boldsymbol{x}}{\mathrm{d}t} = \boldsymbol{v}(t, \boldsymbol{x})\,.$$

Along the trajectories we have

$$(2)\qquad \boldsymbol{x} = \boldsymbol{f}(t, \boldsymbol{x}_0)\,.$$

Let us consider two neighbouring trajectories and denote by $\delta\boldsymbol{x}$ the displacement vector between the positions on the two trajectories. $\delta\boldsymbol{x}$ satisfies the linear equation

$$(3)\qquad \frac{\mathrm{d}}{\mathrm{d}t}\,\delta\boldsymbol{x} = \left(\delta\boldsymbol{x}\cdot\frac{\partial}{\partial \boldsymbol{x}}\right)\boldsymbol{v}(t, \boldsymbol{v}) = \frac{\partial \boldsymbol{v}}{\partial \boldsymbol{x}}\,\delta\boldsymbol{x}\,, \qquad \frac{\mathrm{d}}{\mathrm{d}t}\,\delta = \delta\,\frac{\mathrm{d}}{\mathrm{d}t},$$

$\partial\boldsymbol{v}/\partial\boldsymbol{x}$ being a dyadic. Hence

$$(4)\qquad \delta\boldsymbol{x} = L(t, \boldsymbol{x}_0)\,\delta\boldsymbol{x}_0\,, \qquad \frac{\mathrm{d}}{\mathrm{d}t}\,\delta\boldsymbol{x} = \frac{\partial L}{\partial t}\,L^{-1}\,\delta\boldsymbol{x}\,;$$

$L(t, \boldsymbol{x}_0)$ being a dyadic

$$(5)\qquad L(t, \boldsymbol{x}_0) = \frac{\partial \boldsymbol{x}}{\partial \boldsymbol{x}_0}\,, \qquad \frac{\partial L}{\partial t} = \frac{\partial \boldsymbol{v}}{\partial \boldsymbol{x}}\,L\,.$$

Since

$$\frac{\mathrm{d}}{\mathrm{d}t}(\boldsymbol{v}\cdot\delta\boldsymbol{x}) = \frac{\mathrm{d}\boldsymbol{v}}{\mathrm{d}t}\cdot\delta\boldsymbol{x} + \boldsymbol{v}\cdot\delta\boldsymbol{v} = \frac{\mathrm{d}\boldsymbol{v}}{\mathrm{d}t}\cdot\delta\boldsymbol{x} + \delta\frac{\boldsymbol{v}^2}{2}, \tag{6}$$

we get from the Euler equation

$$m\frac{\mathrm{d}}{\mathrm{d}t}(\boldsymbol{v}\cdot\delta\boldsymbol{x}) = e\left(\boldsymbol{E} + \frac{\boldsymbol{v}}{c}\wedge\boldsymbol{H}\right)\cdot\delta\boldsymbol{x} + \delta\left(\frac{m\boldsymbol{v}^2}{2} + \frac{\hbar^2}{2m}\frac{\Delta R}{R}\right). \tag{7}$$

It is easily seen that

$$\left(\boldsymbol{E} + \frac{\boldsymbol{v}}{c}\wedge\boldsymbol{H}\right)\cdot\delta\boldsymbol{x} = \delta\left(\frac{\boldsymbol{v}}{c}\cdot\boldsymbol{A} - A_0\right) - \frac{1}{c}\frac{\mathrm{d}}{\mathrm{d}t}(\boldsymbol{A}\cdot\delta\boldsymbol{x}). \tag{8}$$

Hence

$$\frac{\mathrm{d}}{\mathrm{d}t}(\boldsymbol{u}\cdot\delta\boldsymbol{x}) = \delta\left(\frac{m\boldsymbol{v}^2}{2} - eA_0 + \frac{e}{c}\boldsymbol{v}\cdot\boldsymbol{A} + \frac{\hbar^2}{2m}\frac{\Delta R}{R}\right). \tag{9}$$

By integrating both sides of (9) with respect to t we get

$$\boldsymbol{u}\cdot\delta\boldsymbol{x} - \boldsymbol{u}_0\cdot\delta\boldsymbol{x}_0 = \delta\chi, \tag{10}$$

$$\chi = \int_0^t \left\{\frac{m\boldsymbol{v}^2}{2} - e\left(A_0 - \frac{\boldsymbol{v}}{c}\cdot\boldsymbol{A}\right) + \frac{\hbar^2}{2m}\frac{\Delta R}{R}\right\}\mathrm{d}t. \tag{11}$$

Equation (10) leads immediately to the circulation theorem for $\boldsymbol{u}$

$$\int_C \boldsymbol{u}\cdot\delta\boldsymbol{x} = \int_{C_0}\boldsymbol{u}_0\cdot\delta\boldsymbol{x}_0. \tag{12}$$

The circulation theorem means that $\int_C \boldsymbol{u}\cdot\delta\boldsymbol{x}$ is an integral invariant of order 1 of the motion of the elements of the fluid. Equation (12) can be transformed by means of the Stokes theorem as follows

$$\int_S \boldsymbol{\eta}\cdot\boldsymbol{n}\,\mathrm{d}S = \int_{S_0}\boldsymbol{\eta}_0\cdot\boldsymbol{n}_0\,\mathrm{d}S_0, \tag{13}$$

S and S_0 being formed by the same elements of fluid at the times t and 0, respectively, and limited by the contours C and C_0. $\boldsymbol{n}$ and $\boldsymbol{n}_0$ denote unit vectors on the normals to S and S_0, respectively. The choice of S being ar-

bitrary in (13), we must have

$$\boldsymbol{\eta}\cdot\delta_1\boldsymbol{x}\wedge\delta_2\boldsymbol{x}=\boldsymbol{\eta}_0\cdot\delta_1\boldsymbol{x}_0\wedge\delta_2\boldsymbol{x}_0\,, \tag{14}$$

for arbitrary $\delta_1\boldsymbol{x}$, $\delta_2\boldsymbol{x}$. Equation (14) is the differential form of (13).

It is well known that the adjoint $K^\dagger$ of a dyadic K is defined by the equation

$$\boldsymbol{a}\cdot K\boldsymbol{b}=\boldsymbol{b}\cdot K^\dagger\boldsymbol{a}\,, \tag{15}$$

$\boldsymbol{a}$ and $\boldsymbol{b}$ being arbitrary vectors. The determinant $|K|$ of the matrix of K satisfies the equation

$$|K|\boldsymbol{a}\wedge\boldsymbol{b}\cdot\boldsymbol{c}=K\boldsymbol{a}\wedge K\boldsymbol{b}\cdot K\boldsymbol{c}=\boldsymbol{c}\cdot\{K^\dagger(K\boldsymbol{a}\wedge K\boldsymbol{b})\}\,, \tag{16}$$

for any vectors $\boldsymbol{a}$, $\boldsymbol{b}$, $\boldsymbol{c}$. Therefore we have

$$|K|\boldsymbol{a}\wedge\boldsymbol{b}=K^\dagger(K\boldsymbol{a}\wedge K\boldsymbol{b})\,. \tag{17}$$

By taking into account that

$$(K^\dagger)^{-1}=(K^{-1})^\dagger \tag{18}$$

we get

$$|L|\boldsymbol{\eta}_0\cdot\delta_1\boldsymbol{x}_0\wedge\delta_2\boldsymbol{x}_0=\boldsymbol{\eta}_0\cdot L^\dagger(L\,\delta_1\boldsymbol{x}_0\wedge L\,\delta_2\boldsymbol{x}_0)=(L\boldsymbol{\eta}_0)\cdot\delta_1\boldsymbol{x}\wedge\delta_2\boldsymbol{x}\,. \tag{19}$$

It follows from (14) and (19) that there is an equation for $\boldsymbol{\eta}$ similar to that of Cauchy for the vorticity in hydrodynamics

$$|L|\boldsymbol{\eta}=L\boldsymbol{\eta}_0=\left(\boldsymbol{\eta}_0\cdot\frac{\partial}{\partial\boldsymbol{x}_0}\right)\boldsymbol{x}\,. \tag{20}$$

Since

$$|L|\,\delta_1\boldsymbol{x}_0\wedge\delta_2\boldsymbol{x}_0\cdot\delta_3\boldsymbol{x}_0=\delta_1\boldsymbol{x}\wedge\delta_2\boldsymbol{x}\cdot\delta_3\boldsymbol{x}=\frac{\varrho_0}{\varrho}\,\delta_1\boldsymbol{x}_0\wedge\delta_2\boldsymbol{x}_0\cdot\delta_3\boldsymbol{x}_0\,, \tag{21}$$

because of the conservation of the mass of a fluid element during the motion. Hence

$$\varrho\,|L|=\varrho_0\,. \tag{22}$$

It follows from (20) *and* (22) *that the vector* $\boldsymbol{\eta}/\varrho$ *changes during the motion in the same way as a* $\delta\boldsymbol{x}$

$$\frac{\boldsymbol{\eta}}{\varrho} \overset{\delta x}{=} L\frac{\boldsymbol{\eta}_0}{\varrho_0}. \tag{23}$$

Let $\delta\boldsymbol{x}_0$ be an element of a η-line at the time 0

$$\delta\boldsymbol{x}_0 = \alpha\frac{\boldsymbol{\eta}_0}{\varrho_0}, \qquad (\alpha = \text{number}). \tag{24}$$

It follows from (4) and (23) that the corresponding $\delta\boldsymbol{x}$ will also be an element of a η-line at the time t: $\delta\boldsymbol{x} = \alpha\boldsymbol{\eta}/\varrho$. Hence

The elements of the Madelung fluid lying on a η*-line at the time* 0 *will also lie on a* η*-line at any other instant of time.*

The η*-surfaces being formed by* η*-lines, the elements of the fluid lying on a* η*-surface at the time* 0 *will also lie on a* η*-surface at any other instant of time. This holds in particular for the* η*-tubes. Equation* (13) *expresses the invariance of the strength of a* η*-tube during the motion.*

The above reasoning shows that equations (23) and (13) are equivalent. Let $\boldsymbol{\gamma}$ be a vector such that $\int_S \boldsymbol{\gamma}\cdot\boldsymbol{n}\,\mathrm{d}S$ be an integral invariant

$$\int_S \boldsymbol{\gamma}\cdot\boldsymbol{n}\,\mathrm{d}S = \int_{S_0} \boldsymbol{\gamma}_0\cdot\boldsymbol{n}_0\,\mathrm{d}S_0; \tag{25}$$

we have

$$\frac{\boldsymbol{\gamma}}{\varrho} = L\frac{\boldsymbol{\gamma}_0}{\varrho_0}. \tag{26}$$

Therefore the Helmholtz theorems hold for any such vector $\boldsymbol{\gamma}$, except the theorem on the invariance of the strength of a tube, because the strength of a γ-tube has only a meaning when the flux of $\boldsymbol{\gamma}$ is the same through all the sections of the tube and this does not happen for any tube, unless $\operatorname{div}\boldsymbol{\gamma} = 0$.

It follows from (12) that

$$\frac{\mathrm{d}}{\mathrm{d}t}\int_C \boldsymbol{v}\cdot\delta\boldsymbol{x} = -\frac{e}{mc}\frac{\mathrm{d}}{\mathrm{d}t}\int_C \boldsymbol{A}\cdot\delta\boldsymbol{x} = -\frac{e}{mc}\frac{\mathrm{d}}{\mathrm{d}t}\int_S \boldsymbol{H}\cdot\boldsymbol{n}\,\mathrm{d}S. \tag{27}$$

The rate of variation of the circulation of the velocity is proportional to the rate of variation of the magnetic flux through the contour C.

It follows from (23) and the second equation (5) that

$$\frac{\mathrm{d}}{\mathrm{d}t}\left(\frac{\boldsymbol{\eta}}{\varrho}\right) = \frac{\partial \boldsymbol{v}}{\partial \boldsymbol{x}}\,\frac{\boldsymbol{\eta}}{\varrho} = \left(\frac{\boldsymbol{\eta}}{\varrho}\cdot\frac{\partial}{\partial \boldsymbol{x}}\right)\boldsymbol{v}\,. \tag{28}$$

This equation corresponds to that of Helmholtz in hydrodynamics. It is of the same form as the first equation (3). The Helmholtz equation shows that in any infinitesimal time interval $\boldsymbol{\eta}/\varrho$ varies as a $\delta\boldsymbol{x}$, it is the differential form of the Cauchy equation. The equation (23) follows immediately from (28) by taking into account the second equation (5). We shall now prove that the Helmholtz equation expresses the law of variation of the angular momentum of the elements of the fluid.

Let us consider an element of fluid Ω whose barycentric ellipsoid of inertia at the time t is a sphere. Denoting by G the center of gravity of the fluid element and by $\boldsymbol{r}$ the barycentric position vector of a generic point, the moment of the forces $\boldsymbol{F}$ acting on the element with respect to G is

$$\mathcal{M} = \int_{\Omega} \boldsymbol{r} \wedge \left\{ \boldsymbol{F}_G - \left(\frac{\partial \boldsymbol{F}}{\partial \boldsymbol{x}}\right)_G \boldsymbol{r} \right\} \varrho \,\mathrm{d}\boldsymbol{r} = \int_{\Omega} \boldsymbol{r} \wedge \left(\frac{\partial \boldsymbol{F}}{\partial \boldsymbol{x}}\right)_G \boldsymbol{r}\varrho \,\mathrm{d}\boldsymbol{r} = \tag{29}$$

$$= \sum_{k,l} \boldsymbol{i}_k \wedge \left(\frac{\partial \boldsymbol{F}}{\partial \boldsymbol{x}}\right)_G \boldsymbol{i}_l \int_{\Omega} r_k r_l \varrho \,\mathrm{d}\boldsymbol{r} = \frac{I}{3m} \sum_k \boldsymbol{i}_k \wedge \left(\frac{\partial \boldsymbol{F}}{\partial \boldsymbol{x}}\right)_G \boldsymbol{i}_k = \frac{I}{3m} (\mathrm{rot}\, \boldsymbol{F})_G \,.$$

(I = moment of inertia with respect to G)

the $\boldsymbol{i}_k$ being the unit vectors of the coordinate axes and the r_k the components of $\boldsymbol{r}$. The angular momentum of Ω with respect to G is

$$\boldsymbol{M} = m \int_{\Omega} \boldsymbol{r} \wedge \left\{ \boldsymbol{v}_G + \left(\frac{\partial \boldsymbol{v}}{\partial \boldsymbol{x}}\right)_G \boldsymbol{r} \right\} \varrho \,\mathrm{d}\boldsymbol{r} = m \int_{\Omega} \boldsymbol{r} \wedge \left(\frac{\partial \boldsymbol{v}}{\partial \boldsymbol{x}}\right)_G \boldsymbol{r}\varrho \,\mathrm{d}\boldsymbol{r}\,. \tag{30}$$

Since

$$\frac{\mathrm{d}\boldsymbol{r}}{\mathrm{d}t} = \boldsymbol{v} - \boldsymbol{v}_G = \left(\frac{\partial \boldsymbol{v}}{\partial \boldsymbol{x}}\right)_G \boldsymbol{r}\,, \tag{31}$$

we have

$$\frac{\mathrm{d}\boldsymbol{M}}{\mathrm{d}t} = m \int_{\Omega} \boldsymbol{r} \wedge \left(\frac{\mathrm{d}}{\mathrm{d}t}\,\frac{\partial \boldsymbol{v}}{\partial \boldsymbol{x}}\right)_G \boldsymbol{r}\varrho \,\mathrm{d}\boldsymbol{r} + m \int_{\Omega} \boldsymbol{r} \wedge \left(\frac{\partial \boldsymbol{v}}{\partial \boldsymbol{x}}\right)_G^2 \boldsymbol{r}\varrho \,\mathrm{d}\boldsymbol{r} = \tag{32}$$

$$= \frac{I}{3} \sum_k \boldsymbol{i}_k \wedge \left\{ \left(\frac{\mathrm{d}}{\mathrm{d}t}\,\frac{\partial \boldsymbol{v}}{\partial \boldsymbol{x}}\right)_G + \left(\frac{\partial \boldsymbol{v}}{\partial \boldsymbol{x}}\right)_G^2 \right\} \boldsymbol{i}_k = \frac{I}{3}\,\frac{\mathrm{d}}{\mathrm{d}t} \sum_k \boldsymbol{i}_k \wedge \left(\frac{\partial \boldsymbol{v}}{\partial \boldsymbol{x}}\right)_G \boldsymbol{i}_k + \frac{I}{3} \sum_k \boldsymbol{i}_k \wedge \left(\frac{\partial \boldsymbol{v}}{\partial \boldsymbol{x}}\right)_G^2 \boldsymbol{i}_k =$$

$$= \frac{I}{3}\left(\frac{\mathrm{d}\boldsymbol{\zeta}}{\mathrm{d}t} + \boldsymbol{\zeta}\,\mathrm{div}\,\boldsymbol{v} - \frac{\partial \boldsymbol{v}}{\partial \boldsymbol{x}}\,\boldsymbol{\zeta}\right)_G,$$

$$\boldsymbol{\zeta} = \mathrm{rot}\,\boldsymbol{v}\,. \tag{33}$$

By taking into account the equation of continuity, we get

$$\frac{\mathrm{d}\boldsymbol{M}}{\mathrm{d}t} = \frac{I\varrho_a}{3}\left\{\frac{\mathrm{d}}{\mathrm{d}t}\left(\frac{\boldsymbol{\zeta}}{\varrho}\right) - \frac{\partial \boldsymbol{v}}{\partial \boldsymbol{x}}\,\frac{\boldsymbol{\zeta}}{\varrho}\right\}_a . \tag{34}$$

Therefore the variation of the angular momentum of Ω is given by the equation

$$\frac{\mathrm{d}}{\mathrm{d}t}\left(\frac{\boldsymbol{\zeta}}{\varrho}\right) - \frac{\partial \boldsymbol{v}}{\partial \boldsymbol{x}}\,\frac{\boldsymbol{\zeta}}{\varrho} = \frac{1}{\varrho m}\,\mathrm{rot}\,\boldsymbol{F} . \tag{35}$$

It is easily seen that

$$\frac{1}{\varrho}\,\mathrm{rot}\,\boldsymbol{F} = \frac{e}{\varrho}\,\mathrm{rot}\left(\boldsymbol{E} + \frac{\boldsymbol{v}}{c}\wedge\boldsymbol{H}\right) = \frac{e}{c}\,\frac{\partial \boldsymbol{v}}{\partial \boldsymbol{x}}\,\frac{\boldsymbol{H}}{\varrho} - \frac{e}{c}\,\frac{\mathrm{d}}{\mathrm{d}t}\left(\frac{\boldsymbol{H}}{\varrho}\right) . \tag{36}$$

The Helmholtz equation (28) follows immediately from (35) and (36).

The way in which we derived equation (20) shows that it is equivalent to the circulation theorem (12). *The Cauchy equation and the circulation theorem for* $\boldsymbol{u}$ *are therefore equivalent.*

It follows from the identity (6) that for any closed curve C

$$\frac{\mathrm{d}}{\mathrm{d}t}\int_C m\boldsymbol{v}\cdot\delta\boldsymbol{x} = \int_C m\,\frac{\mathrm{d}\boldsymbol{v}}{\mathrm{d}t}\cdot\delta\boldsymbol{x} . \tag{37}$$

The identity (8) shows that

$$\frac{\mathrm{d}}{\mathrm{d}t}\int_C \frac{e}{c}\boldsymbol{A}\cdot\delta\boldsymbol{x} = -\int_C e\left(\boldsymbol{E} + \frac{\boldsymbol{v}}{c}\wedge\boldsymbol{H}\right)\cdot\delta\boldsymbol{x} . \tag{38}$$

From (37) and (38) we get the following identity

$$\frac{\mathrm{d}}{\mathrm{d}t}\int_C \boldsymbol{u}\cdot\delta\boldsymbol{x} = \int_C\left\{m\,\frac{\mathrm{d}\boldsymbol{v}}{\mathrm{d}t} - e\left(\boldsymbol{E} + \frac{\boldsymbol{v}}{c}\wedge\boldsymbol{H}\right)\right\}\cdot\delta\boldsymbol{x} . \tag{39}$$

The left hand side vanishes as a consequence of (12). Therefore the circulation theorem is equivalent to the equation

$$\mathrm{rot}\left\{m\,\frac{\mathrm{d}\boldsymbol{v}}{\mathrm{d}t} - e\left(\boldsymbol{E} + \frac{\boldsymbol{v}}{c}\wedge\boldsymbol{H}\right)\right\} = 0 . \tag{40}$$

3. – Introduction of the Clebsch Parameters.

It is well known from the theory of the Pfaff expressions that the differential form $\omega = \sum_{i=1}^{n} X_i(x)\,\delta x_i$ can be reduced to one of the canonical

forms

$$\omega = \sum_{r=1}^{s} y_r \, \delta z_r \,, \tag{1}$$

$$\omega = \sum_{r=1}^{s} y_r \, \delta z_r + \delta z_{s+1} \,; \tag{2}$$

$2s$ or $2s+1$ being the minimum number of independent variables in terms of which ω can be expressed, the y and z being independent functions of the x. This minimum number is called the class of ω. It is at most equal to the number n.

In the particular case of a differential form $\sum_{i=1}^{3} X_i \, \delta x_i$ in a three dimensional space, there are only three canonical forms: δz, $y \, \delta z$, $y \, \delta z + \delta z_1$. We are interested in the differential form $\boldsymbol{u} \cdot \delta \boldsymbol{x}$, the time t being considered as a parameter. When $\boldsymbol{u} \cdot \delta \boldsymbol{x}$ is of class 1, $\boldsymbol{u}$ is the gradient of a function S, i.e. the motion of the Madelung fluid is quasi-irrotational. $\boldsymbol{u} \cdot \delta \boldsymbol{x}$ is of class 2 when it admits an integrating factor, without being an exact differential. It is well known that the condition for the existence of an integrating factor is

$$\boldsymbol{u} \cdot \boldsymbol{\eta} = \boldsymbol{u} \cdot \operatorname{rot} \boldsymbol{u} = 0 \,, \tag{3}$$

$\boldsymbol{u} \cdot \delta \boldsymbol{x}$ is of class 3 when $\boldsymbol{u} \cdot \boldsymbol{\eta} \neq 0$.

When $\boldsymbol{u} \cdot \delta \boldsymbol{x}$ is reduced to the canonical form, we have

$$\boldsymbol{u} \cdot \delta \boldsymbol{x} = \delta S + \lambda \, \delta \mu \,, \qquad \boldsymbol{u} = \frac{\partial S}{\partial \boldsymbol{x}} + \lambda \frac{\partial \mu}{\partial \boldsymbol{x}} \,. \tag{4}$$

In the case of class 1 we can take $\lambda = \mu = 0$, more generally, λ as a function of t and μ. In the case of class 2, we can take $S = 0$, λ and μ being independent. More generally, we can take λ and μ independent and S as a function of t and μ. In the case of class 3, S, λ and μ are independent functions of x_1, x_2 and x_3. Thus we have proven the existence of the Clebsch parameters S, λ, μ by means of the theory of the reduction to the canonical forms.

The existence of the Clebsch parameters can be easily established by the consideration of the η-lines. Let us assume that the η-lines at the time t are defined by the equations

$$\lambda_1(t, \boldsymbol{x}) = \text{const.} \,, \qquad \mu(t, \boldsymbol{x}) = \text{const.} \tag{5}$$

The η-line passing through a point is orthogonal to the vectors $\partial \lambda_1 / \delta \boldsymbol{x}$ and $\partial \mu / \partial \boldsymbol{x}$, since it lies on the two surfaces $\lambda_1 = \text{constant}$ and $\mu = \text{constant}$ passing

through the point. Hence

$$\boldsymbol{\eta} = \gamma \frac{\partial \lambda_1}{\partial \boldsymbol{x}} \wedge \frac{\delta \mu}{\delta \boldsymbol{x}}, \tag{6}$$

γ being a function of t and $\boldsymbol{x}$. Since

$$\frac{\partial \gamma}{\partial \boldsymbol{x}} \cdot \frac{\partial \lambda_1}{\partial \boldsymbol{x}} \wedge \frac{\partial \mu}{\partial \boldsymbol{x}} = \operatorname{div} \boldsymbol{\eta} = 0, \tag{7}$$

γ, λ_1 and μ are not independent functions of $\boldsymbol{x}$

$$\gamma = F(t, \lambda_1, \mu). \tag{8}$$

Let us introduce the function $\lambda(t, \boldsymbol{x})$

$$\lambda = \int \gamma \, \mathrm{d}\lambda_1. \tag{9}$$

It is easily seen that

$$\boldsymbol{\eta} = \frac{\partial \lambda}{\partial \boldsymbol{x}} \wedge \frac{\partial \mu}{\partial \boldsymbol{x}}, \qquad \operatorname{rot} \boldsymbol{u} = \operatorname{rot}\left(\lambda \frac{\partial \mu}{\partial \boldsymbol{x}}\right). \tag{10}$$

It follows from (10) that there are functions S such that

$$\boldsymbol{u} - \lambda \frac{\partial \mu}{\partial \boldsymbol{x}} = \frac{\partial S}{\partial \boldsymbol{x}}. \tag{11}$$

We shall now prove that it is possible to choose the Clebsch parameters λ and μ as constants of the motion. It follows from the equation (10) of section 2 that

$$\delta S(t, \boldsymbol{x}) + \lambda(t, \boldsymbol{x}) \, \delta\mu(t, \boldsymbol{x}) = \delta S(0, \boldsymbol{x}_0) + \lambda(0, \boldsymbol{x}_0) \, \delta\mu(0, \boldsymbol{x}_0) + \delta\chi. \tag{12}$$

Since (12) is equivalent to the equations of motion for S, λ and μ, we can take

$$\lambda(t, \boldsymbol{x}) = \lambda(0, \boldsymbol{x}_0), \quad \mu(t, \boldsymbol{x}) = \mu(0, \boldsymbol{x}_0), \quad S(t, \boldsymbol{x}) = S(0, \boldsymbol{x}_0) + \chi, \tag{13}$$

in order to get the solution of the Euler equations that corresponds to the initial distribution of velocities given by the Clebsch parameters $S(0, \boldsymbol{x}_0)$, $\lambda(0, \boldsymbol{x}_0)$, $\mu(0, \boldsymbol{x}_0)$. Any motion can be obtained in this way, because any initial

distribution of the velocities can be obtained by a suitable choice of the initial values of S, λ and μ.

It follows from the third equation (13) and the equation (11) of section 2 that

$$\frac{\partial S}{\partial t} + \boldsymbol{v}\cdot\left(\frac{\partial S}{\partial \boldsymbol{x}} - \boldsymbol{u}\right) + \frac{1}{2m}\left(\frac{\partial S}{\partial \boldsymbol{x}} - \frac{e}{c}\boldsymbol{A} + \lambda\frac{\partial \mu}{\partial \boldsymbol{x}}\right)^2 + eA_0 - \frac{\hbar^2}{2m}\frac{\Delta R}{R} = 0\,. \tag{14}$$

Since

$$\frac{\partial \lambda}{\partial t} + \boldsymbol{v}\cdot\frac{\partial \lambda}{\partial \boldsymbol{x}} = 0\,, \qquad \frac{\partial \mu}{\partial t} + \boldsymbol{v}\cdot\frac{\partial \mu}{\partial \boldsymbol{x}} = 0\,, \tag{15}$$

as a consequence of the two first equations (13), we have

$$\frac{\partial S}{\partial t} + \lambda\frac{\partial \mu}{\partial t} + \frac{1}{2m}\left(\frac{\partial S}{\partial \boldsymbol{x}} - \frac{e}{c}\boldsymbol{A} + \lambda\frac{\partial \mu}{\partial \boldsymbol{x}}\right)^2 + eA_0 - \frac{\hbar^2}{2m}\frac{\Delta R}{R} = 0\,. \tag{16}$$

Equations (15) and (16) associated to the continuity equation

$$\frac{\partial R^2}{\partial t} + \operatorname{div}\left\{\frac{R^2}{m}\left(\frac{\partial S}{\partial \boldsymbol{x}} - \frac{e}{c}\boldsymbol{A} + \lambda\frac{\partial \mu}{\partial \boldsymbol{x}}\right)\right\} = 0\,, \tag{17}$$

describe completely the motions of the Madelung fluid.

In order to get the most general choice of the Clebsch parameters let us take the substantial derivatives of both sides of (12)

$$\frac{\mathrm{d}}{\mathrm{d}t}(\delta S + \lambda\,\delta\mu) = -\delta\left(\frac{m\boldsymbol{v}^2}{2} + eA_0 - \boldsymbol{u}\cdot\boldsymbol{v} - \frac{\hbar^2}{2m}\frac{\Delta R}{R}\right); \tag{18}$$

δ corresponds to the passage from a fluid element to a neighbouring one, therefore δ and $\mathrm{d}/\mathrm{d}t$ do commute. Equation (18) can be written as follows

$$\delta\left(\frac{\partial S}{\partial t} + \lambda\frac{\partial \mu}{\partial t} + \frac{m\boldsymbol{v}^2}{2} + eA_0 - \frac{\hbar^2}{2m}\frac{\Delta R}{R}\right) = \delta\lambda\frac{\mathrm{d}\mu}{\mathrm{d}t} - \delta\mu\frac{\mathrm{d}\lambda}{\mathrm{d}t}\,. \tag{19}$$

since

$$\frac{\mathrm{d}S}{\mathrm{d}t} - \boldsymbol{u}\cdot\boldsymbol{v} = \frac{\partial S}{\partial t} + \lambda\frac{\partial \mu}{\partial t} - \lambda\frac{\mathrm{d}\mu}{\mathrm{d}t}\,. \tag{20}$$

The form of the right-hand side of (19) shows that the left-hand side is the

δ differential of a function of t, λ and μ, so that

$$\frac{\partial S}{\partial t} + \lambda \frac{\partial \mu}{\partial t} + \frac{m\boldsymbol{v}^2}{2} + eA_0 - \frac{\hbar^2}{2m}\frac{\Delta R}{R} = K(t, \lambda, \mu)\,. \tag{21}$$

Furthermore we have the analogue of the Stuart equations [9]

$$\frac{\mathrm{d}\mu}{\mathrm{d}t} = \frac{\partial K}{\partial \lambda}\,, \qquad \frac{\mathrm{d}\lambda}{\mathrm{d}t} = -\frac{\partial K}{\partial \mu}\,. \tag{22}$$

Equation (19) is satisfied with any choice of the function K. The conditions (15) correspond to the choice $K = 0$.

The above results can be obtained in a more interesting form by using the basic equation (12). Let us introduce the notations

$$\lambda_0(\boldsymbol{x}_0) = \lambda(0, \boldsymbol{x}_0), \qquad \mu_0(\boldsymbol{x}_0) = \mu(0, \boldsymbol{x}_0), \qquad S_0(\boldsymbol{x}_0) = S(0, \boldsymbol{x}_0)\,. \tag{23}$$

It follows from (12) that

$$\delta(S - S_0 - \chi - \lambda_0\mu_0) = -\lambda\,\delta\mu - \mu_0\,\delta\lambda_0\,; \tag{24}$$

$S - S_0 - \chi - \lambda_0\mu_0$ is therefore a function of t, μ and λ_0

$$S - S_0 - \chi - \lambda_0\mu_0 = \Lambda(t, \mu, \lambda_0) \tag{25}$$

and we have

$$\lambda\,\delta\mu + \mu_0\,\delta\lambda_0 = -\delta\Lambda\,. \tag{26}$$

Hence

$$\lambda = -\frac{\partial \Lambda}{\partial \mu}\,, \qquad \mu_0 = -\frac{\partial \Lambda}{\partial \lambda_0}\,. \tag{27}$$

Equation (26) shows that λ, μ are related to λ_0, μ_0 by a contact transformation whose generating function is $-\Lambda$. Λ can be taken arbitrarily, as long as it defines a contact transformation. By taking $\Lambda = -\mu\lambda_0$ we get the equations (13). Equations (27) give the finite contact transformation corresponding to the solution of the Stuart equations (22). By taking the substantial time derivatives of both sides of equation (25) we get an equation

[9] T. STUART: *Dublin Dissertation* (1900).

equivalent to (21)

$$\frac{\partial S}{\partial t} + \lambda \frac{\partial \mu}{\partial t} + \frac{m\boldsymbol{v}^2}{2} + eA_0 - \frac{\hbar^2}{2m}\frac{\Delta R}{R} = \frac{\partial \Lambda}{\partial t}\,. \tag{28}$$

We get from (28) and (21) the following Hamilton-Jacobi equation

$$K\left(t, -\frac{\partial \Lambda}{\partial \mu}, \mu\right) - \frac{\partial \Lambda}{\partial t} = 0\,. \tag{29}$$

Let $\int \boldsymbol{w}\cdot\delta\boldsymbol{x}$ be any relative integral-invariant of order 1. We have

$$\boldsymbol{w}\cdot\delta\boldsymbol{x} - \boldsymbol{w}_0\cdot\delta\boldsymbol{x}_0 = \delta\Theta\,. \tag{30}$$

$\Theta(t, \boldsymbol{x}_0)$ being some function. By introducing Clebsch parameters for the vector field $\boldsymbol{w}$

$$\boldsymbol{w} = \frac{\partial T}{\partial \boldsymbol{x}} + \nu\frac{\partial \sigma}{\partial \boldsymbol{x}}\,, \tag{31}$$

we get

$$\delta T + \nu\,\delta\sigma = \delta T_0 + \nu_0\,\delta\sigma_0 + \delta\Theta\,, \tag{32}$$

$$\frac{\mathrm{d}}{\mathrm{d}t}(\delta T - \delta\Theta + \nu\,\delta\sigma) = 0. \tag{33}$$

Hence

$$\delta\left(\frac{\mathrm{d}T}{\mathrm{d}t} - \frac{\mathrm{d}\Theta}{\mathrm{d}t} + \nu\frac{\mathrm{d}\sigma}{\mathrm{d}t}\right) = \frac{\mathrm{d}\sigma}{\mathrm{d}t}\,\delta\nu - \frac{\mathrm{d}\nu}{\mathrm{d}t}\,\delta\sigma, \tag{34}$$

and we must have

$$\frac{\mathrm{d}\sigma}{\mathrm{d}t} = \frac{\partial G}{\partial \nu}\,, \qquad \frac{\mathrm{d}\nu}{\mathrm{d}t} = -\frac{\partial G}{\partial \sigma}\,, \qquad (G = G(t, \nu, \sigma))\,, \tag{35}$$

with

$$G = \frac{\mathrm{d}}{\mathrm{d}t}(T - \Theta) + \nu\frac{\mathrm{d}\sigma}{\mathrm{d}t}\,. \tag{36}$$

The function G can be taken arbitrarily, since with any choice of G the

equation (34) is satisfied. Different choices of G correspond to different choices of the Clebsch parameters T, ν, σ. The choice $G = 0$ leads to ν and σ that are constants of the motion.

The above reasoning shows that the circulation theorem for $\boldsymbol{w}$ leads to equations of the Stuart type for ν and σ. We shall now prove that the circulation theorem follows from the equations (35). Indeed, we have

$$\frac{\mathrm{d}}{\mathrm{d}t}(\delta_1\nu\,\delta_2\sigma - \delta_2\nu\,\delta_1\sigma) = \delta_2\left(\frac{\partial G}{\partial \nu}\,\delta_1\nu + \frac{\partial G}{\partial \sigma}\,\delta_1\sigma\right) - \delta_1\left(\frac{\partial G}{\partial \nu}\,\delta_2\nu + \frac{\partial G}{\partial \sigma}\,\delta_2\sigma\right) = \tag{37}$$

$$= \delta_2(\delta_1 G) - \delta_1(\delta_2 G) = 0\,.$$

Since

$$\delta_1\nu\,\delta_2\sigma - \delta_2\nu\,\delta_1\sigma = \left(\frac{\partial \nu}{\partial \boldsymbol{x}}\cdot\delta_1\boldsymbol{x}\right)\left(\frac{\partial \sigma}{\partial \boldsymbol{x}}\cdot\delta_2\boldsymbol{x}\right) - \left(\frac{\partial \nu}{\partial \boldsymbol{x}}\cdot\delta_2\boldsymbol{x}\right)\left(\frac{\partial \sigma}{\partial \boldsymbol{x}}\cdot\delta_1\boldsymbol{x}\right) = \tag{38}$$

$$= \left(\frac{\partial \nu}{\partial \boldsymbol{x}}\wedge\frac{\partial \sigma}{\partial \boldsymbol{x}}\right)\cdot(\delta_1\boldsymbol{x}\wedge\delta_2\boldsymbol{x}) = \operatorname{rot}\boldsymbol{w}\cdot\delta_1\boldsymbol{x}\wedge\delta_2\boldsymbol{x}\,,$$

equation (37) shows that

$$\operatorname{rot}\boldsymbol{w}\cdot\delta_1\boldsymbol{x}\wedge\delta_2\boldsymbol{x} = \operatorname{rot}_{x_0}\boldsymbol{w}_0\cdot\delta_1\boldsymbol{x}_0\wedge\delta_2\boldsymbol{x}_0\,. \tag{39}$$

Hence

$$\int_S \operatorname{rot}\boldsymbol{w}\cdot\boldsymbol{n}\,\mathrm{d}S = \int_{S_0}\operatorname{rot}_{x_0}\boldsymbol{w}_0\cdot\boldsymbol{n}_0\,\mathrm{d}S_0\,, \tag{40}$$

S denoting an open surface limited by a contour C. Equation (40) can be transformed into the circulation theorem for $\boldsymbol{w}$

$$\int_C \boldsymbol{w}\cdot\delta\boldsymbol{x} = \int_{C_0}\boldsymbol{w}_0\cdot\delta\boldsymbol{x}_0\,.$$

The circulation theorem for $\boldsymbol{w}$ is equivalent to the proposition that the Clebsch parameters ν, σ satisfy equations of the Stuart type.

Let us consider the differential form Ω_d

$$\Omega_d = \boldsymbol{u}\cdot\mathrm{d}\boldsymbol{x} - \left(\frac{m\boldsymbol{v}^2}{2} + eA_0 - \frac{\hbar^2}{2m}\,\frac{\Delta R}{R}\right)\mathrm{d}t\,. \tag{42}$$

It follows from (16) that

$$\Omega_d = \mathrm{d}S + \lambda\,\mathrm{d}\mu\,. \tag{43}$$

The class of Ω_d is less than 4, since it can be expressed in terms of the three functions S, λ, μ. Conversely, to assume that the class of Ω_d is less than 4 is equivalent to assume the existence of three functions S, λ, μ satisfying (43), so that they are Clebsch parameters for $\boldsymbol{u}$ satisfying (16). Hence

The Euler equations imply that Ω_d is of class less than 4 and also that it is possible to choose λ and μ as constants of the motion. Conversely, to assume that the class of Ω_d is less than 4 and that it is possible to write $\Omega_d = \mathrm{d}S + \lambda\,\mathrm{d}\mu$ with λ, μ being constants of the motion leads to the Euler equations.

The quasi-irrotational motions are determined by the condition that the class of Ω_d is 1, i.e. that Ω_d is an exact differential. Indeed, Ω_d being an exact differential, there are functions S such that for any $\mathrm{d}\boldsymbol{x}$ and $\mathrm{d}t$

$$\boldsymbol{u}\cdot\mathrm{d}\boldsymbol{x} - \left(\frac{m\boldsymbol{v}^2}{2} + eA_0 - \frac{\hbar^2}{2m}\,\frac{\Delta R}{R}\right)\mathrm{d}t = \mathrm{d}S\,. \tag{44}$$

Hence

$$\boldsymbol{u} = \frac{\partial S}{\partial \boldsymbol{x}}\,, \qquad \frac{\partial S}{\partial t} + \frac{1}{2m}\left(\frac{\partial S}{\partial \boldsymbol{x}} - \frac{e}{c}\,\boldsymbol{A}\right)^2 + eA_0 - \frac{\hbar^2}{2m}\,\frac{\Delta R}{R} = 0\,. \tag{45}$$

By taking the gradients of both sides of the second equation (45) we get the Euler equation for quasi-irrotational motions

$$\frac{\partial \boldsymbol{u}}{\partial t} = -\frac{\partial}{\partial \boldsymbol{x}}\left(\frac{m\boldsymbol{v}^2}{2} + eA_0 - \frac{\hbar^2}{2m}\,\frac{\Delta R}{R}\right). \tag{46}$$

4. – Transformations of the Clebsch Parameters.

We shall now discuss the different possible choices of the Clebsch parameters for the same state of motion of the fluid. Since

$$\boldsymbol{\eta} = \frac{\partial \lambda}{\partial \boldsymbol{x}} \wedge \frac{\partial \mu}{\partial \boldsymbol{x}}\,, \tag{1}$$

λ and μ are both solutions of the partial differential equation

$$\boldsymbol{\eta}\cdot\frac{\partial f}{\partial \boldsymbol{x}} = 0\,, \tag{2}$$

which has only two independent solutions. Therefore the parameters λ' and μ' of another set must be functions of t, λ and μ

$$\lambda' = f_1(t, \lambda, \mu)\,, \qquad \mu' = f_2(t, \lambda, \mu)\,, \tag{3}$$

provided λ and μ be independent functions of $\boldsymbol{x}$, as we shall assume.

Since

$$\frac{\partial \lambda'}{\partial \boldsymbol{x}} \wedge \frac{\partial \mu'}{\partial \boldsymbol{x}} = \frac{D(f_1, f_2)}{D(\lambda, \mu)} \frac{\partial \lambda}{\partial \boldsymbol{x}} \wedge \frac{\partial \mu}{\partial \boldsymbol{x}}, \tag{4}$$

we have the necessary condition

$$\frac{D(f_1, f_2)}{D(\lambda, \mu)} = 1 . \tag{5}$$

Let us regard μ as a « coordinate » q and λ as its « conjugate momentum ». Equation (5) shows that the Poisson bracket of μ' and λ' is 1

$$\frac{\partial \mu'}{\partial \mu} \frac{\partial \lambda'}{\partial \lambda} - \frac{\partial \mu'}{\partial \lambda} \frac{\partial \lambda'}{\partial \mu} = 1 . \tag{6}$$

It is well known that (6) is a necessary and sufficient condition for the existence of a function $\Gamma(t, \mu, \mu')$ such that

$$\lambda \, \delta\mu - \lambda' \, \delta\mu' = \delta\Gamma \tag{7}$$

or

$$\lambda \frac{\partial \mu}{\partial \boldsymbol{x}} - \lambda' \frac{\partial \mu'}{\partial \boldsymbol{x}} = \frac{\partial \Gamma}{\partial \boldsymbol{x}} . \tag{8}$$

It follows from (8) that equation (5) is also a sufficient condition for λ' and μ' to be Clebsch parameters, because

$$\boldsymbol{u} = \frac{\partial}{\partial \boldsymbol{x}} (S + \Gamma) + \lambda' \frac{\partial \mu'}{\partial \boldsymbol{x}} . \tag{9}$$

Hence

$$S' = S + \Gamma + \text{arbitrary function of } t = S + \Gamma + F(t) . \tag{10}$$

The function Γ may be taken arbitrarily, provided the equations

$$\lambda = \frac{\partial \Gamma}{\partial \mu} , \qquad \lambda' = -\frac{\partial \Gamma}{\partial \mu'} , \tag{11}$$

do define λ', μ' in terms of t, λ and μ.

In order that λ' and μ' be constants of the motion

$$\frac{\mathrm{d}\lambda'}{\mathrm{d}t} = 0\,, \qquad \frac{\mathrm{d}\mu'}{\mathrm{d}t} = 0\,, \tag{12}$$

we must have

$$\frac{\partial f_1}{\partial t} + \frac{\partial f_1}{\partial \lambda}\,\frac{\mathrm{d}\lambda}{\mathrm{d}t} + \frac{\partial f_1}{\partial \mu}\,\frac{\mathrm{d}\mu}{\mathrm{d}t} = 0\,, \qquad \frac{\partial f_2}{\partial t} + \frac{\partial f_2}{\partial \lambda}\,\frac{\mathrm{d}\lambda}{\mathrm{d}t} + \frac{\partial f_2}{\partial \mu}\,\frac{\mathrm{d}\mu}{\mathrm{d}t} = 0\,. \tag{13}$$

When λ and μ are constants of the motion, these equations become

$$\frac{\partial f_1}{\partial t} = 0\,, \qquad \frac{\partial f_2}{\partial t} = 0\,, \tag{14}$$

so that

$$\lambda' = f_1(\lambda, \mu)\,, \qquad \mu' = f_2(\lambda, \mu)\,. \tag{15}$$

Therefore, in this case, we can get the transformations of the Clebsch parameters by means of functions $\Gamma(\mu, \mu')$ not involving t.

It follows from (11) that

$$\lambda\,\frac{\partial \mu}{\partial t} - \lambda'\,\frac{\partial \mu'}{\partial t} = \frac{\partial \Gamma}{\partial \mu}\,\frac{\partial \mu}{\partial t} + \frac{\partial \Gamma}{\partial \mu'}\,\frac{\partial \mu'}{\partial t}\,. \tag{16}$$

Denoting by $(\partial\Gamma/\partial t)_{\mathrm{tot}}$ the total derivative of Γ with respect to t, equation (16) can be written as follows

$$\lambda\,\frac{\partial \mu}{\partial t} - \lambda'\,\frac{\partial \mu'}{\partial t'} = \left(\frac{\partial \Gamma}{\partial t}\right)_{\mathrm{tot}} - \frac{\partial \Gamma}{\partial t}\,. \tag{17}$$

When λ, μ and λ', μ' are constants of the motion, Γ can be taken as a function of μ and μ' only, so that

$$\lambda\,\frac{\partial \mu}{\partial t} - \lambda'\,\frac{\partial \mu'}{\partial t'} = \left(\frac{\partial \Gamma}{\partial t}\right)_{\mathrm{tot}}\,. \tag{18}$$

It follows from (8) and (18) that:

A transformation of the Clebsch parameters λ, μ, which are constants of the motion, into another set λ', μ' with the same property corresponds to a gauge transformation of the second kind of the quantities $-\lambda\,\partial\mu/\partial \boldsymbol{x}$, $(\lambda/c)\,\partial\mu/\partial t$.

By choosing Γ as a function of μ and μ' only and taking $F(t) = 0$ in equation (10), *the system of equations* (15)-(16)-(17) *of section* **3** *becomes invariant for the transformation of the Clebsch parameters* $(S, \lambda, \mu) \to (S', \lambda', \mu')$.

We shall now discuss the behaviour of the equations (15-(16)-(17) of section **3** for a change of gauge of the electromagnetic potentials

$$\boldsymbol{A}' = \boldsymbol{A} + \frac{\partial \varphi}{\partial \boldsymbol{x}}, \qquad A_0' = A_0 - \frac{1}{c}\frac{\partial \varphi}{\partial t}. \tag{19}$$

The velocity $\boldsymbol{v}$ must be invariant. Hence $\boldsymbol{u}$ is transformed as follows

$$\boldsymbol{u}' = \boldsymbol{u} + \frac{e}{c}\frac{\partial \varphi}{\partial \boldsymbol{x}}, \tag{20}$$

and the gauge transformation induces a transformation of the Clebsch parameters

$$\delta S' + \lambda' \delta \mu' = \delta S + \lambda \delta \mu + \frac{e}{c}\delta \varphi. \tag{21}$$

The general solution of (21) can be obtained in the same way, as that of equation (12) of section **3**

$$\lambda = \frac{\partial \Gamma}{\partial \mu}, \qquad \lambda' = -\frac{\partial \Gamma}{\partial \mu'}, \qquad S' = S + \Gamma + \frac{e}{c}\varphi + F(t), \tag{22}$$

in terms of an arbitrary function $\Gamma(t, \mu, \mu')$ and of another arbitrary function $F(t)$. By taking $F(t) = 0$ and a Γ depending only on μ and μ', the equations (15)-(16)-(17) of section **3** remain invariant. We can take simply

$$S' = S + \frac{e}{c}\varphi, \qquad \lambda' = \lambda, \qquad \mu' = \mu, \tag{23}$$

in order to get a gauge transformation of the first kind of the wave function Ψ

$$\Psi = R \exp\left[\frac{i}{\hbar} S\right], \tag{24}$$

$$\Psi' = \Psi \exp\left[\frac{ie}{\hbar c}\varphi\right]. \tag{25}$$

5. – Quasi-Irrotational and η-Regions of the Madelung Fluid.

At any instant of time the fluid is formed by a quasi-irrotational part and a part in which $\eta \neq 0$. We shall denote by Ω_t the region of space where the motion is quasi-irrotational and its boundary surface by Σ_t. The region where $\eta \neq 0$ will be denoted by $\overline{\Omega}_t$.

Σ_t is in general a surface of discontinuity for the partial derivatives of the components of the velocity $\boldsymbol{v}$. This surface of discontinuity has special properties of propagation, because it is always formed by the same elements of the fluid. Thus its velocity of propagation at any point coincides with the component of the velocity of the fluid at the point in the direction of the normal to Σ_t.

Within Ω_t the Clebsch parameters λ and μ can be taken null and the first formula (5) of section **1** is still valid; the equations (16) and (17) of section **3** go over into the equations (2) and (3) of section **1**. Hence

By taking $\lambda = \mu = 0$ in Ω_t, the Schrödinger equation still holds, the wave function being $\Psi = R \exp[(i/\hbar)S]$.

There is an important circumstance to be taken into account: *the function S will in general not be single-valued in Ω_t, when Ω_t is not a simply-connected region.* This corresponds to the well known fact that the potential of velocities of an ordinary fluid moving irrotationally in a multiply-connected region is cyclic. Let $n+1$ be the order of connectivity of Ω_t. The circulation of $\boldsymbol{u}$ along any closed path C within Ω_t is a linear combination of the cyclic constants $K_1, K_2, \ldots, K_n$

$$\oint_C \boldsymbol{u} \cdot \delta \boldsymbol{x} = \sum_{l=1}^{n} p_l K_l \,, \tag{1}$$

the coefficients p being integers. The cyclic constants K, as well as n, are invariants of the motion.

In order that Ψ be single valued in the case of a multiply-connected region Ω_t, it is necessary and sufficient that the cyclic constants K_l be integral multiples of $2\pi\hbar = h$

$$K_l = m_l h \,, \qquad m_l = \text{integer} \,, \tag{2}$$

since by starting at a point of Ω_t and describing a closed path in Ω_t, the value of S will be increased by $\sum_l p_l K_l$. The equations (2) are restrictions on the initial conditions. Let us consider the case in which the multiple connection of Ω_t is due to the existence of n η-rings. The ciclic constants K_l are simply

the values of the strengthes of the rings. Therefore the condition (2) lead to the quantization of the strengthes of the η-rings:

In order that Ψ be single-valued in Ω_t, it is necessary that the strengthes of the existing η-rings be integral multiples of h.

It is not necessary to take λ and μ null in Ω_t. In order that $\boldsymbol{\eta}$ be zero it is sufficient that $\partial\lambda/\partial\boldsymbol{x} \wedge \partial\mu/\partial\boldsymbol{x}$ be 0, i.e. that λ be a function of t and μ

$$\lambda = f(t, \mu) . \tag{3}$$

When λ and μ are chosen as constants of the motion, the condition (3) requires that λ be a function of μ alone

$$\lambda = f(\mu) , \tag{3a}$$

so that

$$\lambda \frac{\partial \mu}{\partial \boldsymbol{x}} = \frac{\partial}{\partial \boldsymbol{x}} \int \lambda \, \mathrm{d}\mu , \qquad \lambda \frac{\partial \mu}{\partial t} = \frac{\partial}{\partial t} \int \lambda \, \mathrm{d}\mu . \tag{4}$$

By taking

$$S' = S + \int \lambda \, \mathrm{d}\mu = S + \int f(\mu) \, \mathrm{d}\mu , \tag{5}$$

and μ as any constant of the motion

$$\frac{\partial \mu}{\partial t} + \boldsymbol{v} \cdot \frac{\partial \mu}{\partial \boldsymbol{x}} = 0 , \tag{6}$$

the equations (15) of section **3** will be satisfied and (16)-(17) take the form of equations (2) and (3) of section **1**. Thus we get again the Schrödinger equation for $\Psi' = R \exp[(i/\hbar)S']$.

6. – Generalization of the Schrödinger Equation for the General Motions of the Fluid.

The Euler equations and the continuity equation are valid for any motion of the Madelung fluid and, by replacing the Schrödinger equation by them, we obtain a generalization of the Schrödinger theory. This remark was made independently by TAKABAYASHI [2] and by us [3]. TAKABAYASHI introduced the Clebsch parameters and the equations (15), (16) and (17) of section **3**. We

have obtained the same equations starting from a generalized form of the classical Hamilton-Jacobi equation ([4]). Those equations are not a good analogue of the Schrödinger equation, because they separate the amplitude and the phase of the wave function. It is precisely interesting to see that the Schrödinger equation can be generalized by the introduction of an extra scalar potential and an extra vector potential, without losing the usual form

$$i\hbar \frac{\partial \Psi}{\partial t} = \frac{1}{2m}\left(\frac{\hbar}{i}\frac{\partial}{\partial \boldsymbol{x}} - \frac{e}{c}\boldsymbol{A} + \lambda \frac{\partial \mu}{\partial \boldsymbol{x}}\right)^2 \Psi + \left(eA_0 + \lambda \frac{\partial \mu}{\partial t}\right)\Psi . \tag{1}$$

This equation was given by us in reference ([4]). It is equivalent to the set (16)-(17) of section **3**, with

$$\Psi = R \exp\left[\frac{i}{\hbar} S\right] . \tag{2}$$

It is obvious that (1) leads to a continuity equation, no matter how λ and μ be taken

$$\frac{\partial \varrho}{\partial t} + \operatorname{div} \boldsymbol{j} = 0 , \qquad \varrho = \Psi^* \Psi , \qquad \boldsymbol{j} = \varrho \boldsymbol{v} , \tag{3}$$

$$\boldsymbol{j} = \frac{1}{2m}\left\{\Psi^*\left(\frac{\hbar}{i}\frac{\partial}{\partial \boldsymbol{x}} - \frac{e}{c}\boldsymbol{A} + \lambda \frac{\partial \mu}{\partial \boldsymbol{x}}\right)\Psi - \Psi\left(\frac{\hbar}{i}\frac{\partial}{\partial \boldsymbol{x}} + \frac{e}{c}\boldsymbol{A} - \lambda \frac{\partial \mu}{\partial \boldsymbol{x}}\right)\Psi^*\right\} . \tag{4}$$

It follows from (3) and (4) that

$$m\boldsymbol{v} + \frac{e}{c}\boldsymbol{A} = \frac{\partial S}{\partial \boldsymbol{x}} + \lambda \frac{\partial \mu}{\partial \boldsymbol{x}} . \tag{5}$$

It is remarkable that the equations (15) of section **3** can be obtained together with (1) from the ordinary Schrödinger variational principle

$$\delta \int \Psi^*\left\{i\hbar \frac{\partial \Psi}{\partial t} - \frac{1}{2m}\left(\frac{\hbar}{i}\frac{\partial}{\partial \boldsymbol{x}} - \frac{e}{c}\boldsymbol{A} + \lambda \frac{\partial \mu}{\partial \boldsymbol{x}}\right)^2 \Psi - \left(eA_0 + \lambda \frac{\partial \mu}{\partial t}\right)\Psi\right\} \mathrm{d}t\, \mathrm{d}\boldsymbol{x} = 0 , \tag{6}$$

by giving arbitrary variations to the wave function Ψ and the functions λ and μ, as we showed in reference ([4]). Equation (1) follows from the variation of Ψ^* and the equations (15) of section **3** from the variation of λ and μ.

We have seen in section **4** that the most general change of the Clebsch parameters S, λ, μ, such that the new parameters λ' and μ' be constants of the motion, corresponds to a gauge transformation of the second kind of $-\lambda\, \partial\mu/\partial \boldsymbol{x}$ and $\lambda\, \partial\mu/\partial t$

$$\left\{\begin{aligned} \lambda' \frac{\partial \mu'}{\partial \boldsymbol{x}} &= \lambda \frac{\partial \mu}{\partial \boldsymbol{x}} - \frac{\partial \Gamma}{\partial \boldsymbol{x}} , \\ \lambda' \frac{\partial \mu'}{\partial t} &= \lambda \frac{\partial \mu}{\partial t} - \frac{\partial \Gamma}{\partial t} , \end{aligned}\right. \tag{7}$$

Γ being an arbitrary real function $\Gamma(\lambda, \mu)$ of λ and μ not involving explicitly the time t, provided λ and μ be independent functions of $\boldsymbol{x}$. $\partial\Gamma/\partial t$ denotes now the $(\partial\Gamma/\partial t)_{\text{tot}}$ of section **4**. To the transformation of the λ and μ we can associate the following transformation of S

$$S' = S + \Gamma , \tag{8}$$

which leads to a gauge transformation of the first kind of Ψ

$$\Psi' = \Psi \exp\left[\frac{i}{\hbar}\Gamma\right]. \tag{9}$$

The invariance of the generalized Schrödinger equation for the transformation (7)-(9) follows immediately from the variational principle (6), since for any real function Γ we have

$$\begin{cases} \Psi'^*\left\{i\hbar\dfrac{\partial}{\partial t} - \left(eA_0 + \lambda'\dfrac{\partial\mu'}{\partial t}\right)\right\}\Psi' = \Psi^*\left\{i\hbar\dfrac{\partial}{\partial t} - \left(eA_0 + \lambda\dfrac{\partial\mu}{\partial t}\right)\right\}\Psi , \\ \Psi'^*\left(\dfrac{\hbar}{i}\dfrac{\partial}{\partial \boldsymbol{x}} - \dfrac{e}{c}\boldsymbol{A} + \lambda'\dfrac{\partial\mu'}{\partial \boldsymbol{x}}\right)^2\Psi' = \Psi^*\left(\dfrac{\hbar}{i}\dfrac{\partial}{\partial \boldsymbol{x}} - \dfrac{e}{c}\boldsymbol{A} + \lambda\dfrac{\partial\mu}{\partial \boldsymbol{x}}\right)^2\Psi . \end{cases} \tag{10}$$

Therefore it is not necessary to impose on Γ the condition of being a function of λ and μ only. When λ and μ are independent, it follows from (7) that Γ must be a function of λ and μ. Indeed, the equations (7) are equivalent to the following equation

$$\lambda'\,\mathrm{d}\mu' = \lambda\,\mathrm{d}\mu - \mathrm{d}\Gamma . \tag{11}$$

The class of the Pfaff expression $\lambda'\,\mathrm{d}\mu'$ is at most 2, so that the class of $\lambda\,\mathrm{d}\mu - \mathrm{d}\Gamma$ cannot be larger than 2. When λ and μ are independent the class of $\lambda\,\mathrm{d}\mu - \mathrm{d}\Gamma$ is 3, unless Γ is a function of λ and μ.

When λ and μ are not independent, the generalized Schrödinger equation goes over into the ordinary Schrödinger equation. Indeed, by taking

$$\mathrm{d}\Gamma = \lambda\,\mathrm{d}\mu , \tag{12}$$

we get

$$\lambda'\frac{\partial\mu'}{\partial \boldsymbol{x}} = 0 , \qquad \lambda'\frac{\partial\mu'}{\partial t} = 0 , \tag{13}$$

and Ψ' satisfies the ordinary Schrödinger equation.

Let us consider now the transformation

$$\Psi' = C\Psi\,, \qquad \Psi'^{*} = C^{*}\Psi'\,, \tag{14}$$

C being an arbitrary real or complex constant. Since

$$R^2\boldsymbol{v} = \frac{1}{2m}\left\{\Psi^{*}\left(\frac{\hbar}{i}\,\frac{\partial}{\partial \boldsymbol{x}} - \frac{e}{c}\boldsymbol{A} + \lambda\frac{\partial\mu}{\partial\boldsymbol{x}}\right)\Psi - \Psi\left(\frac{\hbar}{i}\,\frac{\partial}{\partial\boldsymbol{x}} + \frac{e}{c}\boldsymbol{A} - \lambda\frac{\partial\mu}{\partial\boldsymbol{x}}\right)\Psi^{*}\right\}, \tag{15}$$

the velocity $\boldsymbol{v}$ is not changed by the transformation (14), λ and μ being kept unchanged. *Thus from any solution Ψ, λ, μ of the generalized Schrödinger equation we can derive other solutions $C\Psi^{*}$, λ, μ corresponding to the same distribution of velocities $\boldsymbol{v}(t, \boldsymbol{x})$, the density being everywhere multiplied by the constant factor $|C|^2$.*

The gauge-invariance of the generalized Schrödinger equation can be easily checked. The gauge transformation (19) of section 4 corresponds to the transformation of the wave function

$$\Psi' = \Psi \exp\left[\frac{ie}{\hbar c}\varphi\right], \qquad \lambda' = \lambda\,, \qquad \mu' = \mu\,, \tag{16}$$

which can also be combined with a transformation of the parameters S, λ and μ of the type (7).

Since the generalized Schrödinger equation has the same form as an ordinary Schrödinger equation for a particle moving in the electromagnetic field described by the potentials $A_{0,\mathrm{in}} = (\lambda/e)\,\partial\mu/\partial t$, $A_{\mathrm{in}} = -(c\lambda/e)\,\partial\mu/\partial\boldsymbol{x}$, we may associate to any motion of the Madelung fluid a quantal state of motion of a single particle described by the wave functions Ψ. This association requires the condition of single-valuedness of the wave function which leads to the quantization of the strengthes of the η-rings, as shown in section 5.

Let us denote by $\boldsymbol{E}_{\mathrm{in}}$ and $\boldsymbol{H}_{\mathrm{in}}$ the electric and magnetic fields corresponding to the potentials $(\lambda/e)\,\partial\mu/\partial t$ and $-(c\lambda/e)\,\partial\mu/\partial\boldsymbol{x}$

$$\boldsymbol{H}_{\mathrm{in}} = -\frac{c}{e}\,\frac{\partial\lambda}{\partial\boldsymbol{x}}\wedge\frac{\partial\mu}{\partial\boldsymbol{x}} = -\frac{c}{e}\boldsymbol{\eta}\,, \qquad \boldsymbol{E}_{\mathrm{in}} = -\frac{\boldsymbol{v}}{c}\wedge\boldsymbol{H}_{\mathrm{in}} = \frac{\boldsymbol{v}}{e}\wedge\boldsymbol{\eta}\,. \tag{17}$$

The second equation (17) *shows that the Lorentz force due to the «inner» field vanishes.* The Helmholtz equation (28) of section 2 gives the equation of motion of the «inner» field

$$\frac{\mathrm{d}}{\mathrm{d}t}\,\frac{\boldsymbol{H}_{\mathrm{in}}}{\varrho} - \left(\frac{\boldsymbol{H}_{\mathrm{in}}}{\varrho}\cdot\frac{\partial}{\partial\boldsymbol{x}}\right)\boldsymbol{v} = 0\,. \tag{18}$$

It is obvious that the equations of motion of the Madelung fluid can be written as follows

$$
(19)\qquad \begin{cases} i\hbar\dfrac{\partial\Psi}{\partial t} = \dfrac{1}{2m}\left(\dfrac{\hbar}{i}\dfrac{\partial}{\partial \boldsymbol{x}} - \dfrac{e}{c}(\boldsymbol{A} + \boldsymbol{A}_{\mathrm{in}})\right)^2\Psi + e(A_0 + A_{0,\mathrm{in}})\Psi, \\ \boldsymbol{H}_{\mathrm{in}} = \mathrm{rot}\,\boldsymbol{A}_{\mathrm{in}}\,, \qquad \boldsymbol{E}_{\mathrm{in}} = -\dfrac{\partial \boldsymbol{A}_{0,\mathrm{in}}}{\partial \boldsymbol{x}} - \dfrac{1}{c}\dfrac{\partial \boldsymbol{A}_{\mathrm{in}}}{\partial t}\,, \\ \left(\dfrac{\mathrm{d}}{\mathrm{d}t} - \dfrac{\partial \boldsymbol{v}}{\partial \boldsymbol{x}}\right)\dfrac{\boldsymbol{H}_{\mathrm{in}}}{\varrho} = 0\,, \qquad \boldsymbol{E}_{\mathrm{in}} = -\dfrac{\boldsymbol{v}}{c}\wedge\boldsymbol{H}_{\mathrm{in}}\,. \end{cases}
$$

These equations do not involve any more the Clebsch parameters. The equations of motion of the Madelung fluid are equivalent to the system formed by the generalized Schrödinger equation, the Helmholtz equation in the form (18) *and the condition on the Lorentz force due to the « inner » field to vanish* $\boldsymbol{E}_{\mathrm{in}} + \boldsymbol{v}/c \wedge \boldsymbol{H}_{\mathrm{in}} = 0$.

7. – Steady Motions of the Madelung Fluid.

In the steady motions, the velocity and the density at any point are time independent

$$
(1)\qquad \frac{\partial \varrho}{\partial t} = 0, \qquad \frac{\partial \boldsymbol{v}}{\partial t} = 0\,.
$$

We shall assume that the external electromagnetic field is time independent and that the potentials do not depend on t. In this case the Euler equation becomes

$$
(2)\qquad \frac{\partial W}{\partial \boldsymbol{x}} = \boldsymbol{v}\wedge\boldsymbol{\eta}\,,
$$

$$
(3)\qquad W = \frac{m\boldsymbol{v}^2}{2} + eA_0 - \frac{\hbar^2}{2m}\frac{\Delta R}{R}\,,
$$

as is easily seen by taking into account the identity $(\partial/\partial \boldsymbol{x})\boldsymbol{v}^2/2 = (\boldsymbol{v}\cdot\partial/\partial \boldsymbol{x})\boldsymbol{v} + \boldsymbol{v}\wedge\mathrm{rot}\,\boldsymbol{v}$. Since

$$
(4)\qquad \frac{\partial W}{\partial \boldsymbol{x}}\cdot\boldsymbol{v} = 0,
$$

W is a constant of the motion. In the present case the trajectories coincide with the streamlines and W has the same value at all the points of a stream-

line. When

$$\boldsymbol{v}\wedge\boldsymbol{\eta}=0 \qquad \text{(everywhere)}. \tag{5}$$

W has the same value at all the points of the fluid. Condition (5) is satisfied in the quasi-irrotational motions.

When $\boldsymbol{v}\wedge\boldsymbol{\eta}\neq 0$, the value of W is not constant in the whole fluid. This is an essential difference between the general and the quasi-irrotational steady motions of the Madelung fluid.

In the steady motions of the Madelung fluid

$$\frac{\partial W}{\partial \boldsymbol{x}}\cdot\boldsymbol{\eta}=0\,, \tag{6}$$

so that W can be taken as a Clebsch parameter, provided $\boldsymbol{v}\wedge\boldsymbol{\eta}\neq 0$. Let us take

$$\lambda = W\,. \tag{7}$$

We must determine the parameter μ by the conditions

$$\boldsymbol{\eta}=\frac{\partial\lambda}{\partial\boldsymbol{x}}\wedge\frac{\partial\mu}{\partial\boldsymbol{x}}\,, \qquad \frac{\partial\mu}{\partial t}+\boldsymbol{v}\cdot\frac{\partial\mu}{\partial\boldsymbol{x}}=0\,. \tag{8}$$

It follows from (7) and (2) that

$$\frac{\partial\lambda}{\partial\boldsymbol{x}}\wedge\frac{\partial\iota}{\partial\boldsymbol{x}}=\frac{\partial W}{\partial\boldsymbol{x}}\wedge\frac{\partial\mu}{\partial\boldsymbol{x}}=(\boldsymbol{v}\wedge\boldsymbol{\eta})\wedge\frac{\partial\mu}{\partial\boldsymbol{x}}=\left(\boldsymbol{v}\cdot\frac{\partial\mu}{\partial\boldsymbol{x}}\right)\boldsymbol{\eta}-\left(\boldsymbol{\eta}\cdot\frac{\partial\mu}{\partial\boldsymbol{x}}\right)\boldsymbol{v}\,. \tag{9}$$

The vector $\boldsymbol{\eta}$ is orthogonal to $\partial\mu/\partial\boldsymbol{x}$, as a consequence of the first equation (8). Hence

$$\frac{\partial\lambda}{\partial\boldsymbol{x}}\wedge\frac{\partial\mu}{\partial\boldsymbol{x}}=\left(\boldsymbol{v}\cdot\frac{\partial\mu}{\partial\boldsymbol{x}}\right)\boldsymbol{\eta}=-\frac{\partial\mu}{\partial t}\,\boldsymbol{\eta}\,, \tag{10}$$

and we get

$$\frac{\partial\mu}{\partial t}=-1\,, \qquad \mu=-t+\nu(\boldsymbol{x})\,. \tag{11}$$

When $\boldsymbol{v}\wedge\boldsymbol{\eta}\neq 0$ the two equations

$$\boldsymbol{v}\cdot\frac{\partial f}{\partial\boldsymbol{x}}=0\,, \qquad \boldsymbol{\eta}\cdot\frac{\partial f}{\partial\boldsymbol{x}}=0\,, \tag{12}$$

admit only common solutions of the form $F(t, W)$, F denoting an arbitrary function. Therefore, in that case, a time independent Clebsch parameter λ or μ which is also a constant of the motion must be a function of W. When $\boldsymbol{v}\wedge\boldsymbol{\eta}=0$, the two equations (12) are not distinct and it is possible to choose λ and μ as time independent constants of the motion. Let us assume that $\boldsymbol{v}\wedge\boldsymbol{\eta}=0$ and $\boldsymbol{\eta}\neq 0$. The second equation (12) has two independent solutions f_1 and f_2, that are also time independent constants of the motion. $\boldsymbol{\eta}$, being orthogonal to $\partial f_1/\partial\boldsymbol{x}$ and $\partial f_2/\partial\boldsymbol{x}$, is parallel to $\partial f_1/\partial\lambda\wedge\partial f_2/\partial\boldsymbol{x}$

$$\boldsymbol{\eta}=\alpha\frac{\partial f_1}{\partial\boldsymbol{x}}\wedge\frac{\partial f_2}{\partial\boldsymbol{x}}. \tag{13}$$

Since

$$\operatorname{div}\boldsymbol{\eta}=0=\frac{\partial\alpha}{\partial\boldsymbol{x}}\cdot\frac{\partial f_1}{\partial\boldsymbol{x}}\wedge\frac{\partial f_2}{\partial\boldsymbol{x}}, \tag{14}$$

we have

$$\alpha=\Phi(f_1, f_2). \tag{15}$$

Let F_1 and F_2 be two independent functions of f_1, f_2. Since

$$\frac{\partial F_1}{\partial\boldsymbol{x}}\wedge\frac{\partial F_2}{\partial\boldsymbol{x}}=\frac{D(F_1, F_2)}{D(f_1, f_2)}\cdot\frac{\partial f_1}{\partial\boldsymbol{x}}\wedge\frac{\partial f_2}{\partial\boldsymbol{x}}=\frac{\boldsymbol{\eta}}{\alpha}\,\frac{D(F_1, F_2)}{D(f_1, f_2)}, \tag{16}$$

by choosing the F in order that

$$\frac{D(F_1, F_2)}{D(f_1, f_2)}=\alpha, \tag{17}$$

we can take

$$\lambda=F_1, \qquad \mu=F_2. \tag{18}$$

In order that time independent constants of the motion may be taken as Clebsch parameters in a steady motion of the Madelung fluid, it is necessary and sufficient that $\boldsymbol{v}\wedge\boldsymbol{\eta}=0$.

The flux through any section of a stream tube has a value independent of the choice of the section, in a steady motion. Hence

$$\int_S\varrho\boldsymbol{v}\cdot\boldsymbol{n}\,\mathrm{d}S=\int_{S_0}\varrho_0\boldsymbol{v}_0\cdot\boldsymbol{n}_0\,\mathrm{d}S_0. \tag{19}$$

In a steady motion $\varrho \boldsymbol{v}$ is a γ-vector. By the application of the formula (26) of section 2, we get

$$\boldsymbol{v} = \left(\boldsymbol{v}_0 \cdot \frac{\partial}{\partial \boldsymbol{x}_0}\right) \boldsymbol{x} \,. \tag{20}$$

The dyadic that transforms $\boldsymbol{v}_0$ into $\boldsymbol{v}$ transforms also $\boldsymbol{\eta}_0/\varrho_0$ into $\boldsymbol{\eta}/\varrho$, in any steady motion of the Madelung fluid.

It follows from the above theorem that $\boldsymbol{v}_0 \wedge \boldsymbol{\eta}_0 = 0$ leads to $\boldsymbol{v} \wedge \boldsymbol{\eta} = 0$ at the points of the streamline passing through $\boldsymbol{x}_0$ and to the constancy of $\eta/\varrho v$

$$\frac{\eta}{\varrho v} = \frac{\eta_0}{\varrho_0 v_0} \,. \tag{21}$$

$\eta/\varrho v$ is a constant of the motion in the steady motions in which the streamlines coincide with the η-lines, i.e. in the steady motions in which W is constant through the whole fluid. This theorem corresponds to that of Beltrami for ordinary inviscid fluids. We shall call Beltrami motions those satisfying the condition $\boldsymbol{v} \cdot \boldsymbol{\eta} = 0$. *In the Beltrami motions the «inner» electric field $\boldsymbol{E}_{\text{in}}$, defined in section 6 is null.*

We are led to the Beltrami motions by considering the motions of the Madelung fluid with wave functions of the stationary quantum mechanical type

$$\Psi(t, \boldsymbol{x}) = \boldsymbol{\Phi}(\boldsymbol{x}) \exp\left[-\frac{i}{\hbar} Et\right], \qquad E = \text{constant}, \tag{22}$$

with time independent λ and μ. In this case the generalized Schrödinger equation becomes

$$\left(\frac{\hbar}{i} \frac{\partial}{\partial \boldsymbol{x}} - \frac{e}{c} \boldsymbol{A} + \lambda \frac{\partial \mu}{\partial \boldsymbol{x}}\right)^2 \boldsymbol{\Phi} + e A_0 \boldsymbol{\Phi} = E \boldsymbol{\Phi} \,, \tag{23}$$

$$\boldsymbol{v} \cdot \frac{\partial \lambda}{\partial \boldsymbol{x}} = 0 \,, \qquad \boldsymbol{v} \cdot \frac{\partial \mu}{\partial \boldsymbol{x}} = 0 \,. \tag{24}$$

The existence of the constant W in the steady motions of the Madelung fluid corresponds to the Bernoulli theorem, which expresses the conservation of the total energy of any element of the fluid during its motion. The total energy per mass m is the sum of the kinetic energy $m\boldsymbol{v}^2/2$, the external potential energy eA_0 and the internal energy $-(\hbar^2/2m)\Delta R/R$. In the steady Beltrami motions, the energy per unit mass is the same for all the elements of the fluid. This happens in particular in the quasi-irrotational steady motions described by the ordinary Schrödinger equation.

It is interesting to notice that the steady motions corresponding to discrete eigenvalues of the hamiltonian are characterized by the conditions of having wave functions Ψ that are regular everywhere and tend to zero at infinity with sufficient rapidity to render $\int_{-\infty}^{+\infty} |\Psi|^2 \, \mathrm{d}\boldsymbol{x}$ *finite and of having* $\boldsymbol{\eta} = 0$ *everywhere.*

8. – Simple Case of Beltrami Motion.

Beltrami discussed, in hydrodynamics, the motion of an incompressible fluid with the following distribution of velocities

$$\boldsymbol{v} = \boldsymbol{\omega} \wedge \boldsymbol{x} + \sqrt{2}\sqrt{a^2 - r^2}\,\boldsymbol{\omega} \qquad (r \leqslant a)(r^2 = x_1^2 + x_2^2), \tag{1}$$

$\boldsymbol{\omega}$ = constant vector parallel to the x_3-axis.

It is easily seen that

$$\operatorname{rot} \boldsymbol{v} = \sqrt{2}\sqrt{a^2 - r^2}\,\boldsymbol{v}, \qquad \operatorname{div} \boldsymbol{v} = 0 \qquad (r \leqslant a). \tag{2}$$

We shall assume the distribution of velocities (1) for $r > a$ and take

$$\boldsymbol{v} = \boldsymbol{\omega} \wedge \frac{a^2 \boldsymbol{x}}{r^2}, \qquad (r > a). \tag{3}$$

It is easily seen that

$$\operatorname{rot} \boldsymbol{v} = 0, \qquad \operatorname{div} \boldsymbol{v} = 0. \qquad (r > a). \tag{4}$$

Equations (1) and (3) define a distribution of velocities satisfying everywhere the condition $\boldsymbol{v} \wedge \boldsymbol{\eta} = 0$, in the absence of magnetic fields. We shall assume that there are no electromagnetic fields. Since $\mathrm{d}r/\mathrm{d}t = 0$, we have

$$\begin{cases} m \dfrac{\mathrm{d}\boldsymbol{v}}{\mathrm{d}t} = m\boldsymbol{\omega} \wedge \boldsymbol{v} = -\, m\omega^2 \boldsymbol{r}, & r \leqslant a, \\ m \dfrac{\mathrm{d}\boldsymbol{v}}{\mathrm{d}t} = \dfrac{ma^2}{r^2}\, \boldsymbol{\omega} \wedge \boldsymbol{v} = -\, \dfrac{m\omega^2 a^4}{r^4}\, \boldsymbol{r}, & r > a, \\ \boldsymbol{r} = x_1 \boldsymbol{i}_1 + x_2 \boldsymbol{i}_2 . \end{cases} \tag{5}$$

The density mR^2 is now a constant of the motion, since $\operatorname{div} \boldsymbol{v} = 0$. R can be

taken as a function of r satisfying the equations

$$\frac{\hbar^2}{2m}\frac{\mathrm{d}}{\mathrm{d}r}\frac{\Delta R}{R} = \begin{cases} -m\omega^2 r\,, & r \leqslant a, \\ -\dfrac{m\omega^2 a^4}{r^3}\,, & r > a. \end{cases} \tag{6}$$

Hence

$$\frac{\Delta R}{R} = \begin{cases} -\dfrac{m^2\omega^2}{\hbar^2}(r^2 - 2a^2) - k^2\,, & r \leqslant a, \\ \dfrac{m^2\omega^2 a^4}{\hbar^2 r^2} - k^2\,, & r > a. \end{cases} \tag{7}$$

(k^2 = constant of integration).

It follows from the equations (1) and (2) of section 5 that we must take

$$m\omega a^2 = l\hbar \qquad (l = \text{positive integer}). \tag{8}$$

since

$$2\pi\int_0^a \boldsymbol{i}_3 \cdot \operatorname{rot} \boldsymbol{v}\, r\,\mathrm{d}r = 2\pi\omega a^2\,. \tag{9}$$

We get from (7)

$$\begin{cases} \dfrac{\mathrm{d}^2R}{\mathrm{d}r^2} + \dfrac{1}{r}\dfrac{\mathrm{d}R}{\mathrm{d}r} + \left\{\dfrac{l^2}{a^4}(r^2 - 2a^2) + k^2\right\}R = 0\,, & r < a, \\ \dfrac{\mathrm{d}^2R}{\mathrm{d}r^2} + \dfrac{1}{r}\dfrac{\mathrm{d}R}{\mathrm{d}r} + \left(k^2 - \dfrac{l^2}{r^2}\right)R = 0\,, & r > a. \end{cases} \tag{10}$$

Hence

$$R = \alpha J_l(kr) + \beta N_l(kr)\,, \qquad r > a \quad (\alpha \text{ and } \beta = \text{constants}), \tag{11}$$

J_l and N_l denoting the Bessel and Neumann functions of order l, respectively. The first equation (10) has only one solution regular at $r = 0$, we shall denote it by $G(r)$, with the normalization $G(0) = 1$. The fitting conditions at the boundary of the vortex tube

$$\begin{cases} G(a) = \alpha J_l(ka) + \beta N_l(ka)\,, \\ G'(a) = k\{\alpha J_l'(ka) + \beta N_l'(ka)\}\,, \end{cases} \tag{12}$$

determine α and β

$$(13)\qquad \begin{cases} \alpha = \dfrac{\pi a}{2}\{kG(a)N_l'(ka) - G'(a)N_l(ka)\}, \\ \beta = -\dfrac{\pi a}{2}\{kG(a)J_l'(ka) - G'(a)J_l(ka)\}. \end{cases}$$

The trajectories of the elements of the fluid are helices in the vortex tube and circles outside the tube. It is easily seen that the value of W is everywhere the same

$$(14)\qquad W = \frac{m\boldsymbol{v}^2}{2} - \frac{\hbar^2}{2m}\frac{\Delta R}{R} = \frac{\hbar^2 k^2}{2m}.$$

We can take for $r < a$

$$(15a)\qquad S = -Wt + l\hbar\varphi\left(2 - \frac{r^2}{a^2}\right),\quad \lambda = \frac{l\hbar}{a^2}\sqrt{2(a^2 - r^2)},\quad \mu = x_3 - \sqrt{2(a^2 - r^2)}\varphi,$$

and for $r > a$

$$(15b)\qquad S = -Wt + l\hbar\varphi,\quad \lambda = 0,\quad \mu = 0,$$

φ denoting the azimuthal angle around the x_3 axis

$$(16)\qquad \operatorname{tg}\varphi = \frac{x_2}{x_1}.$$

The above choice of the Clebsch parameters leads to a multiple valued Ψ for $r < a$. A single valued wave function can be obtained by taking for $r < a$

$$(17)\quad S = -Wt + \frac{l\hbar x_3}{\sqrt{2}a^2}\sqrt{a^2 - r^2} + l\hbar\varphi,\ \lambda = \frac{l\hbar}{\sqrt{2}a^2}(a^2 - r^2),\ \mu = \frac{x_3}{\sqrt{a^2 - r^2}} - \sqrt{2}\varphi.$$

Equation (2) shows that the component of the vorticity tangent to the cirles $x_3 = \text{const}$ $r = a$ is infinite. Situations in which the vorticity becomes infinite on a surface are well known in hydrodynamics.

9. – Discontinuous Motions and Vortex Sheets.

We shall now examine some cases of discontinuous motion associated to vortex sheets. Let us discuss firstly a simple case of steady motion, in the

absence of electromagnetic fields, whose velocity distribution is

$$\boldsymbol{v} = \begin{cases} v_{\mathrm{I}}\,\boldsymbol{i}_3\,, & x_1 > 0\,, \\ v_{\mathrm{II}}\boldsymbol{i}_3\,, & x_1 < 0\,, \end{cases} \tag{1}$$

$$R = \text{constant} \qquad v_{\mathrm{I}},\ v_{\mathrm{II}} = \text{constants} \tag{2}$$

The Euler and continuity equations are obviously satisfied for $x_1 \neq 0$. Although $\boldsymbol{v}$ is discontinuous, we can give a meaning to the equations of motion even when $x_1 = 0$, since

$$\lim_{x_1 \to 0+} \left\{ m\frac{\partial \boldsymbol{v}}{\partial t} + m\left(\boldsymbol{v}\cdot\frac{\partial}{\partial \boldsymbol{x}}\right)\boldsymbol{v} - \frac{\hbar^2}{2m}\,\frac{\partial}{\partial \boldsymbol{x}}\,\frac{\Delta R}{R} \right\} = \tag{3}$$

$$= \lim_{x_1 \to 0-} \left\{ m\frac{\partial \boldsymbol{v}}{\partial t} + m\left(\boldsymbol{v}\cdot\frac{\partial}{\partial \boldsymbol{x}}\right)\boldsymbol{v} - \frac{\hbar^2}{2m}\,\frac{\partial}{\partial \boldsymbol{x}}\,\frac{\Delta R}{R} \right\} = 0\,,$$

$$\lim_{x_1 \to 0+} \left\{ \frac{\partial \varrho}{\partial t} + \operatorname{div}(\varrho \boldsymbol{v}) \right\} = \lim_{x_1 \to 0-} \left\{ \frac{\partial \varrho}{\partial t} + \operatorname{div}(\varrho \boldsymbol{v}) \right\} = 0\,. \tag{4}$$

Denoting by $\delta(x)$ the Dirac singular function, we have

$$\operatorname{rot} \boldsymbol{v} = (v_{\mathrm{II}} - v_{\mathrm{I}})\,\delta(x_1)\boldsymbol{i}_2\,. \tag{5}$$

The discontinuity surface $x_1 = 0$ is a vortex sheet. The distribution of velocities (1) can be described by means of discontinuous Clebsch parameters

$$S = m|\boldsymbol{v}|x_3\,, \qquad \lambda = -x_3\,, \qquad \mu = m|\boldsymbol{v}|\,. \tag{6}$$

The above results can be easily extended to more general cases. Let Σ be a surface dividing the space into two regions in which the vector field $\boldsymbol{w}(\boldsymbol{x})$ is continuous and has continuous derivatives, there being a jump of the tangential component of $\boldsymbol{w}$ across Σ. Let $\boldsymbol{n}(\boldsymbol{x})$, $\boldsymbol{\tau}_1(\boldsymbol{x})$, $\boldsymbol{\tau}_2(\boldsymbol{x})$ be three mutually orthogonal continuous unit vectors such that $\boldsymbol{n} = \boldsymbol{\tau}_1 \wedge \boldsymbol{\tau}_2$ and $\boldsymbol{n}(\boldsymbol{x})$ be normal to Σ when $\boldsymbol{x}$ lies on Σ. Since

$$\operatorname{div} \boldsymbol{\omega} = \left(\boldsymbol{\tau}_1\cdot\frac{\partial}{\partial \boldsymbol{x}}\right)\boldsymbol{\omega}\cdot\boldsymbol{\tau}_1 + \left(\boldsymbol{\tau}_2\cdot\frac{\partial}{\partial \boldsymbol{x}}\right)\boldsymbol{\omega}\cdot\boldsymbol{\tau}_2 + \left(\boldsymbol{n}\cdot\frac{\partial}{\partial \boldsymbol{x}}\right)\boldsymbol{\omega}\cdot\boldsymbol{n}, \tag{7}$$

we can define $\operatorname{div}\boldsymbol{w}$ on Σ when $(\boldsymbol{\tau}_1\cdot\partial/\partial\boldsymbol{x})\,\boldsymbol{w}\cdot\boldsymbol{\tau}_1 + (\boldsymbol{\tau}_2\cdot\partial/\partial\boldsymbol{x})\,\boldsymbol{w}\cdot\boldsymbol{\tau}_2 + (\boldsymbol{n}\cdot\partial/\partial\boldsymbol{x})\boldsymbol{w}\cdot\boldsymbol{n}$ tends to a defined value, independent of the path, as $\boldsymbol{x}$ approaches any point of Σ. $\operatorname{div}\boldsymbol{w}$ can be finite on Σ, notwithstanding the discontinuity of the tangential

component of $\boldsymbol{w}$. The situation with rot $\boldsymbol{w}$ is essentially different. Since

$$\text{rot}\,\boldsymbol{\omega} = \boldsymbol{\tau}_1 \wedge \left(\boldsymbol{\tau}_1 \cdot \frac{\partial}{\partial \boldsymbol{x}}\right)\boldsymbol{\omega} + \boldsymbol{\tau}_2 \wedge \left(\boldsymbol{\tau}_2 \cdot \frac{\partial}{\partial \boldsymbol{x}}\right)\boldsymbol{\omega} + \boldsymbol{n} \wedge \left(\boldsymbol{n} \cdot \frac{\partial}{\partial \boldsymbol{x}}\right)\boldsymbol{\omega}\,, \tag{8}$$

and

$$\boldsymbol{n} \wedge \left(\boldsymbol{n} \cdot \frac{\partial}{\partial \boldsymbol{x}}\right)\boldsymbol{w} = \boldsymbol{n} \wedge \frac{\partial \boldsymbol{w}}{\partial n} = \frac{\partial}{\partial n}(\boldsymbol{n} \wedge \boldsymbol{w}) + \boldsymbol{w} \wedge \left(\boldsymbol{n} \cdot \frac{\partial}{\partial \boldsymbol{x}}\right)\boldsymbol{n}\,, \tag{9}$$

rot $\boldsymbol{w}$ has a delta-like singularity arising from the derivation of the discontinuous tangential vector $\boldsymbol{n} \wedge \boldsymbol{w}$. By the application of the above results to the velocity, we see that:

The discontinuity of the tangential component of the velocity across a surface Σ is associated to the existence of a vortex sheet on Σ corresponding to a delta-like singularity of the tangential component of rot $\boldsymbol{v}$. *It may nevertheless be possible to define the divergence of $\boldsymbol{v}$ on Σ and the value of* div $\boldsymbol{v}$ *may be finite on Σ.*

The surface Σ may either contain always the same elements of the fluid or propagate in the mass of the fluid as a wave of discontinuity. In the case of a fixed Σ containing always the same elements of the fluid, their trajectories lie on Σ, so that the normal component of the velocity is continuous and null on Σ. In order that the equations of motion be satisfied on Σ, it is necessary that

$$m \frac{\partial \boldsymbol{v}}{\partial t} + m\left(\boldsymbol{v} \cdot \frac{\partial}{\partial \boldsymbol{x}}\right)\boldsymbol{v} - \frac{\hbar^2}{2m} \frac{\partial}{\partial \boldsymbol{x}} \frac{\Delta R}{R} - \boldsymbol{E}\,,$$

and

$$\frac{\partial \varrho}{\partial t} + \boldsymbol{v} \cdot \frac{\partial \varrho}{\partial \boldsymbol{x}} + \varrho\,\text{div}\,\boldsymbol{v}\,,$$

tend to zero as $\boldsymbol{x}$ approaches Σ, independently of the path. There is no difficulty with the terms involving the derivatives of $\boldsymbol{v}$, as we have shown. With respect to this point the situation is similar to that of the dynamics of ordinary compressible fluids, but the requirements on the behaviour of the density are essentially different, because the force derived from the quantum potential involves derivatives of the third order of the density.

We shall now discuss another example of steady motions with vortex sheets, corresponding to a potential $V(r)$ depending only on the distance to the x_3 - axis. Let $R(r)\exp[il\varphi - (i/\hbar)Et]$ be a stationary solution of the ordinary Schrödinger equation for the potential $V(r)$, corresponding to the eigenvalue E of the energy. The trajectories of the elements are circles $r = \text{const.}$ $x_3 = \text{const.}$

described in uniform motion, the velocity being $(lh/mr^2)\boldsymbol{i}_3\wedge\boldsymbol{r}$. Let us consider the motion in which the density distribution is the same as in that stationary state, the distribution of the velocities being

$$\boldsymbol{v}=\begin{cases}\dfrac{lh}{mr^2}\,\boldsymbol{i}_3\wedge\boldsymbol{r}+v_{\mathrm{I}}\,\boldsymbol{i}_3\,, & r<a,\\[2ex] \dfrac{lh}{mr^2}\,\boldsymbol{i}_3\wedge\boldsymbol{r}+v_{\mathrm{II}}\boldsymbol{i}_3\,, & r>a,\end{cases}\tag{10}$$

$$(v_{\mathrm{I}},\ v_{\mathrm{II}}=\text{constants})\,.$$

In the present case Σ is the cylinder $r=a$. It is easily seen that the Euler equation and the equation of continuity are satisfied everywhere. The motion is irrotational for $r\neq a$ but the cylinder $r=a$ is a vortex sheet

$$\operatorname{rot}\boldsymbol{v}=\delta(r-a)(v_{\mathrm{I}}-v_{\mathrm{II}})\boldsymbol{i}_3\wedge\frac{\boldsymbol{r}}{r}\,.\tag{11}$$

It follows from the equation (8) of section 1 that the stress $\boldsymbol{T}$ acting on a surface element $d\sigma$ of the fluid is in general not directed along the normal $\boldsymbol{n}$

$$\boldsymbol{T}=\frac{h^2}{m}\,\frac{\partial R}{\partial n}\,\frac{\partial R}{\partial \boldsymbol{x}}-\frac{h^2}{4m}\,\Delta\varrho\,\boldsymbol{n}\,.\tag{12}$$

A necessary and sufficient condition for $\boldsymbol{T}$ to be normal is

$$\frac{\partial R}{\partial n}\,\frac{\partial R}{\partial \boldsymbol{x}}\wedge\boldsymbol{n}=0\,,\tag{13}$$

This condition is satisfied in the motion defined by (10) on Σ.

RIASSUNTO (*)

Si discutono i moti generici del mezzo continuo (fluido di Madelung) i cui moti irrotazionali sono descritti dall'equazione di Schrödinger. Si dimostra che molti dei teoremi fondamentali del moto vorticoso dei fluidi barotropici non viscosi sono validi anche per il fluido di Madelung. Si dà una discussione dettagliata dei parametri di Clebsch. Si dimostra l'esistenza di uno speciale tipo di moti permanenti, simili ai moti di Beltrami, in cui le linee di flusso coincidono con le linee di vorticosità, che corrisponde a una stretta generalizzazione degli ordinari stati stazionari. Si discute la quantizzazione dei tubi di vorticosità. Si dànno esempi di moti di Beltrami e di moti discontinui del fluido di Madelung. Si dimostra che i moti generici del fluido di Madelung possono essere interpretati anche fisicamente in termini degli ordinari stati quantici di una particella.

(*) *Traduzione a cura della Redazione*

IL NUOVO CIMENTO Vol. I, N. 4 1° Aprile 1955

Une analyse en déphasages de la diffusion et de la polarisation dans les collisions proton-proton à grande énergie.

C. A. Klein

Laboratoire de Physique de l'École Normale Supérieure - Paris

(ricevuto il 5 Gennaio 1955)

Résumé. — Les résultats des mesures de la diffusion et de la polarisation dans les expériences de collision simple et double, aux énergies comprises entre 100 et 400 MeV, ont été analysés en utilisant les déphasages affectant d'une part l'onde ^1S, d'autre part les ondes ^3P_j correspondant à un moment cinétique total $j = 0, 1, 2$. Seul un nombre restreint de solutions est en mesure de fournir un accord satisfaisant avec l'expérience, tant du point de vue diffusion que polarisation. Parmi ces solutions, il en existe qui sont susceptibles de rendre compte de l'inversion des niveaux nucléaires suggérée par la théorie de Mayer-Jensen du modèle des couches et qui correspondent, du moins en ce qui concerne le déphasage ^1S, à un potentiel nucléaire central muni d'un cœur répulsif du type Jastrow. A noter toutefois que la variation angulaire de la polarisation aux environ de 300 MeV ne peut être reproduite qu'en utilisant en outre les déphasages associés aux états ^3F.

Les divers potentiels phénoménologiques, proposés depuis quelques années en vue de décrire l'interaction entre deux nucléons subissant un choc à grande énergie, se sont tous révélés plus ou moins décevants, au fur et à mesure que se sont précisées, d'une part les mesures de la diffusion, en particulier aux petits angles, et d'autre part les mesures de la polarisation dans les expériences de collision double. Aussi Breit [1] a-t-il récemment proposé de renoncer provisoirement à l'étude de types de potentiels particuliers, pour se limiter à l'examen des « déphasages » créés par l'interaction, sans faire d'hypothèse à priori à son sujet. En ce qui concerne l'interaction proton-proton, une première tentative de ce genre a été entreprise par Garren [2]. Négligeant les effets cou-

[1] G. Breit: *Proceeding of the 4 annual Rochester Conference oh High Energy Nuclear Physics* (1954), p. 19.

[2] A. Garren: *Phys. Rev.*, **92**, 213 and 1587 (1953).

lombiens, cet auteur a montré qu'il doit être possible de décrire l'isotropie de la section efficace différentielle, la valeur de cette section efficace ainsi que le pourcentage de polarisation, mesurés par OXLEY et ses collaborateurs [3] de l'Université de Rochester avec des protons de 240 MeV, en utilisant les déphasages correspondant aux seules ondes S et P. Nous nous sommes proposés d'étudier dans quelle mesure une telle analyse, c'est-à-dire ne faisant appel qu'aux quatre paramètres associés à l'interaction dans les états $^1S_0$, $^3P_0$, $^3P_1$ et $^3P_2$, est susceptible de rendre compre de l'ensemble des résultats de la diffusion et de la polarisation proton-proton, dont on dispose à l'heure actuelle dans le domaine compris entre 100 et 400 MeV.

1. – La méthode mise en oeuvre.

Dans la diffusion proton-proton, la section efficace différentielle résulte de trois contributions: l'interaction nucléaire, l'interaction coulombienne, et les effets dus à l'interférence de ces deux interactions

$$\sigma(k,\theta) = \sigma_{\text{nucl}}(k,\theta) + \sigma_{\text{coul}}(k,\theta) + \sigma_{\text{int}}(k,\theta)\,. \tag{1}$$

Négligeant le déphasage dans les états à moment cinétique orbital supérieur à un, et utilisant les notations de BREIT et de ses collaborateurs [4] (soit en particulier $^1K_0$ pour le déphasage de l'onde singulet $^1S_0$, et δ_0, δ_1, δ_2 pour celui des ondes triplet $^3P_0$, $^3P_1$, $^3P_2$ correspondant respectivement a $j=0$, 1 et 2), ces contributions se présentent de la façon suivante:

$$\sigma_{\text{nucl}}(k,\theta) = \frac{1}{k^2}\left\{\sin^2{}^1K_0 + \sum_{j=0}^{2}(2j+1)\sin^2\delta_j + P_2(\cos\theta)\left[\frac{3}{2}\sin{}^2\delta_1 + \right.\right.$$
$$\left.\left. + \frac{7}{2}\sin^2\delta_2 + 4\sin\delta_0\sin\delta_2\cos(\delta_0-\delta_2) + 9\sin\delta_1\sin\delta_2\cos(\delta_1-\delta_2)\right]\right\}, \tag{2}$$

$$\sigma_{\text{coul}}(k,\theta) = \frac{1}{k^2}\left\{\frac{\eta^2}{4}\left[\sin^{-4}\frac{\theta}{2} + \cos{}^4\frac{\theta}{2} - \sin{}^2\frac{\theta}{2}\cos^{-2}\frac{\theta}{2}\cos\left(\eta\log\operatorname{tg}^2\frac{\theta}{2}\right)\right]\right\}, \tag{3}$$

$$\sigma_{\text{int}}(k,\theta) = \frac{1}{k^2}\left\{\frac{\eta}{2}X_0\sin{}^1K_0\cos{}^1K_0 + \frac{\eta}{2}Y_0\sin^2K_0 + \right.$$
$$\left. + P_1(\cos\theta)\left[\frac{\eta}{2}X_1\sum_{j=0}^{2}(2j+1)\sin\delta_j\cos\delta_i + \frac{\eta}{2}Y_1\sum_{j=0}^{2}(2j+1)\sin^2\delta_j\right]\right\}. \tag{4}$$

[3] C. L. OXLEY et R. D. SCHAMBERGER: *Phys. Rev.*, **85**, 416 (1952); C. L. OXLEY, W. F. CARTWRIGHT, J. ROUVINA, E. BASKIR, D. KLEIN et W. SKILLMAN: *Phys. Rev.*, **91**, 419 (1953).

[4] R. M. THALER et J. BENGSTON: *Phys. Rev.*, **94**, 679 (1954).

De nombreuses expériences ont établi que, lorsque l'énergie des protons incidents est comprise entre 100 et 400 MeV, la diffusion se fait à intensité constante dans les angles compris entre 25° et 165° du système barycentrique (5). Or, à ces énergies, les contributions coulombiennes et interférentielles sont pratiquement sans importance pour $40° < \theta < 140°$. Il en résulte que l'isotropie de la section efficace différentielle ne peut être assurée, que si le coefficient de $P_2(\cos\theta)$ dans (2) est identiquement nul. Cette condition nous fournit une première relation à imposer aux déphasages:

$$0 = 3\sin^2\delta_1 + 7\sin^2\delta_2 + 8\sin\delta_0\sin\delta_2\cos(\delta_0 - \delta_2) + \\ + 18\sin\delta_1\sin\delta_2\cos(\delta_1 - \delta_2)\,. \tag{5}$$

Dans ces conditions, la section efficace différentielle à 90° est donnée par:

$$k^2\sigma(k, 90°) = \sin^2{}^1K_0 + \sin^2\delta_0 + 3\sin^2\delta_1 + 5\sin^2\delta_2\,. \tag{6}$$

Wolfenstein et Ashkin (6) ont montré d'une façon générale que si l'interaction entre deux nucléons comporte un terme du type $(\boldsymbol{\sigma}, \boldsymbol{r})$, c'est-à-dire si elle n'est pas purement centrale, le nucléon diffusé dans l'angle θ est partiellement polarisé. Soit $\mathcal{P}(k, \theta)$ cette polarisation en pourcentage. Si l'on se restreint aux états P, $\mathcal{P}(k, \theta)$ se présente en fonction des déphasages de la façon suivante (7):

$$\frac{k^2\sigma(k, \theta)}{\sin 2\theta}\,\mathcal{P}(k, \theta) = 3\sin\delta_0\sin\delta_2\sin(\delta_0 - \delta_2) + \frac{9}{2}\sin\delta_1\sin\delta_2\sin(\delta_1 - \delta_2)\,. \tag{7}$$

On sait que cette polarisation a été indiscutablement mise en évidence aux énergies supérieures à 100 MeV et étudiée en fonction de θ dans de nombreuses expériences de collision double. La précision atteinte est de l'ordre de 20 %, mais le signe de la polarisation n'a pas pu être déterminé. On dispose ainsi d'une troisième condition à imposer aux déphasages.

Observant que les relations (5) et (7) ne font intervenir que les déphasages triplet, la méthode qui s'impose consiste à:

---

(5) Au delà de 400 MeV la situation parait à l'heure actuelle confuse. Selon R. B. Sutton, T. H. Fields, J. G. Fox, J. A. Kane, W. E. Mott et R. A. Stallwood: *Phys. Rev.*, **95**, 663 (1953), $\sigma(\theta)$ mesuré à 437 MeV s'élèverait d'environ 20 % en passant de 90° à 17° (système barycentrique), alors que J. Marshall, L. Marshall et V. A. Nedzel: (*Phys. Rev.*, **92**, 834 (1953)) ont au contraire observé à 429 MeV une section efficace différentielle au comportement usuel.

(6) L. Wolfenstein: *Phys. Rev.*, **75**, 1664 (1949); **76**, 541 (1949); L. Wolfenstein et J. Askin: *Phys. Rev.*, **85**, 947 (1952).

(7) L. J. B. Goldfarb et D. Feldman: *Phys. Rev.*, **85**, 1099 (1952).

a) Étudier l'intersection de la « surface d'isotropie » (5) avec la « surface de polarisation » (7). Nous avons reproduit (fig. 1) quelques courbes d'intersection en projection sur le plan (δ_1, δ_0), lorsqu'on se limite aux solutions fondamentales conformément à la notion de déphasage. Notons que dans le cas d'une polarisation positive, seuls se sont révélés possibles des déphasages δ_2 positifs. Dans le cas d'une polarisation négative, les courbes sont identiques, à condition de remplacer tous les δ_j par $-\delta_j$.

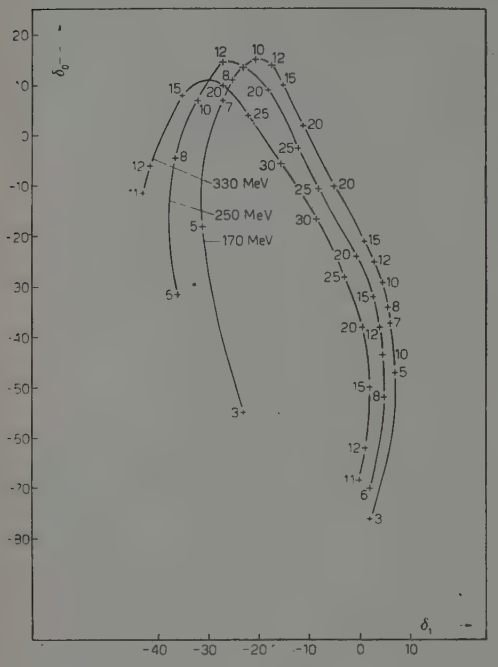

Fig. 1. – Intersection de la surface d'isotropie avec la surface de polarisation à 170, 260 et 330 MeV, en projection sur le plan (δ_1, δ_0). Les chiffres portés le long des courbes indiquent les valeurs correspondantes des déphasages δ_2. Tous les angles sont exprimés en degrés.

b) Associer à chaque triplet δ_0, δ_1, δ_2 fourni par la courbe d'intersection et vérifiant l'inégalité

$$(8) \qquad \sum_{j=0}^{2} (2j+1) \sin^2 \delta_j < k^2 \sigma(k, 90^\circ)$$

les deux valeurs positive et négative, de ${}^1K_0$, assurant une section efficace différentielle correcte à 90°.

c) Essayer de sélectionner les ensembles $({}^1K_0, \delta_0, \delta_1, \delta_2)$ réalisant par l'intermédiaire du terme d'interférence (4) un ajustage optimum aux résultats de la diffusion dans les angles compris entre 10° et 25° (système barycentrique), où les effets d'interférence sont susceptibles d'être assez notables.

Cette méthode nous a effectivement permis de sélectionner, à toutes les énergies, du moins dans l'hypothèse d'une polarisation positive, un nombre restreint d'ensembles de valeurs pour ${}^1K_0$ et les δ_j, présentant une continuité certaine, et fournissant à la fois de bons résultats en ce qui concerne la diffusion et des ordres de grandeur corrects pour la polarisation.

2. – Le résultat des calculs.

Le terme d'interférence se révélant fort sensible aux variations des déphasages, le succès de la méthode dépend essentiellement de la qualité des mesures

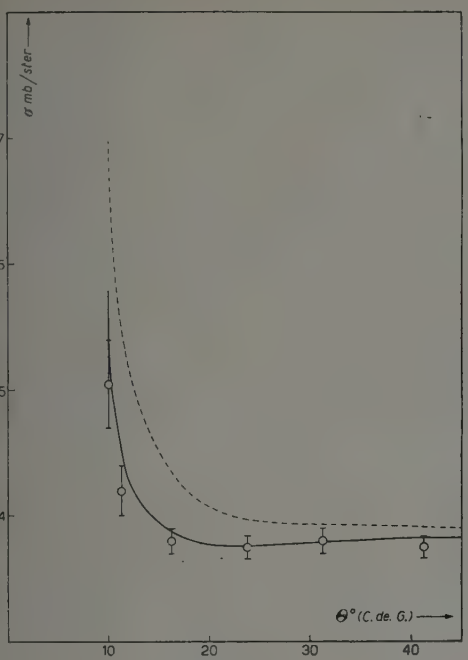

Fig. 2*a*.

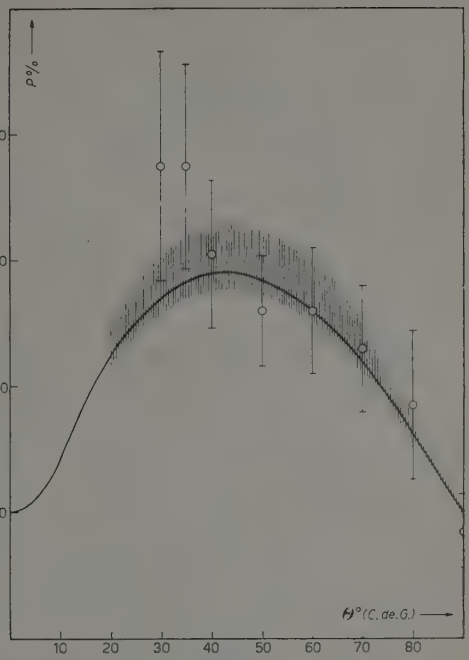

Fig. 2*b*.

Fig. 2*a*. – Diffusion dans une collision p-p à 170 MeV. Les points représentent les résultats experimentaux obtenus par CHAMBERLAIN et GARRISON à cette énergie, munis des erreurs affectant la distribution angulaire. Les courbes ont été calculées à l'aide des déphasages indiqués au tableau I: en trait interrompu $\sigma_{\text{nucl}} + \sigma_{\text{coul}}$; en trait continu

$$\sigma_{\text{nucl}} + \sigma_{\text{coul}} + \sigma_{\text{int}}.$$

Fig. 2*b*. – Polarisation dans une collision p-p à 170 MeV. Les points représentent les résultats expérimentaux obtenus par DICKSON et SALTER à $\sim$ 130 MeV, affectés de leur erreur totale. La courbe a été calculée à l'aide des déphasages indiqués au tableau I. Les hachures recouvrent les valeurs possibles pour la polarisation, lorsqu'on tient compte de l'incertitude sur la section efficace différentielle.

de diffusion aux petits angles. De telles mesures viennent d'être effectuées par le Laboratoire de Berkeley ([8]) à 170, 260 et 330 MeV, apparemment dans de très bonnes conditions. Ce sont elles qui ont servi de base aux calculs effectifs.

([8]) O. CHAMBERLAIN et J. D. GARRISON: *Phys. Rev.*, **95**, 1349 (1954); D. FISCHER et G. GOLDHABER: *Phys. Rev.*, **95**, 1350 (1954).

Ces expériences donnent toutes, au-delà de 20° (système barycentrique), une section efficace différentielle de 3.75 $\pm$ 0.25 mb/stérad. Elles sont donc en net désaccord avec les résultats plus anciens de Rochester et de Harwell, soit environ 5 mb/sterad. Notons que l'équipe d'Harward (O. E. KRUSE, J. M. TEEM et N. F. RAMSEY: *Phys. Rev.*, **94**,

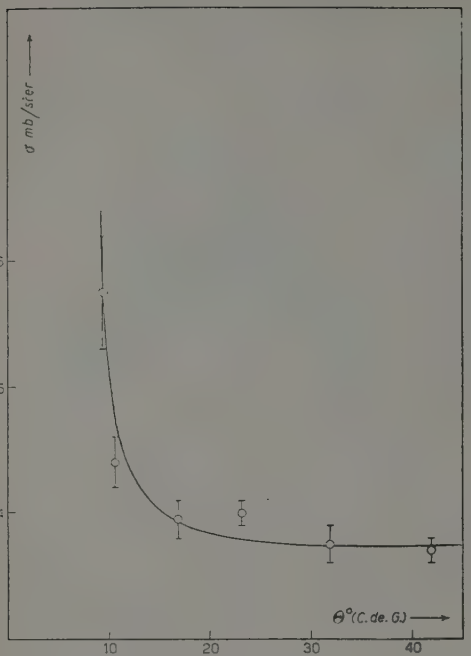

Fig. 3*a*.

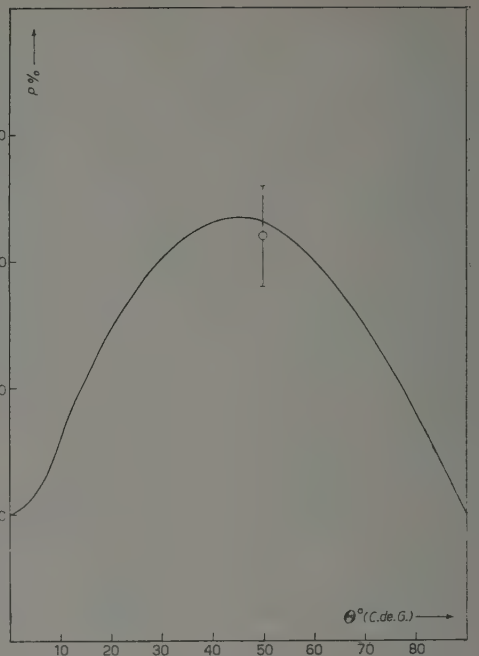

Fig. 3*b*.

Fig. 3*a*. Diffusion dans une collision p-p à 260 MeV. Les points représentent les résultats expérimentaux obtenus par CHAMBERLAIN et GARRISON à cette énergie, munis des erreurs affectant la distribution angulaire. La courbe a été calculée à l'aide des déphasages indiqués au tableau I et correspond à une σ_{int} pratiquement nulle.

Fig. 3*b*. – Polarisation dans une collision p-p à 260 MeV. Le point représente le résultat experimental obtenu par OXLEY *et al.* à ~ 210 MeV, affecté de son erreur totale. La courbe a été calculée à l'aide des déphasages indiqués au tableau I.

Les mesures de la polarisation induite par une collision proton-proton ont établi que celle-ci ne subit pas de modification essentielle, lorsqu'on passe de 100 à 400 MeV. Aussi avons-nous cru pouvoir utiliser pour l'analyse à

a) 170 MeV, les mesures de polarisation effectuées à Harwell aux environs de 130 MeV [9].

b) 260 MeV, la valeur obtenue à Rochester pour la polarisation d'un proton d'environ 210 MeV diffusé dans l'angle $\theta = 50°$ (C. DE G.) [10].

1795 (1954)) a effectué une série de mesures de section efficace différentielle à 90° entre 40 et 90 MeV qui, à notre avis, pourraient signifier qu'il faut peut-etre préférer les mesures de Berkeley et Chicago à celles de Rochester et Harwell.

[9] J. M. DICKSON et D. C. SALTER: *Nature*, **173**, 946 (1954).

[10] C. L. OXLEY, W. F. CARTWRIGHT et J. ROUVINA: *Phys. Rev.*, **93**, 806 (1954).

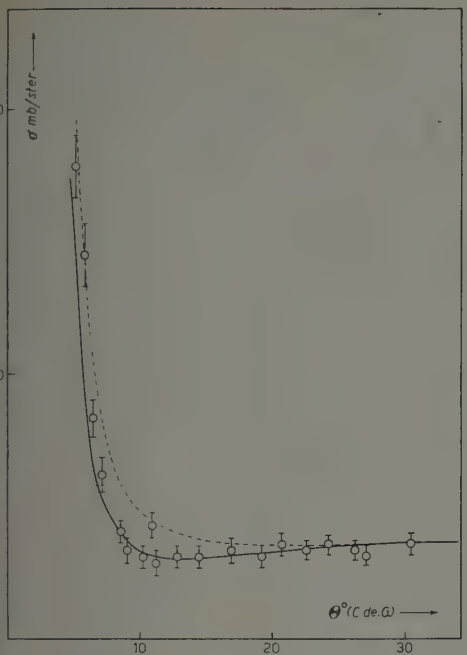

Fig. 4*a*.

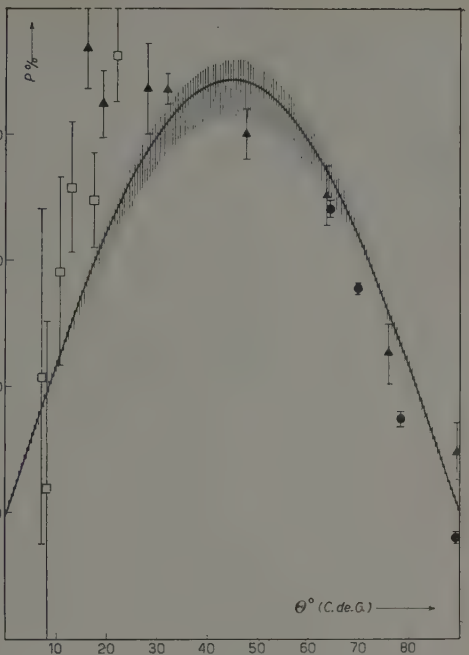

Fig. 4*b*.

Fig. 4*a*. – Diffusion dans une collision p-p à 330 MV. Les points représentent les résultats experimentaux obtenus par FISCHER et GOLDHABER à cette énergie, munis des erreurs affectant la distribution angulaire. Les courbes ont été calculées à l'aide des déphasages indiqués au tableau I: en trait interrompu $\sigma_{\text{nucl}} + \sigma_{\text{coul}}$ et en trait continu $\sigma_{\text{nucl}} + \sigma_{\text{coul}} + \sigma_{\text{Int}}$.

Fig. 4*b*. – Polarisation dans une collision p-p à 330 MeV. Les points représentent les résultats experimentaux obtenus par CHAMBERLAIN *et al.* à ~ 300 MeV, affectés de leur erreur totale. La courbe a été calculée à l'aide des déphasages indiqués au tableau I. Les hachures recouvrent les valeurs possibles pour la polarisation, lorsqu'on tient compte de l'incertitude sur la section efficace differentielle.

c) 320 MeV, les nombreuses mesures de Berkeley aux alentours de 300 MeV ([11]), mesures qui précisent en particulier la polarisation aux petits angles de diffusion, et permettent ainsi d'évaluer le rôle des états à $l > 1$.

Le résultat de nos calculs est illustré fig. 2, 3 et 4, et résumé au tableau I. Les déphasages correspondant à une même énergie donnent tous des courbes pratiquement identiques.

([11]) O. CHAMBERLAIN, G. PETTENGILL, E. SEGRE et C. WIEGAND: *Phys. Rev.*, **95**, 1348 (1954).

TABLEAU I. — *Valeurs acceptables obtenues pour les déphasages* ${}^1K_0$ *et* δ_j *à* 170, 260 *et* 330 MeV, *dans l'hypothèse d'une polarisation positive ou négative.*

E (MeV)		$\mathcal{P} > 0$				$\mathcal{P} < 0$			
		${}^1K_0$	δ_0	δ_1	δ_2	${}^1K_0$	δ_0	δ_1	δ_2
170	1	24	13	— 23	9	27	— 14,5	21	— 9,8
	2	— 26	— 8,5	— 14	16	— 13	— 4,5	28	— 6,8
	3	— 37	— 24	2,5	12,5				
	4	7	— 57,5	7	4				
260	1	23	6	— 32,5	9,8	35	— 12,5	21,5	— 16
	2	— 35	13	— 22	15,6	— 27	— 9,5	20,5	— 10,7
	3	— 43	— 50	5	8,6				
330	1	29	9,5	— 26,5	20 4				
	2	— 10	— 4,5	— 16,5	28,8				
	3	— 25	— 21	— 6	28,2				

On notera que:

a) Sauf éventuellement à 260 MeV, l'interférence de la diffusion nucléaire avec la diffusion coulombienne provoque des effets nettement destructifs, ce qui permet de sélectionner avec assez de précision les seuls ensembles de solutions possibles. En particulier, à 330 MeV, il n'y a plus de combinaison satisfaisante susceptible de donner des polarisations négatives.

b) La prise en considération des seuls déphasages δ_j ne permet pas de traduire correctement la variation angulaire de la polarisation a 330 MeV. Une analyse de Fourier montre en effet que:

$$\mathcal{P}(\theta) = K \sin\theta \cos\theta \,(a + b\cos^2\theta + c\cos^4\theta)\,, \tag{9}$$

ce qui parait confirmer l'intervention des ondes ${}^3F$, comme il faut d'ailleurs s'y attendre à ces énergies.

c) Parmi les solutions obtenues dans l'hypothèse d'une polarisation positive, il existe une série, la série 3, vérifiant strictement l'inégalité

$$\delta_0 < \delta_1 < \delta_2 \tag{10}$$

et correspondant d'une part à une répulsion dans l'état $^3P_0$ et d'autre part à une attraction dans l'état $^3P_2$: Ceci parait conforme à ce que donne l'interaction du type spin-orbite envisagée en vue de l'interprétation de la formation de couches dans les noyaux lourds. Notons que, dans ces conditions, le déphasage S s'annule aux environ de 130 MeV et devient ensuite fortement négatif, ce qui correspond à peu près à ce que donnerait un potentiel central rectangulaire, muni d'un cœur répulsif de 0,6 à $0{,}7 \cdot 10^{-13}$ cm de rayon, et ajusté de façon à reproduire les propriétés de la diffusion singulet aux basses énergies ([12]).

Ce travail à été effectué dans le cadre des activités du Groupe de Physique Théorique du Laboratoire de Physique de l'École Normale Supérieure, sous la direction de Monsieur M. Levy, Maitre de Conférences. Je remercie Mr. Levy d'avoir bien voulu me confier cette étude.

([12]) M. Matsumoto et W. Watari: *Progr. Theor. Phys.*, **11**, 63 (1954).

RIASSUNTO (*)

I risultati delle misure di diffusione e di polarizzazione nelle esperienze di collisione semplice e doppia, ad energie comprese tra 100 e 400 MeV sono stati analizzati utilizzando gli sfasamenti subiti da un lato dall'onda ^1S, dall'altro dalle onde ^3P corrispondenti a un impulso totale $j = 0, 1, 2$. Soltanto un numero ristretto di soluzioni è in grado di dare un accordo soddisfacente con l'esperienza, dal punto di vista sia della diffusione che della polarizzazione. Tra queste soluzioni ne esistono alcune in grado di dare ragione dell'inversione dei livelli nucleari suggerita dalla teoria di Mayer-Jensen del modello degli strati, che corrispondono, almeno per quanto riguarda lo sfasamento ^1S, a un potenziale nucleare centrale dotato di nocciolo repulsivo di tipo Jastrow. È da notare, tuttavia, che la variazione angolare della polarizzazione in prossimità dei 300 MeV non può essere riprodotta se non utilizzando inoltre gli sfasamenti associati agli stati ^3F.

(*) *Traduzione a cura della Redazione.*

IL NUOVO CIMENTO Vol. I, N. 4 1° Aprile 1955

The Construction of Potentials from the S-Matrix for Systems of Differential Equations.

R. G. Newton (*) and R. Jost

The Institute for Advanced Study - Princeton, New Jersey

(ricevuto il 10 Gennaio 1955)

Summary. — The procedure for constructing all potentials belonging to a given S-matrix and prescribed eigenvalue is generalized to systems of equations of the type of the Schrödinger equation for S-states. The determination of the spectral function from the S-matrix is found to be essentially more complicated here than in the case of a single equation, and it leads to restrictions on the S-matrix to make the existence of a short range potential possible. If such a potential exists, it is uniquely determined by the S-matrix, the eigenvalues, and as many real, symmetric, positive semi-definite matrices as there are eigenvalues.

1. – Introduction.

In physics the problem arises of determining the potential which causes a given differential scattering cross-section (analysed in terms of phase shifts) and no bound states, or bound states with given energies. It has been shown [1,7] that under the assumption that the potential has a short range (i.e., its first and second absolute moments exist), is spherically symmetric and spin independent, it is uniquely determined by the phase shift of one angular mo-

(*) Frank B. Jewett Fellow.

(1) V. Bargmann: *Phys. Rev.*, **75**, 301 (1949).

(2) V. Bargmann: *Rev. Mod. Phys.*, **21**, 488 (1949).

(3) N. Levinson: *Kgl. Danske Videnskab Selsab, Mat.-fys. Medd.*, **25**, No. 9 (1949).

(4) R. Jost and W. Kohn: *Phys. Rev.*, **87**, 977 (1952).

(5) R. Jost and W. Kohn: *Phys. Rev.*, **88**, 382 (1952).

(6) R. Jost and W. Kohn: *Kgl. Danske Videnskab Selsab, Mat.-fys. Medd.*, **27**, No. 9 (1953).

(7) N. Levinson: *Phys. Rev.*, **89**, 755 (1953).

mentum, l, as a functilon of the energy, the energies of the, say L_l, bound states of that angular momentum, and a set of L_l parameters C_n.

The present paper represents a first step towards generalizing the procedure to certain types of non-central potentials such as that of the tensor force ([8, 9]) with spin-orbit coupling ([9]). It will not be general enough to include the « centrifugal barrier » which is always present with non-central and spin-orbit forces, and will therefore have no direct physical meaning. It must be regarded as mathematical in nature, and preparatory to work in progress now to include the r^{-2} singularity of the physically real case.

From a mathematical point of view, the problem treated in references ([1]) to ([7]) is that of determining all functions $q(r)$ such that those solutions of the equation

$$-\frac{\mathrm{d}^2}{\mathrm{d}r^2}y(r) + q(r)y(r) = Ey(r)\,, \qquad 0 \leqslant r < \infty\,, \tag{1.0}$$

which vanish at $r = 0$ have a prescribed asymptotic (for large r) phase, given for all $E > 0$, and such that (1.0) has a given set of eigenvalues E_n. The present paper deals with the generalization to finite systems of differential equations of the type (1.0). It is the restriction to function $q_{ij}(r)$ whose first and second absolute moments exist that makes it physically unrealistic.

Section 2 introduces the types of solutions needed, and the S-matrix. Section 3 deals with the eigenvalues and the point $E = 0$. The problem with eigenvalues is reduced to that without. In Section 4 an expression for the spectral function is derived, and the Gel'fand Levitan integral equation ([10, 11, 6]) is generalized to the matrix case. One thereby obtains the potential from the spectral function. Section 5 describes the procedure for obtaining the spectral function from the S-matrix (or the asymptotic phase) and the eigenvalues and a set of as many real, symmetric, positive semi-definite, matrices as there are eigenvalues. This step in the construction is much more intricate than in the case of only one equation (1.0). It leads to certain necessary restrictions on the S-matrix in order that it can be associated with a « short range » potential. Section 6 summarises the construction.

There are three appendixes: Appendix A contains a necessary and sufficient condition for the inverse of a matrix valued analytic function to have a simple pole. Appendix B proves a number of inequalities and estimates for solutions of the differential equation; they are mostly generalizations of such estimates

([8]) W. Rarita and J. Schwinger: *Phys. Rev.*, **59**, 436 (1941).

([9]) J. M. Blatt and V. F. Weisskopf: *Theoretical Nuclear Physics* (New York and London, 1952), pp. 94 ff; ([8]) and ([9]) are examples of references to this subject.

([10]) I. M. Gel'fand and B. M. Levitan: *Dokl. Akad. Nauk SSSR*, n. Ser., **77**, 557 (1951).

([11]) I. M. Gel'fand and B. M. Levitan: *Izv. Akad. Nauk SSSR*, **15**, 309 (1951).

contained in reference ([3]). Appendix C contains the proof that the S-matrix satisfies a Hölder condition under an assumption (2.3′) on the potential that is slightly more restrictive than the existence of the first two absolute moments. Such a Hölder condition proves to be a convenient sufficient condition for the processes in Section 5.

2. – Preliminaries.

Consider a system of differential equations of the type ([12])

$$y''_\alpha(E, r) + Ey_\alpha(E, r) = \sum_{\beta=1}^{N} y_\beta(E, r)V_{\beta\alpha}(r) , \qquad \alpha = 1, 2, ..., N, \tag{2.0}$$

where $V_{\alpha\beta}(r)$ is a real, symmetric $(N \times N)$-matrix. By analogy with the physical case where (2.0) is the Schrödinger equation, E and V will occasionally be referred to, respectively, as the energy and the potential. A set of N vector solutions of (2.0) can be put into the form of an $(N \times N)$-matrix, so that the former are the rows of the latter. This matrix then satisfies the differential equation

$$\psi''(E, r) + E\psi(E, r) = \psi(E, r)V(r) . \tag{2.1}$$

Instead of discussing a set of N vector solutions of the set of N equations (2.0) we shall always refer to a matrix solution to the equation (2.1).

It will be useful to introduce a norm in the space of $(N \times N)$-matrices:

$$|M| \equiv N \max_{\alpha,\beta=1,...,N} (|M_{\alpha\beta}|) , \tag{2.2}$$

which is readily seen to satisfy the triangle and Schwarz's inequalities. We assume that

$$\begin{cases} \int_0^\infty r|V(r)|\,dr < \infty , \\ \int_0^\infty r^2|V(r)|\,dr < \infty . \end{cases} \tag{2.3}$$

When convenient we shall strengthen (2.3) to read, for all α satisfying

$$1 - \varepsilon \leqslant \alpha \leqslant 2 + \varepsilon ,$$

([12]) Differentiation with respect to r is denoted by a prime.

$$(2.3') \qquad \int_0^\infty r^\alpha |V(r)|\,dr < \infty\,, \quad \text{and} \quad \lim_{R\to 0} R^{-\varepsilon}\int_0^\infty dr\,r\,|V(r+R) - V(r)| < \infty\,,$$

for some $\varepsilon > 0$.

We are interested in the following two solutions of (2.1): $F(k, r)$ is defined by the boundary condition

$$(2.4) \qquad \lim_{r\to\infty} \exp[ikr]\,F(k, r) = \mathbf{1}\,,$$

where $k^2 = E$, $G(k^2, r)$ is defined by boundary condition

$$(2.5) \qquad G(k^2, 0) = 0\,, \qquad G'(k^2, 0) = \mathbf{1}\,.$$

With assumption (2.3) on the potential such solutions always exist ([13]) and have the properties ([13]) for all r, that F is an analytic function of k for $\operatorname{Im} k < 0$, continuous and continuously differentiable for $\operatorname{Im} k \leqslant 0$, and G is an entire function of k. Just as in the case of ([3]) $N = 1$, it can be shown ([13]) that for large $|k|$

$$(2.6) \qquad G(k^2, r) = \mathbf{1}\,\frac{\sin kr}{k} + o(|k|^{-1}\exp[|\operatorname{Im} k|\,r])\,,$$

and for large $|k|$, $\operatorname{Im} k \leqslant 0$,

$$(2.7) \qquad F(k, r) = \mathbf{1}\exp[-ikr] + o(\exp[\operatorname{Im} kr])\,.$$

The Wronskian matrix ([14])

$$(2.8) \qquad W(\psi_1, \psi_2) \equiv \psi_1'\psi_2^\dagger - \psi_1\psi_2'^\dagger\,,$$

between two solutions of the same equation (2.1) is, by virtue of the symmetry of V, independent of r. It is, therefore, readily seen that the functions F and G satisfy

$$(2.9) \qquad W(F, F) = W(G, G) = 0\,,$$

since they do so for $r \to \infty$ or $r = 0$, respectively.

([13]) See Appendix B.

([14]) We use a dagger for hermitian conjugation, i.e., transposition and complex conjugation; a star for complex conjugation, and a superscript T for transposition.

A third solution of interest is $F(-k, r)$. For [15] real k

$$F(-k, r) = F^*(k, r)\,, \tag{2.10}$$

and one readily verifies that

$$W(F(k, r), F(-k, r)) = -2ik\,\mathbf{1}\,. \tag{2.11}$$

One then obtains with the help of (2.9) and its equivalent for $F(-k, r)$ (in an obvious notation)

$$\begin{pmatrix} F(k,r) & F'(k,r) \\ F(-k,r) & F'(-k,r) \end{pmatrix}\begin{pmatrix} F'^{T}(-k,r) & -F'^{T}(k,r) \\ -F^{T}(-(k,r) & F^{T}(k,r) \end{pmatrix} = 2ik\,\mathbf{1}. \tag{2.12}$$

Therefore the solutions $F(k, r)$ and $F(-k, r)$ form a fundamental system for $k \neq 0$ and (2.12) allows us to express G explicitly in terms of them by inverting the equation

$$(G(k^2, r), G'(k^2, r)) = (A(k), B(k))\begin{pmatrix} F(k,r) & F'(k,r) \\ F(-k,r) & F'(-k,r) \end{pmatrix} \tag{2.13}$$

for $r = 0$ and using (2.5):

$$G(k^2, r) = (2ik)^{-1}\big[F^T(k)F(-k, r) - F^T(-k)F(k, r)\big]\,, \tag{2.14}$$

where we have defined

$$F(k) = F(k, 0)\,. \tag{2.15}$$

Insertion of (2.5) in (2.14) yields the important relation

$$F^T(k)F(-k) = F^T(-k)F(k)\,. \tag{2.16}$$

In view of (2.16), equation (2.14) can be written

$$G(k^2, r) = -(2ik)^{-1}F^T(-k)\big[F(k, r) - S(k)F(-k, r)\big], \tag{2.17}$$

where [16]

$$S(k) = F(k)F^{-1}(-k) = S^T(k). \tag{2.18}$$

[15] From here on for the remainder of this section, k will be kept real.

[16] For. $k \neq 0$, $\operatorname{Im} k = 0$, $F^{-1}(k, r)$ always exists. This is easily proved by multiplying (2.11) on the left by a vector a, on the right by $a^\dagger$; and using (2.10):

$$a(F'\,F^\dagger - FF'^\dagger)a^\dagger = -2ikaa^\dagger\,.$$

If $aF = 0$, then the left hand side vanishes and the right hand side then shows that $a = 0$.

This impies that

$$S^{-1}(k) = S(-k), \tag{2.19}$$

and by (2.10), therefore, S is unitary:

$$S(k)\,S^{\dagger}(k) = \mathbf{1}\,. \tag{2.20}$$

By analogy with the case where (2.0) is the Schrödinger equation in physics, we call the symmetric and unitary matrix $S(x)$ the scattering matrix ([17]).

3. – Bound State and zero Energy Singularities.

If four a given k_0, $\operatorname{Im} k_0 < 0$, there exists a vector $a \neq 0$ so that $aF(k_0) = 0$, then an $aF(k_0, r)$ is a vector solution of (2.0) which vanishes both at $r = 0$ and $r \to \infty$. Hence k_0^2 is an eigenvalue of (2.0). It is shown in the standard fashion that all eigenvalues are real. We can therefore write $k_0 = -iK_0$, and, in view of physical applications, call $-K_0^2$ the energy of a bound state. The bound states therefore correspond exactly to the points in $\operatorname{Im} k < 0$ where $\det F(k) = 0$ and where, therefore, $F^{-1}(k)$ has a pole. For $\operatorname{Im} k = 0$, $k \neq 0$, $F^{-1}(k)$ is continuous, because F is so and by footnote ([16]); for $\operatorname{Im} k < 0$, $\operatorname{Re} k \neq 0$, $F^{-1}(k)$ is analytic; for $\operatorname{Im} k < 0$, $\operatorname{Re} k = 0$, $F^{-1}(k)$ may have a finite ([18]) number of poles and no other singularities.

We shall now prove the *theorem*:

All singularities of $F^{-1}(k)$ *in* $\operatorname{Im} k < 0$ *are simple poles.*

Differentiation of (2.1) with respect to k (indicated by a dot), transposition, multiplication by F on the left and subtraction from (2.1) multiplied by $\dot{F}^T$ on the right, yields, after integration and use of the boundary condition, for $\operatorname{Re} K > 0$

$$F(-iK, r)\,\dot{F}'^{T}(-iK, r) - F'(-iK, r)\,\dot{F}^{T}(-iK, r) = -2iK\int_r^{\infty} \mathrm{d}t\, F(-iK, t)\,F^{T}(-iK, t)\,. \tag{3.1}$$

Suppose that $F(-iK)$, $K > 0$, is a singular matrix, i.e., there exists a

([17]) C. MØLLER: *Kgl. Danske Videnskab Selsab, Mat.-fys. Medd.*, **22**, No. 19, (1946), p. 19.

([18]) This follows from the fact that $F(k) = \mathbf{1} - o(1)$ as $|k| \to \infty$, by (2.7), and (B.37). Since, thus, neither $|k| = \infty$ nor $k = 0$ can be a point of accumulation of zeros of $\det F(k)$ and the latter is analytic for $\operatorname{Im} k < 0$, it cannot vanish on the negative imaginary axis, except at a finite number of points.

vector $a \neq 0$ so that

$$aF(-iK) = 0 . \tag{3.2}$$

Due to the reality of the Schrödinger equation and the boundary condition for $F(-iK, r)$, $F(-iK, r)$ must be real, and a can therefore be chosen real too. Eq. (3.1) then shows that (where [19] $aF'(-iK) = \lim_{r\to 0} aF'(-iK, r)$).

$$aF'(-iK)\dot{F}^T(-iK)a^T \neq 0 . \tag{3.3}$$

Now suppose that there exists an $a \neq 0$ that satisfies, in addition to (3.2), the equation

$$bF(-iK) + a\dot{F}(-iK) = 0 \tag{3.4}$$

for some vector b. Multiplication of the transposed of (3.4) by $aF'(-iK)$ on the left and the use of (2.9) as well as (3.2) then yield

$$aF'(-iK)\dot{F}^T(-iK)a^T = 0 . \tag{3.5}$$

The contradiction between (3.3) and (3.5) can be resolved only by dropping the assumption that there exists an $a \neq 0$ that satisfies both (3.2) and (3.4). The theorem of Appendix A then proves the required result: $F^{-1}(k)$ has *simple poles* at the position of the bound states.

For a given eigenvalue there may be several linearly independent vectors [20] that satisfy (3.2). Let P_n be a projection [21] onto the space spanned by them for the n-th bound state [22]:

$$\text{range } P_n \equiv \text{kernel } (\mathbf{1} - P_n) \equiv \text{kernel } F(-iK_n) . \tag{3.6}$$

P_n can, moreover, be assumed hermitian. In view of the reality of $F(-iK_n)$, a^* annihilates $F(-iK_n)$ whenever a does; hence P_n^*, also hermitian, satisfies (3.6). Since there is only one hermitian projection with a given kernel, the hermitian P_n is real:

$$P_n = P_n^* = P_n^T . \tag{3.7}$$

Equations (3.6) and (3.7) determine P_n uniquely.

[19] See Appendix B for the existence of the limit.

[20] In the physical case, where the matrix character of V would mean the interaction of different angular momenta if it were not for the exclusion of the centrifugal term by (2.3), this would mean more than one mixture of angular momenta to form a bound state with the same energy.

[21] We mean by a projection simply an idempotent matrix ($P^2 = P$); hermiticity will not be implied in the definition.

[22] The kernel of a matrix M is the space annihilated by it, i.e., the set of all vectors x such that $xM = 0$; the range of M is the set of all vectors x for which there exist vectors y such that $x = yM$.

The projections P_n can now be used to reduce the case of bound states to that without bound states. This is accomplished by the following theorem.

Let $\{-K_n^2\}$, $n = 1, ..., L$, $0 < K_1 < ... < K_L$, be the bound state energies and $\{P_n\}$ the corresponding projections satisfying (3.6) and (3.7). Define a matrix $R = R_L(k)$ as follows:

$$R_0 = \mathbf{1}\,, \tag{3.8}$$

$$R_n(k) = \left(\mathbf{1} - P_n' \frac{2iK_n}{k + iK_n}\right) R_{n-1}(k)\,, \qquad n = 1, ..., L, \tag{3.9}$$

where

$$\text{range } P_n' = \text{kernel } (\mathbf{1} - P_n') = \text{kernel } \left[R_{n-1}(-iK_n) P_n R_{n-1}^{-1}(-iK_n)\right], \tag{3.10}$$

and

$$(P_n')^T = P_n'\,. \tag{3.11}$$

The new S-matrix

$$S_N(k) = R(k)\, S(k)\, R^{-1}(-k)\,, \tag{3.12}$$

which for real k is unitary and symmetric, can be written

$$S_N(k) = F_N(k)\, F_N^{-1}(-k)\,, \tag{3.13}$$

where $F_N(k)$ and $F_N^{-1}(k)$ are analytic in $\text{Im } k < 0$ and continuous in $\text{Im } k \leqslant 0$, except possibly at $k = 0$. For $\text{Im } k < 0$,

$$\lim_{|k| \to \infty} F_N(k) = \mathbf{1}\,. \tag{3.14}$$

Finally,

$$F(k) = R^{-1}(k) F_N(k)\,. \tag{3.15}$$

In order to prove this theorem we remove the bound state singularities from $F^{-1}(k)$ one by one. Let

$$F^{(1)}(k) = R_1(k)\, F(k)\,, \tag{3.16}$$

$$R_1(k) = \mathbf{1} - P_1 \frac{2iK_1}{k + iK_1}\,. \tag{3.17}$$

In a neighborhood of $k = -iK_1$ confined to the lower half plane, $F(k)$ can be expanded

$$F(k) = F_0 + (k + iK_1) F_1 + \ldots\,. \tag{3.18}$$

Equations (3.16) and (3.17) then yield

$$F^{(1)}(k) = -\frac{2iK_1}{k+iK_1} P_1F_0 + (F_0 - 2iK_1P_1F_1) + \dots . \tag{3.19}$$

But by (3.6),

$$P_1F_0 = 0 , \tag{3.20}$$

and hence $F^{(1)}(k)$ is analytic at $k = -iK_1$. Furthermore, suppose

$$xQ = 0 , \tag{3.21}$$

$$Q = F_0 - 2iK_1P_1F_1 . \tag{3.22}$$

Then (3.20) to (3.22) can be written

$$-2iK_1xP_1' = y , \tag{3.23}$$

$$\begin{cases} yF_0 = 0 , \\ xF_0 + yF_1 = 0 . \end{cases} \tag{3.24}$$

The last two equations are of the same form as (3.2) and (3.4), where it was proved that they imply $y = 0$. Hence by the second equation in (3.24),

$$xF_0 = 0 , \tag{3.25}$$

and therefore, by (3.6),

$$x = xP_1 . \tag{3.26}$$

But since $y = 0$, (3.23) and (3.26) show that $x = 0$. This proves that $F^{(1)}(-iK_1)$ possesses an inverse, and $(F^{(1)})^{-1}$ is regular at $k = -iK_1$. Clearly R_1^{-1} is regular everywhere in the lower half-plane, and so is R_1, except at $k = -iK_1$. No new singularities are thus introduced. Furthermore, as $|k| \to \infty$, $\lim R_1 = \mathbf{1}$. Fo real k, by (3.7),

$$R_1(-k) = (R_1^T(k))^{-1} = R_1^*(k). \tag{3.27}$$

It follows that $F^{(1)}(k)$ has all the relevant properties of $F(k)$: analyticity in the open lower half plane, continuity in the closed lower half plane, the limit $\mathbf{1}$ as $k \to \infty$; for real k it satisfies (2.10) with $r = 0$, and (2.16). Moreover, its inverse has singularities only at $k = -iK_n$, $n = 2, \dots, L$. The new S-matrix

$$S_1(k) = R_1(k)\, S(k)\, R_1^{-1}(-k) = F_1(k)\, F_1(-k)^{-1} \tag{3.28}$$

is, for $\operatorname{Im} k = 0$, unitary and symmetric and satisfies (2.19).

By a repetition of this method, all bound state singularities can be removed. Before the above procedure can be repeated, however, new projections must be defined. The matrix P_2 does not satisfy (3.6) with respect to $F_1(-iK_2)$, but with respect to $F(-iK_2)$. In view of the facts that for any non-singular matrix M

$$\text{kernel } (MA) \equiv (\text{kernel } A)M^{-1},$$

and

$$\text{kernel } (AM) \equiv \text{kernel } A,$$

it is clear that

$$P_2'' = R_1(-iK_2)\,P_2R_1^{-1}(-iK_2) \tag{3.29}$$

is a projection and satisfies

$$\text{range } P_2'' \equiv \text{kernel } (1 - P_2'') \equiv \text{kernel } F_1(-iK_2)\,. \tag{3.30}$$

Since $R_1(-iK_2)$ is not unitary, P_2'' is not hermitian. There exists, however, a hermitian projection P_2' with the same range; it is uniquely defined by (3.10) and (3.11) for $n = 2$. P_2' is, in fact, real, because $R_1(-iK_2)$ is real; it therefore satisfies (3.7) and (3.6) with respect to F_1. The procedure used for the removal of the singularity at $k = -iK_1$ may now be repeated to remove that at $k = -iK_2$. The theorem has thus been proved.

In contrast to the one dimensional case, it is, in general, not possible to remove the singularity at $k = 0$, if there is one, and still keep the S-matrix either unitary or symmetric. It will, nevertheless, be necessary to know the kernel of $F(0)$. This knowledge can be obtained from the S-matrix.

Equations (B.33) and (B.37) show that for $\operatorname{Im} k < 0$ one may write near $k = 0$

$$F(k) = F_0 + kF_1 + o(k)\,, \tag{3.33}$$

$$F^{-1}(k) = k^{-1}N_{-1} + R(k)\,, \qquad R(k) = o(k^{-1})\,. \tag{3.34}$$

Then by (B.39) and (B.40)

$$S(0) = F_0R(0) - F_1N_{-1} = 1 - 2F_1N_{-1}\,. \tag{3.35}$$

Equations (B.38) and (B.39) show that F_1N_{-1} is a projection of the type (3.6):

$$\text{range } (F_1N_{-1}) \equiv \text{kernel } (1 - F_1N_{-1}) \equiv \text{kernel } F(0)\,. \tag{3.36}$$

Therefore,

$$\text{kernel } F(0) \equiv \text{range } \tfrac{1}{2}(1 - S(0)) \equiv \text{kernel } \tfrac{1}{2}(1 + S(0))\,. \tag{3.37}$$

This can be expressed as follows: On the kernel space of $F(0)$,

$$S(0) = -\mathbf{1}\,, \tag{3.38}$$

while on the quotient space, in which elements whose difference lies in the kernel of $F(0)$ are identified,

$$S(0) = \mathbf{1}\,. \tag{3.39}$$

Equations (3.38) and (3.39) are the proper generalization of the scalar case, where $S(0) = 1$ if $f(0) \neq 0$, $S(0) = -1$, if $f(0) = 0$.

In view of (3.36), (3.37), (2.20), and (2.18), the projection

$$P_0 \equiv \tfrac{1}{2}(\mathbf{1} - S_N(0)) \tag{3.40}$$

satisfies (3.6) and (3.7) for F_N at $k = 0$ and can be used like the P_n's. The function

$$F_{N0}(k) \equiv R_0(k) F_N(k)\,, \tag{3.41}$$

with

$$R_0(k) = \mathbf{1} - P_0 i\varepsilon k^{-1}\,, \qquad \varepsilon > 0\,, \tag{3.42}$$

and its inverse are analytic for $\operatorname{Im} k < 0$, continuous for $\operatorname{Im} k \leqslant 0$. It also satisfies (3.14). The new S-matrix, however,

$$S_{N0}(k) \equiv F_{N0}(k)\, F_{N0}^{-1}(-k) = R_0(k)\, S_N(k)\, R_0^{-1}(-k)\,, \tag{3.43}$$

is in general no longer symmetric or unitary unless $S_N(0) = S(0) = \mathbf{1}$, i.e., $F^{-1}(0)$ exists. Nevertheless, it is still true that

$$S_{N0}(k) S_{N0}(-k) = \mathbf{1}\,, \tag{3.44}$$

and since, for $\operatorname{Im} k = 0$

$$R_0(-k) = R_0^*(k)\,,$$

(2.10) also holds for $F_{N0}(k)$.

One can obtain partial information about the bound states and a possible singularity at $k = 0$ from consideration of the determinant. The determinant of $F(k)$ will, in general, have multiple zeros at the position of the bound states. We shall prove the *theorem*:

The multiplicity of the zero of $\det F(k)$ at $k = -iK$ equals the dimensionality of the kernel of $F(-iK)$.

By (3.16),

$$f(k) \equiv \det F(k) = \det R_1^{-1}(k) \times \det F_1(k)\,, \tag{3.45}$$

where

$$R_1^{-1} = \mathbf{1} + P_1 \frac{2iK_1}{k - iK_1} \,. \tag{3.46}$$

There always exists a coordinate system in which P_1 is diagonal. Its diagonal elements will then be p_1 ones, where p_1 is the dimensionality of the kernel of $F(-iK_1)$, and the remainder, zeros. Therefore,

$$f(k) = \left(1 + \frac{2iK_1}{k - iK_1}\right)^{p_1} \det F_1(k) = \left(\frac{k + iK_1}{k - iK_1}\right)^{p_1} \det F_1(k) \,. \tag{3.47}$$

Since $\det F_1(-iK_1) \neq 0$, this proves the theorem.

Equations (3.33) and (3.37) can be used quite similarly to prove that near $k = 0$, $\operatorname{Im} k \leqslant 0$

$$f(k) = k^q(a_0 + o(1)) \,, \qquad a_0 \neq 0 \,, \tag{3.48}$$

if q is the dimensionality of the kernel of $F(0)$.

We now write

$$f(k) = |f(k)| \exp\left[i\eta(k)\right], \tag{3.49}$$

and it follows that

$$\frac{1}{2\pi i} \int \mathrm{d} \log f(k) = m \,, \tag{3.50}$$

where the integral extends over the path in Fig. 1 so that all zeros of $f(k)$ in $\operatorname{Im} k < 0$ are included; and m is the sum of the multiplicities of all zeros of $f(k)$ in $\operatorname{Im} k < 0$. As $R \to \infty$, the contribution from the large semi-circle vanishes. That from the small one is

$$\int \mathrm{d} \log f(k) = -iq\pi \,. \tag{3.51}$$

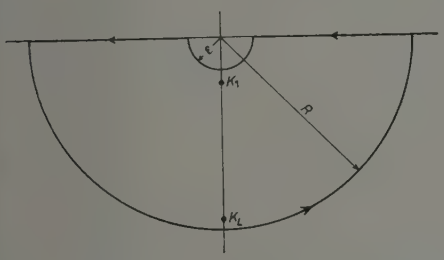

Fig. 1. – Path of integration in the complex k-plane, surrounding all zeros $-iK_1, \ldots, iK_L$ of $F(k)$.

Equations (3.50) and (3.51) readily yield

$$\lim_{\varepsilon \to 0} \lim_{R \to \infty} \left[-\eta(R) + \eta(-R) + \eta(\varepsilon) - \eta(-\varepsilon) + i \log \begin{vmatrix} f(R) & f(-\varepsilon) \\ f(-R) & f(\varepsilon) \end{vmatrix} \right] = 2\pi(m + \tfrac{1}{2} q). \tag{3.52}$$

Equation (2.10) shows that the logarithm vanishes, and therefore

$$\eta(0+) - \eta(0-) - \eta(\infty) + \eta(-\infty) = 2\pi(m + \tfrac{1}{2} q) \,. \tag{3.53}$$

Now (2.10) implies also that

$$\eta(-k) + \eta(k) = 2\pi n \,, \tag{3.54}$$

where n is an integer. If we demand that $\eta(k)$ be continuous in $(0, \infty)$ which we can since $f(k)$ is so and has no zeros there, then addition of (3.54) for $k \to \infty$ to (3.53) and subtraction of (3.54) for $k \to 0$, results in

$$\eta(0+) - \eta(\infty) = \pi(m + \tfrac{1}{2}q). \tag{3.55}$$

Finally, from the fact that $\det(F^{-1}) = (\det F)^{-1}$, and (2.18) and (2.20), it follows that we may define

$$\tfrac{1}{2} \log \det S(k) = i\eta(k) \,. \tag{3.56}$$

4. – Spectral Function and Potential.

The spectral function is obtained in the course of deriving the completeness relation. Consider, for an arbitrary matrix function $\mathcal{F}(r)$ sufficiently regular,

$$\Phi_1(k, r) = -\int_{r-\varepsilon}^{r} \mathrm{d}t \mathcal{F}(t) G^T(k^2, t) F^{-1}(k) F(k, r), \qquad \varepsilon > 0 \,. \tag{4.1}$$

If the bound state singularities are at $k = -iK_n$, $n = 1, \ldots, L$, $F^{-1}(k)$ has simple poles there whose residues we call $N^{(n)}_{-1}$, while F and G are analytic. Therefore

$$\int k \,\mathrm{d}k \, \Phi_1(k, r) = 2\pi \sum_{n=1}^{L} K_n \int_{r-\varepsilon}^{r} \mathrm{d}t \mathcal{F}(t) G_n^T(t) N^{(n)}_{-1} F_n(r) \,, \tag{4.2}$$

where $G_n(r) \equiv G(-K_n^2, r)$, $F_n(r) \equiv F(-iK_n, r)$ and the integral on the left extends over the contour of Fig. 1, enclosing all bound states. Due to (3.34), the radius of the small semi-circle can be allowed to shrink to zero.

Owing to the first line of (A.4), where $M_0 = F_0^{(n)}$, and (2.5),

$$N^{(n)}_{-1} F_n(r) = N^{(n)}_{-1} F_n'(0) G_n(r) \,. \tag{4.3}$$

We now define

$$C_n = 2iK_n N^{(n)}_{-1} F_n'(0) \,. \tag{4.4}$$

Due to (2.9), C_n is a real symmetric matrix. Multiplication of (3.1) by $N^{(n)}_{-1}$

on the left, by $N_{-1}^{(n)T}$ on the right, and use of (4.3), (4.4), (2.9), and (A.4), then lead to [23]

$$C_n = \int_0^\infty C_n G_n(r) G_n^T(r) C_n \, \mathrm{d}r = -4K_n^2 N_{-1}^{(n)} \left[\int_0^\infty \mathrm{d}r \, F_n(r) F_n^T(r) \right] N_{-1}^{(n)T} , \tag{4.5}$$

from which it follows that the quadratic form xCx^T is non-negative.

It follows from (3.1) that $aF_0^{(n)} = aF_n'(0) = 0$ implis $a = 0$. Since by (A.4), furthermore,

$$\text{range } N_{-1}^{(n)} \equiv \text{kernel } F_0^{(n)} , \tag{4.6}$$

(3.6) shows that

$$N_{-1}^{(n)} = N_{-1}^{(n)} P_n ,$$

and by (4.4),

$$\text{kernel } C_n \equiv \text{kernel } N_{-1}^{(n)} . \tag{4.7}$$

In view of (4.4), (4.5), and the symmetry of C_n we can therefore write

$$C_n = -N_{-1}^{(n)} A_n N_{-1}^{(n)T} , \tag{4.8}$$

where, by (3.7) and (4.5),

$$A_n = 4K_n^2 P_n \left[\int_0^\infty \mathrm{d}r \, F_n(r) F_n^T(r) \right] P_n \tag{4.9}$$

is a real, symmetric matrix with a non-negative associated quadratic form. Equations (4.7), (4.6), (3.6) and (4.9) show that

$$\text{kernel } A_n \equiv \text{kernel } P_n . \tag{4.10}$$

Equation (4.2) now becomes

$$\int k \, \mathrm{d}k \, \Phi_1(k, r) = -i\pi \sum_{n=1}^{L} \int_{r-\varepsilon}^{r} \mathrm{d}t \, \mathcal{F}(t) G_n^T(t) C_n G_n(r) . \tag{4.11}$$

For the integral over the large semi-circle, the asymptotic expressions for G and F, (2.6) and (2.7), can be used:

$$\int_{\text{s.c.}} \mathrm{d}k \exp[-ikr] \int_{r-\varepsilon}^{r} \mathrm{d}t \, \mathcal{F}(t) \sin kt = \frac{i\pi}{2} \mathcal{F}(r) + R(k, r) ,$$

[23] This is the proper generalization of the first equation in (1.10) of reference [6].

where $\lim R(k, r) = 0$ as $|k| \to \infty$. Therefore,

$$\mathcal{F}(r) = \frac{2i}{\pi} \int_{-\infty}^{\infty} k \, \mathrm{d}k \int_{r-\varepsilon}^{r} \mathrm{d}t \, \mathcal{F}(t) G^T(k^2, t) F^{-1}(k) F(k, r) + \\ + 2 \sum_{n=1}^{L} \int_{r-\varepsilon}^{r} \mathrm{d}t \, \mathcal{F}(t) G_n^T(t) C_n G_n(r) . \tag{4.12}$$

The fact that G is an even function of k, and equations (2.14) and (2.16) then yield, on adding to the k-integrand its value for $k \to -k$:

$$\mathcal{F}(r) = 2\pi^{-1} \int_{-\infty}^{\infty} k^2 \, \mathrm{d}k \int_{r-\varepsilon}^{r} \mathrm{d}t \, \mathcal{F}(t) G^T(k^2, t) \left[F^T(k) F(-k)\right]^{-1} G(k^2, r) + \\ + 2 \sum_{n=1}^{L} \int_{r-\varepsilon}^{r} \mathrm{d}t \, \mathcal{F}(t) G_n^T(t) C_n G_n(r) . \tag{4.13}$$

If we now define a symmetric matrix function $P(E)$ by

$$\begin{cases} P(-\infty) = 0, & \\ \dfrac{\mathrm{d}P(E)}{\mathrm{d}E} = \begin{cases} \pi^{-1} \sqrt{E} \left[F^T(\sqrt{E}) F(-\sqrt{E})\right]^{-1}, & E > 0 , \\ \sum\limits_n C_n \delta(E - E_n) , & E \leqslant 0 , \end{cases} \end{cases} \tag{4.14}$$

then

$$\mathcal{F}(r) = 2 \int_{r-\varepsilon}^{r} \mathrm{d}t \, \mathcal{F}(t) \int G^T(E, t) \, \mathrm{d}P(E) G(E, r) . \tag{4.15}$$

In the same way one obtains

$$\mathcal{F}(r) = 2 \int_{r}^{r+\varepsilon} \mathrm{d}t \, \mathcal{F}(t) \int G^T(E, t) \, \mathrm{d}P(E) G(E, r) \tag{4.16}$$

from

$$\Phi_2 = - \int_{r}^{r+\varepsilon} \mathrm{d}t \, \mathcal{F}(t) F^T(k, t) \left(F^T(k)\right)^{-1} G(k^2, r) . \tag{4.17}$$

Addition of (4.15) and (4.16) proves the completeness:

$$\mathcal{F}(r) = \int_{r-\varepsilon}^{r+\varepsilon} \mathrm{d}t \, \mathcal{F}(t) \int G^T(E, t) \, \mathrm{d}P(E) G(E, r) , \tag{4.18}$$

which can alxo be written

$$\int G^T(E, t) \, \mathrm{d}P(E) G(E, r) = \delta(t - r) , \tag{4.19}$$

and consequently,

$$(4.19') \qquad \int_0^\infty \mathrm{d}r\, \mathcal{F}(r)\mathcal{F}^T(r) = \int \left[\int_0^\infty \mathrm{d}r\, \mathcal{F}(r)\, G^T(E, r)\right] \mathrm{d}P(E) \left[\int_0^\infty \mathrm{d}r\, \mathcal{F}(r)\, G^T(E, r)\right]^T .$$

This proves that $P(E)$, defined by (4.14), is the spectral function. It depends only upon the bound state energies, the matrices C_n, and $F(k)$. The Gel'fand Levitan procedure finally connects the spectral function directly with the potential.

Equations (2.1) and (2.5) readily yield

$$(4.20) \qquad \int_0^r \mathrm{d}t\, G(E, t)\, G^T(E', t) = (E' - E)^{-1}\, W\big(G(E, r),\, G(E', r)\big) .$$

Using this equation, one obtains by precisely the same procedure as in reference ([6]), the equation corresponding to (1.12) there:

$$(4.21) \qquad G(E, r) = G_1(E, r) + \int_0^r \mathrm{d}t\, G_1(E, t)\, K(t, r),$$

where

$$(4.22) \qquad K(t, r) = \int G_1^T(E, t) \mathrm{d}\left[P_1(E) - P(E)\right] G(E, r) ,$$

and $G_1(E, r)$, $P_1(E)$ are the solution and spectral function, respectively, belonging to a suitable comparison potential $V_1(r)$ that satisfies (2.3). Again as in reference ([6]), (4.22) leads to the Gel'fand Levitan equation

$$(4.23) \qquad K(s, r) + g(s, r) + \int_0^r \mathrm{d}t\, g(s, t)\, K(t, r) = 0,$$

with

$$(4.24) \qquad g(s, r) = -\int G_1^T(E, s) \mathrm{d}\left[P_1(E) - P(E)\right] G_1(E, r) .$$

One obtains

$$(4.25) \qquad V(r) = V_1(r) + 2\frac{\mathrm{d}}{\mathrm{d}r} K(r, r)$$

by using

$$(4.26) \qquad \frac{\partial^2}{\partial r^2} K(t, r) - K(t, r) V(r) = \frac{\partial^2}{\partial t^2} K(t, r) - V_1(t)\, K(t, r) ,$$

and

$$(4.27) \qquad K(0, r) = 0 .$$

The proof that the homogeneous form of (4.23) has no solution also follows exactly reference ([6]) and rests on the statement immediately following (4.5). Equation (4.23), therefore, has a unique solution.

It remains to be checked whether the construction process yields a symmetric potential from a symmetric spectral function. If the constructed potential satisfies (2.3), then it follows with the help of (4.11), (2.6), (2.7), (2.17), (3.38), (3.39), and (4.19) that

$$\mathcal{G}(r, t) = -\int G^T(E, r)\, \mathrm{d}P(E)\, G(E, t) E^{-1} \tag{4.28}$$

exists for any r and t and is a Green's function for (2.1) with $E = 0$. If P is symmetric, then the Green's function satisfies.

$$\mathcal{G}(r, t) = \mathcal{G}^T(t, r) .$$

The same must then be true for its inverse, which exists uniquely and is given by (2.1). It thus follows that $V(r)$ is a symmetric matrix.

The construction of the potential from the spectral function $P(E)$ thus proceeds in precisely the same way as in the case of $N = 1$. The difficulty which remains is the transition from $S(k)$, the position of the bound state energies $-K_n^2$, $n = 1, \ldots, L$, and the corresponding real, symmetric positive semi-definite matrices A_n to the spectral function $P(E)$. According to (4.8) and (4.14), this transition is obtained, if we construct, from the mentioned quantities, the function $F(k)$. The next section is devoted to that. The matrices $N_{-1}^{(n)}$, needed for C_n, are then obtained from $F(k)$ as

$$N_{-1}^{(n)} = \lim_{k \to -iK_n} (k + iK_n) F^{-1}(k) . \tag{4.29}$$

If $S(k)$ is symmetric, then $F(k)$ satisfies (2.16), and $P(E)$ is symmetric.

5. – Construction of $F(k)$.

From a given S-matrix, we first remove the bound states and the singularity of $F^{-1}(k)$ at $k = 0$, if there is such, by means of the procedure of Section 3. For this purpose one needs, in addition to the bound state energies $-K_n^2$, the projection P_n of (3.6) and (3.7). They are obtained from the matrices A_n by (4.10) and (3.7). The new S-matrix is S_{N0} of (3.43). We shall see that there exist certain necessary restrictions on $S_{N0}(k)$ so that it can belong to a potential that satisfies (2.3) (or (2.3′)). We are, however, not going to prove that these restrictions suffice. The question of sufficient conditions for the

S-matrix to lead to such a potential (or, that of the asymptotic behavior of $V(r)$) is still open even in the scalar case ($N = 1$).

The construction of $F(k)$ from $S(k)$ has to proceed here quite differently from the scalar case ([3]). Most of following techniques are due to J. PLEMELJ ([24])

It will be convenient for the following to work in the unit circle rather than in the lower half plane. We therefore perform the transformation

$$z = \frac{k+i}{k-i} \tag{5.1}$$

and define

$$F_{N0}(k) \equiv \Phi_+(z) \quad \text{for} \quad \operatorname{Im} k \leqslant 0 . \tag{5.2}$$

The points on the circumference of the unit circle, $|z| = 1$, are denoted by t, and we define

$$S_{N0}(k) \equiv M(t) , \quad \text{for} \quad \operatorname{Im} k = 0 . \tag{5.3}$$

It is proved in Appendix C that under the assumption (2.3′) on the potential $M(t)$ satisfies a Hölder condition ([25]); due to (3.14), (2.10), (3.34), and (3.44), it fulfils the following equations

$$\begin{cases} M(1) = \mathbf{1} , \\ M(t)M(t^{-1}) = \mathbf{1} , \quad M(t^{-1}) = M^*(t) . \end{cases} \tag{5.4}$$

Further, we say that a (matrix valued) function $H_+(z)$ belongs to the class K_+ if $H_+(z)$ and $H_+^{-1}(z)$ are analytic in $|z| < 1$ and continuous in $|z| \leqslant 1$; $H_-(z)$ belongs to the class K_- if $H_-(z^{-1}) = K_+$. The intersection of K_+ and K_- is the set of all constant non-singular matrices.

The problem of solving (3.43) for $F_{N0}(k)$ is now that of solving

$$\begin{cases} M(t) = \Phi_+(t)\Phi_+^{-1}(t^{-1}) , \\ \text{with} \quad \Phi_+(1) = \mathbf{1} \quad \text{and} \quad \Phi_+(z) \varepsilon K_+ . \end{cases} \tag{5.5}$$

Lemma 1: If (5.5) has a solution, then this solution is unique. To prove this, let Φ_+ and Ψ_+ both satisfy (5.5) and introduce

$$A_+(z) = \Psi_+^{-1}(z)\Phi_+(z) .$$

([24]) J. PLEMELJ: *Monatsh. f. Math. u. Phys.*, **19**, 211 (1908).

([25]) A function $f(x)$ satisfies a Hölder condition if there exist two positive constants A and μ so that for any two points x_1 and x_2

$$|f(x_1) - f(x_2)| \leqslant A\,|x_1 - x_2|^{\mu} .$$

Then (5.5) and its equivalent for $\Psi_+(z)$ show that $A_+(z)\varepsilon K_+$ and $A_+(z)=A_+(z^{-1})$, so that $A_+(z)\varepsilon K_-$.

Therefore $A_+(z)=\text{const.}$, and by the boundary condition in (5.5), $A_-(z)\equiv\mathbf{1}$.

This proves Lemma 1.

Lemma 2: If the system

$$H_+(t) = M(t)H_-(t)\,, \qquad H_+(z)\varepsilon K_+\,, \qquad H_-(z)\varepsilon K_-\,, \tag{5.6}$$

has a solution, then (5.5) also has a solution.

For the proof we first show that any solution of (5.6) can be written as

$$\begin{cases} H_+(z) = H_+^0(z)C\,, \\ H_-(z) = H_-^0(z)C\,, \end{cases} \tag{5.7}$$

where C is a constant matrix, and H_+^0, H_-^0 is a special solution of (5.6). Equation (5.6) immediately yields

$$C = (H_+^0(z))^{-1}H_+(z) = (H_-^0(z))^{-1}H_-(z)\varepsilon K_+ \cap K_-\,,$$

and therefore (5.7), and C is constant. We can now impose the boundary condition

$$H_+(1) = H_-(1) = \mathbf{1}\,; \tag{5.8}$$

$H_+(z)$ and $H_-(z)$ are then uniquely defined. But by virtue of (5.4), we also have

$$H_-(t^{-1}) = M(t)H_+(t^{-1})\,,$$

and hence

$$H_+(z) = H_-(z^{-1})\,,$$

which shows that $H_+(z)$ solves (5.5) and proves Lemma 2.

Let us call K_+' the class of all vector values functions $\varphi_+(z)$ analytic in $|z|<1$ and continuous in $|z|\leqslant 1$; K_-' is the class of all vector valued functions $\varphi_-(z)$ such that $\varphi_-(z^{-1})\varepsilon K_-'$. Let n vectors $\varphi_+^{(1)}(z), \ldots, \varphi_+^{(n)}(z)$, $\varphi_-^{(i)}(z)\varepsilon K_-'$, $i=1,\ldots,n$, be called linearly independent if no linear combination

$$\varphi_+(z) = \sum_{i=1}^{n} C_i\varphi_+^{(i)}(z)\,, \qquad C_i = \text{const.}, \; i=1,\ldots,n,$$

has a zero inside the closed unit circle unless $C_1 = \ldots = C_n = 0$. We define

linear independence for members of K'_-, $\varphi_-(z)$, by requiring it in the above sense of $\varphi_-(z^{-1})$. From these definitions one immediately obtains

Lemma 3: If

$$\varphi_+(t) = M(t)\varphi_-(t)\,, \qquad \varphi_+(z)\varepsilon K'_+\,, \qquad \varphi_-(z)\varepsilon K'_-\,, \tag{5.9}$$

has N linearly independent solutions $\varphi_+^{(1)}(z)$, ..., $\varphi_+^{(N)}(z)$ and $\varphi_-^{(1)}(z)$, ..., $\varphi_-^{(N)}(z)$, then (5.6) has a solution, and vice versa.

If (5.6) has a solution, H_+ and H_-, then the vector

$$C = H_-^{-1}\varphi_- = H_+^{-1}\varphi_+\,, \tag{5.10}$$

where φ_+ and φ_- form an arbitrary solution of (5.9), must be constant. If, now, $\varphi_-^{(z)}(z_0) = 0$ for any $|z_0| \geqslant 1$, including $|z| = \infty$, then $C = 0$ and hence $\varphi_-(t) \equiv 0$. As a corollary of this statement one has

Lemma 4:. If (5.6) has a solution, then (5.9) has no non-trivial solution such that

$$\varphi_-(\infty) = 0\,. \tag{5.11}$$

We shall now show that if (5.9) has solutions, they can be found by solving a Fredholm equation. For that purpose we introduce the Hilbert transform operator, $\mathcal{H}$, defined on all square integrable functions on the circumference of the unit circle ([26]) by

$$(\mathcal{H}f)(t) = \frac{1}{\pi i} P \oint \frac{f(t')\,\mathrm{d}t'}{t - t'}\,, \tag{5.12}$$

where the integral extends over the circumference of the unit circle and P denotes the Cauchy principal value. The projection operator

$$\Pi = \tfrac{1}{2}(1 + \mathcal{H}) \tag{5.13}$$

has the following properties ([26]):

$$\varphi_+ \varepsilon K'_+ \quad \text{if and only if} \quad \Pi\varphi_+ = \varphi_+\,, \tag{5.14}$$

$$\varphi_- \varepsilon K'_- \quad \text{and} \quad \varphi_-(\infty) = \mu\,, \quad \text{if and only if} \quad (1 - \Pi)\varphi_- = \varphi_- - \mu\,. \tag{5.15}$$

It follows from this and the fact that Π is a projection operator, that for any square integrable (vector valued) function φ,

$$\Pi\varphi\varepsilon K'_+\,, \qquad (1 - \Pi)\varphi\varepsilon K'_- \quad \text{and} \quad [(1 - \Pi)\varphi](\infty) = 0\,. \tag{5.16}$$

([26]) E. C. TITCHMARSH: *Theory of Fourier Integrals* (Oxford, 1937), pp. 119 ff. The extension to vector and matrix valued function is trivial.

We can now say that (5.9) is equivalent to the following pair of equations:

$$M^{-1}(1-\Pi)M\varphi_- = 0\,, \tag{5.17a}$$

$$\Pi(\varphi_- - \mu) = 0\,. \tag{5.17b}$$

Adding these two equations one obtains

$$M^{-1}(1-\Pi)M\varphi_- + \Pi\varphi_- = \mu\,, \tag{5.18}$$

or, using (5.14) and (5.12),

$$\varphi_-(t) - \frac{1}{2\pi i}\oint \mathrm{d}t'\,\frac{M^{-1}(t)M(t') - \mathbf{1}}{t-t'}\,\varphi_-(t') = \mu\,. \tag{5.18'}$$

Since $M(t)$ satisfies a Hölder condition, this is a Fredholm equation.

Theorem I. (5.6) has a solution if and only if $M(t)$ satisfies the following conditions:

a) No non-trivial solution of ([27]) (5.18$'_o$) satisfies (5.17*b*) with $\mu = 0$.

b) For every given constant vector $\mu \neq 0$, (5.18′) has a solution that satisfies (5.17*b*).

Proof.: The necessity follows readily from Lemmata 3 and 4.

To show that *a*) and *b*) together are sufficient, we choose a system of N constant linearly independent vectors, $\mu^{(1)}, \ldots, \mu^{(N)}$. According to *b*), for each of them there exists a solution, $\varphi_-^{(i)}(z)$, of (5.18) which satisfies (5.17*a*) and (5.17*b*) separately, and hence solves (5.9). They must be linearly independent; for if

$$\varphi\ (z) \quad \sum_{i=1}^{N} C_i \varphi_-^{(i)}(z)$$

had a zero at $z = z_0$, $|z_0| \geqslant 1$, then

$$\psi_-(z) \equiv (z - z_0)^{-1}\varphi_-(z)$$

would be a solution of (5.9) which vanishes for $|z| \to \infty$. The function $\psi_-(z)$ would then solve (5.18) and (5.17*b*), both with $\mu = 0$. According to *a*), then, $\psi = 0$ and hence ([28]) $C_1 = \ldots = C_N = 0$. By Lemma 3, (5.6) has therefore a solution. This proves the theorem.

([27]) We refer to the homogeneous form of an integral equation by putting a subscript « *o* » on the number of the inhomogeneous equation.

([28]) Strictly speaking, the case $|z_0| = 1$ requires additional reasoning. It can be found in reference ([29]).

Theorem I, in a sense, solves the problem of finding the additional restrictions on $M(t)$, or $S_{N^0}(k)$, so that a short range potential can belong to it. We shall now treat further the case where $M(t)$ is symmetric and unitary. In view of Section 3 (the paragraph containing equations (3.40) to (3.44)), this will be the case when the original S-matrix equals **1** for $k = 0$. We call this the *normal case*. Finally we shall give a short account of the general theory of solving (5.9), due to PLEMELJ ([24]).

We now turn to the treatment of the normal case. The matrix $M(t)$ then satisfies, besides (5.4),

$$M^T(t) = M(t) . \tag{5.19}$$

Lemma 4': If, in the normal case, (5.6) has a solution, then neither (5.9) nor

$$\psi_+(t) = M^{-1}(t)\psi_-(t) , \qquad \psi_+(z)\varepsilon K'_+ , \qquad \psi_-(z)\varepsilon K'_- , \tag{5.9*}$$

have solutions which vanish at infinity.

The proof of this lemma is obtained directly from the application of Lemma 4 to the result of using (5.19) in (5.6):

$$(H_+^{-1}(t))^T = M^{-1}(t)(H_-^{-1}(t))^T . \tag{5.20}$$

Lemma 5: If, in the normal case, (5.6) is solvable, then $(5.18'_0)$ has only the trivial solution $\varphi \equiv 0$.

According to Lemma 4', no non-trivial solution of (5.18_0) can satisfy (5.17*a*) and (5.17*b*). The functions

$$\psi_+ \equiv -\Pi\varphi , \qquad \psi_- \equiv (1-\Pi)M\varphi , \tag{5.21}$$

which, by (5.16), have the properties

$$\psi_+\varepsilon K'_+ , \qquad \psi_-\varepsilon K'_- , \qquad \psi_-(\infty) = 0 , \tag{5.22}$$

are therefore not identically zero. But with (5.21) and (5.22), (5.18) reads exactly like (5.9*), while $\psi_-(\infty) = 0$. The contradiction with Lemma 4' can be resolved only if $\varphi \equiv 0$. Lemma 5 is thus proved.

The problem (5.9*) has a Fredholm equation associated with it in the same sense in which (5.18') is that of (4.9):

$$M(1-\Pi)M^{-1}\psi_- + \Pi\psi_- = \nu , \tag{5.18*}$$

or

$$\psi_-(t) - \frac{1}{2\pi i}\oint \mathrm{d}t' \frac{M(t)\,M^{-1}(t') - \mathbf{1}}{t - t'}\,\psi_-(t') = \nu , \tag{5.18*'}$$

where $v = \psi_-(\infty)$. Due to (5.19), the adjoint of the corresponding homogeneous equation reads

$$\chi(t) + \frac{1}{2\pi i} \oint dt' \frac{M^{-1}(t) M(t') - \mathbf{1}}{t - t'} \chi(t') = 0 . \tag{5.18'*T}$$

According to Lemma 4', the analogue of Lemma 5 for $(5.18_o'^*)$ also holds, and hence for $(5.18_o'^{*T})$ too:

Lemma 6: If, in the normal case, (5.6) has a solution, then $(5.18_o'^{*T})$ has only the trivial solution.

Lemmata 5 and 6 prove the second part of

Theorem II. In the normal case, (5.6), has a solution if and only if neither $(5.18_o')$ nor $(5.18_o'^{*T})$ have non-trivial solutions.

All we need supply now is the sufficiency proof. If $(5.18_o'^{*T})$ has no solution, then neither do $(5.18_o'^*)$ or (5.18_o^*). Thus (5.9*) has no non-trivial solution that vanishes at infinity. Since, by hypothesis, $(5.18_o')$ has no solution either, (5.18') can be solved for arbitrary μ. Put

$$\Pi(\varphi_- - \mu) \equiv -\psi_+ ; \qquad (1 - \Pi) M \varphi_- \equiv \psi_- , \tag{5.23}$$

where φ_- is a solution of (5.18'); then, by (5.16), ψ_+ and ψ_- solve (5.9*) and ψ_- vanishes at infinity. It follows that $\psi_+ \equiv \psi_- \equiv 0$, and hence that φ_- solves both equations (5.17) and consequently (5.6). This completes the proof of the theorem.

The condition in Theorem II can be stated as follows: The two equations

$$\tfrac{1}{2}(M^\dagger \hbar M - \hbar \mathbf{1})\chi = \pm \chi \tag{5.24}$$

must have no (non-trivial) solution; i.e., the Fredholm integral operator $\frac{1}{2}(M^\dagger \hbar M - \hbar \mathbf{1})$ must not have the eigenvalue ± 1. It is readily proved that this is equivalent to requiring that

$$\tfrac{1}{2} |\hbar M - M \hbar| < 1 , \tag{5.25}$$

where $|A|$ is the least upper bound of the operator A.

Finally we return to the general case and cite the fundamental

Theorem of Plemelj: Every matrix $M(t)$ that satisfies a Hölder condition can be written in the following form:

$$M(t) = H_+(t) N(t) H_-(t) , \qquad H_+ \varepsilon K_+ , \qquad H_- \varepsilon K_- , \tag{5.26}$$

where

$$N_{ij}(z) = \delta_{ij} z^{\mu_i} . \tag{5.27}$$

and the integers $\mu_1 \leqslant \mu_2 \leqslant \ldots \leqslant \mu_N$ are uniquely determined.

A way of constructing H_+, H_-, and the integers μ_i can be found in references ([24]) and ([29]). In terms of them, the conditions for (5.6) to have a solution in the general case can be stated as follows:

Theorem III. (5.6) has a solution if and only if

$$\mu_1 = \mu_2 = \ldots = \mu_N = 0 .$$

As a last result of the general theory we mention that $H_-(t)$ and $H_-(t)$, and therefore $\Phi_+(t)$ of (5.2), satisfy a Hölder condition ([29]).

6. – Summary.

We summarize the construction procedure:

Let a symmetric and unitary matrix valued function $S(k)$ that satisfies (2.19) and a Hölder condition (C.26), (5.1); a set of L positive numbers K_n, $n = 1, \ldots, L$; and a set of L real, symmetric, positive semi-definite matrices A_n, $n = 1, \ldots, L$, be given. Then one constructs the L projections, P_n, uniquely defined by (4.10) and (3.7), from the A_n, and forms $S_{N0}(k)$ by means of Section 3. In the normal case, $S(0) = \mathbf{1}$, one may test $S_{N0}(k)$ by Theorem II; if either of the equations (5.24) has a non-trivial solution, then there exists no short range potential corresponding to S; if neither do, or if (5.25) is fulfilled, then $F(k)$ can be constructed from solutions of the Fredholm equation (5.18′). In case $S(0) \neq \mathbf{1}$, Theorem I or Theorem III contain the necessary conditions for the existence of a short range potential; if (and only if) they are fulfilled, $F(k)$ can be constructed by solving (5.18′).

From $F(k)$ one obtains $N_{-1}^{(n)}$ by (4.29); the latter are then used in conjunction with the A_n to form the C_n by (4.8), which in turn are used, together with $F(k)$, to build the spectral function, $P(E)$, by (4.14). The Gel'fand Levitan equation, (4.23), finally leads to the potential (4.25). If that potential satisfies (2.3), then it leads to the S-matrix $S(k)$, bound states of energy $-K_n^2$ and mixtures given by the kernel of A_n, and to wave functions that satisfy (4.9). The total number of bound states, each counted as many times as they are degenerate, is directly given by (3.55).

([29]) N. I. MUSKELISHVILI: *Singular Integral Equations* (Groningen, Holland, 1953), pp. 381 ff.

Appendix A

Theorem. If $M(z)$ is a $(N\times N)$-matrix valued function of z, analytic for $|z|<1$, and so that $\det M(0)=0$, $\det M(z)\neq 0$ for $0<|z|<1$, then a necessary and sufficient condition for $M^{-1}(z)$ to have a simple pole at $z=0$ is that the system

$$\text{(A.0)}\qquad \begin{cases} aM(0)=0\,, \\ bM(0)+aM'(0)=0\,, \end{cases}$$

($M'(z)\equiv \mathrm{d}M/\mathrm{d}z$) implies that $a=0$.

The intuitive meaning of the criterion is that there must not exist a vector valued function $f(z)$, analytic and different from zero in a neighborhood including $z=0$, such that $fM=o(|z|)$.

Proof of the theorem: From the construction of the inverse it is clear that $M^{-1}(z)$ cannot have any singularities for $|z|<1$ other than a pole of finite order at $z=0$. Therefore, there must exist an n such that

$$\text{(A.1)}\qquad M^{-1}(z)=z^{-n}N_{-n}+z^{-n+1}N_{-n+1}+\dots\,,$$

$$\text{(A.2)}\qquad M(z)=M_0+zM_1+\dots\,.$$

The matrices N_m must satisfy the equations

$$\text{(A.3)}\qquad \sum_{i=0}^{m}M_iN_{i+m-n}=\sum_{i=0}^{m}N_{i+m-n}M_i=\mathbf{1}\delta_{mn}\,,\qquad m=0,1,\dots\,.$$

Now if M^{-1} has a *simple* pole at $z=0$, then $N_{-n}=\dots=N_{-2}=0$, $N_{-1}\neq 0$ and the equations

$$\text{(A.4)}\qquad \begin{cases} M_0N_{-1}=N_{-1}M_0=0\,, \\ M_0N_0+M_1N_{-1}=N_0M_0+N_{-1}M_1=\mathbf{1}\,, \end{cases}$$

have a solution $N_{-1}\neq 0$. Suppose (A.4) has such a solution and at the same time the system (A.0) ($M'(0)=M_1$) has a solution. Then by the first line of (A.0) and the second line of (A.4), $a=aM_1N_{-1}$ and therefore, by (A.0) $bM_0N_{-1}=-a$. The first equation in (A.4) then proves that $a=0$. This proves the *necessity* of the criterion.

Suppose now that the system (A.0) implies $a=0$. Equation (A.3) then shows that $N_{-n}=0$, and therefore $N_{-n+1}=0$, etc., until one arrives at (A.4). Thus M^{-1} has *at most* a simple pole at $z=0$. It is however clear that $M^{-1}(z)$ has to have a pole at $z=0$. The criterion is therefore also sufficient.

Appendix B

The purpose of this appendix is to derive some necessary estimates and inequalities under the assumption (2.3).

Define

$$\text{(B.1)}\qquad \mathcal{F}(k,r)=\exp[ikr]F(k,r)\,,$$

so that

$$\lim_{r\to\infty} \mathcal{F}(k, r) = \mathbf{1}\,, \qquad \operatorname{Im} k \leqslant 0\,. \tag{B.2}$$

Since $F(k, r)$ satisfies the integral equation

$$F(k, r) = \mathbf{1}\exp[ikr] + \int_r^\infty \mathrm{d}t\, k^{-1}\sin k(t-r)\,F(k, t)\,V(t)\,, \tag{B.3}$$

$\mathcal{F}(k, r)$ is the solution of the equation

$$\mathcal{F}(k\,r) = \mathbf{1} + \int_r^\infty \mathrm{d}t\, \mathcal{G}(k, t-r)\mathcal{F}(k, t)V(t)\,, \tag{B.4}$$

where

$$\mathcal{G}(k, t-r) = (2ik)^{-1}(1 - \exp[-2ik(t-r)])\,. \tag{B.5}$$

This Green's function is readily shown to satisfy the inequalities, for $t \geqslant r$:

$$|\mathcal{G}(k, t-r)| = \left|\int_0^{t-r} \mathrm{d}\varrho \exp[-2ik\varrho]\right| \leqslant t-r \leqslant t\,, \tag{B.6}$$

$$|\mathcal{G}(k, t-r)| \leqslant \frac{2(t-r)}{1+|k|\,(t-r)}\,. \tag{B.7}$$

Eq. (B.4) defines $\mathcal{F}(k, r)$ by means of successive approximations:

$$\mathcal{F}(k, r) = \sum_{n=0}^{\infty} \mathcal{F}_n(k, r)\,, \tag{B.8}$$

$$\begin{cases} \mathcal{F}_0(k, r) = \mathbf{1}\,, \\ \mathcal{F}_{n+1}(k, r) = \displaystyle\int_r^\infty \mathrm{d}t\, \mathcal{G}(k, t-r)\,\mathcal{F}_n(k, t)V(t)\,. \end{cases} \tag{B.9}$$

Eq. (B.6) shows that $\{\mathcal{F}_n\}$ is dominated by $\{\mathcal{H}_n\}$, where

$$\mathcal{H}_0 = 1, \qquad \mathcal{H}_{n+1}(r) = \int_r^\infty \mathrm{d}t\, t\,|V(t)|\,\mathcal{H}_n(t)\,, \tag{B.10}$$

and thus

$$\mathcal{H}_n(r) = (J(r))^n/n!, \tag{B.11}$$

where

$$J(r) = \int_r^\infty \mathrm{d}t\, t\,|V(t)|\,. \tag{B.12}$$

It follows that

$$|\mathcal{F}(k,r)| \leqslant \exp[J(r)] \leqslant \exp[J(0)] = K\ ; \tag{B.13}$$

$\mathcal{F}(k,r)$ is uniformly bounded. Resubstitution of (B.13) in (B.1) and use of (B.7) yield

$$|\mathcal{F}(k,r) - \mathbf{1}| \leqslant 2K \int_r^\infty \mathrm{d}t\, |V(t)|\, \frac{t-r}{1+|k|(t-r)} \leqslant 2\int_r^\infty \mathrm{d}t\, |V(t)|\, \frac{t}{1+|k|t}\,. \tag{B.14}$$

The right hand side of (B.14) shows that, as $|k| \to \infty$ in $\operatorname{Im} k \leqslant 0$, the left hand side vanishes, *uniformly in* r; or, with $z = -\operatorname{Im} k$

$$F(k,r) = \mathbf{1}\exp[-ikr] + o(\exp[-zr]) \quad \text{as} \quad |k| \to \infty\,. \tag{B.15}$$

Eq. (B.14) also immediately yields the non-uniform estimate

$$|F(k,r) - \mathbf{1}\exp[-ikr]| \leqslant \frac{2K}{|k|}\exp[-zr]\int_r^\infty \mathrm{d}t\, |V(t)|\,. \tag{B.16}$$

From the integral equation

$$G(k^2,r) = \mathbf{1}k^{-1}\sin kr + \int_0^r \mathrm{d}t\, k^{-1}\sin k(r-t)\, G(k^2,t)V(t) \tag{B.17}$$

one obtains similarly for $|k| \to \infty$,

$$G(k^2,r) = \mathbf{1}k^{-1}\sin kr + o(|k|^{-1}\exp[|z|r])\,. \tag{B.18}$$

Differentiation of (B.4) and (B.5) leads to

$$\mathcal{F}'(k,r) = -\int_r^\infty \mathrm{d}t \exp[-2ik(t-r)]\,\mathcal{F}(k,t)V(t)\,, \tag{B.19}$$

which exists for $r > 0$. But by (B.13) for $r \leqslant 1$,

$$|r\,\mathcal{F}'(k,r)| \leqslant K\int_r^\infty \mathrm{d}t\, r\,|V(t)| \leqslant K\left[\int_r^{\sqrt{r}} \mathrm{d}t\, t\,|V(t)| + \sqrt{r}\int_{\sqrt{r}}^\infty \mathrm{d}t\, t\,|V(t)|\right], \tag{B.20}$$

and therefore

$$\lim_{r\to 0} r\,\mathcal{F}'(k,r) = 0\,. \tag{B.21}$$

From the existence of $\int_0^\infty \mathrm{d}t\, t^2|V(t)|$ it follows similarly that

$$\lim_{r\to 0} \frac{\partial}{\partial k}\,\mathcal{F}'(k,r) = 0\,. \tag{B.22}$$

Since $\lim rf'(r) =$ implies $\lim rf(r) = 0$, as $r \to 0$, (B.21) and (B.22) yield

$$\lim_{r\to 0} rF'(k,r) = \lim_{r\to 0} r\dot{F}'(k,r) = 0\,. \tag{B.23}$$

Now consider, for $z = -\operatorname{Im} k \geqslant \varepsilon |k|$, $\varepsilon > 0$,

$$\text{(B.24)} \qquad \left| k \int_r^\infty \mathrm{d}t \left[F(k,t) F^T(k,t) - \mathbf{1} \exp[-2ikt] \right] \right| \leqslant$$

$$\leqslant |k| \int_r^\infty \mathrm{d}t \left| F(k,t) - \mathbf{1} \exp[-ikt] \right| \left| F(k,t) + \mathbf{1} \exp[-ikt] \right| =$$

$$= |k| \int_0^\infty \mathrm{d}t \exp[-2tz] \left| \mathcal{F}(k,t) - \mathbf{1} \right| \left| \mathcal{F}(k,t) + \mathbf{1} \right| \leqslant$$

$$\leqslant 2K|k| \int_0^\infty \mathrm{d}t \exp[-2tz] J(t) \leqslant 2K|k| \left[\int_0^{z^{-\frac{1}{2}}} \mathrm{d}t \exp[-2tz] J(o) + \right.$$

$$\left. + \int_0^\infty \mathrm{d}t \exp[-2tz] J(z^{-\frac{1}{2}}) \right] \leqslant 2K \left[J(o) \varepsilon^{-\frac{1}{2}} |k|^{\frac{1}{2}} + \tfrac{1}{2} J(|k|^{-\frac{1}{2}}) \varepsilon^{-1} \right] \to 0 \quad \text{as} \quad |k| \to 0 .$$

Therefore, if the k origin is approached inside a cone $\operatorname{Im} k = -\varepsilon' \operatorname{Re} k$, $\varepsilon > 0$ then

$$\text{(B.25)} \qquad \lim_{k \to 0} k \int_r^\infty \mathrm{d}t \, F(k,t) F^T(k,t) = \mathbf{1} \lim_{k \to 0} k \int_r^\infty \mathrm{d}t \exp[-2ikt] = -\tfrac{1}{2} i \mathbf{1} .$$

Now precisely as (3.1) was derived, one obtains for $\operatorname{Im} k \leqslant 0$,

$$\text{(B.26)} \qquad F(k,r) \dot{F}'^T(k,r) - F'(k,r) \dot{F}^T(k,r) = 2k \int_r^\infty \mathrm{d}t \, F(k,t) F^T(k,t) .$$

If $F(0)$ is singular, i.e., if there exists a vector $a \neq 0$ so that

$$\text{(B.27)} \qquad aF(0) = 0 ,$$

then $aF'(k,r)$ must be continuous at $k = r = 0$ because then there must exist a vector b so that $aF(0,r) = bG(0,r)$. Therefore

$$\lim_{r \to 0} aF(0,r) \dot{F}'^T(0,r) = \lim_{r \to 0} \left(aF(0,r)/r \right) \left(r \dot{F}'^T(0,r) \right) =$$

$$= \lim_{r \to 0} aF'(0,r) \lim_{r \to 0} r \dot{F}'^T(0,r) = 0 ,$$

by (B.23). Equations (B.25) and (B.26) then yield

$$\text{(B.28)} \qquad aF'(0) \dot{F}^T(0) a^T = iaa^T .$$

Suppose there exists a vector b so that

$$\text{(B.29)} \qquad bF(0) + a\dot{F}(0) = 0 .$$

One then obtains

$$aF'(0)\dot{F}^T(0)a^T = 0 \tag{B.30}$$

in the same manner as (3.5) from (3.4). Comparison of (B.30) and (B.28) shows that the equations (B.27) and (B.29) imply $a=0$. The theorem of Appendix A then proves that the inverse of

$$f(k) \equiv F(0) + k\dot{F}(0) \tag{B.31}$$

has a simple pole at the origin:

$$f^{-1}(k) = N_{-1}k^{-1} + N_0 + \dots . \tag{B.32}$$

By the mean value theorem, for $\operatorname{Im} k \leqslant 0$, near $k = 0$

$$F(k) = f(k) + R_0(k), \qquad R_0(k) = o(|k|). \tag{B.33}$$

We then define

$$R_1(k) = F^{-1}(k) - f^{-1}(k) \tag{B.34}$$

and readily obtain

$$R_1 = -f^{-1}[R_0 f^{-1}(\mathbf{1} + R_0 f^{-1})^{-1}], \tag{B.35}$$

where $R_0 f^{-1} = o(1)$. It follows that

$$R_1(k) = o(|k|^{-1}) \quad \text{near} \quad k = 0, \tag{B.36}$$

so that

$$F^{-1}(k) = N_{-1}k^{-1} + o(|k|^{-1}). \tag{B.37}$$

The following equations must, of course, be satisfied:

$$F(0)N_{-1} = N_{-1}F(0) = 0, \tag{B.38}$$

$$\dot{F}(0)N_{-1} + F(0)R_1(0) = N_{-1}\dot{F}(0) + R_1(0)F(0) = \mathbf{1}, \tag{B.39}$$

where

$$F(0)R_1(0) \equiv \lim_{|k|\to 0} F(0)R_1(k) \tag{B.40}$$

must exist, even if $R_1(0)$ does not.

Appendix C

In this appendix we shall use (2.3′) to prove that, after transferring the real line onto the unit circle via (5.1), the S-matrix satisfies a Hölder condition there.

Substitution of (B.13) into (B.4) yields for $r = 0$ and by (B.7)

$$(C.1)\qquad |F(k)-\mathbf{1}| \leqslant K\left|\int_0^\infty \mathrm{d}r\, \mathcal{G}(k,r)V(r)\right| \leqslant 2K\int_0^\infty \frac{\mathrm{d}r\, r}{1+|k|r}\,|V(r)| \leqslant$$

$$\leqslant 2K\left[\int_0^{|k|^{-1}} 2\,\mathrm{d}r\, r^{1-\varepsilon}|V|\,|k|^{-\varepsilon} + \int_{|k|^{-1}}^\infty \mathrm{d}r\, r^{1-\varepsilon}|V|\,|k|^{-1+1-\varepsilon}\right] = 2K|k|^{-\varepsilon}\int_0^\infty \mathrm{d}r\, r^{1-\varepsilon}|V|\,.$$

With the assumption (2.3′), therefore,

$$(C.2)\qquad F(k) = \mathbf{1} + 0(|k|^{-\varepsilon}) \quad \text{as} \quad |k| \to \infty\,.$$

Next we differentiate (B.4) with respect to k:

$$(C.3)\qquad \dot{\mathcal{F}}(k,r) = \int_r^\infty \mathrm{d}t\left[\dot{\mathcal{G}}(k,t-r)\mathcal{F}(k,t) + \mathcal{G}(k,t-r)\dot{\mathcal{F}}(k,t)\right]V(t)\,.$$

The first integral on the right hand side of

$$(C.4)\qquad \left|\int_r^\infty \mathrm{d}t\,(\dot{\mathcal{G}}(k,t-r))\mathcal{F}(k,t)V(t)\right| \leqslant K\int_0^\infty \mathrm{d}t\,|V(t)|\,|\mathcal{G}(k,t)|\,|k|^{-1} -$$

$$+\,|k|^{-1}\left|\int_r^\infty \mathrm{d}t(t-r)\mathcal{F}(k,t)\,V(t)\exp\left[2ik(r-t)\right]\right|,$$

is of the same form as (C.1), and hence $0(|k|^{-1-\varepsilon})$ as $|k| \to \infty$. Consider the second:

$$(C.5)\qquad I = \int_{-\infty}^\infty \mathrm{d}t\, v(t)\exp\left[-2ikr\right],$$

where

$$(C.6)\qquad v(t) = \begin{cases} t\mathcal{F}(k,t+r)V(t+r)\,, & t \geqslant 0\,,\\ 0\,, & t < 0\,. \end{cases}$$

By a shift of the origin of r by $\xi = \pi|k|^{-1}$ and addition of the result to (C.5) one obtains

$$I = -\int_{-\infty}^\infty \mathrm{d}t v(t+\xi)\exp\left[-2ikt\right] = \tfrac{1}{2}\int_{-\infty}^\infty \mathrm{d}t\big(v(t) - v(t+\xi)\big)\exp\left[-2ikt\right],$$

and therefore by (B.13) and (2.3′), for sufficiently large $|k|$,

$$(C.7)\qquad |I| \leqslant \tfrac{1}{2}\int_{-\infty}^{\infty} dt\, |v(t) - v(t+\xi)| \leqslant \tfrac{1}{2}K \int_{0}^{\xi} dt\, t\, |V(t+r)| +$$

$$+ \tfrac{1}{2}K\int_{0}^{\infty} dt\, t\, |V(t+r+\xi) - V(t+r)| + \tfrac{1}{2}\int_{0}^{\infty} dt\, t\, |V(t+r))|\, \mathcal{F}(k, t+r+\xi) -$$

$$- \mathcal{F}(k, t+r)| + \tfrac{1}{2}K\xi^{\varepsilon}\int_{\xi}^{\infty} dt\, |V(t+r)| \leqslant \tfrac{1}{2}K\xi^{\varepsilon}\int_{0}^{\infty} dt\, t^{1-\varepsilon}\, |V(t)| +$$

$$+ \tfrac{1}{2}K\xi^{\varepsilon}\left[\xi^{-\varepsilon}\int_{0}^{\infty} dt\, t\, |V(t+\xi) - V(t)|\right] + \tfrac{1}{2}K\xi^{\varepsilon}\int_{0}^{\infty} dt\, t\, |V(t)| +$$

$$+ \tfrac{1}{2}K\xi^{\varepsilon}\int_{0}^{\infty} dt\, t^{1-\varepsilon}\, |V(t)| \leqslant K'\xi^{\varepsilon} = K''\, |k|^{-\varepsilon},$$

because it is readily proved by (B.4), (B.13), and (B.6) that as a consequence of (2.3′)

$$(C.8)\qquad |\mathcal{F}(k, t+\xi) - \mathcal{F}(k, t)| \leqslant K\xi^{\varepsilon}.$$

Substitution of (C.4) and (C.8) in (C.3) therefore leads to

$$(C.9)\qquad |\dot{\mathcal{F}}(k, r)| \leqslant |K|\, |k|^{-1-\varepsilon} + \left|\int_{r} dt\, \mathcal{G}(k, t-r)\dot{\mathcal{F}}(k, t)V(t)\right|.$$

If one sets $K^{-1}\, k^{1+\varepsilon}\, \mathcal{F}(k, r) = f(k, r)$, one obtains precisely as (B.13) was derived, that $f(k, r)$ is uniformly bounded, and thus for $r = 0$

$$(C.10)\qquad \dot{F}(k) = 0(|k|^{-1-\varepsilon}) \quad \text{as} \quad |k| \to \infty.$$

We now prove from (C.2) and (C.10), and the fact that $F(k)$ is continuous and has a continuous derivative for all real k, that it satisfies a Hölder condition on the unit circle after the transformation (5.1). It follows from the mean value theorems and (C.10) that there exists a K and a ν_0 so that for all $|k| > K$, $0 < \nu \leqslant \nu_0$, $|k| \leqslant |k'| \leqslant \nu|k|$,

$$(C.11)\qquad |F(\nu k) - F(k)| \leqslant |\dot{F}(k')|\, |\nu - 1|\, |k| \leqslant C\, |k|^{-\varepsilon}\, |\nu - 1| \leqslant$$

$$\leqslant C'\left|\frac{k\nu - k}{(k+i)(k\nu+i)}\right|^{\varepsilon};$$

similarly, for $|k| \geqslant K$, $\nu \geqslant \nu_0$, by (C.2)

$$(C.12)\qquad |F(\nu k) - F(k)| \leqslant C''\, |k|^{-\varepsilon} \leqslant C'''\left|\frac{k\nu - k}{(k+i)(k\nu+i)}\right|^{\varepsilon}.$$

Thus for $|k_1| > K$ and any k_2

$$|F(k_1) - F(k_2)| \leqslant A \left| \frac{k_1 - k_2}{(k_1 + i)(k_2 + i)} \right|^{\varepsilon}. \tag{C.13}$$

On the other hand, (C.13) certainly holds if $|k_1| \leqslant K$ and $k_2 \leqslant K_1$ since $F(k)$ is continuously differentiable. If k_1 and k_2 are interchanged, (C.13) must hold for $|k_2| \geqslant K$ and any k_1. Therefore, (C.13) is true for any k_1 and any k_2.

We now perform the transformation (5.1) and set

$$F(k) = F_1(z). \tag{C.14}$$

Equation (C.13) then readily leads to

$$|F_1(z_1) - F_1(z_2)| \leqslant C|z_1 - z_2|^{\varepsilon} \tag{C.15}$$

for any z_1 and z_2 with $|z_1| = |z_2| = 1$.

In order to prove the Hölder condition for $S(z)$, a strengthening of (B.37) is required. This we obtain from (2.3′) again. We write (C.3) as

$$\begin{aligned} \dot{\mathcal{F}}(k, r) - \dot{\mathcal{F}}(0, r) = \int_r^{\infty} \mathrm{d}r \big[& (\dot{\mathcal{G}}(k, t-r) - \dot{\mathcal{G}}(0, t-r)) \mathcal{F}(k, t) + \\ & + \dot{\mathcal{G}}(0, t-r)(\mathcal{F}(k, t) - \mathcal{F}(0, t)) + (\mathcal{G}(k, t-r) - \mathcal{G}(0, t-r)) \dot{\mathcal{F}}(k, t) + \\ & + \mathcal{G}(0, t-r)(\dot{\mathcal{F}}(k, t) - \dot{\mathcal{F}}(0, t)) \big] V(t). \end{aligned} \tag{C.16}$$

Now by (B.13) and (2.3′)

$$\begin{aligned} & \left| \int_0^{\infty} \mathrm{d}t \, (\dot{\mathcal{G}}(k, t) - \dot{\mathcal{G}}(0, t)) \mathcal{F}(k, t) V(t) \right| \leqslant \\ & \leqslant K \int_0^{\infty} \mathrm{d}t \, |V(t)| \, |\dot{\mathcal{G}}(k, t) - \dot{\mathcal{G}}(0, t)| \leqslant K' \int_0^{\infty} \mathrm{d}r \, r^2 |V| \, \frac{r|k|}{1 + r|k|} \leqslant \\ & \leqslant K' \left[\int_0^{R} \mathrm{d}r \, r^2 |V| \, |k|^{\mu} + \int_R^{\infty} \mathrm{d}r \, r^{2+\varepsilon} |V| \, |k|^{\mu} \right] \leqslant K'' |k|^{\mu}, \end{aligned} \tag{C.17}$$

where $R = |k|^{-1+\mu}$, $\mu = \varepsilon/(1 + \varepsilon)$. Furthermore as $k \to 0$,

$$\int_r^{\infty} \mathrm{d}t \, \dot{\mathcal{G}}(0, t-r)(\mathcal{F}(k, t) - \mathcal{F}(0, t)) V(t) = 0(|k|), \tag{C.18}$$

$$\int_r^{\infty} \mathrm{d}t \, (\mathcal{G}(k, t-r) - \mathcal{G}(0, t-r)) \dot{\mathcal{F}}(k, t) V(t) = 0(|k|), \tag{C.19}$$

and hence one obtains from (C.16), for $|k|$ sufficiently small,

$$\dot{\mathcal{F}}(k,r)-\dot{\mathcal{F}}(0,r) \leqslant C|k|^{\mu}+\int_{r}^{\infty} dt\,(t-r)(\dot{\mathcal{F}}(k,t)-\dot{\mathcal{F}}(0,t))V(t) \quad \text{(C.20)}$$

It follows, as (C.10) does from (C.9) that

$$\dot{F}(k)=\dot{F}(0)+0(|k|^{\mu}), \quad \text{as} \quad k\to 0. \quad \text{(C.21)}$$

The mean value theorem leads to

$$\begin{cases} \dot{F}(k) = \dot{F}(0)+k\ddot{F}(0)+R_0(k), \\ R_0(k)=0(|k|^{1+\mu}), \quad \text{as} \quad k\to 0, \end{cases} \quad \text{(C.22)}$$

which replaces (B.33). It is then readily seen that (B.37) is replaced by

$$\dot{F}^{-1}(k)=N_{-1}k^{-1}+0(|k|^{-1+\mu}), \quad \text{(C.23)}$$

and that

$$\dot{F}_0R_1(k)=\mathbf{1}-\dot{F}(0)N_{-1}+0(|k|^{\mu}). \quad \text{(C.24)}$$

This equation finally strengthens (3.35) to read

$$S(0)=\mathbf{1}-2F_1N_{-1}+0(|k|^{\mu}) \quad \text{as} \quad k\to 0. \quad \text{(C.25)}$$

After transforming to the unit circle, it readily follows from (C.15), (C.25) and the fact that $F^{-1}(k)$ is continuous and differentiable in the open intervals $(0,\infty)$ and $(-\infty,0)$, that $S_1(z)=S(k)$ satisfies a Hölder condition for $z=1$:

$$|S_1(z_1)-S_1(z_2)|\leqslant A|z_1-z_2|^{\mu}. \quad \text{(C.26)}$$

RIASSUNTO (*)

Si generalizza a sistemi di equazioni del tipo dell'equazione di Schrödinger per gli stati S il procedimento per la costruzione di tutti i potenziali appartenenti a una matrice S data e degli autovalori assegnati. Si trova che la determinazione della funzione spettrale a partire dalla matrice S è in questo caso intrinsecamente più complicata che non nel caso di una equazione singola e conduce a restrizioni sulla matrice S tali da render possibile l'esistenza di un potenziale di « short-range ». Se un tale potenziale esiste, è unicamente determinato dalla matrice S, dagli autovalori, e da tante matrici semidefinite, positive, simmetriche, reali quanti sono gli autovalori.

(*) *Traduzione a cura della Redazione.*

IL NUOVO CIMENTO Vol. X, N. 4 1° Aprile 1955

Energy Levels of ^{56}Fe and ^{27}Al by the Inelastic Scattering of 15 MeV Neutrons.

R. Ramanna (*), N. Veeraraghavan and P. K. Iyengar

Tata Institute of Fundamental Research - Bombay, India

(ricevuto il 18 Gennaio 1955)

Summary. — A stilbene scintillation spectrometer has been used to study the neutrons inelastically scattered by iron and aluminium for an incident monoenergetic beam of 15 MeV neutrons. Using good geometry counts were taken with and without the scatterer in position and the results were analysed by a ratio method. For iron, levels have been obtained at 7.6, 5.8, 4.5 and 1.9 MeV. For aluminium, levels have been obtained at 8.1, 5.8, 4.0 and 3.0 MeV. Comparison with existing data from γ-ray measurements is given.

The energy levels of intermediate and heavy nuclei can be obtained by studying the energy distribution of inelastically scattered neutrons from a monoenergetic beam of fast neutrons incident on the scatterer. In the process of scattering a compound nucleus is formed with an excitation energy equal to the sum of the incident energy and the binding energy of the neutron. The neutrons are re-emitted by the compound nucleus in energy groups leaving the target nucleus in various excited states. The energy of each excited level is given by the difference in the energy of the incident neutrons and the various scattered groups. If the incident neutron energy is high enough to excite the target nucleus to the region of overlapping levels, the scattered neutron spectrum will have, besides the groups due to lower energy levels, a maxwellian distribution of neutrons of low energy. From the maxwellian distribution the nuclear temperature of the scattering nucleus corresponding to the incident excitation energy can be calculated [1].

(*) Reactor group, Atomic Energy Commission.

[1] B. G. Whitmore: *Phys. Rev.*, **92**, 654 (1953); G. K. O'Neill: *Phys. Rev.*, **95**, 1235 (1954).

The residual nucleus which is left in an excited state decays by emission of γ-rays. A study of these γ-rays also gives the energy levels. In general, the energies of these γ-rays correspond to the energy levels of the scattering nucleus and can be obtained with a resolution of the order of 10% depending on the energy of the γ-rays. However, it is difficult to establish the levels uniquely by this method since the γ-rays may be emitted in cascade. It is therefore necessary to determine the levels by the study of scattered neutron groups.

Fast neutron spectra are usually obtained by using proton recoil detectors. Cloud chambers ([2]) and photographic plates ([3]) have been used in the past, but they suffer from the disadvantage of the tediousness of reading and evaluating proton recoil tracks. With scintillation counters or proportional counters ([4]) filled with hydrogen or helium and employing electrical counting a high degree of statistical accuracy is possible.

Using scintillation neutron counters with anthracene and stilbene crystals POOLE ([5]) and ELIOT *et al.* ([6]) have studied the energy levels of various elements up to 2.5 MeV with D-D neutron source. SCHERRER *et al.* ([7,8]) have estimated the γ-ray energies emitted in inelastic scattering by various elements for incident neutrons of 14 MeV from the D(t, n)-^{4}He reaction. They have used a NaI scintillation γ-ray spectrometer and their work indicates the difficulties in measuring high energy γ-rays. BROWNE *et al.* ([9]) have determined the energy levels of ^{27}Al up to 6 MeV by the inelastic scattering of 8 MeV protons. In the present investigation neutron groups inelastically scattered by iron and aluminium in the energy region 7 to 15 MeV have been studied using scintillation spectroscopy and the energy levels have been determined in a direct manner.

1. – Neutron Source and Experimental Arrangement.

The neutrons were produced by D(t, n)-^{4}He reaction using 300 keV deuterons from a Cockcroft and Walton type accelerator and a zirconium-tritium target. For this incident deuteron energy the neutron beam has 14.2 and

([2]) R. N. LITTLE, R. W. LONG and C. E. MANDEVILLE: *Phys. Rev.*, **69**, 414 (1946).
([3]) P. H. STELSON and W. M. PRESTON: *Phys. Rev.*, **86**, 132 (1952).
([4]) H. H. BARSCHALL, M. E. BATTAT, W. C. BRIGHT, E. R. GRAVES, T. JORGENSEN and J. H. MANLEY: *Phys. Rev.*, **72**, 881 (1947).
([5]) M. J. POOLE: *Phil. Mag.*, **44**, 1398 (1953).
([6]) E. A. ELIOT, D. HICKS, L. E. BEGHIAN and H. HALBAN: *Phys. Rev.*, **94**, 144 (1954).
([7]) V. E. SCHERRER, R. B. THEUS and W. R. FAUST: *Phys. Rev.*, **89**, 1268 (1953).
([8]) V. E. SCHERRER, R. B. THEUS and W. R. FAUST: *Phys. Rev.*, **91**, 1476 (1953).
([9]) C. P. BROWNE, S. F. ZIMMERMAN and W. W. BUECHNER: *Phys. Rev.*, **96**, 725 (1954).

15.4 MeV energies at 90° and 0° respectively. The scatterer and detector were arranged in good geometry as shown in Fig. 1. The aluminium and iron scatterers were rectangular blocks ($10 \times 7 \times 4$ cm each), the maximum dimension being of the order of the mean free path for scattering in these elements for 15 MeV neutrons. The scintillation spectrometer consisted of an E.M.I. 6260 photomultiplier with three identical stilbene crystals ($1.5 \times 1.5 \times 0.9$ cm each) mounted on the photocathode side by side. The last four stages of the photomultiplier were shorted and it was worked at 935 V. The crystals were shielded from the direct neutron beam by a polythene cone absorber and neutrons scattered at 90° to the incident beam were detected. Pulses from the photomultiplier were amplified and analysed by a forty channel pulse analyser. A second scintillation counter was used to monitor the neutron intensity.

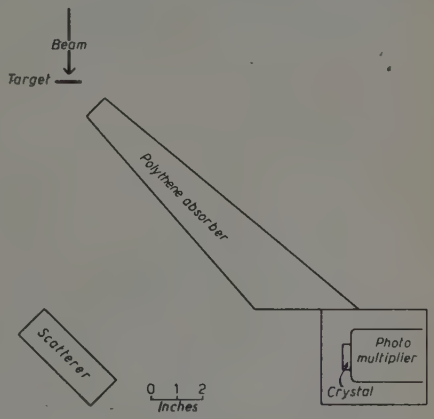

Fig. 1. Experimental arrangement.

2. – Experimental Procedure.

A preliminary experiment was performed to calibrate the spectrometer. The scintillation counter was arranged to detect the 14.2 MeV neutrons at 90° to the incident deuteron beam. The proton recoil pulse distribution obtained with the analyser is shown in Fig. 2. This agrees with the expected proton recoil distribution for incident monoenergetic neutrons. This spectrum was differentiated and the pulse height corresponding to 14.2 MeV proton recoil was obtained from the position of the maximum. For organic crystals the pulse height versus the energy of the particles is not strictly linear. BIRKS [10] has computed the relative pulse heights against proton energy for anthracene. Using this relationship for stilbene also, since stilbene is known to behave

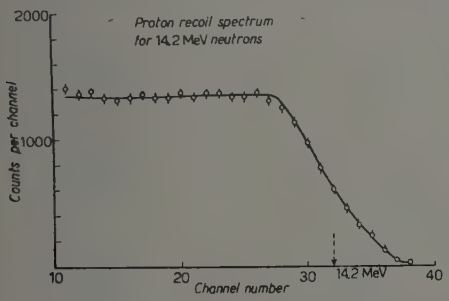

Fig. 2. Proton recoil spectrum for 14.2 MeV neutrons.

[10] J. B. BIRKS: *Proc. Phys. Soc.*, **64** A, 874 (1951).

similar to anthracene, the pulse heights were converted to proton recoil energies and thus the energy scale obtained for the scintillation counter. This calibration is shown in Fig. 3 and 4.

Pulse analyser readings were taken with and without the scatterer in position. Because of low intensity counts had to be taken for long durations extending over several days. The pulse

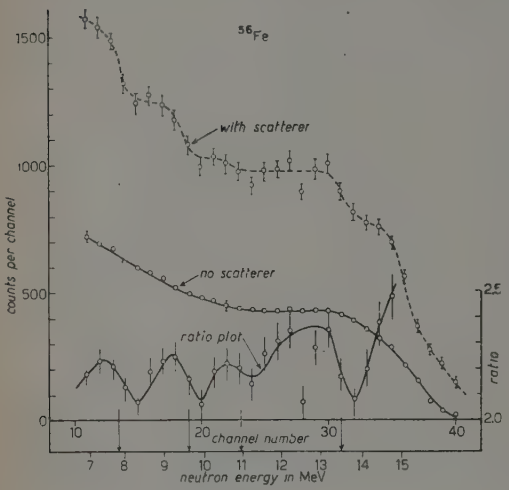

Fig. 3.

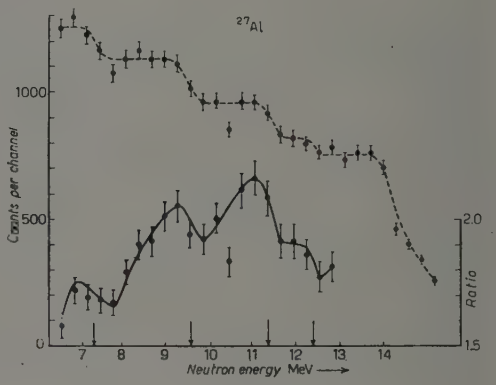

Fig. 4.

height distributions obtained for iron and aluminium are shown in Fig. 3 and 4. The curve with the scatterer in position shows steps which correspond to neutron groups. Since the polythene cone does not cut off the direct neutrons completely, the curve without the scatterer shows a smooth pulse height distribution due to degraded neutrons leaking through the cone. The ratio of the counts per channel with the scatterer in position to that without the scatterer in position is plotted in Fig. 3 and 4. This is done to bring out the positions of the scattered neutron groups more clearly as explained by ELIOT *et al.* (6). However since in this case the background is not due to direct monoenergetic neutrons the steps in the ratio plot are not separated by plateaus but by slow rises. From the ratio plot the energy of the scattered neutron groups is taken as shown in Fig. 3 and 4.

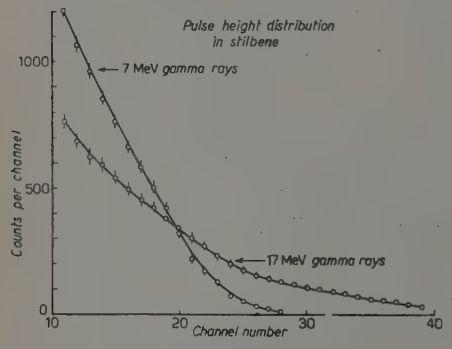

Fig. 5. Pulse height distribution in stilbene.

In order to study the effect of γ-rays accompanying inelastic scattering, the pulse height spectra due to monoenergetic 7 MeV γ-rays from the ^{19}F(p, γ)

reaction and 17 MeV γ-rays from the $^{7}Li(p, \gamma)$ reaction incident on the detector were obtained and are shown in Fig. 5. As expected they have a smoothly decreasing pulse height distribution and hence it was concluded that the steps in the proton recoil pulse height distribution with the scatterer in position are not due to γ-rays.

3. – Results and Discussion.

The overall stability of the electronic equipments was better than 2%. The resolution of the spectrometer as obtained from the D-t spectrum at 90° was found to be 10 %.

^{56}Fe. – From the ratio plot (Fig. 3) neutron groups were observed at 7.8, 9.6, 10.9 and 13.5 MeV corresponding to energy levels at 7.6, 5.8, 4.5 and 1.9 MeV respectively.

KIEHN and GOODMAN ([11]) have, by studying the γ-rays emitted in inelastic scattering of 2.5 MeV neutrons by iron, established levels at 0.85, 2.09 and 2.25 MeV. The 1.9 MeV level observed in the present work agrees well with the latter two levels obtained by them within experimental error.

SCHERRER *et al.* ([7]) have estimated γ-ray energies at 3.3, 4.4, 5.8, 7.1 and 8.75 MeV due to inelastic scattering of 14 MeV neutrons by iron. Of these the 4.4, 5.8 and 7.1 MeV γ-rays could be interpreted as due to the direct transitions to the ground state from levels at 4.5, 5.8 and 7.6 MeV observed in the present work. The two sets of values agree within experimental error. The 3.3 MeV γ-rays in their work could be either due to a transition from the 4.5 to 0.85 MeV level, 5.8 to 1.9 MeV level or from the 7.6 to 4.5 MeV level, since no neutron group is observed corresponding to the 3.3 MeV level. As our investigation of the neutron spectrum is only from 7 MeV to 15 MeV, the 8.75 MeV level could not be verified.

^{27}Al. – From the ratio plot (Fig. 4) neutron groups were observed at 7.3, 9.6, 11.4 and 12.4 MeV corresponding to energy levels at 8.1, 5.8, 4.0 and 3.0 MeV respectively. SCHERRER *et al.* ([8]) have estimated γ-ray energies at 1.7, 4.5 and 5.4 MeV due to inelastic scattering of 14 MeV neutrons by aluminium. These workers ([12]) have also observed γ-rays at 0.05, 0.89, 1.05, 1.20, 1.70 and 2.20 MeV for inelastic scattering of 3.2 MeV neutrons by aluminium.

In the following table the results of the present work are compared with those of γ-ray measurements.

([11]) R. M. KIEHN and C. GOODMAN: *Phys. Rev.*, **93**, 177 (1954).

([12]) V. E. SCHERRER, B. A. ALLISON and W. R. FAUST: *Phys. Rev.*, **96**, 386 (1954).

Scatterer	Energy levels by Neutron groups (Present Work) MeV	Gamma ray energies (other workers) MeV	Remarks
Iron	—	8.75	Not verified.
	7.6	7.1	Agreement within exp. error.
	5.8	5.8	»
	4.5	4.4	»
	—	3.3	Probably due to cascade emission.
	1.9	2.25 2.09	Agreement within exp. error.
	—	0.85	Not possible to observe.
Aluminium	8.1	—	—
	5.8	5.4	Agreement within exp. error.
	4.0	4.5	»
	3.0	—	—
	—	2.20	Not observed.
	—	1.70 1.20 1.05 0.89 0.05	Not possible to observe.

Our thanks are due to Mr. B. V. Joshi for changing the ion source to a radio-frequency type. Our thanks are also due to Messrs. P. N. Rama Rao, M. P. Navalkar, C. S. Somanathan and S. K. Amberdaker for running the accelerator and for help in taking counts for many hours over extended periods.

RIASSUNTO (*)

Uno spettrometro a scintillazione a stilbene è stato usato per lo studio dello scattering anelastico dei neutroni da parte del ferro e dell'alluminio per un fascio monoenergetico incidente di neutroni di 15 MeV. Con una buona disposizione sperimentale si sono eseguiti conteggi con e senza interposizione dello « scatterer » e i risultati sono stati analizzati per mezzo di rapporti. Si sono ottenuti per il ferro livelli a 7,6, 5,8, 4,5 e 1,9 MeV. Per l'alluminio si sono ottenuti livelli a 8,1, 5,8, 4,0 e 3,0 MeV. Si confrontano i risultati delle misure coi dati esistenti.

(*) *Traduzione a cura della Redazione.*

On the Interpretation of Fission Asymmetry According to the Liquid Drop Nuclear Model.

U. L. Businaro
Laboratori CISE - Milano

S. Gallone
Istituto di Fisica dell'Università e Laboratori CISE - Milano

(ricevuto il 19 Gennaio 1955)

Summary. — The possibility is examined, on the liquid drop-model, that the asymmetrization in the low energy nuclear fission may take place after the system, in evolving along its reaction path, has passed the symmetric saddle. The energy surface is investigated beyond the symmetric saddles both by extrapolating well-known formulae, valid in the small deformation range, and by using a representation in which the energy of shapes slightly different from an arbitrarily prolated basic ellipsoid may be calculated. The results obtained seem to indicate that along the effective symmetric reaction path there exists an « inversion » point, beyond which, in the case of incipient motion, a small asymmetric deformation would tend to grow.

1. – Introduction.

The marked asymmetry exhibited in the low energy fission of heavy nuclei has not yet been completely interpreted in terms of a theory based on the simple liquid-drop model. This may be due, among other reasons, to the analytical difficulties encountered in the computation of the energy of a deformed nucleus for sufficiently general and large deformations.

Among various works [1-3] on this subject, the ENIAC computations of Frankel and Metropolis are the most complete. These authors do not find asymmetric saddles, in particular the effect due to the addition of a small

(1) N. Bohr and J. A. Wheeler: *Phys. Rev.*, **56**, 426 (1939).
(2) R. D. Present and J. K. Knipp: *Phys Rev.*, **57**, 751, 1188 (1940).
(3) S. Frankel and J. K. Metropolis: *Phys. Rev.*, **72**, 914 (1947).

asymmetric deformation to the symmetric saddle shape, is not energetically favoured (4). They thus think, according to the mentioned results, that the liquid-drop model does not favour fission asymmetry.

In a recent work (5), HILL and WHEELER reexamine the situation and show, on dynamical grounds, that an asymmetric fission is indeed possible even with a saddle of symmetrical character. They also think that asymmetrical saddles may exist for nuclei sensibly lighter than Uranium.

On the base of these last observations it might be of some interest to find out whether an asymmetrization of the nucleus could be favoured for configurations following the passing of the symmetrical saddle. The results of the calculations seem to indicate that such a circumstance may actually occur.

The results of Section 1 are based on the extrapolation of known formulae whose validity is restricted to the small deformation range. In Section 2 an attempt is made to extend the conclusions of section 1 to a case in which the validity of the calculation is not necessarily restricted to shapes differing only slightly from the sphere.

1. – Following PRESENT and KNIPP (2), the nuclear shape may be described with a Legendre expansion of the following type:

$$R(\mu) = R_0 \left[1 + a_0 + \sum_{i=1}^{\infty} a_i P_i(\mu) \right], \tag{1}$$

where R_0 is the radius of the undeformed nucleus, a_0 is determined by the condition of volume conservation (nuclear fluid incompressibility) and a_1 by the condition of center of mass fixity. Under these conditions these authors give for the energy of the deformed nucleus an expression which is valid for small values of the deformation parameters. The relevant terms for the considerations which will follow are given here:

$$\begin{aligned} \frac{\Delta E}{E_s} = {} & \frac{2}{5}(1-x)a_2^2 - \frac{4}{105}(1+2x)a_2^3 - \frac{1}{175}\left(38 - \frac{314}{7}x\right)a_2^4 - \\ & - \frac{4}{35}(1+3x)a_2^2 a_4 + \left(1 - \frac{10}{27}x\right)a_4^2 + \frac{2}{7}\left(\frac{5}{2} - \frac{10}{7}x\right)a_3^2 - \\ & - \frac{8}{105}\left(1 + \frac{23}{7}x\right)a_2 a_3^2 + \ldots . \end{aligned} \tag{2}$$

x is the well-known parameter introduced by BOHR and WHEELER (1) and E_s indicates the surface energy of the undeformed nucleus.

If the even terms of (2) are considered, the condition that the deform-

(4) The range of nuclei studied by FRANKEL and METROPOLIS extends up to $x = 0.65$.
(5) D. L. HILL and J. A. WHEELER: *Phys. Rev.*, **89**, 1102 (1953).

ation energy be stationary leads to an expression for the fission threshold valid in the neighbourhood of $x = 1$. This expression is identical, up to the order considered in $(1 - x)$, to that calculated by BOHR and WHEELER using different deformation parameters which will be used in the following section.

One obtains for the fission threshold:

$$\frac{\Delta E_f}{E_s} = \frac{98}{135}(1-x)^3 - \frac{11\,368}{34\,425}(1-x)^4 + \dots . \tag{3}$$

The equilibrium deformation, to the first order in $(1 - x)$, is defined by the following value of the deformation parameter a_2:

$$\bar{a}_2 = \frac{7}{3}(1-x) - \dots . \tag{4}$$

This deformation represents, for values of x slightly less than 1, an elongated shape of unstable equilibrium (saddle shape), while, for x slightly greater than 1, the equilibrium form is flattened and unstable only with respect to non-axial deformations.

For $x > 1$ the spherical form is of unstable equilibrium, while for $x < 1$ it corresponds to stable equilibrium. This situation is illustrated in Fig. 1, where x is plotted as a function of a_2.

The asymmetry terms in a_3 allow the study of nuclear stability with respect to deformations of P_3 type. It is seen that the spherical form corresponds to stable equilibrium with respect to this type of deformation when x is less than 7/4. One may ask what the effect of such a deformation would be if superimposed on a deformation a_2 of P_2 type.

For values of x slightly less than 7/4 the deformation of P_3 type becomes energetically favoured as a_2 reaches the « inversion » value:

$$a_2^i = \frac{50}{63}\left(\frac{7}{4} - x\right) + \dots , \tag{5}$$

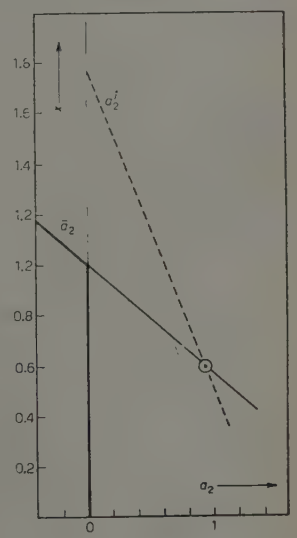

Fig. 1*a*. – Line $\bar{a}_2$ (as given by (4)) indicates the non spherical equilibrium shape. The x axis corresponds to equilibrium in the spherical form. The thick line means stable equilibrium (*) and the thin line unstable equilibrium. The « inversion » line a_2^i (given by (5)) is also shown in the figure.

(*) For the line a_2 in the region $x > 1$ the equilibrium is stable with respect to to axial deformations only.

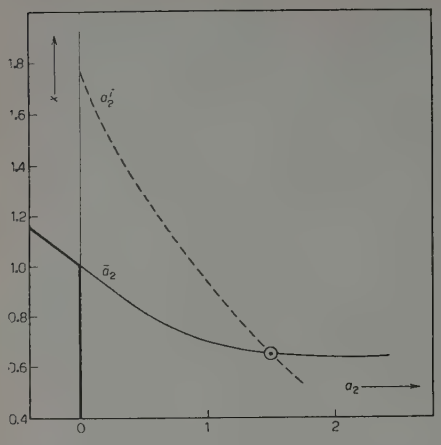

Fig. 1*b*. – As for 1*a*. Curve $\bar{a}_2$ comes from the work of FRANKEL and METROPOLIS ([3]). Curve a_2^i represents a further approximation of (5) and is deduced from the formula of PRESENT and KNIPP ([2]).

for which the second derivative of the potential energy with respect to a_3 changes sign. Equation (5) thus defines an « inversion » line which is plotted in Fig. 1*a*. The geometrical significance of such an « inversion » on the energy surface is illustrated in Fig. 2*a*, which refers to a value of x slightly less than 7/4. As for the character of the motion in the neighbourhood of a_2^i, the analysis of Appendix II shows, supposing incipient motion, that the frequency of the lowest normal mode of asymmetric oscillations vanishes, or is already imaginary, when a_2 reaches the value a_2^i. This last consideration remains valid even for incipient motions around symmetrical configurations of « inversion » greatly different from the sphere.

There remains to examine the existence of « inversion » along the effective symmetrical reaction path, for the values of x of practical interest ($x < 1$).

In order to simplify the analytical difficulties connected with the solution of this problem a fictitious reaction path corresponding to pure ellipsoidal deformations is substituted to the effective one (Section 2). A linear extrapolation of the results obtained in the case of small deformations would lead however to the following conclusions illustrated in Fig. 1*a* and 2*b*.

For $x \sim 0.6$ the linear series $\bar{a}_2$ bifurcates and new equilibrium shapes, corresponding to asymmetric saddles, come into existence. Other asymmetric equilibrium figures slightly differing from the sphere appear when x approaches 7/4, because for this value of x the linear equilibrium series corresponding to the spherical form becomes unstable for a deformation of P_3 type. It is however not very likely that these

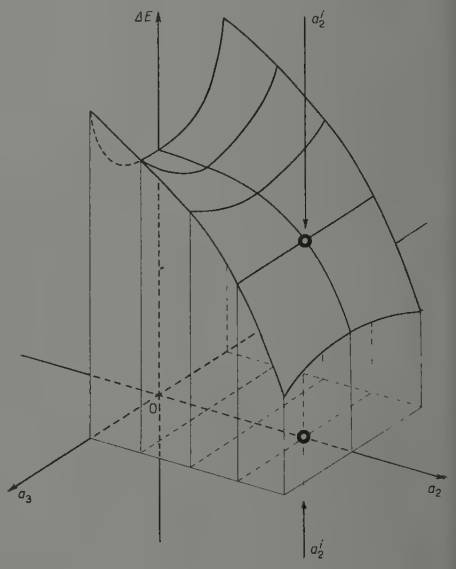

Fig. 2*a*. – A qualitative representation of the energy surface for a value of x slightly less than 7/4, as a function of a_2 and a_3. The position of the « inversion » point is shown.

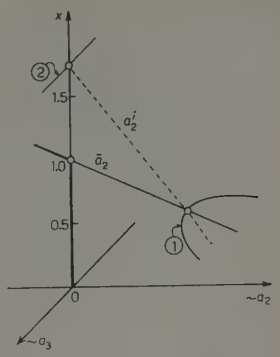

Fig. 2*b*. – Another version of Fig. 1*a* in which the possible equilibrium configurations for various x values are indicated as a function of a_2 and a_3. In addition to the lines already shown in Fig. 1*a* curves 1 and 2 which emerge normally to the plane (x, a_2) are also indicated. Curve 1 indicates the asymmetric equilibrium figures which bifurcate from the linear series $\bar{a}_2$. These asymmetric figures would correspond to asymmetric saddles on the energy surface. Line 2 indicates the beginning of a series of asymmetric equilibrium shapes, which initiates by bifurcation of the spherical series at

$$x = 7/4.$$

asymmetric equilibrium shapes have anything to do with the asymmetric fission of heavy nuclei ($x \sim 0.75$) at low energy.

The existence of the « inversion » point seems to favour, on the contrary, a progressive amplification of the asymmetrical components of nuclear motion once the « inversion » elongation has been reached.

Fig. 1*b* illustrates a refinement of the linear extrapolation of Fig. 1*a* concerning the existence and the position of the « bifurcation » shape.

2. – In order to accomplish the analytical investigation mentioned at the end of section 1, a representation already used by WICK (6), which is suitable for the description of small deformations around a basic ellipsoid of revolution, may be adopted. The advantage of this parametrisation lies in the possibility of calculating the deformation energy of rather elongated shapes, the eccentricity of the basic ellipsoid being an arbitrary parameter.

In the system of curvilinear coordinates defined by

$$\text{(6)} \qquad \begin{cases} x = \sqrt{r^2 - e^2} \cdot \sqrt{1 - \mu^2} \cos\varphi\,, \\ y = \sqrt{r^2 - e^2} \cdot \sqrt{1 - \mu^2} \sin\varphi\,, \\ z = r\mu\,, \end{cases}$$

the surface $r = a$ represents an ellipsoid of revolution around the z-axis, whose intersection with a meridian plane $\varphi = \text{const.}$ is an ellipse with semi-major axis equal to a and semi-minor axis equal to $\sqrt{a^2 - e^2}$.

The shape of the deformed nucleus is described by a Legendre expansion of the following type:

$$\text{(7)} \qquad r(\mu) = a\left[1 + \sum_{i=1}^{\infty} \alpha_i P_i(\mu)\right].$$

(6) G. C. WICK: *Nuovo Cimento*, serie VIII, **16**, 229 (1939).

In order to calculate the deformation energy with respect to the spherical shape (see Appendix I) the condition of volume conservation and center of mass fixity must be imposed to (7).

Introducing the eccentricity $y = e/a$ the deformation energy of the nucleus, up to the second order in the coefficients α_i, is given by:

$$\frac{\Delta E}{E_s} = \left[\bar{A}(y) - 1 + 2x(A(y) - 1)\right] + \sum_i \alpha_i (B_i(y) + 2x B_i(y)) + \tag{8}$$
$$+ \sum_{is} (C_{is}(y) + 2x C_{is}(y)) \alpha_i \alpha_s .$$

The square bracket term on the right hand side of (8) represents the deformation energy of the ellipsoid; one obtains for this term (7):

$$\begin{cases} A(y) = (1 - y^2)^{\frac{1}{3}} \dfrac{Q_0}{y} , \\ \bar{A}(y) = \dfrac{1}{2}\left[(1 - y^2)^{\frac{1}{3}} + (1 - y^2)^{-\frac{1}{6}} \dfrac{\arcsin y}{y}\right] . \end{cases} \tag{9}$$

The surface energy coefficients (B_i, $\bar{C}_{is}$) are:

$$\begin{cases} \bar{B}_i(y) = \bar{A}(y) \dfrac{4}{15} \dfrac{y^2}{1 - y^2} \delta_{i2} + \dfrac{1}{2} (1 - y^2)^{-\frac{1}{2}} \displaystyle\int_{-1}^{+1} \frac{2 - y^2 - y^2\mu^2}{(1 - y^2\mu^2)^{\frac{1}{2}}} P_i(\mu)\, \mathrm{d}\mu , \\ C_{is}(y) - \bar{C}_{si}(y) = \left[2(2i + 1) y^4 \delta_{i2} \delta_{s2} - 225(1 - y^2)\, \delta_{is}\right] \dfrac{2\bar{A}(y)}{225(2i + 1)(1 - y^2)^2} \\ \qquad + \dfrac{2}{15} \dfrac{y^2}{1 - y^2} (\bar{B}_i \delta_{s2} + \bar{B}_s \delta_{i2}) + \dfrac{E_{is}(y) + F_{is}(y)}{(1 - y^2)^{\frac{3}{2}}} , \end{cases} \tag{10}$$

where δ_{is} is the Kronecker symbol, and:

$$\begin{cases} E_{is}(y) = \dfrac{1}{4} \dfrac{1}{(1 - y^2)^{\frac{3}{2}}} \displaystyle\int_{-1}^{+1} \frac{-y^6\mu^4 + (-y^6 + 6y^4 - 3y^2)\mu^2 + (-3y^2 + 2)}{(1 - y^2\mu^2)^{\frac{3}{2}}} P_i(\mu) P_s(\mu)\, \mathrm{d}\mu , \\ F_{is}(y) = \dfrac{1}{4} \dfrac{1}{(1 - y^2)^{\frac{3}{2}}} \displaystyle\int_{-1}^{+1} (1 - \mu^2)(1 - y^2\mu^2)^{\frac{1}{2}} \frac{\mathrm{d}P_i(\mu)}{\mathrm{d}\mu} \frac{\mathrm{d}P_s(\mu)}{\mathrm{d}\mu}\, \mathrm{d}\mu . \end{cases} \tag{10'}$$

(7) From here on, P_n and Q_n indicate, respectively, the first and the second kind Legendre functions of order n. When not otherwise specified the argument is meant to be $1/y$.

The Coulomb energy is given by (8):

$$(11)\quad \begin{cases} B_i(y) = \dfrac{2}{3}\dfrac{y^2}{1-y^2}A(y)\,\delta_{i2} + \dfrac{1}{y(1-y^2)^{\frac{5}{3}}}\left[(5A_{02}Q_0 - A_{22}Q_2)\,\delta_{i2} - A_{24}Q_2\,\delta_{i4}\right] \\ C_{is}(y) = C_{si}(y) = -\left[4(2i+1)y^4\,\delta_{i2}\,\delta_{s2} + 225(1-y^2)\,\delta_{is}\right]\dfrac{A(y)}{45(2i+1)(1-y^2)^2} + \\ + \dfrac{y^2}{3(1-y^2)}(B_i\,\delta_{s2} + B_s\,\delta_{i2}) + \\ + \dfrac{5}{2y(2i+1)(1-y^2)^{\frac{5}{3}}}\left[2(1-y^2)(Q_0 - P_2Q_2)\,\delta_{is} + 3(2i+1)\sum_{n=0}^{\infty} g_n A_{ni}A_{ns}\right], \end{cases}$$

where

$$(11')\quad \begin{cases} g_n = \dfrac{1}{(2n+1)y^2}\left[y^2Q_nP_n + Q_2 - Q_0 + y\right], \\ A_{ni} = \left(1 - \dfrac{y^2}{3}\right)\delta_{ni} - (2n+1)\dfrac{y^2}{3}\displaystyle\int_{-1}^{+1} P_2(\mu)\,P_n(\mu)\,P_i(\mu)\,\mathrm{d}\mu\,. \end{cases}$$

In Appendix IV an algebraic reduction of the coefficients B_i, $\bar{B}_i$, C_{is}, C_r is given for the cases used in the numerical computations.

Formula (8) is renormalized on the volume of the undeformed nucleus. The condition of center of mass fixity (up to α_i^2 order in the expression of $\Delta E/E_s$) is (see Appendix I):

$$(12)\qquad \alpha_1 = \frac{6}{7}\frac{y^2}{5-3y^2}\,\alpha_3\,.$$

A power series development of formula (8), setting

$$(13)\qquad \alpha = \frac{y^2}{3}\,,$$

(8) The parameters a_n used by WICK (6) are related to the α_n by the following relation:

$$a_n = \frac{\sqrt{\pi(2n+1)}}{y(1-y^2)}\sum_i \alpha_i A_{ni}$$

where the A_{ni} are given in the text. In the α_n scheme of parameters the integral $\int \xi^2\,\mathrm{d}\omega$, contained in formula (21) of (6), reduces simply to

$$\frac{4\pi}{y^2}\sum_n \frac{\alpha_n^2}{2n+1}\,.$$

yields for the deformation energy (9):

$$(14)\qquad \frac{\Delta E}{E_s} = \frac{2}{5}(1-x)\alpha^2 + \frac{4}{105}(29-32x)\alpha^3 + \frac{1}{35}(101-116x)\alpha^4 +$$

$$+ \frac{2}{35}(1-8x)\alpha^2\alpha_4 + \left(1-\frac{10}{27}x\right)\alpha_4^2 + \frac{2}{7}\left(\frac{5}{2}-\frac{10}{7}x\right)\alpha_3^2 + \frac{8}{35}\left(8-\frac{41}{7}x\right)\alpha\alpha_3^2 + \ldots$$

The symmetrical terms of (14) in α and α_4 coincide with those calculated by BOHR and WHEELER (1,2).

One may repeat on the symmetric and asymmetric parts of (14) the considerations already made starting from formula (2). The results are still expressed by formulae (4) and (5) where α_2 must now be substituted by α. The discussion condensed in Fig. 1*a* still holds; but one may observe that in the present case $\varkappa$ and $\varkappa'$ intersect in a region which is external to the interval of existence of α:

$$0 < \alpha < \tfrac{1}{3}\,.$$

Following the programme of Section **1**, the calculation of y^i (the eccentricity for which the second derivative of the deformation energy vanishes) was performed starting from formulae (8) and (12). The result is given in Fig. 3 where y^i is compared to y which is the eccentricity of the « saddle ellipsoid » that is the value of the eccentricity (function of x) for which the deformation energy of the simple ellipsoid is stationary. In this connection one may observe that the effective saddle shape is represented with sufficient accuracy by an ellipsoid, only if x is slightly less than 1.

In Appendix III, Fig. 1, III the effective reaction path (3) is compared with that of a purely ellipsoidal deformation; the effect of a deformation α_2 of a P_2 type is also examined in a first rough approximation. One may see that it is not possible to neglect this type of deformation in the description of the saddle shape for values of x smaller of say 0.9. In Fig. 3 the curve y (corresponding to stationary configurations for the case of P_4 deformation added to the basic ellipsoid) is also shown for comparison.

(9) Expression (14) has been calculated by Dr. F. GUARINO (private communication) with more terms than those included in (14). Some of these are given below:

$$\frac{\Delta E}{E_3} = \ldots + \frac{4}{5}(1-x)\alpha\alpha_2 + \frac{4}{35}(18-21x)\alpha^2\alpha_2 + \frac{8}{7}\left(\frac{127}{25}-\frac{46}{7}x\right)\alpha^3\alpha_2 +$$

$$+ \frac{4}{35}(8-11x)\alpha\alpha_2^2 + \frac{2}{35}\left(\frac{271}{5}-\frac{599}{7}x\right)\alpha^2\alpha_2^2 + \frac{6}{385}\left(333-\frac{20\,936}{77}x\right)\alpha^2\alpha_3^2 +$$

$$+ \frac{48}{35}(1-x)\alpha\alpha_1\alpha_3 - \frac{12}{35}\left(1+\frac{8}{7}x\right)\alpha_1\alpha_2\alpha_3 + \ldots\,.$$

The inspection of Fig. 3 shows that the value of the « inversion » eccentricity is $y^i \sim 0.93$ for heavy nuclei. This value of the eccentricity corresponds to an ellipsoid whose major axis is about twice the minor one. This moderately elongated ellipsoid is comparable with the effective saddle shape for the same heavy nuclei (see again Fig. 1, III). This circumstance seems to favour, although not to prove, the existence of an « inversion » point on the effective reaction path beyond the saddle.

Independently from these last considerations, the existence of configurations whose evolution results in a growth of an eventual initial asymmetry, seems to favour the possibility of interpretation of fission asymmetry according to the simple liquid-drop model.

The authors are deeply indebted to Prof. J. A. WHEELER for a helpful discussion on the whole subject of this work during the Parma Conference of the Italian Physical Society.

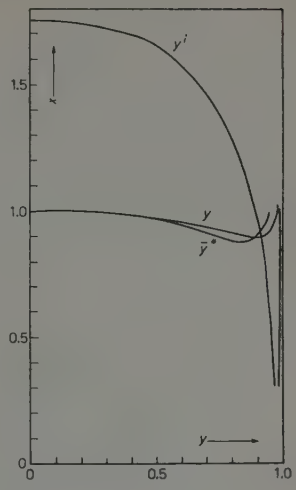

Fig. 3. – Curves $\bar{y}$ and $\overline{y^*}$ give the « saddle shape » for purely ellipsoidal deformation and ellipsoidal deformation plus P_4 deformation (up to the second order) respectively. y^i is the « inversion » curve.

APPENDIX I

Center of Mass Corrections.

In evaluating whether a small asymmetric deformation is energetically favoured or not, one must make sure that the asymmetry is not merely apparent, i.e. is simply caused by a translation of the initial symmetrical figure ([3]). Let us consider a small asymmetric deformation characterized by the parameters a_1, a_3, ... superimposed on a symmetrical shape defined by a_2, a_4, ... The resultant displacement δ of the center of mass is, in the first approximation, given by:

$$\frac{\delta}{R_0} = a_1 + \frac{6}{5} a_2 a_1 + \frac{27}{35} a_2 a_3 + \dots . \tag{1.I}$$

In a reference system whose origin coincides with the center of mass the shape is represented by the following expansion:

$$R'(\mu') = R(\mu') - \delta P_1(\mu') - \frac{R_0 \delta}{R(\mu')} \sum_{i=1}^{\infty} a_i \frac{i(i+1)}{2i+1} (P_{i+1} - P_{i-1}) + 0(\delta^2) , \tag{2.I}$$

where $R(\mu) = R_0 \sum_{i=0}^{\infty} a_i P_i(\mu)$ is the expansion of the shape referred to the former origin, δ is the displacement which characterizes the new position of the center of mass and R' and μ' are the new coordinates.

It is seen that the coefficients of even order in the expansion of R' differ from the corresponding ones in the expansion of R by a quantity which is of the order of the square of the small asymmetric deformations.

This alteration in the expansion of the symmetrical part of the shape may be neglected, as observed by FRANKEL and METROPOLIS ([3]), if the original symmetrical shape is of equilibrium; in this case, in fact, the symmetric part of the deformation energy is unvaried up to second order terms in the small asymmetric deformations.

If however the initial symmetrical shape is not of equilibrium, the condition of center of mass fixity prevents the introduction of apparent variations of second order with respect to asymmetric deformations in the symmetrical part of the deformation energy.

Following PRESENT and KNIPP the condition $\delta = 0$, which fixes the center of mass in the origin must be imposed. This condition may be expressed in the following way:

$$a_1 = -\frac{27}{35} a_2 a_3 + \dots . \tag{3.I}$$

In the case of spheroidal coordinates, formulae (1.I), (2.I) and (3.I) are now written:

$$\frac{\delta}{a} = \alpha_1 + \frac{37}{10}\alpha\alpha_1 - \frac{18}{35}\alpha\alpha_3 + \frac{27}{35}\alpha_2\alpha_3 + \frac{6}{5}\alpha_2\alpha_1 , \tag{1'.I}$$

$$R'(\mu') = R(\mu') - \delta \frac{R^2(\mu') - e^2}{R^2(\mu') - e^2\mu'^2} P_1(\mu') - \frac{R^2(\mu') - e^2}{R^2(\mu') - e^2\mu'^2} \frac{a\delta}{R(\mu')} \sum_{i=1}^{\infty} \alpha_i \frac{i(i+1)}{2i+1} (P_{i+1} - P_{i-1}) + 0(\delta^2) , \tag{2'.I}$$

where $R(\mu) = a \sum_{i=0}^{\infty} \alpha_i P_i(\mu)$,

$$\alpha_1 = \frac{18}{35}\alpha\alpha_3 - \frac{27}{35}\alpha_2\alpha_3 . \tag{3'.I}$$

APPENDIX II

Dynamical Considerations.

The following considerations can help in clarifying the dynamical significance of the « inversion ».

The variation of the deformation energy of the drop in the neighbourhood of a symmetrical configuration defined by the even parameters a_i may be

written:

$$V = \sum V_i \delta a_i + \sum V_{ik} \delta a_i \delta a_k + \sum V_{rs} b_r b_s , \tag{1.II}$$

where δa_i are small variations in the symmetric coordinates, while b_r represent small variations of the asymmetric coordinates. In a similar way, and making the hypothesis of incipient motion, one obtains for the kinetic energy:

$$T = \sum T_{ik} \dot{\delta} a_i \dot{\delta} a_k + \sum T_{rs} \dot{b}_r \dot{b}_s . \tag{2.II}$$

It is seen that formulae (1.II) and (2.II) do not contain terms of the type $\delta a_i b_r$, because V and T must be invariant under the change of sign of the b_r, this operation being equivalent to an inversion of the figure around the origin.

The absence of such mixed terms in the expression of the Lagrangian permits the separation of the symmetric coordinates from the asymmetric ones in the equations governing the incipient motion of the system.

The character of the asymmetric component of the incipient motion may be studied by applying to the Lagrangian:

$$L = \sum T_{rs} \dot{b}_r \dot{b}_s - \sum V_{rs} b_r b_s , \tag{3.II}$$

the well-known methods of the analysis of small oscillations.

According to the theorems of Rayleigh on the introduction of bonds in an oscillating system, $V_{kk} = 0$ is a sufficient condition for instability. Thus $V_{33} < 0$, which is true beyond the « inversion » point, means that in such a region a small asymmetry would tend to grow during the incipient phase of the motion.

The frequency of the P_3 oscillation around the saddle shape has been calculated on the hypothesis of irrotational motion of the nuclear fluid.

Indicating with O the surface tension and with MA the nuclear mass, one gets, as a first approximation:

$$\bar{\omega}_3^2 = \frac{45}{28}\left[1 - \frac{164}{45}(1-x)\right]\frac{32\pi O}{3MA} . \tag{4.II}$$

This result is obtained both with the PRESENT and KNIPP ([2]) formula and with that of the Bohr and Wheeler type (14), provided one has calculated the kinetic energy corresponding to both cases. Up to

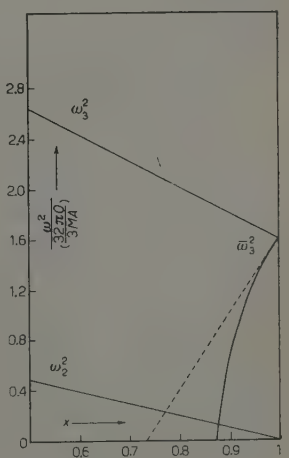

Fig. 1, II. – The frequency $\bar{\omega}_3$ as given by (4, II) is indicated (dotted line). The full line also indicated with $\bar{\omega}_3$ represents the oscillation frequency of P_3 type around the « saddle ellipsoid ». The frequencies of oscillation ω_2 and ω_3 around the spherical shape are also indicated.

the first order in $(1-x)$, (4.II) coincides with the frequency of the lowest mode of normal asymmetric oscillations. The frequency of the P_3 oscillation around an arbitrarily prolated ellipsoid has been also calculated, taking into due account the center of mass corrections.

The calculated frequency however does not correspond in this case to that of a normal asymmetric mode around the « saddle ellipsoid ». These results are illustrated in Fig. (1.II).

Appendix III

On the Scheme of Parameters Adopted in Section 2.

The curve $\bar{y}$ giving the eccentricity of the « saddle ellipsoid » is shown in Fig. 3. As may be seen in the figure, the minimum value of x for which an energy maximum is found for a nucleus undergoing a purely ellipsoidal deformation is about 0.89.

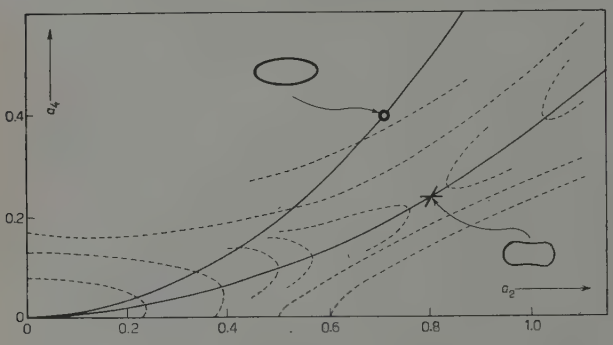

Fig. 1, III. – Of the heavy curves shown in the figure the one below represents, in the plane (a_2, a_4), the reaction path, as calculated by Frankel and Metropolis [3], while that above is the projection in that plane of the ellipsoidal path. The contours of the energy surface are plotted for $x=0.74$ (as calculated in reference [3]). The saddle shape and the « inversion » ellipsoid are also sketched for $x=0.74$.

This result is not surprising since the path followed in the a_i-space with ellipsoidal deformations differs sensibly from the «reaction path » as calculated by Frankel and Metropolis. Fig. 1.III illustrates such different paths in the plane a_2, a_4. The contours of the energy surface as calculated by Frankel and Metropolis for $x = 0.74$ are also shown: it is seen that along the path corresponding to ellipsoidal deformation the energy increases monotonically. In connection with the preceding observations it might be useful to illustrate, at least in a first approximation, the behaviour of the deformation energy as a function of α and α_2. In the neighbourhood of $x = 1$ and for small α and α_2, this energy is given by,

$$\frac{\Delta E}{E_s} = \frac{2}{5}(1-x)(\alpha+\alpha_2)^2 + \frac{4}{35}(\alpha+\alpha_2)^3 , \tag{1.III}$$

which shows that α and α_2 are additive in a first approximation.

Extrapolating such a behaviour to large deformations and to values of x sensibly different from 1, it is seen, noting that α must be less than $\frac{1}{3}$, that

for $x < 0.86$ it is not possible to find an energy maximum under the condition $\alpha_2 = 0$.

One may pass from the representation used by PRESENT and KNIPP and the one adopted in section 2, by applying the following formulae which are valid up to terms of order α^2:

$$(2.\text{III}) \qquad \begin{cases} a_1 = \alpha_1 + \alpha\alpha_1 - \frac{9}{7}\alpha\alpha_3 , \\ a_2 = \alpha + \alpha_2 + \frac{10}{7}\alpha^2 + \frac{9}{7}\alpha\alpha_2 - \frac{12}{7}\alpha\alpha_4 , \\ a_3 = \alpha_3 + \frac{4}{3}\alpha\alpha_3 + \frac{20}{11}\alpha\alpha_5 , \\ a_4 = \alpha_4 + \frac{27}{35}\alpha^2 + \frac{18}{35}\alpha\alpha_2 + \frac{86}{77}\alpha\alpha_4 - \frac{36}{143}\alpha\alpha_6 , \\ a_5 = \alpha_5 + \frac{20}{21}\alpha\alpha_3 + \frac{119}{117}\alpha\alpha_5 + \frac{213}{65}\alpha\alpha_7 . \end{cases}$$

APPENDIX IV

Algebraic Reduction of Some Energy Coefficients.

In order to permit numerical computation it is useful to reduce the formulae (10) and (11) to simpler expressions.

The algebraic reduction has to be made coefficient by coefficient and the result may be expressed in the following way for the coefficients $C_{i,s}$ and $\bar{C}_{i,s}$:

$$(1.\text{IV}) \qquad \begin{cases} C_{is} = \dfrac{1}{y^{i+s}} \dfrac{1}{(1-y^2)^{\frac{3}{2}}} \cdot \left[R_{is}(y) + S_{is}(y) \dfrac{Q_0}{y} \right] , \\ \bar{C}_{is} = \dfrac{1}{y^{i+s}} \dfrac{1}{(1-y^2)^{\frac{3}{2}}} \cdot \left[M_{is}(y) + N_{is}(y) \dfrac{1}{1-y^2} \dfrac{\arcsin y}{y} \right] , \end{cases}$$

where R_{is}, S_{is}, M_{is}, N_{is} are polynomials whose expression is given as follows for the cases useful in the

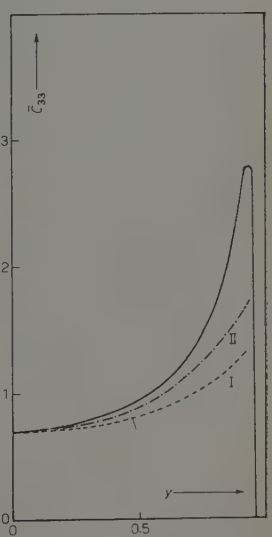

Fig. 1, IV. – The full line gives the actual value of $\bar{C}_{33}$; while dotted lines give the first and second approximation of $\bar{C}_{33}$ in powers of y^2.

performed numerical calculations:

$$
\text{(2.IV)}\quad
\begin{cases}
R_{11}(y) = \dfrac{1}{21}\,(12y^2 - 33)\,, \\[2ex]
R_{13}(y) = \dfrac{1}{63}\,(119y^4 - 606y^2 + 675)\,, \\[2ex]
R_{33}(y) = \dfrac{1}{2\,772}\,(7\,009y^6 - 36\,501y^4 + 57\,375y^2 - 30\,375)\,, \\[2ex]
R_{44}(y) = \dfrac{1}{576\,576}\,(342\,207y^{10} - 2\,995\,425y^8 + 13\,757\,850y^6 - \\
\qquad\qquad - 33\,254\,550y^4 + 37\,258\,375y^2 - 15\,563\,625)\,,
\end{cases}
$$

$$
\text{(3.IV)}\quad
\begin{cases}
S_{11} = \dfrac{1}{21}\,(2y^4 - 23y^2 + 33)\,, \\[2ex]
S_{13} = \dfrac{1}{63}\,(9y^6 - 261y^4 + 831y^2 - 675)\,, \\[2ex]
S_{33} = \dfrac{1}{2\,772}\,(1\,359y^8 - 16\,056y^6 + 52\,926y^4 - 67\,500y^2 + 30\,375)\,, \\[2ex]
S_{44} = \dfrac{1}{576\,576}\,(140\,805y^{12} - 785\,162y^{10} + 5\,783\,495y^8 - \\
\qquad - 22\,255\,500y^6 + 44\,290\,575y^4 - 42\,446\,250y^2 + 15\,563\,625)\,,
\end{cases}
$$

$$
\text{(4.IV)}\quad
\begin{cases}
M_{11} = \dfrac{1}{48}\,(-8y^4 + 62y^2 - 57)\,, \\[2ex]
M_{13} = \dfrac{1}{48}\,(-16y^6 - 308y^4 + 912y^2 - 585)\,, \\[2ex]
M_{33} = \dfrac{1}{21\,504}\,(-12\,160y^8 + 74\,992y^6 - 261\,576y^4 + \\
\qquad\qquad + 363\,510y^2 - 165\,375)\,, \\[2ex]
M_{44} = \dfrac{1}{294\,912}\,(142\,624y^{10} - 999\,104y^8 + 7\,905\,780y^6 - \\
\qquad\qquad - 18\,289\,220y^4 + 19\,773\,075y^2 - 7\,254\,450)\,,
\end{cases}
$$

$$
\text{(5,IV)}\quad
\begin{cases}
N_{11} = \dfrac{1}{48}\,(40y^4 - 100y^2 + 57)\,, \\[2ex]
N_{13} = \dfrac{1}{48}\,(-144y^6 + 864y^4 - 1\,302y^2 + 585)\,, \\[2ex]
N_{33} = \dfrac{1}{21\,504}\,(27\,264y^8 - 208\,704y^6 + 489\,216y^4 - \\
\qquad\qquad - 473\,760y^2 + 163\,375)\,, \\[2ex]
N_{44} = \dfrac{1}{294\,912}\,(20\,736y^{12} - 682\,624y^{10} + 5\,498\,560y^8 - \\
\qquad - 19\,314\,720y^6 + 31\,826\,430y^4 - 24\,609\,375y^2 + 7\,254\,450)\,.
\end{cases}
$$

For the coefficients B_i and $\bar{B}_i$ the expressions of B_4 and B_4 are:

$$(6.\text{IV}) \qquad \begin{cases} B_4 = \dfrac{2}{21}\dfrac{1}{(1-y^2)^{\frac{3}{2}}}\left[-3+(3-y^2)\dfrac{Q_0}{y}\right], \\ \bar{B}_4 = \dfrac{1}{384}\dfrac{1}{y^4}\dfrac{1}{(1-y^2)^{\frac{3}{2}}}\left[(-735+1\,040y^2-308y^4)+\right. \\ \qquad \left.+(735-1\,530y^2+936y^4-144y^6)\dfrac{1}{\sqrt{1-y^2}}\dfrac{\arcsin y}{y}\right]. \end{cases}$$

In general the behaviour of the modulus of these coefficients presents a maximum followed by a divergency for $y \to 1$. One may compare this behaviour with the power series development (with respect to y^2) of these coefficients.

The comparison is indicated, as an example, for the coefficient $\bar{C}_{33}$ in Fig. 3,IV.

RIASSUNTO

Nell'ambito del modello a goccia, si esamina la possibilità che la asimmetrizzazione nella fissione dei nuclei pesanti a bassa energia, avvenga dopo che il sistema, nel suo evolversi lungo il cammino di reazione, abbia superato la sella simmetrica. A tale scopo si studia la superficie energia al di là delle selle simmetriche, sia estrapolando formule note valide per piccole deformazioni attorno alla sfera, sia adoperando una rappresentazione che permette di calcolare l'energia per figure poco diverse da un ellissoide di base comunque allungato. I risultati ottenuti sembrano indicare che lungo il cammino effettivo di reazione simmetrico esista un punto di « inversione » al di là del quale, per moti incipienti, una piccola asimmetria iniziale tende ad amplificarsi.

On the Range-Energy Relation for Slow α-Particles in Argon.

G. Bertolini and M. Bettoni

Istituto di Fisica Sperimentale del Politecnico - Milano

(ricevuto il 2 Febbraio 1955)

Summary. — The range-ionization curve for α-particles in argon has been obtained in the region of 0.25-3.5 MeV. A grid ionization chamber containing two sources of α-particles was used for measurements. The sources were placed in such a way as to emit particles in the direction of and perpendicularly to the field. The different rise time of the tracks running parallel and perpendicular to the electric field enables us to know the range of the α-particles, while the amplitude enables us to know the energy. The range-energy curve is obtained by assuming a strict proportionality between the total ionization produced and the energy of the α-particle. By comparison with the Bethe range-energy curve in air, the stopping power in argon is obtained.

1. – Introduction.

The relation range-energy for α-particles in the air was studied theoretically by Livingston and Bethe [1] in 1937 and later corrected by Bethe [2] after the results obtained by Jesse and Sadauskis [3] which demonstrated that the average energy expended to produce an ion pair in the air was not constant. The Bethe theory is applicable for energies exceeding 5 MeV but its usefulness is limited to lower energies because it did not take into account the binding effect for L, M shell, nor the capture and loss of electrons by α-particles, phenomena which are more conspicuous as the energy of the particle is lower.

(1) M. S. Livingston and H. A. Bethe: *Rev. Mod. Phys.*, **9**, 261 (1937).
(2) H. A. Bethe: *Rev. Mod. Phys.*, **22**, 213 (1950).
(3) W. P. Jesse and J. Sadauskis: *Phys. Rev.*, **78**, 1 (1950).

In the case of argon there exist only calculations for low energy α by HIRSCHFELDER and MAGEE (4) which however have not proved strictly correct. Recently COOK and coll. (5) have made an accurate measurement of the range of the α-particles from 20 to 250 keV by determining the behaviour of the specific ionization along the tracks produced by α-particles in a cloud chamber. In the past the range for α-particles between 5 and 10 MeV was measured for naturally occuring emitters. The relative results are collected in an article by GRAY (6).

The purpose of the present work was to establish experimentally the range-energy relation for α-particles in the region between 250 keV to 3.5 MeV.

2. – Method.

In the low energy region it is not possible to have natural emitting substances. In order to study this region, α sources were made from ^{210}Po with alluminium absorber and variable length collimators. The ionization from a single α-particle was measured with a grid argon filled ionization chamber. The value of the range of a single α was obtained from the rise time of the pulse at the collector. The rise time depends on the drift velocity of the electrons and on the length of the projection of the track in the direction of the electric field; the rate of rise depends on the specific ionization of the α-particle along the track. The voltage of the collector will start to rise as the first electrons pass through the grid into the grid-collector region, and continue to increase until the last electron reaches the collector.

If an α-particle ionizes in the direction of the field, the rise time of the pulse is given by

$$t_1 = \frac{R}{v} + \frac{d}{v'} , \tag{1}$$

where R is the range of the α-particles, d the distance grid-collector, v and v' the drift velocities in the cathode-grid and grid-collector fields respectively. This relation is satisfied by the hypothesis that the value R is less than cathode-grid distance.

An α-particle running parallel to the plates in the chamber, gives a pulse which rise-time is equal to

$$t_t = \frac{d}{v'} .$$

(4) J. O. HIRSCHFELDER and J. L. MAGEE: *Phys. Rev.*, **73**, 207 (1948).
(5) C. J. COOK, E. JONES and T. JORGENSEN: *Phys. Rev.*, **91**, 1417 (1953).
(6) L. H. GRAY: *Proc. Camb. Phys. Soc.*, **40**, 72 (1944).

For shortness' sake we shall call the tracks perpendicular to the field as transversal tracks and those in the direction of the field as longitudinal tracks.

In this way it was possible to measure the range corresponding to a given ionization. From the measured ionization we can have directly the energy of the particle. Recent measurements by JESSE and SADAUSKIS [3] have shown that the energy expended in producing a pair of ions in argon is indipendent of the α-particle's energy. Hence there exists a strict proportionality between the total ionization produced and the energy of the α-particles.

3. – Apparatus.

The grid ionization chamber was set up with the first stage of the preamplifier being inside the chamber. In this way it is possible to have a small capacity of the collector in order to reveal α-particles of low energies [7]. The chamber was filled with argon of a purity higher than 99.9% and the pressure was measured with a precision vacuum system (accuracy to one part in 100). The cathode voltage assured a complete collection of the electrons at all the pressures. The grid voltage, obtained from a potential divider, was adjusted so that the grid-collector field was 2.2 times the cathode-grid field. With this ratio the grid does not capture electrons.

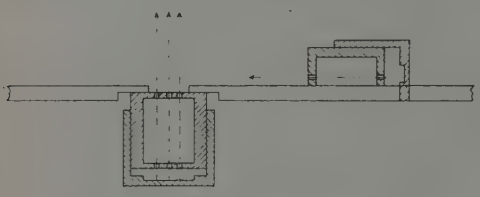

Fig. 1. – Cathode of the ionization chamber with collimators.

The collimation of the α-particles was obtained by two brass collimators, 1 cm long and carrying two holes of 0.3 mm diameter (Fig. 1). The collimator mounted on the back of the cathode was a source of longitudinal tracks; the transversal tracks were obtained with the collimator mounted on the top of the cathode with the axis being perpendicular to the force lines of the field. In these conditions the error in the range is about 0.1%. On the source it was possible to put Al absorbers, 1 to 5 μ thick (equivalent to an absorption of 0.24 and 1.2 MeV respectively) in order to have α-particles of different energies. The pressure in the chamber was so regulated as to maintain the range of the particles around 2.5 cm, irrespective of the energy. In this way the rise time of the pulse was always sufficiently long to be measured without a big error.

The single α-particle pulse was amplified using a model 100 linear amplifier [8] (rise time 0.5 μs and decay time 100 μs). With these time constants,

[7] G. BERTOLINI e A. BISI: *Nuovo Cimento*, **9**, 1022 (1952).

[8] W. C. ELMORE and M. SANDS: *Electronics Experimental Techniques* (New York, 1949), p. 165.

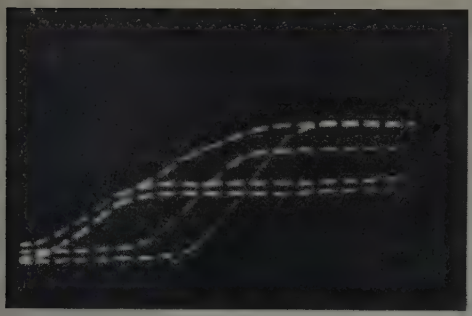

2*a*

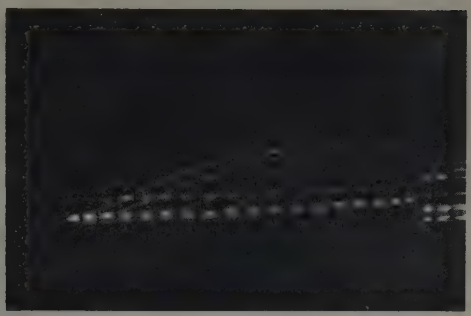

2*b*

2*c*

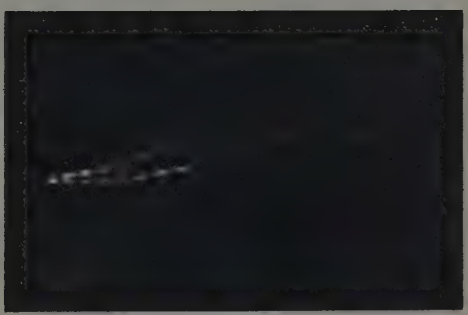

2*d*

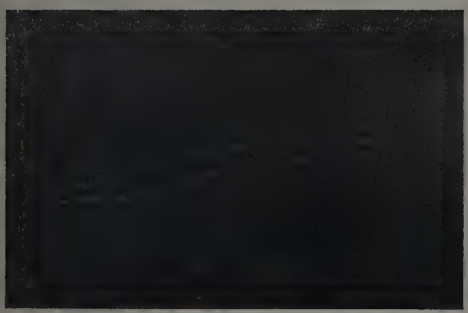

2*e*

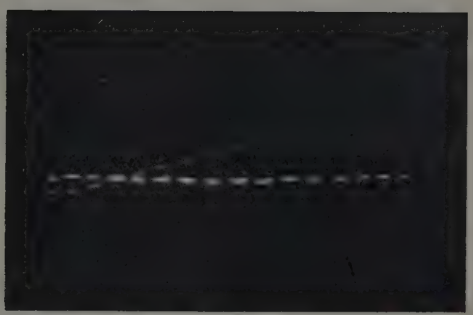

2*f*

Fig. 2. – α-particles pulses. The pulses with short rise time correspond to transversal tracks, the pulses with long rise time to longitudinal tracks. *a*) α-particle of 3.25 MeV; *b*) α-particle of 2 MeV; *c*) α-particle of 1.35 MeV; *d*) α-particle of .7 MeV; *e*) α-particle of .45 MeV; *f*) α-particle of .40 MeV.

the height variation of the output pulses is practically negligible even when the rise time varies noticeably (9). The output pulse was sent to the vertical plates of a Du Mont oscillograph type 248/B. The sweep of the oscillograph was triggered by the pulse induced on the grid by the electrons of the track and suitably amplified. The pulse on the grid begins to rise some μs before the one on the collector. This assures a delay between the start of the sweep and the beginning of the vertical pulse allowing a clear observation of the pulse.

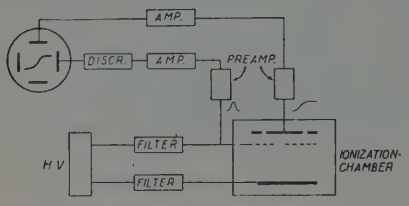

Fig. 3. Block diagram of the experimental apparatus.

The single pulses corresponding to transversal and longitudinal tracks were photographed with a Cossor camera model 1428. Fast films Ferrania X 3 V were used. Fig. 2 shows some photographs for α of different energy. The time markers of the oscillograph were calibrated with a cristal-oscillator. The linearity of the complete set-up was established by examining photographs of variable amplitude test pulses. The block diagram of the experimental apparatus is shown in Fig. 3.

4. – Experimental Results.

The rise time t_r of the transversal track pulses gives the drift velocity v^r of the electrons under the conditions of our experiment. From a series of photographs of such tracks in argon with different X/p ratio we were able to obtain the drift velocity of the electrons as function of X/p.

The drift velocity was taken from the slope of the track. We have found a diagram similar to that of COLLI and FACCHINI (10).

The rise time and amplitude of individual longitudinal tracks was evaluated. From the amplitude it was possible to know the energy of the single α-particle by means of comparing it with pulses given by α-particles of a thin ^{210}Po source directly on top of the negative electrod. The source was prepared by evaporation of a RaD + RaE + RaF solution. The rise time was evaluated by assuming that the pulse was approaching zero with a parabolic arc. Having determined the drift velocity, it is possible to obtain the range of the α-particle by means of this evaluation and by formula (1).

A single run consisted of about 100 photographs made consecutively in about eight minutes. In each photograph pulses corresponding to transversal

(9) G. BERTOLINI, M. BETTONI and A. BISI: *Nuovo Cimento*, **11**, 458 (1954).
(10) L. COLLI and U. FACCHINI: *Rev. Scient. Instr.*, **23**, 39 (1952).

and longitudinal α-particles appear. The evaluation of the drift velocity was made by averaging all the transversal tracks of the single run. v is the value corresponding to X/p in the cathode-grid region, directly obtainable from the drift velocity — X/p diagram.

The range R calculated from formula (1) was corrected in order to take into account the diffusion of the track. When electrons are drifting in an electric field the average distance diffused by an electron in a given time is [11]:

$$\delta = \sqrt{\frac{4Dt}{\tau}},$$

D is the diffusion which may be obtained from the relation:

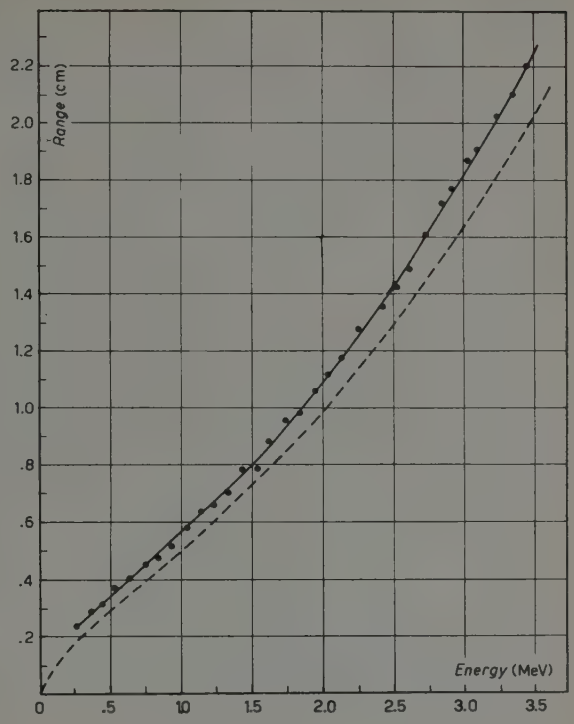

Fig. 4. – Range-energy curve for α-particles in argon. The dotted line represents the Bethe range-energy curve for α-particles in air.

$$\frac{V}{D} = \frac{40.3X}{\eta},$$

where X is the field in V/cm and η the ratio of the energy of agitation of free electrons to agitation energy of gas molecules. η is a function of X/p and the numerical factor refers to a temperature of 15 °C. The correction for the diffusion of the track is from 9 to 15 %.

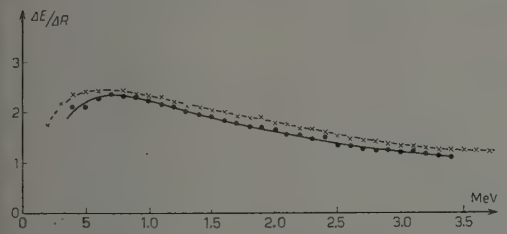

Fig. 5. – $\Delta E/\Delta R$ as function of the energy for α-particles stopped in argon (solid line) and in air (dotted line) $\Delta E = 0.2$ MeV.

The experimental results are given in Fig. 4. Every point which served to construct the experimental curve is an average of 20 to 30 tracks. The error is about 3 %. The dotted curve represents the

(11) D. H. Wilkinson: *Ionization Chambers and Counters* (Cambridge, 1950), p. 36.

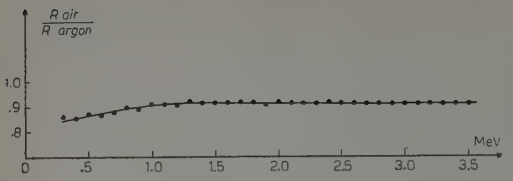

Fig. 6. – Integral stopping power $s = R_{air}/R_{argon}$.

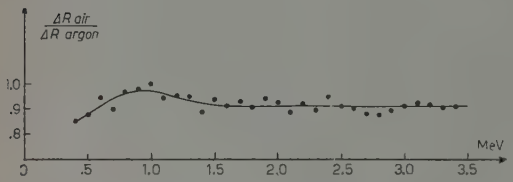

Fig. 7. – Stopping power $\Delta R_{air}/\Delta R_{argon}$ as a function of the energy. ΔR is the range variation corresponding to $\Delta E = 0.2$ MeV.

Bethe range-energy curve for α-particles in air.

The function $\Delta E/\Delta R$ for argon was derived from Fig. 4 and compared with the function of the air derived from Bethe curve (Fig. 5). The dotted curve represents the air function and the continuous curve that of argon. The reciprocal position of the two maximums is similar to that obtained for protons stopped in various materials, for which there is a greater number of measurements than that for α ([12]).

In Fig. 6 is given the ratio of the total range in air and argon as function of the energy of α-particles. This ratio which equals 0.915 remains constant between 1 and 3.5 MeV and decreases at lower energies. Fig. 7 shows the behaviour of the stopping power $\Delta R_{air}/\Delta R_{argon}$, where ΔR is the range variation corresponding to $\Delta E = 0.2$ MeV.

The results of COOK and COW. ([5]) in the region of very low energy agree with our measurements within 2%.

We are greatly indebted to Prof. G. BOLLA for his encouragements and to Dr. A. BISI for very helpful discussions.

([12]) H. A. BETHE and J. ASHKIN: *Experimental Nuclear Physics* (New York, 1953), vol. I, p. 201.

RIASSUNTO

È stata ricavata la curva sperimentale range-ionizzazione per particelle α in argon nell'intervallo 0,25-3,5 MeV. La misura è stata effettuata con una camera a ionizzazione a griglia contenente due sorgenti di particelle α disposte in modo da emettere particelle nella direzione del campo elettrico e perpendicolarmente al campo stesso. Dai differenti tempi di salita degli impulsi si ricava il range delle particelle nella camera e dall'energia la loro ampiezza. Nell'ipotesi che in argon si abbia proporzionalità fra ionizzazione ed energia, si ottiene la curva range-energia. Il confronto con la curva di Bethe per particelle α in aria permette di ricavare il potere frenante dell'argon rispetto all'aria.

On the Total Decay Energy in the Orbital Electron Capture of ^{181}W.

A. Bisi, S. Terrani and L. Zappa

Istituto di Fisica Sperimentale del Politecnico - Milano

(ricevuto il 4 Febbraio 1955)

Summary. — An investigation of the radiations from ^{181}W was made by means of a high transmission β-spectrometer, a proportional counter spectrometer and a scintillation spectrometer. ^{181}W was found to emit only L X- and K X-radiations, characteristic of Ta, arising from L- and K-capture. The decay energy was found to be: $E_0 = 92$ keV, and the transition was classified as once forbidden ($\Delta I = 0, 1$; yes). The pairing effect in the region around $A = 181$ from the Suess-Jensen plot is briefly discussed.

1. – Introduction.

A long-lived radioactive tungsten of mass 181 ($T_{\frac{1}{2}} = 140$ d) was discovered by Wilkinson [1] on bombarding tantalum with high energy deuterons. A similar activity was observed by Burkig and Richardson [2] to arise from proton bombardment of tantalum. Later Lindner [3] was able to produce ^{181}W from capture of thermal neutrons by ^{180}W.

The instability of ^{181}W against orbital electron capture was put in evidence by Wilkinson [1]. The occurrence of γ-rays was reported by several investigators; their results are summarized in Table I. As may be seen the knowledge of the decay of ^{181}W is in a rather unsatisfactory state. No concrete evidence showing the production of the excited levels of ^{181}Ta, whose energies were all known from the decay of ^{181}Hf [4] (Fig. 2) can be found. Moreover

---

[1] G. Wilkinson: *Nature*, **160**, 864 (1947).

[2] J. W. Burkig and J. Reginald Richardson: *Phys. Rev.*, **76**, 586 (1949).

[3] M. Lindner: *Phys. Rev.*, **84**, 240 (1951).

[4] J. M. Hollander, I. Perlman and G. T. Seaborg: *Rev. Mod. Phys.*, **25**, 469 (1953).

according to DER MATEOSIAN and GOLDHABER (5) the 22 μs state (0.613 MeV) is not produced in the decay of ^{181}W.

TABLE I.

Energy of γ-radiation in MeV	References
1.8 (weak) abs.	WILKINSON (1)
0.030, 0.600, 0.800 (weak) scint. spect. (*)	ALBURGER *et al.* (6)
γ abs.	LINDNER (3)
0.1365, 0.1525 (weak) spect. conv.	CORK *et al.* (7)

The adopted symbols and abbreviations are taken from the Table of Isotopes of HOLLANDER, PERLMAN and SEABORG (4).

The electron capture of ^{181}W can be classified as an even-even transition (a proton pair is broken to produce a neutron pair). The knowledge of the total decay energy makes it possible to locate exactly the position of this nuclide in the sequence of isodiapheres (Suess-Jensen plot of the decay energies of odd-A nuclides with constant neutron excess $I = N - Z$, against N (8)). It seems possible therefore to establish the existence of appreciable difference in the pairing terms for odd protons and neutrons in the region around $A = 181$ where reliable decay data are rare.

The aim of this work has been the determination of a reliable value for the total decay energy of ^{181}W through a detailed investigation of the emitted radiations.

2. – Measuring Techniques.

The radiations from ^{181}W were analysed by means of a high transmission β-ray spectrometer, a proportional counter spectrometer and a scintillation spectrometer, described elsewhere (9). The pulse size was measured by means of a single channel (10) and a twenty channels (11) electronic pulse analyser.

(5) M. GOLDHABER and R. D. HILL: *Rev. Mod. Phys.*, **24**, 179 (1952).

(6) D. E. ALBURGER, E. DER MATEOSIAN, G. FRIEDLANDER, M. GOLDHABER, J. W. MIHELICH, G. SCHARFF-GOLDHABER and A. W. SUNYAR: *Report BNL* 82 (1950).

(7) J. M. CORK, W. H. NESTER, J. M. LE BLANC and M. K. BRICE: *Phys. Rev.*, **92**, 119 (1953).

(8) H. E. SUESS and J. H. D. JENSEN: *Ark. för Fys.*, **3**, 577 (1952).

(*) Probably caused by impurities (A. W. SUNYAR: private communication).

(9) A. BISI, S. TERRANI and L. ZAPPA: *Nuovo Cimento* **1**, 291 (1955).

(10) J. E. FRANCIS jr., P. R. BELL and J. C. GUNDLACH: *Rev. Sci. Instr.*, **22**, 133 (1951).

(11) E. GATTI: *Nuovo Cimento*, **11**, 153 (1954).

^{181}W (a carrier-free solution of H_2WO_4 in diluted HCl) was obtained by irradiation of Ta in the cyclotron of Amsterdam.

3. – Experimental Results.

No evidence at all was found of a β^+ emission nor of conversion lines in the β-spectrometer.

In the course of a detailed search with the scintillation spectrometer we were not able to detect any evidence of the γ-rays listed in Table I. In particular an investigation of the γ-spectrum was carried out in the region around 150 keV, after the intense peak of K X-radiation had been thoroughly absorbed. This investigation has shown that the ratio of the intensity of the γ-rays, if present, to K X-rays would be certainly lower than $1/10^5$.

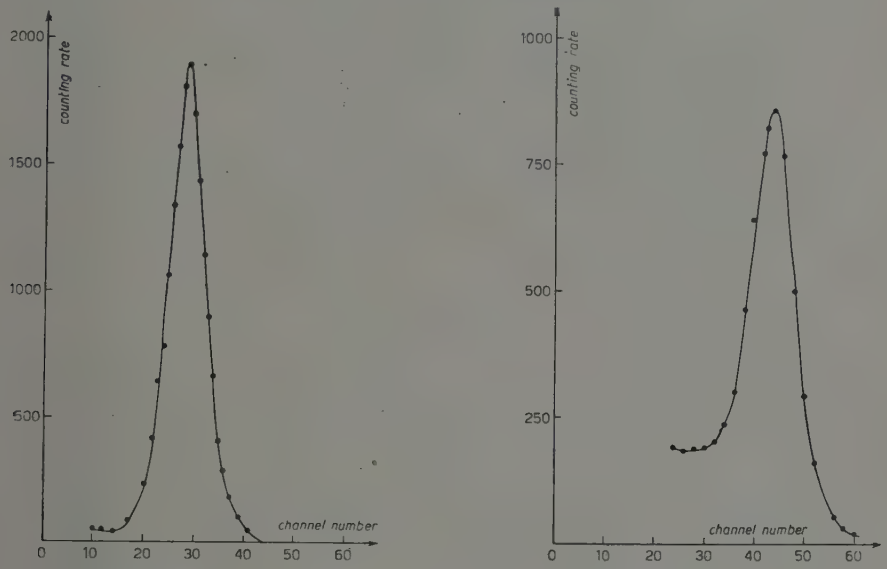

a) L X-radiations from ^{181}W; *b*) K X-radiations from ^{181}W.

Fig. 1.

In the spectra obtained with the proportional counter spectrometer two intense peaks were observed and interpreted as K X- and L X-rays characteristic of Ta (Fig. 1). The value of relative intensities of the L X- and K X-radiation was obtained from the areas under the peaks after subtracting the background and after correction for the detection efficiency of the counter ([12]).

([12]) A. Bisi and L. Zappa: *Nuovo Cimento*, **12**, 211 (1954).

In this way we found:

$$\frac{I_L}{I_K} = 0.39 \pm 0.01 \,. \tag{1}$$

As it will become clear in the following section, the observed K and LX-radiations arise only from orbital electron capture. It is therefore possible to calculate the relative amounts of K- (P_K) and L-capture (P_L) from the result (1).

We have:

$$\frac{P_L}{P_K} = \frac{1}{\omega_{LL}} \left\{ \frac{I_L}{I_K} \omega_K - \omega_{LK} \right\},$$

where: ω_K = K-shell fluorescence yield of Ta;

$\omega_{LK} = \sum_i r_i \omega_{Li}$ L fluorescence yield for the transitions to the L level following the K-capture;

$\omega_{LL} = \sum_i u_i \omega_{Li}$ L fluorescence yield for the transitions to the L level following the L-capture.

ω_{LK} and ω_{LL} can be estimated from the partial fluorescence yield ω_{Li} and from the relative excitations probabilitie u_i, r_i ([9,13]). With the values listed in Table II, we obtain:

$$\frac{P_L}{P_K} = 1.54 \,. \tag{2}$$

TABLE II.

		L_{I}	L_{II}	L_{III}	References
ω_K	0.94				BURHOP [14]
ω_{Li}		$8.0 \cdot 10^{-2}$	$31 \cdot 10^{-2}$	$18 \cdot 10^{-2}$	BISI, TERRANI and ZAPPA [9]
v_i		0	1/3	2/3	BURHOP [14]
u_i		0.95	~ 0.05	0	MARSHAK [15]

[13] B. B. KINSEY: *Canad. Journ. Res.*, A **26**, 494 (1948).

[14] E. H. S. BURHOP: *The Auger Effect and other Radiationless Transitions* (Cambridge, 1952).

[15] E. R. MARSHAK: *Phys. Rev.*, **61**, 431 (1942).

4. – Discussion.

Owing to the fact that no γ-rays were observed it can be reasonably assumed that the ground state of ^{181}W is lower in energy than the first excited state of ^{181}Ta (136 keV). Hence the total decay energy of ^{181}W must lie between 60 keV (K-electron binding energy of W) and 136 keV. This assumption can be tested from the value of the transition energy obtained from eq. (2) as follows: in view of the low value of the decay energy (certainly lower than 500 keV) and the half life of ^{181}W, we can deduce: $6 < \log ft < 8$. This fact suggests that the transition can be classified, according to MAYER, MOSZKOVSKI and NORDHEIM [16], as first forbidden ($\Delta I = 0,1$; yes). The remarkable feature of this group of transitions is the allowed shape of their spectra, within the accuracy of the measurements. Therefore the transition energy of ^{181}W can be evaluated by using the following formula for allowed transitions:

$$\frac{P_L}{P_K} = \left(\frac{\psi_{L_1}}{\psi_K}\right)^2 \left(\frac{W_0 + W_L}{W_0 + W_K}\right)^2 ,$$

where $(\psi_{LI}/\psi_K)^2$ is the ratio of L_I- and K-shell electron densities at the nuclear radius, W_K and W_L the K- and L-shell energies, and W_0 the nuclear energy change. With the value of $(\psi_{LI}/\psi_K)^2$ calculated by ROSE and JACKSON [17] and the values of W_K and W_L deduced from available tables of critical absorption energies [18], we have for the total decay energy of ^{181}W:

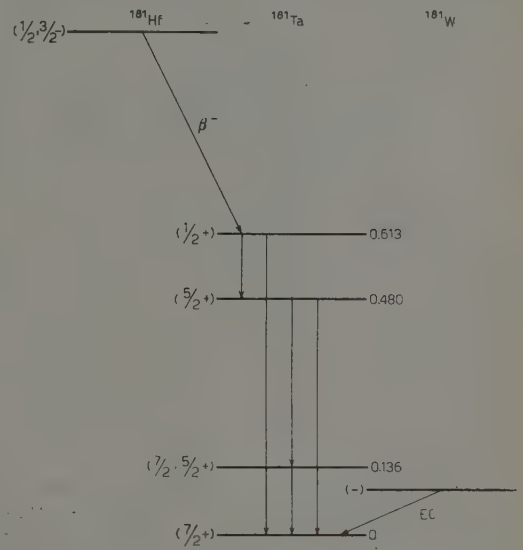

Fig. 2. – Proposed decay scheme for ^{181}W.

$$E_0 = 92 \text{ keV} . \tag{3}$$

We estimate that the uncertainty in the E_0 value is not greater than 10 %. It is worthwhile to note that in the region where $(W_0 + W_L)/(W_0 + W_K)$ is different from 1 the W_0 value varies slowly against P_L/P_K. In our case the

[16] M. G. MAYER, S. A. MOSZKOWSKI and L. W. NORDHEIM: *Rev. Mod. Phys.*, **23**, 315 (1951).

[17] M. E. ROSE and J. L. JACKSON: *Phys. Rev.*, **76**, 1540 (1949).

[18] R. D. HILL, E. L. CHURCH and J. W. MIHELICH: *Rev. Sci. Instr.*, **23**, 523 (1952).

uncertainty in P_L/P_K value arises mostly from the uncertainty in the value of ω_{L_1}. No reasonable value of ω_{L_1} can however raise to E_0 value above 136 keV.

With the value (3), the log ft from graphs and nomographs given by MOSZKOWSKI [19] can be:

$$\log ft \sim 6.4 .$$

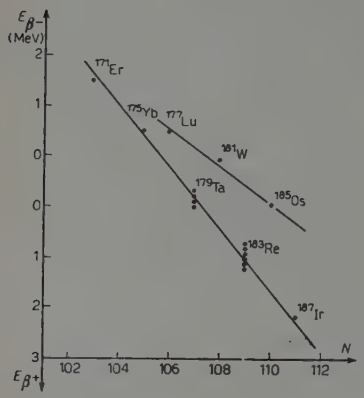

Fig. 3. – Suess-Jensen plot for odd A-nuclides with a change in neutron excess from 33 to 35 (and conversely).

Fig. 2 shows the decay scheme of ^{181}W together with the decay scheme of ^{181}Hf. Fig. 3 shows the Suess and Jensen plot for the isodiaphere corresponding to the change of the neutron excess from 33 to 35. The data are taken from HOLLANDER, PERLMAN and SEABORG [4] and from Nuclear Data [20]. The circles and the crosses indicate respectively the odd-odd and even-even transitions. Our value for the decay energy of ^{181}W is consistent with the decay values for the two odd-Z nuclides ^{177}Lu, ^{185}Os. The discrepancy between even-Z points and odd-Z points is evident, pointing to appearance of a difference in pairing terms for odd protons and neutrons in the region around $A=181$. This pairing effect which as far as we know has been thought to be missing, appears on the contrary to be appreciable, amounting to about $+0.7$ MeV.

We are indebted to Prof. G. BOLLA for his kind interest in this work.

([19]) S. A. MOSZKOWSKI: *Phys. Rev.*, **82**, 35 (1951).

([20]) *Nuclear Data, National Bureau of Standards Circular No. 499* (1950) and *Supplements* (1951).

RIASSUNTO

Vengono studiate le radiazioni emesse dal ^{181}W per mezzo di uno spettrometro β ad alta trasmissione, uno spettrometro a contatore proporzionale ed uno spettrometro a scintillazione. Si trova che il ^{181}W emette soltanto radiazioni L X e K X caratteristiche del Ta provenienti da cattura L e da cattura K. Per l'energia di decadimento si ottiene $E_0=92$ keV. La transizione è classificata 1° proibita ($\Delta I=0, 1$; si). Si segnala infine l'effetto di accoppiamento per protoni e neutroni dispari, nella regione intorno ad $A=181$, ricavabile dal diagramma di Suess e Jensen.

Misure su protoni dei raggi cosmici.

C. Baccalin, P. Bassi e C. Manduchi (*)

Istituto di Fisica dell'Università - Padova

Istituto Nazionale di Fisica Nucleare - Sezione di Padova

(ricevuto il 7 Febbraio 1955)

Riassunto. — Mediante un telescopio di contatori di G. M. in coincidenza ed un contatore di Čerenkov in anticoincidenza abbiamo misurato l'intensità assoluta, la distribuzione zenitale, l'effetto barometrico e la variazione di intensità fra 0 e 2 000 m s.l.m., dei protoni di circa 400 MeV dei raggi cosmici. Con lo stesso dispositivo opportunamente modificato abbiamo poi misurato il rapporto tra le intensità dei neutroni e dei protoni di circa 400 MeV nei raggi cosmici ed i cammini liberi medi di interazione nucleare anelastica in C e Pb per protoni. I risultati si inquadrano nell'attuale descrizione teorica della cascata nucleonica nell'atmosfera ad eccezione del rapporto neutroni-protoni.

I protoni di energia attorno a 400 MeV si possono separare dalle altre componenti dei raggi cosmici mediante l'uso di un « heavy particle selector », che è un dispositivo formato da un telescopio di contatori di Geiger e da un contatore di Čerenkov in anticoincidenza. Il metodo è stato descritto per la prima volta nel 1951 da Duerden e Hyams [1] e ne daremo un breve cenno. In fig. 1 abbiamo riportato la quantità di luce Čerenkov emessa in acqua da mesoni μ e da protoni, in funzione dei rispettivi « range » in piombo. Evidentemente una particella il cui « range » è compreso, per esempio, fra 100 e 200 g/cm^2 di piombo è un mesone se produce luce di Čerenkov, altrimenti è un protone.

Il dispositivo sperimentale che separa i due tipi di particelle è quello di fig. 2: si tratta di un telescopio 1234 di contatori in coincidenza quadrupla,

(*) Attualmente presso il Laboratorio di Chimica Fisica della S. A. Montecatini (Ferrara).

(1) T. Duerden e B. D. Hyams: *Phil. Mag.*, **43**, 717 (1952).

con un assorbitore T che fissa il limite inferiore al range delle particelle, e di un contatore di Čerenkov Č in anticoincidenza che pone invece il limite superiore alla velocità.

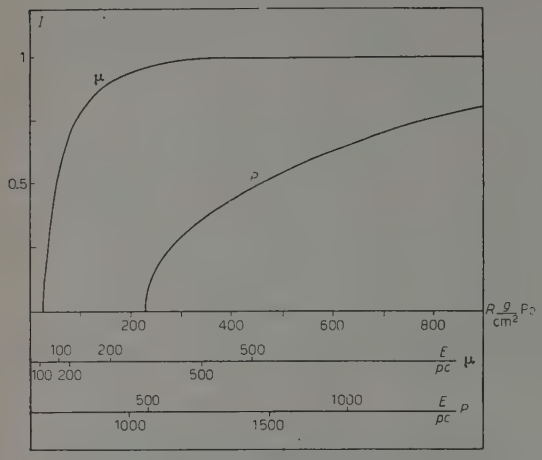

Fig. 1.

Lo schema a blocchi del circuito è anch'esso in fig. 2. I contatori (lunghezza utile cm 30, diametro cm 4) sono collegati a gruppi di 5 o 6, tramite elementi amplificatori - formatori - adattatori, ai circuiti di coincidenza. Il contatore di Čerenkov (lunghezza cm 32, diametro cm 30) è un cilindro, a pareti diffondenti contenente acqua, con un fotomoltiplicatore Dumond 6292 seguito da un amplificatore rapido ([2]) e da un discriminatore. Quest'ultimo ammette soltanto impulsi più alti di 1/20 del valore medio dell'impulso prodotto da una particella relativistica che attraversi l'apparecchio (questo impulso medio corrisponde ad una decina di elettroni al catodo del fotomoltiplicatore). Per

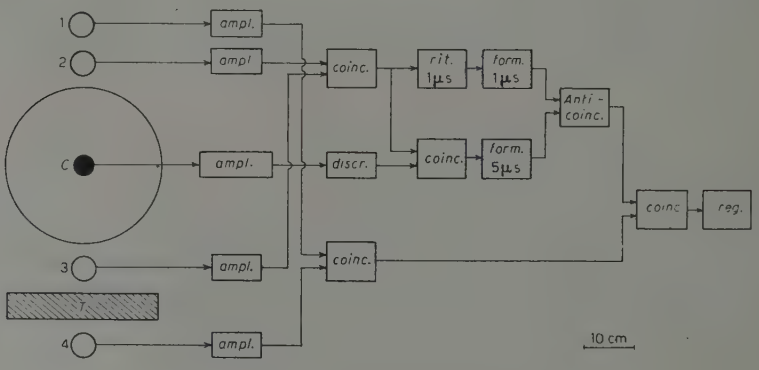

Fig. 2.

diminuire il tempo morto, l'anticoincidenza avviene fra l'impulso di coincidenza doppia ritardato di 1 μs e quello di coincidenza tripla 23 Č opportunamente allungato. L'inefficienza dell'anticoincidenza dipende da vari fattori: *a*) rendimento ottico del contatore di Čerenkov; *b*) sciami laterali; *c*) casuali.

([2]) R. C. Chase e W. A. Higinbotham: *Rev. Sc. Instr.*, **23**, 34 (1952).

Preciseremo in seguito il valore dell'inefficienza, che è comunque dell'ordine di 1‰ nelle diverse disposizioni usate.

Tutte le misure sono state effettuate sotto un tetto di pochi g/cm².

Con un dispositivo del genere si viene a disporre di un fascio piuttosto monocromatico di protoni. Abbiamo eseguito misure relative alla componente protonica dei raggi cosmici nella atmosfera (intensità, variazione con l'altezza, variazione zenitale, effetto barometrico); abbiamo inoltre cercato indicazioni sulla componente neutronica e sulle interazioni nucleari dei protoni in materiali condensati.

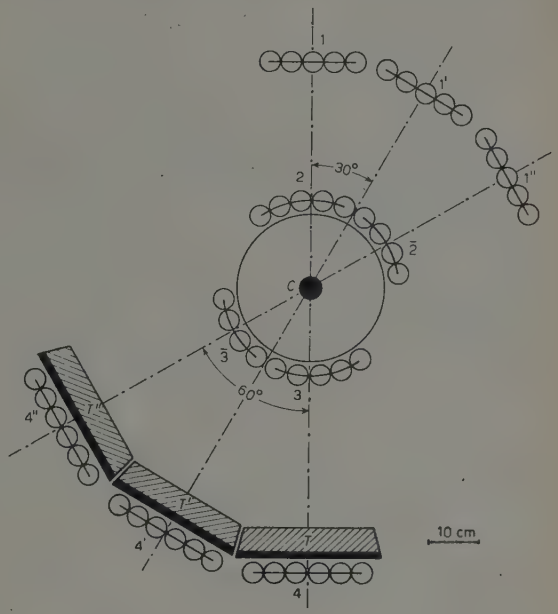

Fig. 3.

1. – La componente protonica dei raggi cosmici.

1·1. *Distribuzione zenitale a livello del mare.* – Abbiamo misurato la distribuzione zenitale al livello del mare, nel piano EW, dei protoni dei raggi cosmici di energie comprese fra 300 e 500 MeV circa (*).

L'apparecchio è disegnato in fig. 3. I contatori 2,$\bar{2}$ e 3,$\bar{3}$ sono normalmente connessi in parallelo; la misura della componente protonica e della totale sono state fatte contemporaneamente nelle tre direzioni zenitali 0°, 30°, 60° a mezzo dei telescopi 1234 che hanno una semiapertura angolare di circa 15°.

Per correggere piccole differenze geometriche fra i canali abbiamo normalizzato i risultati ad un andamento zenitale della totale di tipo $\cos^2 \vartheta$.

L'inefficienza dell'anticoincidenza 1234 — Č si misura ponendo fra i contatori 3 e 4 un assorbitore di piombo di 25 cm: allora tutte le particelle che attraversano il telescopio 1234 sono abbastanza veloci da produrre luce di Čerenkov e debbono venire anticoincise. Si è trovata una inefficienza di $0{,}75 \pm 0{,}06$ particelle per ogni 1000 che attraversano l'apparecchio. Si può avere una indicazione della frazione di inefficienza che è dovuta a sciami laterali ed a casuali usando la coincidenza quadrupla 1 $\bar{2}$ $\bar{3}$ 4 formata da gruppi

(*) Per la valutazione della banda di energia vedi 1·4.

di contatori non allineati: si trova $0{,}14 \pm 0{,}05$ per 1000 particelle che sarebbero registrate dal telescopio 1234. L'inefficienza dovuta a questi fenomeni è dunque dello stesso ordine di grandezza di quella ottica del contatore di Čerenkov.

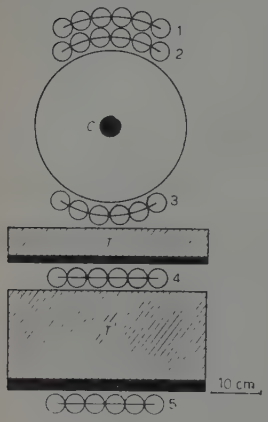

Fig. 4.

Le frequenze di conteggio del canale verticale sono:

— coincidenze 1234 (componente dura): 1009 ± 60 coinc/h;

— anticoincidenze $1234 - \check{C}$ (protoni): $1{,}67 \pm 0{,}10$ coinc/h.

I valori normalizzati dalle frequenze a diversi angoli zenitali sono:

— a 0°: $1 \pm 0{,}06$, a 30°: $0{,}46 \pm 0{,}05$, a 60°: $0{,}15 \pm 0{,}02$;

il valore a 60° è la media di quelli ottenuti in due serie di misure, una a E ed una a W, che coincidono entro gli errori statistici (20%).

1·2. *Variazione d'intensità con l'altezza.* – Per questa misura e per le successive in cui, più che una buona definizione angolare interessava una elevata frequenza di conteggio, abbiamo modificato la geometria dell'apparecchio come risulta in fig. 4: il telescopio 1234 serve per le misure sui protoni, quello 1235 per le misure di inefficienza dell'anticoincidenza.

L'uso dei due telescopi geometricamente diversi dà origine ad alcune difficoltà nella valutazione dell'inefficienza. Infatti mentre è presumibile che il contributo degli sciami sia lo stesso per i due telescopi, quello dovuto alla inefficienza ottica del contatore di Čerenkov è proporzionale al numero di quadruple che ogni telescopio registra.

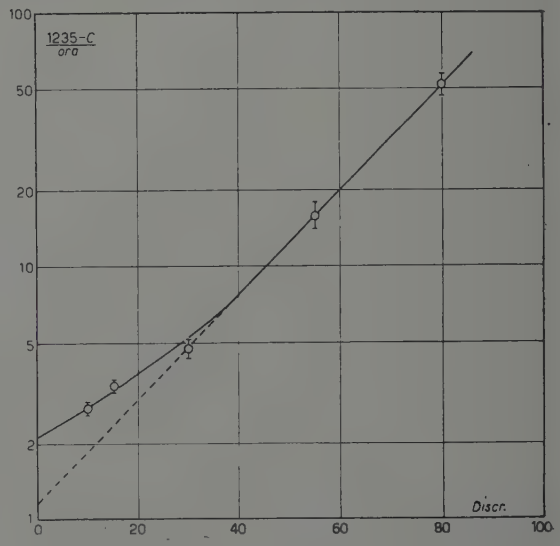

Fig. 5.

Per illustrare come si è tenuto conto di questo fatto riportiamo in fig. 5 le frequenze di conteggio $1235 - \check{C}$ ottenute variando l'altezza degli impulsi d'anticoincidenza ammessi dal discriminatore (questa misura in particolare è

stata fatta a 2000 m dove gli sciami sono più numerosi). La retta tratteggiata indica l'estrapolazione che isola il contributo all'inefficienza da parte del contatore di Čerenkov (proporzionale alle coincidenze quadruple); la differenza fra linea piena e linea tratteggiata è invece il contributo degli sciami (costante). Poichè, nelle misure, il discriminatore era nella posizione 10 della scala arbitraria riportata in ascisse, l'effetto che abbiamo descritto era sensibile: in tutte le misure che seguono abbiamo perciò calcolato l'inefficienza con le precauzioni suddette.

Nelle misure a cui si riferisce la fig. 5, le coincidenze 1235 erano 1900 all'ora. L'inefficienza dell'anticoincidenza è quindi maggiore di quella misurata in 1·1 e ciò è dovuto al fatto che in queste misure e nelle successive abbiamo preferito una vernice bianca per il contatore di Čerenkov che avesse migliori caratteristiche di durata rispetto a quella usata nella misura della distribuzione zenitale (che, d'altra parte era otticamente migliore).

Col dispositivo di fig. 4 abbiamo misurato all'ora:

— al livello del mare: 2780 coincidenze 1234 (componente dura) e $4{,}7 \pm 0{,}3$ anticoincidenze 1234 — Č (protoni);

— a 2000 metri: 3900 coincidenze 1234 e $19{,}9 \pm 0{,}7$ anticoincidenze 1234 — Č.

Il rapporto delle intensità delle componenti protoniche è quindi $4{,}23 \pm 0{,}31$ fra 2000 e zero m s.l.m..

1·3. *Variazione di intensità con la pressione a* 2000 m. – Sempre usando il dispositivo di fig. 4 abbiamo cercato la correlazione fra intensità dei protoni e pressione atmosferica a 2000 m. A tale scopo la registrazione era effettuata a mezzo di un milliamperometro scrivente.

I dati raccolti sono stati suddivisi in gruppi di 12 ore (precisamente dalle 0 alle 12 e dalle 12 alle 24 di ogni giorno) e confrontati con le registrazioni del barografo.

In 35 giorni di misura di è ottenuto un coefficiente barometrico

$$\alpha = -10{,}6 \pm 5{,}0\,\% \text{ per cm Hg}\,.$$

L'errore è stato calcolato dividendo in sei gruppi i dati raccolti e valutando lo scarto quadratico medio fra i risultati parziali. Per controllare la stabilità dell'apparecchio, durante queste misure, abbiamo ancora suddiviso i risultati in gruppi di 2 ore ciascuno ed abbiamo cercato una eventuale correlazione dell'intensità dei protoni col tempo solare. Sempre in 35 giorni di misure, ed usando i valori non corretti per la pressione, il valore medio del numero di protoni è di 1400 circa per ognuno dei gruppi di due ore. La dispersione

intorno a tale media è 2700 ± 1000, che non è in disaccordo con una distribuzione normale.

1·4. *Intensità assoluta al l.d.m. ed a* 2000 m. – Le misure fin qui descritte sono tutte a carattere relativo e d'altra parte lo strumento non è il più indicato per misure assolute d'intensità a causa dei diversi materiali che lo costituiscono e che implicano correzioni per passare dal valore misurato a quello vero.

Calcoleremo comunque il valore assoluto dell'intensità che corrisponde ai nostri risultati. A tale scopo bisogna conoscere i limiti ed il baricentro dello spettro di impulso su cui si è effettuata la misura (*): il limite inferiore è l'impulso di un protone che riesce appena ad attraversare l'apparecchio (890 MeV/c); come limite superiore assumiamo l'impulso di un protone che al centro del contatore di Čerenkov ha la velocità corrispondente alla produzione di 1 elettrone al catodo del fotomoltiplicatore (1200 MeV/c). Il baricentro della banda si ottiene dallo spettro J. G. Wilson [3], opportunamente degradato per le perdite per ionizzazione (circa 1020 MeV/c).

Normalizzando le coincidenze quadruple 1234 col valore assoluto della componente dura dei raggi cosmici in direzione verticale al l.d.m. [4], otteniamo, dalle misure descritte in 1·2,

— a livello del mare: $(4{,}62 \pm 0{,}20) \cdot 10^{-3}$ protoni $cm^{-2}\, s^{-1}\, sterad^{-1}$;

— a 2000 m: $(19{,}54 \pm 0{,}70) \cdot 10^{-3}$ protoni $cm^{-2}\, s^{-1}\, sterad^{-1}$.

Questi valori rappresentano un limite inferiore per due motivi: *a*) i protoni che giungono nel contatore di Čerenkov accompagnati da particelle relativistiche sono da queste anticoincisi; *b*) una parte dei protoni scompare, mentre attraversa l'apparecchio, per interazione nucleare. Trascuriamo il primo effetto e, per calcolare la correzione dovuta al secondo, usiamo i cammini di interazione in materiali condensati misurati da Fox e coll. [5] per neutroni, assumendo che i cammini siano gli stessi per neutroni e protoni. L'apparecchio corrisponde a mezza lunghezza d'interazione complessiva cioè la frequenza dei protoni osservati è ridotta di un fattore 0,6.

Il valore vero per l'intensità assoluta è allora:

— a 0 m s.m. $(7{,}62 \pm 0{,}33) \cdot 10^{-3}$ protoni $cm^{-2}\, s^{-1}\, sterad^{-1}\, (MeV/c)^{-1}$,

— a 2000 m s.m. $(32{,}2 \pm 1{,}15) \cdot 10^{-3}$ protoni $cm^{-2}\, s^{-1}\, sterad^{-1}\, (MeV/c)^{-1}$.

(*) Si valuta lo spettro in impulso per facilitare il confronto con i risultati di altri autori.

[3] M. G. Milroy e J. G. Wilson: *Proc. Phys. Soc.*, A **64**, 404 (1951).

[4] B. Rossi: *Rev. Mod. Phys.*, **20**, 537 (1942).

[5] R. Fox Cheith, L. Wontrs e K. R. MacKenzie: *Phys. Rev.*, **80**, 23 (1950).

1·5. *Discussione.* – Un confronto fra i risultati ottenuti è possibile qualora si faccia l'ipotesi semplificativa di un assorbimento esponenziale lungo l'atmosfera e si trascuri la diffusione angolare. Dalla variazione con la quota, dalla distribuzione zenitale e dall'effetto barometrico si può allora dedurre il cammino di assorbimento della componente protonica di 400 MeV in aria.

I valori che si ottengono dai nostri risultati sono i seguenti:

— dalla variazione con l'altezza: $\Lambda = 148 \pm 8$;

— dalla distribuzione zenitale (*): $\Lambda = 184 \pm 27$;

— dall'effetto barometrico: $\Lambda = 128 \pm 50$.

Se ora teniamo presente che: *a*) il cammino di assorbimento in aria della componente nucleonica di alta energia è 120 g/cm² ([6]); *b*) il « range » residuo in aria di un protone da 500 MeV è 130 g/cm²; appare evidente che i protoni da 500 MeV da soli non possono render ragione di un cammino di assorbimento $\Lambda \sim 148$ g/cm² e devono in massima parte esser prodotti localmente da una componente (neutronica) che ha un cammino di assorbimento, per energie analoghe, di almeno 148 g/cm² e che, presumibilmente, è più numerosa.

Il § 2 è dedicato alla ricerca di indicazioni sulla componente neutronica.

In ultimo possiamo confrontare l'intensità assoluta che abbiamo trovato con quella di altri autori. In una banda dello spettro di impulso che è compreso fra 890 e 1200 MeV/c, con baricentro a 1020 MeV/c, troviamo $I = (7{,}62 \pm \pm 0{,}33) \cdot 10^{-8}$ protoni cm^{-2} s^{-1} sterad^{-1} (MeV/c)$^{-1}$; nella stessa regione MYLROY e WILSON ([3]) trovano circa $5 \cdot 10^{-8}$ e J. BALLAM e P. G. LICHTENSTEIN ([7]) circa $10 \cdot 10^{-8}$.

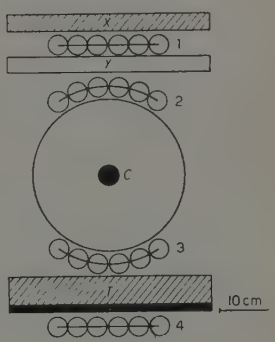

Fig. 6.

2. – La componente neutronica dei raggi cosmici.

2·1. *Rapporto neutroni protoni a* 2000 m s.m. – Un neutrone di 400 MeV che urta un nucleo ha energia abbastanza alta perchè, nella descrizione dell'evento, si possa prescindere dalla struttura nucleare e si possa considerare soltanto l'interazione del neutrone col singolo nucleone urtato. Se quest'ultimo è un protone si ha, per lo più, « scambio di carica » (essendo ancora poco probabile la produzione di mesoni): il protone cioè esce dal nucleo con approssimativamente la stessa energia e la stessa direzione del neutrone incidente.

(*) Considerando solo i valori a 0° e 30° perchè quello a 60° è probabilmente falsato dalla diffusione angolare.

([6]) B. ROSSI: *High Energy Particles* (New York, 1952), cap. 8.

Con l'apparecchio disegnato in fig. 6, confrontando la misura con assorbitore in X e quella con assorbitore in Y, possiamo misurare l'intensità dei protoni (della solita banda energetica 300-500 MeV) prodotti dai neutroni nell'assorbitore X. Lo stesso problema è già stato affrontato da J. BALLAM e P. G. LICHTENSTEIN [7], che usavano un sistema di due camere di Wilson per rivelare i protoni secondari.

Seguendo la loro impostazione

$$N = P \exp\left[-\frac{X}{L}\right]\frac{L_{np}}{X}, \tag{1}$$

ove N è il numero dei neutroni incidenti; P il numero dei protoni che emergono dall'assorbitore X nel quale sono stati prodotti per scambio di carica; L è il cammino di interazione di neutroni e protoni in X e L_{np} è il cammino libero medio dei neutroni per eventi del tipo che ci interessa (assumiamo $L_{np} = (A/Z)L$, ove L è il cammino di interazione nucleare) [5]. Abbiamo usato (fig. 6) assorbitori di piombo $X = Y = 33$ g/cm^2.

Le misure, eseguite a 2000 m hanno dato:

a)	senza assorbitori	$18{,}90 \pm 1$	protoni/ora,
b)	con assorbitore in X	$14{,}44 \pm 0{,}22$	protoni/ora,
c)	con assorbitore in Y	$11{,}87 \pm 0{,}20$	protoni/ora.

La differenza b-c dà direttamente

$$P = 2{,}57 \pm 0{,}30 \text{ protoni/ora}.$$

Dalla formula (1) con $L = 234$ g/cm^2 e (quindi $L_{np} = 590$ g/cm^2) si ricava

$$N = 52{,}8 \pm 6 \text{ neutroni/ora}.$$

Questo numero di neutroni si può confrontare con quello dei protoni misurato senza assorbitori *a*), qualora si trascurino le perdite per ionizzazione e si ammetta che il protone prodotto per scambio di carica conservi esattamente l'energia e la direzione del neutrone. Allora il rapporto $52{,}8/18{,}9 = 2{,}8$ è indicativo delle proporzioni fra neutroni e protoni dei raggi cosmici a 2000 m nell'intorno di 400 MeV di energia e, considerando le ipotesi fatte, 2,8 è un limite inferiore.

2·2. *Discussione.* – Come si era previsto in 1·5 discutendo l'assorbimento dei protoni di 400 MeV in aria, abbiamo trovato che i neutroni, a quella energia,

[7] J. BALLAM e P. G. LICHTENSTEIN: *Phys. Rev.*, **93**, 851 (1954).

sono più numerosi dei protoni. Lo sviluppo della cascata nucleonica in questa zona è quindi determinato dal comportamento dei neutroni.

L'unica esperienza di altri autori con cui si possa istituire un confronto diretto è quella di J. BALLAM e P. G. LICHTENSTEIN [7] che, al livello del mare, in una banda di energia simile alla nostra, trovano un rapporto neutroni-protoni circa 4, con una statistica piuttosto povera. Pensiamo che la differenza fra il nostro risultato ed il loro, se pure è significativa, sia dovuta non tanto ad un effetto della quota, quanto all'aver usato convertitori diversi. È infatti evidente che le ipotesi semplificative fatte nella descrizione dello « scambio di carica » sono più realistiche per il carbonio che per il piombo.

Non riteniamo invece molto significativo il confronto con esperienze di tipo integrale, come quella di J. C. BARTON [8] perchè lo spettro energetico dei neutroni non è sufficientemente noto.

È infine ovvio che l'uso di un sistema di anticoincidenze e di un convertitore a basso numero atomico ci avrebbe dato risultati migliori: la scelta del metodo che abbiamo usato è dovuta solo a ragioni contingenti.

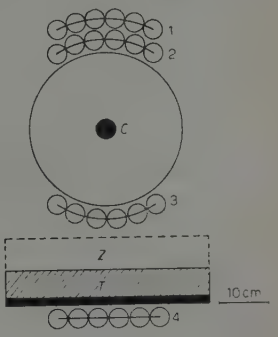

Fig. 7.

3. – Interazione nucleare dei protoni in materiali condensati.

Una grandezza che caratterizza l'interazione dei protoni con i nuclei è il cammino libero medio L, funzione del tipo di nucleo urtato e dell'energia del protone incidente. Descriviamo delle misure che hanno permesso di determinare questo cammino in piombo e carbonio per protoni dei raggi cosmici di circa 400 MeV.

L'apparecchio disegnato in fig. 7, senza assorbitore in Z, riveli N_0 protoni/ora: con assorbitore in Z ne rivelerà $N_1 = \varrho N_0 \exp[-Z/L]$ all'ora, ove $\varrho < 1$ rappresenta le perdite per interazioni elettromagnetiche, mentre $\exp[-Z/L]$ rappresenta quelle per interazioni nucleari. Per determinare il valore di ϱ abbiamo usato uno spettro in range dei protoni a 2 000 m, ottenuto per interpolazione fra quelli sperimentali a 0 ed a 3 500 m s.l.m. [3,9] (che peraltro non differiscono sensibilmente).

Abbiamo poi calcolato qual'è il corrispondente spettro che arriva ai contatori 4 dopo aver attraversato tutto l'apparecchio e l'eventuale assorbitore Z. La banda di questo spettro degradato, che il nostro strumento può rivelare,

---

[8] J. C. BARTON: *Proc. Phys. Soc.*, **6** A, 1042 (1951).

[9] G. E. MILLER, J. E. HENDERSON, D. S. POTTER, J. TODD e A. W. WOTRING: *Phys. Rev.*, **79**, 459 (1950).

ha come limite inferiore zero e come limite superiore il range (all'uscita dell'apparecchio) di un protone che, nel contatore di Čerenkov, aveva velocità sufficiente da produrre un elettrone al catodo del fototubo. ϱ è semplicemente il rapporto tra i valori integrali delle bande con e senza assorbitore.

In tab. I abbiamo riportato i valori di ϱ, Z, N_1, L in piombo e carbonio per $N_0 = 16{,}9 \pm 0{,}6$ protoni/ora. (Gli errori indicati sono quelli statistici).

TABELLA I.

	ϱ	Z (g/cm²)	N_1	L (g/cm²)
Piombo	0,710	33	$9{,}6 \pm 0{,}6$	150 ± 27
Carbonio	0,775	15,7	$10{,}9 \pm 0{,}6$	87 ± 19

L'energia dei protoni al momento dell'interazione si calcola a ritroso dagli spettri usati prima e ne risulta, all'ingresso dell'assorbitore Z, una banda fra 300 e 500 MeV circa.

Trascurando i protoni che sono fatti uscire dall'apparecchio da urti elastici (perchè questo effetto dovrebbe essere compensato, almeno in parte, da quelli che vi entrano per la stessa ragione), e trascurando la produzione di mesoni, possiamo definire il tipo di interazione nucleare a cui si riferisce il cammino libero medio che abbiamo trovato: si tratta, di urti in cui i protoni perdono abbastanza energia per uscire dalla banda 300-500 MeV.

I cammini liberi medi che abbiamo trovato coincidono, entro gli errori, con quelli relativi ad ogni urto anelastico ([10]): risulta allora che, in media, le perdite di energia per interazione nucleare in carbonio e piombo sono di almeno un centinaio di MeV per urto.

4. – Conclusione.

In quanto precede abbiamo descritto uno studio abbastanza accurato svolto sui protoni dei raggi cosmici di circa 400 MeV di energia nella bassa atmosfera. L'ottimo accordo ottenuto con altre esperienze per quel che riguarda il valore assoluto dell'intensità e quello del cammino di interazione nucleare anelastica in Pb e C è un indice dell'attendibilità del metodo.

Abbiamo anche messo in evidenza la possibilità di misurare, con un dispo-

([10]) J. DE JUREN: *Phys. Rev.*, **80**, 27 (1950).

sitivo di contatori, l'intensità e la direzione di arrivo di neutroni di alcune centinaia di MeV.

Cercheremo ora di inquadrare i risultati ottenuti nello schema, in parte noto, della cascata nucleonica. Allo stato attuale della ricerca, lo studio della componente nucleonica di media e bassa energia, nell'atmosfera, non è in grado probabilmente di fornire utili indicazioni sui processi elementari; ha invece interesse per completare il quadro interpretativo e descrittivo dai raggi cosmici (bilancio energetico, origine).

Il panorama sperimentale attuale è ben noto: per energie di oltre qualche GeV il cammino di assorbimento in aria dei protoni e dei neutroni si aggira su 120 g/cm^2; questo cammino cresce ad energie minori, tanto per i neutroni che per i protoni (questi ultimi sotto 1 GeV perdono sensibilmente energia anche per ionizzazione ma sono continuamente riforniti dalla componente neutronica).

L'aumento del cammino di assorbimento non corrisponde necessariamente ad una variazione delle sezioni d'urto elementari, ma sembra si possa spiegare come dovuto, in parte, alla minor pendenza dello spettro primario alle basse energie ([11]), ed in parte ad una variazione del grado di anelasticità nell'urto nucleone-nucleo, con l'energia.

In questo ordine di idee i valori sperimentali del cammino di assorbimento in aria per protoni e neutroni, e specialmente il valore del rapporto neutroni-protoni sotto 1 GeV di energia, forniscono un controllo molto sensibile per la prova di ogni teoria che descriva la cascata nucleonica. La nostra esperienza indica un cammino di assorbimento per protoni di 148 $\pm$ 8 g/cm^2 ed un limite inferiore al rapporto neutroni/protoni di 2,8, sempre per energia attorno ai 400 MeV.

Una teoria della cascata nucleonica valida anche ad energia di qualche centinaio di MeV è stata svolta da E. Clementel, F. Ferrari e G. Puppi ([12,13]): in essa si è tenuto conto: *a*) degli urti nucleari anelastici; *b*) degli urti elastici; *c*) delle perdite per ionizzazione dei protoni. Sempre a 400 MeV si trova un cammino di assorbimento dei protoni nella bassa atmosfera di 145 g/cm^2 ed un rapporto neutroni/protoni = 2.16.

Può avere infine interesse il conoscere l'energia dei protoni primari da cui derivano, in prevalenza, i protoni da noi osservati: ci sembra che l'unica utile indicazione si possa avere dallo studio compiuto da S. Lattimore ([14]) sull'effetto di latitudine di stelle di varia grandezza. Risulterebbe che gli eventi di circa 400 MeV di energia corrispondono ad una banda primaria il cui baricentro è

([11]) W. Heisenberg: *Kosmische Strahlung* (Berlin 1953), cap. V.
([12]) E. Clementel e G. Puppi: *Nuovo Cimento*, **8**, 942 (1951).
([13]) E. Clementel e F. Ferrari: *Nuovo Cimento*, **9**, 572 (1952).
([14]) S. Lattimore: *Phil. Mag.*, **41**, 961 (1950).

minore o al massimo uguale a 15 GeV. Un'indicazione più precisa si potrebbe naturalmente avere dallo studio dell'effetto di latitudine su protoni da 400 MeV, nella bassa atmosfera.

Ringraziamo i Proff. P. Budini, E. Clementel, G. Puppi e A. Rostagni per utili discussioni ed i signori S. Capuzzo e E. Vianello per la parte che hanno avuto nella costruzione e nel controllo degli apparecchi.

SUMMARY

We have used a « heavy particle selector » with a Čerenkov counter in anticoincidence to measure the absolute intensity, the zenith angle distribution, the barometric effect and the altitude variation of cosmic ray protons around 400 MeV energy. We have also measured the neutron to proton ratio in the same energy region, and the anelastic nuclear interaction lenght in C and Pb for protons. With the exception of the neutron proton ratio, all the results are consistent with our present theoretical description of the nucleon cascade in the atmosphere.

IL NUOVO CIMENTO Vol. I, N. 4 1° Aprile 1955

On the Nuclear Interaction of He-Nuclei in the Cosmic Radiation.

M. Ceccarelli, G. Quareni and G. T. Zorn (*)

Istituto di Fisica dell'Università - Padova

Istituto Nazionale di Fisica Nucleare - Sezione di Padova

(ricevuto il 7 Febbraio 1955)

Summary. — 42 stars, produced in photographic emulsions by the nuclear interaction of cosmic ray He-nuclei have been identified. They were selected in a systematic way, based on the identification of the tracks associated with nuclear disintegrations. These disintegrations, as well as those produced by « primary » protons in the same plates were analysed, and the angular and frequency distributions for both types of stars were determined. From a comparison of these distributions it has been concluded that, on the average, only about one half of the nucleons of the He-nucleus contribute appreciably to the destruction of the target nucleus and to the production of mesons.

This paper deals with the interaction of He-nuclei of the Cosmic Radiation with nuclei composing photographic emulsions. The nucleus of Helium, having a small number of nucleons, is particularly suited to the investigation of interactions between nuclei. Photographic emulsion techniques allow the disintegrations so produced to be studied in great detail. However, due to the inherent difficulty of this type of research, very little work has been done on these lines [1] and in any case the greater part only deals with disintegrations at very high energy, with intense production of mesons. We believed it would be interesting to carry out a program of research in which the selection of the dis-

---

(*) Now at Brookhaven National Laboratory, U.S.A.

[1] H. L. Bradt, M. F. Kaplon and B. Peters: *Helv. Phys. Acta*, **23**, 24 (1950); U. Camerini, J. H. Davies, C. Franzinetti, W. O. Lock, D. H. Perkins and G. Yekutieli: *Phil. Mag.*, **42**, 1261 (1951); G. Cortini, A. Manfredini and G. Segrè: *Nuovo Cimento*, **9**, 659 (1952); A. Engler, U. Haber-Schaim and W. Winkler: *Nuovo Cimento*, **12**, 930 (1954).

integrations was as unbiased as possible (i.e. in which the selection criteria were the least restrictive).

1. – Selection of Disintegrations Produced by He-Nuclei.

In this investigation we have used nuclear research emulsions (Ilford G5, 400 μ thick) exposed to the cosmic radiation at an altitude of 95 000 ft for 4 hours at a geomagnetic latitude of 55° N. These plates were kindly lent to us by Professor C. F. POWELL, F.R.S..

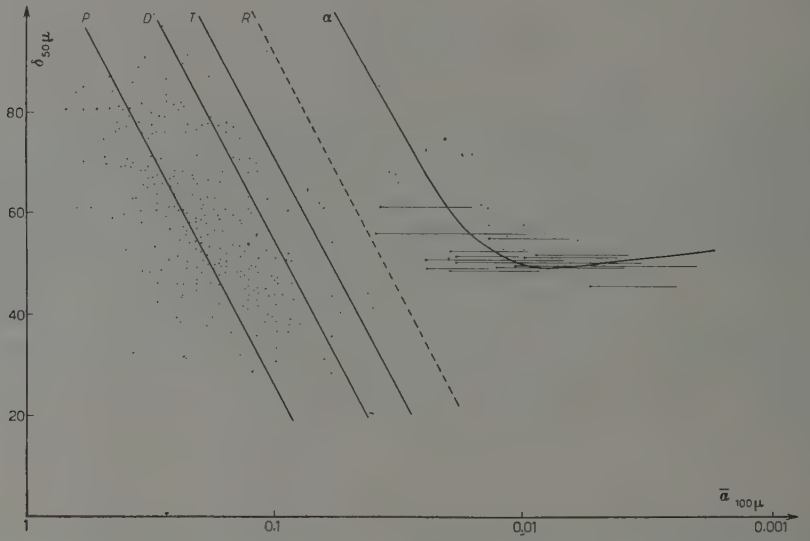

Fig. 1. – Relationship between grain density $\delta_{50\mu}$ and mean angle of scattering. $\bar{\alpha}_{100\mu}$ for tracks associated with nuclear disintegrations. The lines P, D, T and α correspond to protons, deuterons, tritons and α-particles rispectively. Line R was used in selecting the tracks of α-particles. A point accompanied by a horizontal line represents the upper limit for $\bar{\alpha}_{100\mu}$ for that particular track.

Out of a total of 7 900 nuclear disintegrations observed in an emulsion volume of 9.5 cm^3, about 1 000 stars were selected each of which had at least one « grey » or « black » track in the upper hemisphere forming an angle of less than ten degrees with the emulsion plane. We have made grain density and multiple scattering measurements on those tracks longer than 1 000 μ and having grain densities greater than that corresponding to three times the minimum value. The results of measurements on a total of 650 tracks so selected are partially shown in Fig. 1. In this figure the lines P, D, T and He correspond to protons, deuterons, tritons and He-nuclei respectively

and are based on a « best fit » of the proton line to the experimental points. If as a result of the first measurement the point corresponding to a track fell to the right of the T line, it was re-examined in more detail, taking into particular account the « distortion » of the emulsion. If after the second measurement the point fell to the right of the dashed line, the corresponding track was considered to be due to a He-nucleus and we have logically assumed it to be the « primary », thus identifying He-stars without any reference to the disintegration itself. The accuracy of our measurements is indicated by the separation of the points between the He and T lines, and, together with the method outlined above, has enabled us, we believe, to have obtained in an unbiased way a fair sample of the He-disintegrations produced in these plates.

This also seems to be confirmed by a comparison with results deduced from the energy spectrum determined by WADDINGTON of the Bristol group using these same plates. For this comparison we have divided the disintegrations into 2 groups, being those produced by primaries having energies greater and less than 1.6 GeV, and have compared the ratio of the number of stars in each group to the ratio of the number of particles in corresponding energy ranges as deduced from the energy spectrum. Assuming no variations with energy of the mean free path for nuclear interaction, these ratios may be directly compared and it was found that they are identical within statistical errors.

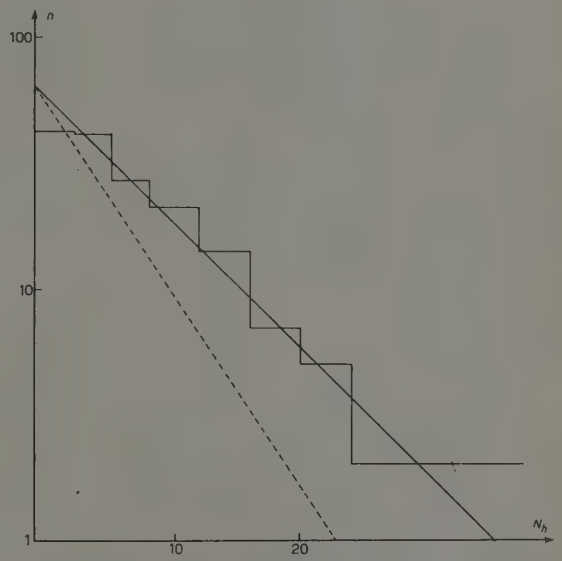

Fig. 2. – Frequency distribution for stars produced by α-particles (solid line) and by protons (broken line) having N_h grey and black prongs.

2. – Results.

The criterion adopted in the study of the interaction of He-nuclei of the cosmic radiation has been that of a comparison in the same emulsions of the disintegrations produced by these particles with those produced by protons. A direct comparison would seem to have its justification in the fact that at high altitudes in the atmosphere both of these types of particles have similarly shaped energy spectra above 1 GeV/nucleon. The selection procedure for He-stars was that described

in the previous section. P-stars were also selected in a systematic way. They were identified with the group of stars which had a « thin » track in the « upper » hemisphere. However, if the star contained a « jet », the track of the singly charged « primary » had to appear opposite to the axis of the jet within its median angle.

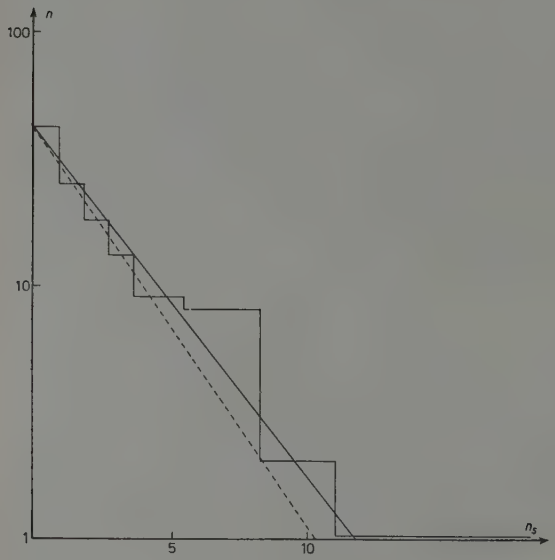

Fig. 3. – Frequency distribution for stars produced by α-particles (solid line) and by protons (broken line) having n_s thin tracks. For α-stars, the numbers n_s have been reduced by one.

For this comparison we have analysed in the same way stars produced by He-nuclei and by protons, and we have grouped the tracks of these stars into three grain density groups: « thin », « grey » and « black », corresponding to specific ionisation losses for singly charged particles of $1 < I/I_0 < 2$, $2 < I/I_0 < 5$, $5 < I/I_0$, respectively. We have used n_s, n_g and n_b for the number of thin tracks (other than the « primary »), grey tracks and black tracks per star, respectively, and have adopted the notation N_h for the sum $n_g + n_b$. The angle of each track with respect to the primary track was also determined, thus making possible a comparison of the angular distributions as well as the frequencies of the disintegration products.

The frequency of stars having N_h grey and black tracks is shown in Fig. 2 for both He-stars and p-stars, and a corresponding frequency distribution of stars having n_s thin tracks is shown in Fig. 3. The curves and histogram of Fig. 2 have been normalized to the same total number of He-stars and p-stars, whereas the curves and histogram presented in Fig. 3 have been normalized to the same number of He-stars having $n_s \geqslant 2$ and p-stars having $n_s \geqslant 1$.

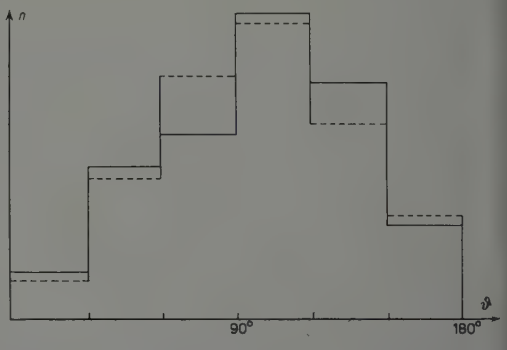

Fig. 4. – Angular distribution of black tracks from α-stars (solid line) and from p-stars (broken line).

The angular distributions of black prongs from the He-stars and from p-stars are shown in Fig 4.

In Fig. 5 are shown the two angular distributions for grey prongs from He-stars having primaries of energy respectively greater and less than 1 GeV. These are compared with the angular distribution of grey prongs from all particles.

The angular distribution of thin tracks associated with He-stars are shown

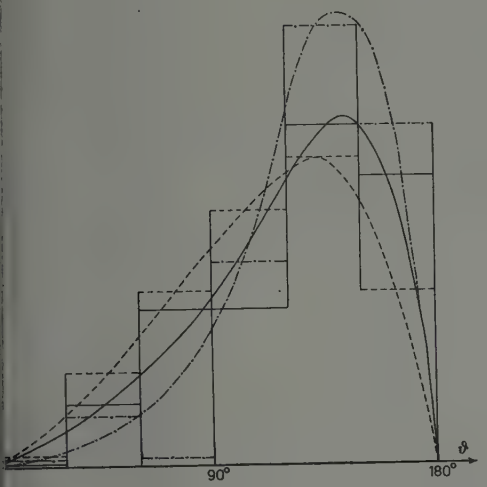

Fig. 5. – Angular distribution of grey prongs for stars produced by protons (broken line), α-particles > 1 GeV (solid line), and α-particles < 1 GeV (alternate dots and dashes).

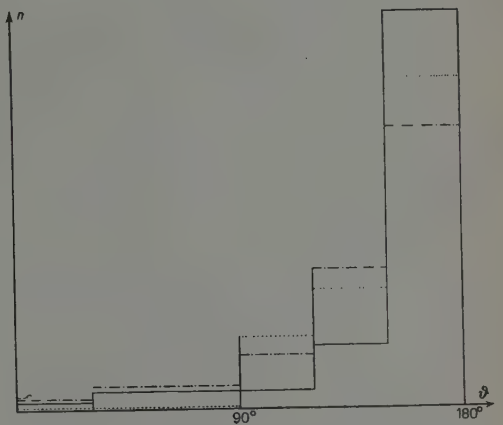

Fig. 6. – Angular distribution of thin tracks from α-stars having $1 \leqslant n_s \leqslant 3$ (solid line) $4 \leqslant n_s \leqslant 9$ (alternate dots and dashes); $10 \leqslant n_s$ (dotted line).

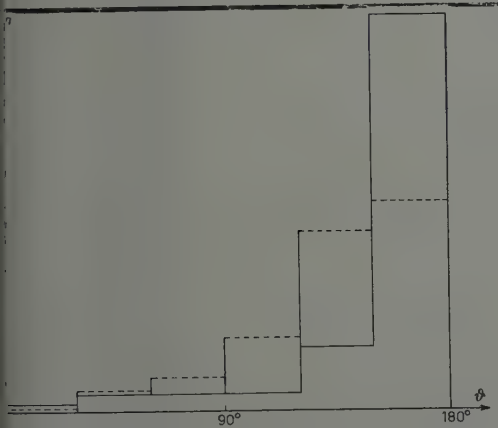

Fig. 7. – Angular distribution of thin tracks from α-stars (solid line) and from p-stars (broken line).

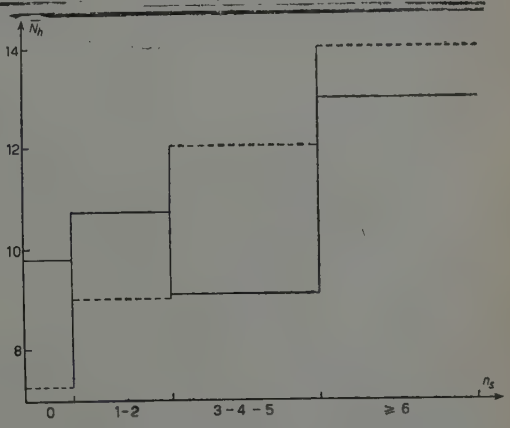

Fig. 8. – Distribution of $\overline{N}_h$ as a function of the number of thin tracks, n_s, from α-stars (solid line) and fromp-stars (broken line).

in Figs. 6 and 7. In Fig. 6 He-stars have been divided into three groups corresponding to different multiplicities (n_s-value) and the angular distributions of thin tracks of these three groups were compared with each other. In Fig. 7 a comparison of the angular distributions of shower particles for He- and p-stars is made in the low multiplicity region ($1 \leqslant n_s \leqslant 3$). Finally the average N_h, N_h, of He and p-stars having the same multiplicity were compared. The result of this comparison is shown in Fig. 8.

3. – Discussion.

The division of the star tracks into categories depending upon the ionization of the associated particles allows us, generally, to identify either the kinds of particle or the phase of the disintegration process in which they were emitted. Thin or « shower » particle tracks are attributed mainly to mesons and to some high energy protons. Grey tracks are generally attributed to the phase of direct emission, and black tracks to the evaporative phase of nuclear destruction.

N_h, the sum of the number of grey and black tracks in a single star gives us an indication of the degree of nuclear disintegration. As is apparent from Fig. 3, the disintegrations produced by He-nuclei result in a larger destruction of the target nucleus than is visible in p-stars. Noting the histograms of Fig. 8, this effect seems to be more pronounced for disintegrations having small n_s and which, therefore, are produced at smaller primary energies. As the average energy increases, i.e. with increasing n_s, one notes that there is a slower increase of N_h for He-stars than for p-stars, until, at the highest multiplicities which have been compared, the star sizes are approximately the same.

Since higher multiplicities are associated with a more frequent re-absorption of mesons, it is reasonable to assume that the nuclear excitation must also depend principally on this same phenomenon. Thus the relatively small contribution, due to the direct interaction of the primary nucleons, does not sensibly affect the size of the stars ([2]).

The histogram of Fig. 4 indicates that the black tracks are distributed almost isotropically, not only for stars produced by protons but also for those produced by He-nuclei. This result seems to confirm that the particles producing these tracks are emitted principally in an evaporation process, the excitation mechanism of which does not depend sensibly on the mode of the nuclear excitation.

For grey tracks from He and p-stars, however, a marked difference in their angular distributions is observed (Fig. 7). In He-stars the grey tracks are much more closely grouped in the direction of the primary than in p-stars.

([2]) M. CECCARELLI and G. T. ZORN: *Nuovo Cimento*, **10**, 540 (1953).

It would be possible to explain this fact if we were to assume that, for He-stars, most of these closely grouped grey tracks are produced by one or both of the two protons which composed the He-nucleus. This hypothesis has its confirmation in the fact the collimation of grey tracks is much more accentuated in the stars produced by He-particles having energies less than 1 GeV, and therefore with ionizations greater than eight times the minimum value (twice minimum produced by doubly charged particles). The fact that the collimation of grey tracks decreases for stars with He primaries of greater energy may be considered as being due to the existence of a lower limit for the grain density used for the selection of grey tracks. It would therefore seem possible to state, based on the evidence thus far presented, that He-nucleons quite often traverse nuclear matter without interacting strongly, and that those particles producing well-grouped tracks in the forward direction may well be He-nucleons which have interacted only very weakly with nuclear matter.

Following this scheme it is evident that when the He primary is very energetic the charged fragments resulting from its disintegration, if non interacting, appear in the category of thin tracks and not in that of grey tracks. This would, therefore, result in a more accentuated collimation for thin tracks associated with He-stars as is observed in Fig. 6. The effect of collimation observed for $1 \leqslant n_s \leqslant 3$ is reduced when $n_s > 3$, that is, when there is a more copious production of mesons. The angular distribution of these mesons would, in general, be much broader than the angular distribution for protons resulting from the fracture of the incident He-nucleus.

The characteristics of the nuclear interaction of the He-nucleus will now be considered in the light of a simple model of its structure. We will make the assumption that, for the process considered, the 4 He nucleons interact with nuclear matter as four isolated particles which traverse the target nucleus. The data available on the cross-section for star production for fast protons indicates an appreciable nuclear transparency.

Assuming in our case a value of 0.7 for the ratio of the effective cross-section to the geometric value for the average nucleus of the photographic emulsion, and assuming that the He-nucleus is composed of four completely independent nucleons (also as regards their position in space), one may calculate the probability that on collision no nucleons of the He particle collide, and that one, two, three or four suffer collisions in a single encounter. These probabilities are listed in Table I. The mean number of interacting nucleons is 2.8 while the most probable is 3.

Also it would seem necessary to consider the space correlation of the 4 nucleons. They are not independent, for, if one interacts, it eliminates the possibility of this interaction for the remaining three nucleons. As a result, the average number of nucleons that interact should perhaps be notably smaller than 2.8, and such a value would seem to be in better agreement with the exper-

imental results. In fact, analysing quantitatively the angular distribution of grey tracks and of shower particle tracks for stars with n_s between 1 and 3, we find that the average number of strongly interacting nucleons of the He nucleus is 2. The analysis was based on the hypothesis that the angular distribution of grey prongs is the same in p-stars and in stars having as primaries He-particles with energies less than 1 GeV, provided that it is possible to exclude tracks produced by the incident nucleons after the collision. The number of

TABLE I.

0	0.008
1	0.0756
2	0.2646
3	0.4116
4	0,2401

tracks which constitute the forward excess in He-stars was, therefore, held to be equal to the number of protons which had come from the fracture of the He-particle, and which had crossed the nucleus without suffering strong interaction. A similar argument has been applied to the forward excess of showers.

The model proposed above would almost preclude a traversal of a target nucleus by a He nucleus without at least one of its nucleons interacting (probability = 0.0081), and this is in fact borne out by the geometric mean free path for nuclear interaction that is observed experimentally ([3]). Whatever model of nuclear interaction is used, it should take into account the spatial correlation of the nucleons, which in turn would imply a knowledge of the problem of a many body interaction. On the other hand, we do not believe that our experimental data is sufficient to permit us to choose in a reliable manner between the various possible models.

From the model proposed it follows that for He-nuclei many more peripheral star-producing collisions occur, together with a large number of interactions with light nuclei. For protons, on the other hand, central collisions with heavy elements resulting in stars are more probable.

This would also seem to be confirmed by two He-events out of the 42 observed in this investigation, in which a process of stripping took place, very probably in a peripheral encounter. The details of these events are given in the following section.

The results that have been previously discussed indicate that approximately two of the He nucleons either do not interact with the target nucleus or do so only weakly. Judging from these results it would appear that on the average only two of the He nucleons should contribute to the production of mesons.

([3]) C. J. WADDINGTON: *Phil. Mag.*, **45**, 1312 (1954).

This may also be confirmed from the comparison of meson production in p-stars. In Fig. 2 one observes that the slope of the normalized curves representing the frequency of stars produced by cosmic ray protons and He-nuclei as a function of their multipliticies (n_s) are not very different.

One should note that we have already substracted one shower particle from each He-star. Considering the model previously proposed, this « excess » of one fast particle may be attributed to the inclusion in the shower of a high energy proton from the break-up of the He-nucleus. Since the number of mesons present in He-stars is not very much larger than in p-stars, we may infer that no more than two nucleons of the He-nucleus contribute to meson production, which agrees with the previous estimate.

4. – Two Unusual Events.

During this investigation two events of an unusual character were observed. They are, indeed, He-stars, but have the apparent characteristic that the He-primary producing the stars, continues on after the nuclear encounter, only slightly deviated in direction and without any change in velocity. The details of these events are presented in Table II.

TABLE II.

	Primary α-particle		Secondary α-particle		Kinetic energy of the α-part.	Type of star (α-part. is not included)	Visible energy of the star	Angle between the two α-tracks
	$\bar{\alpha}_{100\mu}$	$\delta_{50\mu}$	$\bar{\alpha}_{100\mu}$	$\delta_{50\mu}$				
I	0.0021 ± 0.003	76.3 ± 1.6	0.04 ± ?	76.2 ± 1.6	1.4 GeV	7 + 0	650 MeV	1 670
II	0.01 ± ?	50.7 ± 1.1	0.011 ± 0.003	50.4 ± 1.1	5 GeV	3 + 2	900-1 450 MeV	1 770

The stars produced by the interaction of these He nuclei are the result of a high excitation energy and, therefore, may not be explained as being produced by the energy loss that would result from the small angular deviations in the direction of motion of the primary particle. They may, however, be explained as resulting from a « stripping » process in which a ^{6}He or a ^{4}He nucleus is transformed in the encounter into a ^{4}He or a ^{3}He nucleus. Energy considerations would seem to indicate that the first event was produced by

at least two neutrons stripped from a ^{6}He nucleus. The second event could have been produced by a single neutron, thus indicating that the parent particle could have been either a ^{6}He or a ^{4}He nucleus. Since the ^{6}He nucleus is unstable, its presence in the cosmic radiation can only be explained by supposing it to be a result of the fracture of heavier nuclei of the primary radiation.

5. – Conclusion.

The model of nuclear interaction for He-nuclei which has been proposed in this investigation seems to explain in a satisfactory and self-consistent way the results obtained through the comparison of He and p-stars. The He-nucleus according to this model interacts strongly with the target nuclei, but only two of its nucleons contribute substantially to its destruction. The production of mesons as inferred from this model is also consistent with the experimental results and would seem to indicate that on the average not more than 2 of the nucleons of the He-nucleus are responsible for the production of mesons.

Stripping processes in nuclear interaction have also been observed. These, presumably, result from a peripheral encounter with the target nucleus, and are apparently characterized by a very small excitation of the He-nucleus in the encounter.

Aknowledgments.

We wish to thank Prof. ROSTAGNI, the Director of these Laboratories, for the interest with which he has followed our work, and Professors M. DALLAPORTA and G. PUPPI for their useful advice and assistance in discussions. Our thanks must also go to A. BERNARDI and D. SOTTOVIA for their help in scanning and in studying the events.

RIASSUNTO

Nel corso di questa ricerca sono state identificate 42 disintegrazioni nucleari prodotte in emulsione fotografica da nuclei d'elio della radiazione cosmica. L'identificazione è basata sull'analisi diretta delle tracce associate alle stelle e riteniamo quindi che essa sia poco restrittiva. Le disintegrazioni prodotte da particelle α sono state analizzate e confrontate con quelle prodotte nelle stesse lastre da protoni. Da questo confronto è risultato che in media soltanto la metà circa dei nucleoni formanti il nucleo d'elio contribuisce sensibilmente alla disintegrazione del nucleo urtato ed alla produzione di mesoni.

IL NUOVO CIMENTO Vol. I, N. 4 1° Aprile 1955

Singular Integral Equations in Quantum Field Theory.

J. C. TAYLOR

Peterhouse - Cambridge, England

(ricevuto il 7 Febbraio 1955)

Summary. — The covariant theory of meson-nucleon scattering contains a vertex-part equation which is a singular integral equation. Because of this, there is a difficulty about the treatment of a renormalization constant. It is shown here how a consistent use of a high energy cut-off overcomes this difficulty. A related difficulty for the Bethe-Salpeter equation cannot be overcome by the same method.

1. – Introduction.

The study of the covariant integral equation for the meson-nucleon system was begun by FUBINI (1), who showed that, for purposes of renormalization, the equation had to be analysed into a system of subsidiary equations. The renormalized system of equations, which has been given by a number of authors (2), contains a vertex-part equation which has the property of being singular (3). This has the consequence that a renormalization constant, Z^{-1}, which appears as an inhomogeneous term, must be zero. Thus, although the theory is a departure from the perturbation method, infinite constants are still encountered.

Because of the « b-divergences » (4), Z^{-1} appears as a factor in a related self-energy part. Since infinite constants are now appearing as multiplicative

(1) S. FUBINI: *Nuovo Cimento*, **10**, 851 (1953).

(2) N. KROLL: *Procedeings of the Fourth Annual Rochester Conference on High Energy Nuclear Physics*, 156 (1954); M. M. LÉVY: *Phys. Rev.*, **94**, 460 (1954); J. C. TAYLOR: *Nuovo Cimento*, **12**, 148 (1954), etc..

(3) A very similar equation has been studied by S. F. EDWARDS: *Phys. Rev.*, **90**, 284 (1953).

(4) A. SALAM: *Phys. Rev.*, **82**, 217 (1951).

factors (as opposed to additive terms in the perturbation theory), it is necessary to use some sort of cut-off at intermediate stages of the calculation. From the formal correspondence with the perturbation theory, one would expect the final result for observable quantities to be insensitive to the value of the cut-off. The proof of this, however, requires an examination of the uniformity of convergence of the series concerned. In section **2**, this proof is supplied. It rests upon an asymptotic property of the vertex-part function, which is derived in section **3**. The asymptotic property also enables the mechanism of the multiplicative cancellation of infinities to be exhibited.

The Bethe-Salpeter ([5]) equation for the deuteron also has the singular property. Here, it has the consequence that there is not a discrete eigenvalue spectrum. It is the substance of a proposal by GOLDSTEIN ([6]) and by GREEN and MCCARTHY ([7]) that a spectrum be defined as the limit of the spectrum of the cut-off equation (which is discrete). In section **4**, an examination of the asymptotic properties of the equation makes it probable that this prescription would not yield physically reasonable results.

2. – The Vertex-Part Equation.

In pseudo-scalar charge-symmetric meson theory, the renormalized vertex-part equation is ([2]), for the relevant state ($I=\frac{1}{2}$),

$$(1)\quad \Gamma_c(p,k) = -ig^2(2\pi)^{-4}\int \mathrm{d}k'\,\gamma_5[i\gamma(p-k-k')+M]^{-1}\gamma_5[i\gamma(p-k')+M]^{-1}\cdot \cdot\Gamma_c(p,k')(k'^2+\mu^2)^{-1}+\gamma_5 Z^{-1}\,.$$

The renormalization constant Z^{-1} is supposed to be determined by

$$(2)\qquad \Gamma_c(p_0,0)=\gamma_5\,,\qquad i\gamma p_0 + M = 0\,.$$

However, equation (1) can have no solution with $Z^{-1}\neq 0$; for, if it did, $\Gamma_c(p,k)$ would tend to $\gamma_5 Z^{-1}$ for large k, and the integral in (1) would diverge logarithmically. This is the main consequence of the singular property. It means that (1) is effectively an homogeneous equation, and (2) leaves $\Gamma_c(p,k)$ undetermined to within an arbitrary factor $f(p)$ (satisfying $f(p_0)=1$).

The theory also contains a self-energy function, related to $\Gamma_c(p,k)$ by

$$(3)\qquad \Sigma(p) = g^2(2\pi)^{-4}\int \gamma_5[i\gamma(p-k)+M]^{-1}\Gamma_c(p,k)(k^2+\mu^2)^{-1}\,\mathrm{d}k\,.$$

([5]) E. E. SALPETER and H. BETHE: *Phys. Rev.*, **84**, 1232 (1951).
([6]) J. S. GOLDSTEIN: *Phys. Rev.*, **91**, 1516 (1953).
([7]) H. S. GREEN and I. E. MCCARTHY: *Proc. Phys. Soc.*, A **67**, 719 (1954).

The convergent part, Σ_c, is given by

$$\Sigma_b(p) = \Sigma(p) - \Sigma(p_0) - (p - p_0)_\mu [\partial/\partial p_\mu \Sigma(p)]_{p=p_0}, \tag{4}$$

$$\Sigma_c(p) = Z^{-1}\Sigma_b(p). \tag{5}$$

The appearance of the factor Z^{-1} again in (5) is the chief obstacle to a direct acceptance of the result $Z^{-1}=0$.

The formal justification of equation (5), using the iteration solutions for the functions concerned, rests upon SALAM's [4] proof of the cancellation of the « b-divergences » in the general case. In fact, the system of Feynman graphs implicit here is the simplest system having the essential structure made use of in Salam's proof.

Consider now the application to equation (1) of a high-energy cut-off, characterized by a large number X. Then (1) becomes an equation of the Fredholm type, and has a unique solution $\Gamma_X(p, k)$. Moreover, for sufficiently small g^2, the iteration solution converges and the Fredholm solution coincides with it. $Z^{-1}(X)$ will be a non-zero quantity, determined by equation (2). Assuming that a solution of the original equation exists, Γ_X will tend to a finite limit as $X \to \infty$, and $Z^{-1}(X)$ will tend to zero. Defining the solution of (1) to be the limit of Γ_X removes the arbitrary function $f(p)$.

Let $\Sigma^N_{c,X}(p)$ be the iteration solution of the cut-off equation up to the N-th order in g^2. Then the proof of the cancellation of the « b-divergencies » in the power-series shows that $\Sigma^N_{c,X}$ is insensitive to X. For sufficiently small g^2 the power-series converge, and we would like to pass to the limit $N \to \infty$ and deduce that $\Sigma_{c,X}$ is insensitive to X. To justify this step, we require uniform convergence of the iteration solution, regarding the terms as functions of X. In the next section, it is shown that $Z^{-1}(X)$ and $\Sigma_{b,X}$ depend upon X through terms of the form

$$\exp [f(g^2) \log X].$$

The radius of convergence of the g^2-expansion of this expression is independent of X; and so the requirement of uniform convergence is certainly met. Finally, the result extends to all values of g^2 by analytic continuation.

Thus, by using a cut-off which is eventually allowed to become infinite, we should be able to obtain sensible finite answers for both Γ_c and Σ_c. Of more interest than a formal proof, however, is an explanation of how the cancellation of X-dependent factors actually happens. This we attempt to provide in the next section.

3. – The Asymptotic Form.

The singular property of equation (1) is signalled by the coupling constant's being dimensionless. In this section, this fact is exploited to obtain the asymptotic form of $\Gamma_c(p, k)$ for large k^2, and thence to deduce the form of $\Sigma_c(p)$.

First consider equation (1) without a cut-off and with Z^{-1} put zero. For $k^2 \gg M^2$, μ^2, p^2, it is approximately

$$\Gamma_c(p, k) = ig^2(2\pi)^{-4} \int \mathrm{d}k'[i\gamma(k + k')](k + k')^{-2}[i\gamma k'](k'^2)^{-2}\Gamma_c(p, k') . \tag{6}$$

It is proved in the appendix that (6) has solutions $(k^2 - i\varepsilon)^{-\alpha}$ and $(i\gamma k)(k^2 - i\varepsilon)^{-\beta}$, where α and β are roots of

$$(1 - \alpha)\alpha(1 + \alpha) = \lambda = g^2(4\pi)^{-2}, \qquad (2 - \beta)(1 - \beta)\beta = \lambda , \tag{7}$$

respectively. For simplicity, suppose λ to be sufficiently small for the roots α_1, α_2, α_3 and β_1, β_2, β_3 of equations (7) to be real. Then they satisfy

$$\begin{cases} 0 < \alpha_2 < \alpha_1 < 1 , & \alpha_3 < -1 , & \alpha_1 + \alpha_2 + \alpha_3 = 0 ; \\ 0 < \beta_2 < \beta_1 < 1 , & \beta_3 > 2 , & \beta_1 + \beta_2 + \beta_3 = 3 ; \end{cases} \tag{8}$$

and in each case only the first two solutions are admissable. Thus, for the asymptotic form of equation (1) without cut-off, we have

$$\Gamma_c(p, k) \sim \gamma_5 f(p)\{f_1(p)(k^2)^{-\alpha_1} + f_2(p)(k^2)^{-\alpha_2} + \\ + (i\gamma k)[g_1(p)(k^2)^{-\beta_1} + g_2(p)(k^2)^{-\beta_2}]\}, \tag{9}$$

where f_1, f_2, g_1 and g_2 are determinable from the exact equation, but $f(p)$ is undetermined.

Second, consider equation (1) with a high-energy cut-off applied. Since the integrals are only logarithmically divergent, it should make no difference what form of cut-off is used. It is convenient to cut-off as follows: in (1)

$$\text{subtract } (i\gamma k')(k'^2 + XM^2)^{-1} \text{ from } [i\gamma(p - k - k') + M]^{-1} . \tag{10}$$

Then, up to terms of order $1/X$, a solution of the homogeneous equation without cut-off will also be a solution of the inhomogeneous equation with cut-off, provided that

$$Z^{-1}(X) = ig^2(2\pi)^{-4} \int \mathrm{d}k'(i\gamma k')(k'^2 + XM^2)^{-1}[i\gamma(p - k') + M]^{-1} \cdot \\ \cdot \Gamma_c(p, k')(k'^2 + \mu^2)^{-1} + O(1/X) . \tag{11}$$

Inserting (9) into (11) and using the result

$$\int dk'(k'^2+XM^2)^{-1}(k'^2)^{-1-\alpha} = A(XM^2)^{-\alpha}$$

(where A is a constant whose actual value does not matter), it follows that (11) is satisfied if

$$Z^{-1}(X) = f(p)[A_1 f_1(p)(XM^2)^{-\alpha_1} + A_2 f_2(p)(XM^2)^{-\alpha_2} + \\ + (i\gamma p - M)\{B_1 g_1(p)(XM^2)^{-\beta_1} + B_2 g_2(p)(XM^2)^{-\beta_2}\}]. \tag{12}$$

Equation (12) fixes the function $f(p)$. We have also a normalizing equation, derived from (2), which may be taken to be

$$f(p_0) = 1.$$

Then (12) becomes (absorbing powers of M^2 into the constants A and B)

$$Z^{-1}(X) = A_1 f_1(p_0) X^{-\alpha_1} + A_2 f_2(p_0) X^{-\alpha_2} - 2M[B_1 g_1(p_0) X^{-\beta_1} + B_2 g_2(p_0) X^{-\beta_2}].$$

It will be shown later that $g_2(p) \equiv 0$. Anticipating this result, we have

$$Z^{-1}(X) = A_2 f_2(p_0) X^{-\alpha_2}[1 + O(X^{\alpha_2-\beta_1})], \tag{13}$$

where we have used the relations

$$0 < \beta_2 = (1-\alpha_1) < \alpha_2 < \beta_1 = (1-\alpha_2) < \alpha_1 < 1, \tag{14}$$

which follow easily from (7) and (8). Using (12) and (13) to eliminate $f(p)$ from (9),

$$\Gamma_c(p, k) \sim \gamma_5 f_2(p_0)\{(k^2)^{-\alpha_2} + f_1(p)(k^2)^{-\alpha_1}/f_2(p) + \\ + (i\gamma k)/f_2(p)[g_1(p)(k^2)^{-\beta_1} + g_2(p)(k^2)^{-\beta_2}]\} + O(X^{\alpha_2-\beta_1}). \tag{15}$$

The important fact about this expression is that the coefficient of $(k^2)^{-\alpha_2}$ is independent of p.

Consider now the self-energy functions defined by equations (3), (4) and (5). Denote the self-energy subtraction operator by S; so that $\Sigma_b(p) = S\Sigma(p)$. The term proportional to $(k^2)^{-\beta_1}$ in (15) contributes, to Σ_b,

$$-g^2(2\pi)^{-4} f_2(p_0) S\{g_1(p)/f_2(p) \int dk \gamma_5[i\gamma(p-k) + M]^{-1} \cdot \\ \cdot \gamma_5(i\gamma k)(k^2+\mu^2)^{-1}(k^2)^{-\beta_1}\}. \tag{16}$$

The only divergent contribution from (16) is the term in which S acts on $g_1(p)/f_2(p)$ alone. Introducing a cut-off like (10) into (16), the leading term in X is proportional to $X^{1-\beta_1}$. Similarly, the terms in (15) proportional to $(k^2)^{-\alpha_1}$ and $(k^2)^{-\beta_2}$ contribute terms of order $X^{1-\alpha_1}$ and $X^{1-\beta_2}$. The term proportional to $(k^2)^{-\alpha_2}$ on the other hand, contributes only a convergent integral to Σ_b; for, in the expression analogous to (16), there is no function of p before the integral, and so S must act on the integral. Therefore,

$$\Sigma_b(p) = F_1(p)X^{1-\alpha_1} + G_1(p)X^{1-\beta_1} + G_2(p)X^{1-\beta_2} + O(1)\,; \tag{17}$$

and so, from (5) and (13),

$$\Sigma_c(p) = F_1(p)X^{1-\alpha_1-\alpha_2} + G_1(p)X^{1-\beta_1-\alpha_2} + G_2(p)X^{1-\beta_2-\alpha_2} + o(1)\,. \tag{18}$$

From (14), the first term in (18) tends to zero as $X \to \infty$, whilst the the second is independent of X and yields a finite, non-zero contribution to Σ_c. The third term, on the other hand, would give an infinite contribution. Since it was proved in the previous section that this cannot happen, we must have $G_2(p) = 0$, and so $g_2(p) = 0$ in the original solution (9). This is not unexpected, since the term in $g_2(p)$, alone amongst the terms in (9), is unbounded for large k^2. Thus, only the second term in (18) remains, and comparison of (16) and (17) yields a relation between $\Sigma_c(p)$ and the asymptotic form of $\Gamma_c(p, k)$.

The above description of the cancellation of the X-dependent terms is incomplete in some respects. The vanishing of $g_2(p)$ is not fully explained, and it is not certain that the result is independent of the form of the cut-off. Nevertheless, we believe that the main features — the constant coefficient of $(k^2)^{-\alpha_2}$ in (15), and the exact cancellation of the powers of X in the G_1 term in (18) — would be shared by a more rigorous treatment.

4. – The Bethe-Salpeter Equation.

In pseudo-scalar meson theory, the Bethe-Salpeter equation ([5]) in the « ladder » approximation is

$$\chi(k) = -ig^2(4\pi^3)^{-1}\int \mathrm{d}k'[i\gamma^P(p-k) + M]^{-1}[i\gamma^N(p+k) + M]^{-1}\cdot \gamma_5^P\gamma_5^N[(k-k')^2 + \mu^2]^{-1}\chi(k')\,. \tag{17}$$

Here, $2p$ is the total energy, and is regarded as given, whilst g^2 is to be determined as an eigenvalue. Superfixes P and N distinguish the two nucleons.

Goldstein ([6]) has solved (1) for the particular case $p = 0$ (and $\mu = 0$).

His solution confirms that, because of the singular property, the homogeneous equation has a solution for each value of g^2, and so a discrete eigenvalue spectrum is not obtained. GOLDSTEIN also shows that the cut-off prescription defined in section 1 yields a single « eigenvalue » in his particular case.

GREEN and MCCARTHY (7) suggest a definition of « eigenvalues » for singular integral equations, based upon the use of the Fredholm method. The integral in the Fredholm discriminant of equation (17) are all logarithmically divergent. Cutting them off at a large value X, the discriminant has the form

$$\Delta_X(p, g^2) = \exp[-\varphi(g^2) \log X + O(1/X)] \Delta_0(p, g^2) .$$

Thus, for large X, the zeros of Δ_X are insensitive to X, and they tend to the zeros of Δ_0, which are defined to be the « eigenvalues ». Now, since the divergencies concerned are all logarithmic, it makes no difference whether the cut-off is applied term-by-term, or whether it arises from a cut-off inserted in the original equation. This fact establishes the equivalence of this method to the general cut-off prescription.

We now determine the asymptotic properties of χ, and show that these alone are sufficient to determine the « eigenvalue ». The result is that the « eigenvalue » is independent of p, and, in particular, does not tend to zero as $p^2 \to -M^2$. This is clearly unacceptable; and so the cut-off prescription as defined cannot give sensible answers for bound-state energy levels.

The asymptotic form of (17) is

$$\chi(k) = -ig^2(4\pi^3)^{-1}(i\gamma^P k)^{-1}(i\gamma^N k)^{-1}\gamma_5^P\gamma_5^N \int (k-k')^{-2}\chi(k')\,\mathrm{d}k' . \tag{18}$$

This has a solution with the same matrix dependence as Goldstein's exact solution; and then (18) reduces to

$$\psi(k^2) = -ig^2(4\pi^3)^{-1}(k^2)^{-1} \int (k-k')^{-2}\psi(k'^2)\,\mathrm{d}k' . \tag{19}$$

By the methods of the appendix, it follows that (19) has a solution $(k^2)^{-1-\nu}$, where

$$\alpha(1-\alpha) = \lambda' = g^2/4\pi , \tag{20}$$

(provided that $\lambda' < \frac{1}{4}$). Thus

$$\psi(k^2) = h_1(p^2)(k^2)^{-1-\alpha_1} + h_2(p^2)(k^2)^{-1-\alpha_2} , \tag{21}$$

where $0 < \alpha_1 < \frac{1}{2} < \alpha_2 < 1$ are the roots of (20).

Insert a cut-off into equation (17) by subtracting $(k'^2+X\mu^2)^{-1}$ from $[(k-k')^2+\mu^2]^{-1}$. Then (21) is also a solution of the cut-off equation, provided that an equation of the form

$$C_1 h_1(p^2)X^{-\alpha_1} + C_2 h_2(p^2)X^{-\alpha_2} = 0 \tag{22}$$

is satisfied. Whatever the form of h_1 and h_2, any solution of (22) must tend to the limit $\alpha_1 = \alpha_2 = \frac{1}{2}$, $\lambda' = \frac{1}{4}$ as $X \to \infty$ ([8]). Thus, on the assumption that the asymptotic form of χ does have some term with the Goldstein matrix dependence, the prescription always gives the single « eigenvalue » $\lambda' = \frac{1}{4}$.

The author is indebted to Dr. P. T. MATTHEWS for a most helpful discussion.

APPENDIX

Continual use is made of the formula

$$\int_0^\infty dz z^{n-\alpha}(k^2-z)^{-m} = \Gamma(n-\alpha+1)\Gamma(m-n+\alpha-1)[\Gamma(m)]^{-1}(k^2)^{n+1-m-\alpha} \tag{23}$$
$$(0<\alpha<1,\ n\geqslant 0,\ m\geqslant n+1)\,.$$

Inserting the trial function $(k^2)^{-\alpha}$ into the right hand side of equation (6), we obtain

$$-ig^2(2\pi)^{-4}\left\{\int dk'(i\gamma k)(i\gamma k')(k+k')^{-2}(k'^2)^{-2-\alpha} + \int dk'(k+k')^{-2}(k')^{-1-\alpha}\right\}. \tag{24}$$

From (23) with $m=4$, $n=1$, and using standard FEYNMAN ([9]) techniques, the first term in (24) becomes

$$g^2(4\pi)^{-2}k^2\int_0^\infty dz z^{-\alpha}(k^2+z)^{-2}[\Gamma(2-\alpha)\Gamma(2+\alpha)]^{-1}\,.$$

Using formula (23) again, this expression becomes

$$-\lambda(1-\alpha)^{-1}(1+\alpha)^{-1}(k^2)^{-\alpha}\,.$$

([8]) $\lambda' = \frac{1}{4}$ is not an eigenvalue for any finite value of X, for the form (21) is only valid for $\alpha_1 \neq \alpha_2$. Because this points is not stressed by GOLDSTEIN, the equivalence of his cut-off method to our prescription is slightly obscured.

([9]) R. FEYNMAN: *Phys. Rev.*, **67**, 769 (1949).

Similarly (this time using (23) with $m=3$, $n=1$), the second term in (24) becomes

$$\lambda(1-\alpha)^{-1}\alpha^{-1}(k^2)^{-\alpha} ;$$

and hence the first equation (7) is verified.

For the trial function $(i\gamma k)(k^2)^{-\beta}$, formula (23) with $m=4$, $n=2$ is used.

The treatment of equation (19) is identical with that of the second term in (24).

RIASSUNTO (*)

Nella teoria covariante dello scattering mesone-nucleone si incontra l'equazione di una vertex-part che è un'equazione integrale dotata di singolarità. Perciò si incontrano difficoltà di rinormalizzazione. Nel presente lavoro si mostra come queste difficoltà si possano superare mediante un opportuno taglio ad alta energia. Lo stesso artificio non consente di superare una analoga difficoltà che sorge nell'equazione di Bethe-Salpeter.

(*) *Traduzione a cura della Redazione.*

Sull'energia di legame dell'H_3^*.

F. Duimio

Istituto di Scienze Fisiche dell'Università - Milano
Istituto Nazionale di Fisica Nucleare - Sezione di Milano

(ricevuto il 12 Febbraio 1955)

Riassunto. — Con modelli molto semplificati, che si pensa possano tener conto, nelle grandi linee, della regola pari-dispari, si confrontano le energie di legame dei sistemi D* e H_3^*, con quelle dei sistemi D e H_3. I risultati qualitativi (assenza di stati legati per il D* e piccola energia di legame per l'H_3^*) sono in accordo coi dati sperimentali sui frammenti instabili.

Nella fenomenologia delle particelle « nuove » (iperoni, mesoni pesanti, ecc.) occupano un ruolo particolarmente importante i frammenti instabili (1).

Infatti noi siamo in presenza di sistemi legati di iperoni coi nucleoni, ed è chiaro quanto una conoscenza dettagliata di tali sistemi possa essere utile nello studio delle caratteristiche delle particelle nuove.

In questa nota esamineremo, sia pure in modo pressochè qualitativo, i sistemi iperone-nucleone e iperone-due nucleoni.

Il punto di partenza consiste nel supporre valida l'ipotesi (2) secondo cui le interazioni « forti » siano le $(N_0N_0\pi_0)$ e $(N_0N_1\pi_1)$ (oltre alla $(N_1N_1\pi_0)$), cioè che la costante d'accoppiamento sia la stessa (o dello stesso ordine di grandezza) nei due casi. Per la particelle indicata con π_1 (bosone) assumeremo la massa 970 m_e, per la N_1 (fermione) massa 2185 m_e (considereremo nel seguito solo la $N_1^0 \equiv \Lambda^0$ e non le N_1 cariche).

(1) Per una completa bibliografia dei dati sperimentali vedi: R. Levi Setti: *Suppl. Nuovo Cimento* (in corso di pubblicazione), annesso al corso dal prof. B. Rossi alla Scuola Estiva di Varenna, 1954.

(2) A. Pais: *Phys. Rev.*, **86**, 663 (1952). (Nelle notazioni di questo lavoro N_0 e N_1 indicano rispettivamente nucleone e iperone e π_0 e π_1 mesone π e mesone pesante (K).

In questo modo è evidente come le forze $N_0 \cdot N_1$ siano mediate dal campo π_1, allo stesso modo come le ordinarie forze nucleari sono mediate dal campo π_0 [3]. Adotteremo qui lo schema semplificatissimo di buche di potenziale che rappresentino le suddette interazioni. Indichereno con α_0, α_1, V_0, V_1 il range e la profondità di tali buche e per i rapporti tra di essi accetteremo i seguenti (che si ottengono per le buche di Yukawa derivanti dal calcolo perturbativo statico al secondo ordine):

$$(1) \qquad \begin{cases} \alpha_0 = \beta\alpha_1 \\ V_0 = V_1/\beta \end{cases} \qquad \beta = \frac{m_{\pi_1}}{m_{\pi_0}} = \sim 3.5 \ .$$

1. – Sistema $N_0 \cdot N_1$.

Il sistema è completamente analogo al sistema n-p (deutone).

Vogliamo ora vedere se con le ipotesi precedenti riguardo le interazioni $N_0 \cdot N_1$ tramite il mesone π_1, tale sistema ammette stati legati.

Adottando la forma più semplice di potenziale possibile, cioè la buca rettangolare, e supponendo valide le relazioni (1), la condizione perchè esista uno stato legato è, come è noto:

$$(2) \qquad v_1\alpha_1^2 \geqslant \pi^2\hbar^2/8M' \ ,$$

dove M' è la massa ridotta del sistema.

Ma

$$v_1\alpha_1^2 = v_0\alpha_0^2/\beta \ ,$$

e $v_0\alpha_0^2$ è una costante che si determina in base all'energia di legame del D [4]. Sostituendo per M' il suo valore $M' = \sim 1000\ m_e$, si vede che la condizione (2) non è verificata: non esistono dunque stati legati $N_0 \cdot N_1$ e ciò è confortato dall'esperienza: infatti nessun frammento instabile identificabile con un D* è stato finora osservato.

2. – Sistema $N_0 \cdot N_0 \cdot N_1$.

Considereremo in particolare il sistema H_3^*, cioè $p \cdot n \cdot \Lambda^0$.

Il problema che vogliamo affrontare è dunque il seguente: determinare

[3] Ciò naturalmente va inteso in modo qualitativo: basti pensare che non abbiamo fatto ipotesi nemmeno sulla parità e sullo spin del π_1.

[4] $V_0\alpha_0^2$ è costante nel caso di buca rettangolare e varia di poco al variare di α_0 e della corrispondente V_0 che rende conto dell'energia di legame del deutone, per altre forme di buca normalmente usate (gaussiana, di Yukawa, ecc.).

l'energia di legame di un sistema che differisce da un nucleo di H_3 ordinario per la sostituzione di un n con una Λ^0 supponendo che le forze nucleari tra n e p siano rappresentate da una buca di potenziale con parametri α_0 e V_0, mentre le forze $n \cdot \Lambda^0$ e $p \cdot \Lambda^0$ siano rappresentate da buche analoghe con parametri α_1 e V_1.

Il calcolo anche qui sarà semplificato il più possibile: seguiremo un metodo variazionale del tipo di quello usato nel classico lavoro di BETHE e BACHER [5], supponendo che le forze siano tutte del tipo di Majorana, e le buche di potenziale di tipo gaussiano.

Introduciamo le seguenti coordinate:

$$(3) \qquad \begin{cases} \boldsymbol{X} = \dfrac{M_1 \boldsymbol{x}_1 + M_0(\boldsymbol{x}_2 + \boldsymbol{x}_3)}{M_1 + 2M_0} & \text{(baricentro)} \\ \boldsymbol{r} = \boldsymbol{x}_2 - \boldsymbol{x}_3 \\ \boldsymbol{q} = \boldsymbol{x}_1 - \dfrac{\boldsymbol{x}_2 + \boldsymbol{x}_3}{2} \,. \end{cases}$$

Come funzione di prova usiamo la

$$(4) \qquad \psi = \exp\left[-(\nu/2)(r_{12}^2 + r_{13}^2) - (\mu/2) r_{23}^2\right] \qquad r_{ij} = |\boldsymbol{x}_i - \boldsymbol{x}_j| \,,$$

che espressa in funzione delle variabili (3) si scrive:

$$\psi = \exp\left[-(\nu'/2) r^2 - (\mu'/2) q^2\right], \quad \mu' = 2\nu, \quad \nu' = (\nu/2) + \mu.$$

Il metodo variazionale consiste nello scrivere il valore medio dell'energia totale nello stato definito dalla funzione ψ e cercare i valori dei due parametri μ e ν che lo rendono minimo. Tale valore si approssimerà tanto più all'energia dello stato fondamentale quanto più la funzione ψ approssima l'autofunzione vera di tale stato. L'espressione (4) per la ψ è certo un'approssimazione molto rozza, ma per gli scopi qualitativi che ci siamo proposti può essere sufficiente.

Per l'energia cinetica [6] e potenziale si ha:

$$(5) \qquad \begin{cases} T = \dfrac{1}{4}\mu_0 \dot{r}^2 + \dfrac{M_0 M_1}{M_1 + 2M_0} \dot{q}^2 \\ V = -V_1 \exp\left[r_{12}^2/\alpha_1^2\right] - V_1 \exp\left[r_{13}^2/\alpha_1^2\right] - V_0 \exp\left[r_{23}^2/\alpha_0^2\right] . \end{cases}$$

Il valore medio dell'energia totale sarà:

$$E = \frac{\int \psi^* (T+V) \psi \, \mathrm{d}\boldsymbol{q} \, \mathrm{d}\boldsymbol{r}}{\int \psi^* \psi \, \mathrm{d}\boldsymbol{q} \, \mathrm{d}\boldsymbol{r}} \,,$$

[5] H. A. BETHE and R. F. BACHER: *Rev. Mod. Phys.*, **8**, 83 (1936).

[6] Nel sistema del baricentro, cioè trascurando l'energia cinetica di traslazione dell'intero sistema.

che, con qualche calcolo e supponendo che le relazioni tra α_0, V_0 e α_1, V_1 siano ancora del tipo (1), dà

$$(6) \qquad E = \frac{3}{2}\frac{\hbar^2}{M_0}\{\mu + (2\gamma + \tfrac{1}{2})\nu\} - 16 V_0\beta\left\{\frac{\nu(\nu+\mu)}{(\nu+\mu)(5\nu+\mu+4(\beta/\alpha_0)^2}\right\}^{\frac{3}{2}} - \\ - V_0\left\{\frac{\nu+2\mu}{\nu+2\mu+(2/\alpha_0^2)}\right\}^{\frac{3}{2}},$$

con

$$\gamma = \frac{M_1 + 2M_0}{4M_1}.$$

Ponendo (come in [5])

$$p = 2\frac{\nu+2\mu}{5\nu+\mu}, \qquad \sigma = \frac{(5\nu+\mu)\alpha_0^2}{4}, \qquad T = \frac{\hbar^2}{M\alpha_0^2},$$

la (6) si riduce alla

$$(7) \qquad E_{H_3^*} = -2V_0\beta\left\{p\frac{4-p}{1+2p}\frac{\sigma/\beta^2}{(\sigma/\beta^2)+1}\right\}^{\frac{3}{2}} - V_0\left\{\frac{p\sigma}{p\sigma+1}\right\}^{\frac{3}{2}} + \\ + \frac{1}{3}\sigma T\left\{\left(\frac{9}{2} - 2\gamma\right)p + 8\gamma\right\}.$$

Il problema si riduce ora al minimizzare l'espressione (7) rispetto a σ e p. Tale minimo darà l'energia di legame dell'H_3^*. Ora, date tutte le approssimazioni e semplificazioni usate, un risultato numerico avrebbe certo poco senso. Quello che ci importa è un confronto tra tale valore e i valori che si ottengono, con lo stesso grado di approssimazione, per le energie di legame del tritone e del deutone: tali energie infatti si possono ottenere dalla stessa (7) come casi particolari o limite.

Se poniamo nella (7) $\beta = 1$, $\gamma = \frac{3}{4}$ (cioè $M_0 = M_1$), $p = 1$ (cioè $\nu = \mu$) avremo l'energia di legame del tritone (ricordiamolo ancora: con le approssimazioni usate nella deduzione della (7), cioè pure forze di Majorana ecc.)

$$(8) \qquad E_T = -3V_0\left\{\frac{\sigma}{\sigma+1}\right\}^{\frac{3}{2}} + 3\sigma T \qquad \text{con} \qquad \sigma = \frac{3}{2}\alpha_0^2\mu.$$

Poniamo invece $p = 4$: indipendentemente dai valori di β e γ avremo

$$(9) \qquad E_D = -V_0\left\{\frac{\sigma}{\sigma+1}\right\}^{\frac{3}{2}} + \frac{3}{2}\sigma T \qquad \text{con} \qquad \sigma = \alpha_0^2\mu.$$

La (9) dà quindi l'energia di legame del deutone (ciò è chiaro se si pensa che $p = 4$ corrisponde a $\nu = 0$).

I valori che si ottengono dalla (8) e (5) adottando la coppia di valori: $\alpha_0 = 2{,}25 \cdot 10^{-13}$ cm, $V_0 = 35{,}6$ MeV, sono rispettivamente ~ 1 MeV e $\sim 13\,5$ MeV,

ambedue molto lontani dai valori sperimentali di 2,22 e 8,5 MeV rispettivamente.

La determinazione del minimo di $E_{H_3^*}$ in (7) è molto laboriosa e dipende grandemente dal valore di β che si assume. In particolare con $\beta = 3.5$ si ha $E_{H_3^*} > E_D$. Questo lo si può vedere ponendo nella (7) $p\sigma = \sigma'$ e trascrivendola nella forma:

$$(10) \qquad E_{H_3^*} = -2V_0\beta\left\{p\,\frac{4-p}{1+2p}\,\frac{\sigma'/p\beta^2}{(\sigma'/p)\beta^2+1}\right\}^{\frac{3}{2}} - V_0\left\{\frac{\sigma'}{\sigma'+1}\right\}^{\frac{3}{2}} + \\ + \frac{3}{2}\sigma' T + \frac{2}{3}\sigma' T\gamma\left\{\frac{4}{p}-1\right\}.$$

In essa il secondo e il terzo termine hanno la forma (9) e per il β suddetto (con le altre costanti fissate come sopra) la somma tra il quarto termine e il primo è positiva per qualunque valore di p. In tal modo l'H_3^* non risulterebbe stabile.

Osserviamo però come il valore 3,5 di β fosse stato ottenuto in maniera molto semplicistica dal rapporto m_{π_1}/m_{π_0}; questa deduzione sarebbe corretta solo se fosse tale una teoria della interazione mesone-nucleone e π-nucleone per la quale fosse applicabile il metodo perturbativo al secondo ordine, e se detta interazione fosse scalare. Ora l'interazione (π_0, N_0) non solo non è debole, ma è o PS o PV: in tal caso le interazioni al quarto ordine della teoria delle perturbazioni sono almeno altrettanto importanti quanto quelle del second'ordine, e come conseguenza il « range » della buca che approssima la suddetta interazione viene ridotto [7].

Da queste considerazioni è evidente come β possa scostarsi notevolmente dal valore 3,5. Con una scelta opportuna, per quanto arbitraria [8], di β (o di due valori per β nelle equazioni (1a) e (1b) ammettendo l'eventualità che possano essere diversi), è possibile far sì che $E_{H_3^*} < E_D$.

È evidente anche che $E_{H_3^*}$ risulterà di poco minore di E_D per valori ragionevoli di β (ad esempio, tali per cui la relazione (2) non sia verificata, cioè non esiste un D*), e questo spiegherebbe la bassa energia di legame dell'H_3^*, osservata sperimentalmente.

Pur rendendoci conto della grossolanità delle ipotesi da noi assunte in questo lavoro, ci pare tuttavia che i risultati ottenuti autorizzino a ritenere che la regola pari-dispari per il meccanismo di produzione e decadimento delle particelle nuove può rendere conto nelle sue linee essenziali dei fatti sperimen-

(7) G. C. Wick: *Nature*, **142**, 993 (1938).

(8) Bisognerà prendere $\beta < 3,5$ e questa potrebbe essere una indicazione, benchè molto vaga, che il π_1, se ha spin 0, sia scalare piuttosto che PS.

tali riguardanti i frammenti instabili, o per lo meno che tale regola non è in contraddizione con questi [9].

Ringrazio vivamente il prof. CALDIROLA per il suo interesse ed incoraggiamento.

---

[9] È possibile trarre una conclusione analoga anche dal lavoro di CHESTON e PRIMAKOFF (*Phys. Rev.*, **92**, 1537 (1953)) riguardo al problema del decadimento non mesonico dei frammenti instabili.

SUMMARY

Using very simple models we have calculated and compared the binding energies of the normal and excited deuteron and triton systems. These model seem to us to take into account the general principles of the even-odd rule. The qualitative results, i.e. the low binding energy for H_3^*, and the absence of bound states N_0-N_1 (D^*) are in agreement with experimental results on unstable fragments.

IL NUOVO CIMENTO Vol. I, N. 4 1° Aprile 1955

The Interaction of Fast K-Mesons (*).

M. W. Friedlander, D. Keefe and M. G. K. Menon

H. H. Wills Physical Laboratory - University of Bristol

(ricevuto il 22 Febbraio 1955)

Summary. — Two events are described in which heavy mesons interact with nuclei in photographic emulsions, producing small stars and emerging themselves from the collisions. In one example, a relativistic singly charged particle enters the stack and produces a star with only three emergent charged particles, which have been identified as a hyperon, a π-meson and a K-meson respectively. The K-meson creates two stars before it comes to rest and decays with the emission of a slow μ-meson. In the other example, a K-meson enters the stack from outside and, after interacting, comes to rest within the emulsion and decays with the emission of a single lightly ionizing particle. Certain features of interest associated with the scattering properties of heavy mesons are discussed.

1. – Introduction.

Recently we have observed in this laboratory events which appear to correspond to the interactions in flight of heavy mesons with a mass $\sim 1000\ m_e$. This paper reports two events of this type found in stripped emulsion stacks flown in England. The first example, described in § 2, occurs in a stack of 80 stripped emulsions each $20 \times 15 \times 0.06$ cm^3, the second, described in § 3, in a stack of 46 emulsion strips each $15 \times 15 \times 0.06$ cm^3. In each case, the decay at rest of the K-meson was observed in the course of scanning for heavy

(*) The nomenclature K-meson and χ-meson are used throughout in the sense of Powell (*Proc. Roy. Soc.*, A **221**, 278 (1954)), i.e. the term K-meson refers to any particle with a mass intermediate between those of the π-meson and the proton, and χ-meson is a K-meson which decays with the emission of a μ-meson and at least two neutral particles.


D
Star γ
1 + 2p
C1
C3
C2
Out of stack
71·5mm observed
9·75mm
5·58mm
50μ
Star β
3·0×
X
B

Plate 1.

Plate 2.

unstable particles. In the first, the charged product of the decay was a μ-meson of 14.45 MeV, thus establishing the decaying K-particle as a χ-meson, and in the second, the secondary particle was at plateau ionization and was not identified.

2. – The Associated Production and Interactions in Flight of a Heavy Meson.

2·1. *Experimental Details.* – Photomicrographs of this event are shown in Plate 1 and 2, and details of the measurements made on the various tracks are displayed in Table I.

TABLE I.

Track	Length (mm)	No. of plates	g^*	$p\beta$ (MeV/c)	Mass (m_e)	Identity	Energy (MeV)	Momentum (MeV/c)
D	50.20	18	1.02 ± .03	—	—	π(?) ‡	2 320 ± 300 ‡	2 460 ± 300 ‡
C_1	5.56	4	0.96 ± .04	1 100 ± 350	≲ proton	K-meson ‡	796 ± 250	1 190 ± 300
C_2	71.5	25	0.94 ± .03	370 ± 31	< 500	π-meson	278 ± 25	394 ± 31
C_3	9.75	5	2.00 ± .08	470 ± 70	2 020 ± 350	Hyperon	306 ± 15	910 ± 30
econdary of C_3	19.2	21	1.24 ± .05	—	—	L-meson	84 ± 7 at emission	—
B	21.34	5	1.73 ± .05	271 ± 27	950 ± 100	K-meson	158 ± 18	425 ± 27
χ	24.17	7	—	—	850 ± 100	χ-meson	66.3 at emission	265
μ	5.37	3	—	—	197 ± 20	μ-meson	14.45 at emission	—

‡ The reasons for the assignment of these values are discussed in the text.

The track of the charged decay product of the slow K-meson emerging from the last interaction, Star α, is due to a μ-meson of 14.45 MeV which later decays to an electron, and it cannot be reconciled with that due to a π-meson decaying in flight. This K-meson is not therefore an example of the alternative mode of the τ-meson and must be classified as a χ-meson (O'CEAL-

LAIGH [1]). The mass of the $\varkappa$-meson has been determined by gap measurements at several points along the track.

Star α is of type $4+0p$ and in addition to the $\varkappa$-meson contains three short prongs of lengths 124 μ, 75 μ and 5 μ. The first is probably singly charged, the second doubly charged and the third is too short to be identified. The total visible energy contained in these three prongs is about 16 MeV. The primary of this star (track B) is also a heavy meson and its mass from (g^*, $p\beta$) measurements is 950 ± 100 m_e. Track $\varkappa$ emerges from star α at an angle of 147.6° with respect to the direction of track B.

Track B originated in a star of type $3+0p$, the other two prongs being a 307 μ proton track and an unidentifiable recoil of about 1 μ. The direction of track B makes an angle of 32.4° with that of the primary, Track C_1. Track C_1 is about 2 mm/plate and its identity cannot be directly established as the measured value of $p\beta$ was 1100 ± 300 MeV/c. The ionization, g^*, was certainly appreciably below plateau whereas that expected for a proton of this $p\beta$ would be $g^* \approx 1.1$. While this does indicate that the mass is less than that of a proton, it is not strong evidence since this value of $p\beta$ is close to the upper measurable limit imposed by distortion in the plates concerned. Independent arguments will be given below which strongly suggest that track C_1 is, in fact, due to a K-meson rather than to a π-meson or proton.

From the parent star, $(1+2p)$, of track C_1, there emerge two other particles. Track C_2 can be followed for 71.5 mm until it leaves the stack. Taking into account the errors in the (g^*, $p\beta$) measurements, one finds an upper limit of 500 m_e for its mass. The measurements are entirely consistent with its being a π-meson, and this has been assumed in the discussion below. Track C_3 has been identified as due to a hyperon which decays in flight into an L-meson, after traversing 9.75 mm of emulsion. The mass of the primary from (g^*, $p\beta$) measurements is 2020 ± 350 m_e. The secondary track has a g^* of 1.24 and a projected length per plate of 0.74 mm. The Q-value for the decay scheme

$$Y^{\pm} \rightarrow n + \pi^{\pm} + Q$$

(assuming the secondary particle to be a π-meson), is 97 ± 15 MeV, which is consistent with the present accepted value of ~ 110 MeV.

Track D whose direction makes an angle of 77° with the vertical has been assumed to be the primary of star γ. Its projected length per plate is 2.8 mm and measurements of multiple scattering along this track yield a value of $\bar{\alpha} = 0.039°$ per 100 μ. An investigation of the distortion in the plates traversed, however, shows that this value of α almost certainly arises from this cause and can only be considered an upper limit. The directions of emission

[1] C. O'CEALLAIGH: *Phil. Mag.*, **42**, 1032 (1951).

of the K-meson, the π-meson and the hyperon with respect to that of the assumed primary were 11.2°, 2.1° and 9.5° respectively.

2·2. *Discussion.* – The only two tracks in this event — apart from the black prongs — which cannot be directly identified are tracks C_1 and D. In view, however, of the known association in production of hyperons and heavy mesons, and of the fact that track B is due to an interacting K-meson, it would appear reasonable to attribute track C_1 also to a heavy meson. From a consideration of the results of DAHANAYAKE *et al.* (2) and FOWLER and PERKINS (3) on the production of heavy mesons and hyperons in cosmic-ray induced stars, it is possible to estimate quantitatively that the relative probability that track C_1 is due to a π-meson or a relativistic proton is less than 1 % of its being due to a heavy meson. It would thus appear fairly certain that this track was in fact caused by a K-meson and hence that the measured $p\beta$ value was not seriously in error.

Star γ admits of a simple interpretation if it be assumed that track D is that of a π-meson, the three charged products C_1, C_2, C_3, being produced in a reaction of the type:

$$\pi + \mathrm{N} \rightarrow \mathrm{Y} + \mathrm{K} + \pi \qquad (1)$$

a combination of the Brookhaven and Yukawa reactions.

Energy and momentum considerations and the absence of any black prongs associated with the star supports the view that the collision was with a peripheral neutron in the target nucleus. The momentum component of the charged secondary particles (C_1, C_2, C_3) transverse to the direction of the primary is 117^{+65}_{-85} MeV/c, which could quite easily arise from the Fermi momentum of the bound neutron. The longitudinal momentum component of these particles is 2460 ± 300 MeV/c which implies a primary π-meson kinetic energy of 2320 ± 300 MeV. The actual energy (kinetic + excitation) observed amongst the secondary particles is 2263 ± 250 MeV. The discrepancy 197 ± 50 MeV, (*) between these two values can be considered negligible because of possible interference of Fermi momentum with the momentum balance or because of a small residual excitation of the target nucleus after the collision without the production of charged evaporation prongs. Had the primary particle been a proton, then at the given momentum its kinetic energy would have been 1694 ± 280 MeV, which is 570 ± 30 MeV *too low* and so cannot be explained

(2) C. DAHANAYAKE, P. E. FRANCOIS, Y. FUJIMOTO, P. IREDALE, C. J. WADDINGTON and M. YASIN: *Phil. Mag.*, (1955) in course of publication.

(3) P. H. FOWLER and D. H. PERKINS: *Phil. Mag.* (1955), in course of publication.

(*) The discrepancy, 197 MeV, includes the π-meson rest mass. The error $\pm$ 50 MeV is the independent part of the error on the discrepancy.

in terms of residual nuclear excitation. Furthermore, the track of a π-meson of energy ~ 2.3 GeV has plateau grain density in agreement with the observations, whereas that of a proton is significantly below plateau unless the particle has a considerably higher energy (> 7 GeV). However if the proton energy is ~ 2.3 GeV the momentum balance would be ensured by assuming the emission of neutrons in suitable directions. The agreement in the energy and momentum balance with the assumption of a single π-meson/nucleon collision could, of course, have arisen by chance and one cannot exclude the possibility that more than one nucleon was involved, despite the absence of other charged products.

The space angle between the hyperon and the K-meson is 20.3° and if we define a plane (YK) which contains both their directions, then the plane (YK) makes an angle of $\sim 2°$ with the primary particle track and an angle of 3° with that of C_2. The angle made with this (YK) plane by another plane containing the hyperon and its L-meson secondary is 26.9°.

At two points along the track of the K-particle from Star γ occur stars β and α, in both of which a K-particle enters and a K-particle emerges. If the production of a K-particle in star γ — equ. (1) — is analogous to the Brookhaven reaction, then in the collision of a K-meson and a nucleon one would expect either of the following processes to occur:

$$\mathrm{K} + \mathcal{N} \rightarrow \text{intermediate state} \begin{cases} \nearrow \mathrm{Y} + \pi & (2a) \\ \searrow \mathrm{K}' + \mathcal{N}' & (2b) \end{cases}$$

the second of which corresponds to elastic scattering. Alternatively there may be a variety of inelastic scattering processes e.g. the creation of one or more π-mesons corresponding to a production mechanism such as (1) rather than to the ordinary Brookhaven process. Yet another possibility is afforded if among the K-particles there exist different classes (e.g. in lifetime, interactions, spin, etc.); then it might be possible that in the scattering process the final state K′ of the heavy meson belongs to a class other than that of the primary, K. The emergence then of a $\varkappa$-meson from star α does not necessarily imply that the primary of this star was itself a $\varkappa$-particle.

If the nucleon in (2) is bound in a nucleus, in general it will have a Fermi momentum differing from zero up to about 200 MeV/c which must be taken into account in considering the kinematics of the collisions. The stars α and β have been analysed to see if they are consistent with the simple model of a K-meson interacting with a single bound nucleon and this nucleon thereafter producing a disintegration as it recoils in the target nucleus. In the case of star β, the K-meson is scattered through an angle of 31° with a loss in energy of about 630 MeV and a change in momentum $|p| = 850$ MeV/c. This is in no way consistent with the transfer of energy and momentum to a single

nucleon and instead one must demand an interaction with more than one nucleon or the creation of a neutral particle or particles. It is possible that star α is an example of a K-meson/nucleon interaction, since the angle of scattering (147.6°), the loss of energy (92 MeV) and the loss in momentum (238 MeV/c) are all consistent with a collision with a single nucleon if the latter had a Fermi momentum of about 200 MeV/c.

3. – Collision of a Heavy Meson with a Bound Proton.

This event presents the appearance of a star of three branches (cf. Fig. 1). Track *a* is that of a K-meson which came to the end of its range after traversing 17.45 mm in the same emulsion strip, and then decayed with the emission of a steep lightly ionising secondary particle ($g^* \approx 1$). The measured mass of this K-particle, from measurements of the mean gap-length at various points along the range, is 946 ± 60 m_e, and its energy at emission was 54.1 ± 0.8 MeV. The steepness of the secondary decay particle precluded any reliable estimation of its energy. Track *b* is 89.0 mm in length and crosses nine emulsion strips before reaching the edge of the stack. Grain density and scattering measurements yield a mass of $1900 \pm \pm 200$ m_e for the particle producing this track, and so it has been assumed to be a proton. Its energy at emission from the star was 240 ± 5 MeV.

Track *c* has an ionization of $g^* = 1.25 \pm .02$ and a value of $p\beta = 380 \pm 30$ MeV/c, which measurements, when combined, give a mass estimate of 844 ± 90 m_e. This serves to identify this particle as a K-meson, but the observed track length in the stack — 32.28 mm in eight plates — is insufficient to allow a determination of its direction of motion. If one assumes that this particle is outgoing, then the event represents a star induced by a neutral primary in which two K-mesons are produced, both travelling almost vertically upwards in the stack. Since this appears to be an unlikely hypothesis, in what follows it has been assumed

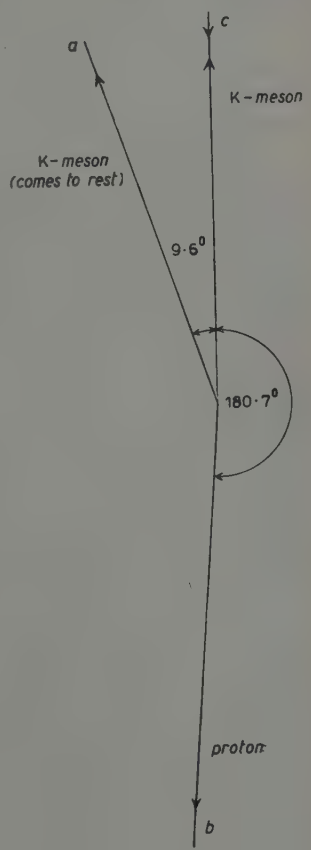

Fig. 1. – Schematic diagram of the event described in § 3; the angles shown are the projected values of the space angles upon the plane of the emulsion.

that this track is approaching and causes the star. This view is further supported by the near coplanarity of the event and the approximate agreement in the momentum and energy balance.

The three tracks, *a*, *b*, *c*, quite clearly depart from exact coplanarity since all dip downwards in the emulsion from the star: the angle between the outgoing proton track and the plane containing the two K-meson tracks is 7°. The angles in space between the tracks are as follows: $\widehat{ab} = 171.2°$, $\widehat{bc} = 178°$, $\widehat{ca} = 11°$.

Apart from these angular measurements the details of the three tracks are given in the table below, where the energies and momenta were calculated assuming a mass of 965 m_e for both K-mesons.

TABLE I.

Track	Length (mm)	Number of plates	Mass (m_e)	Energy at star ↧ (MeV)	Momentum (MeV/c) ↧ at star	Identity
Assumed primary	32.28	8	890 ± 70 (g^*, $p\beta$)	262 ± 9	574 ± 10	K-meson
Stopping K-meson	17.45	1	946 ± 60 (g^*, R)	54.1 ± 0.8	238 ± 2	K-meson
Recoil	89.0	9	$1\,900 \pm 200$ (g^*, $p\beta$)	240 ± 5	714 ± 10	Proton

↧ Calculated assuming $m_K = 965\, m_e$, and $m_p = 1836\, m_e$.

The lack of coplanarity and the unbalance in momentum imply that the K-meson was scattered by a proton bound in a nucleus. The momentum component of the secondary particles transverse to the direction of the primary is 91 ± 2 MeV/c and the total missing momentum is $p = 130 \pm 14$ MeV/c, both of which are consistent with the picture of a collision with a nucleon in motion within a nucleus.

However, the sum of the energies of the outgoing proton and K-meson is 294 ± 5 MeV which *exceeds* that of the primary K-meson by 32 ± 10 MeV. This discrepancy must be further increased by an amount equal to the binding energy of the proton inside the nucleus (~ 8 MeV). This is somewhat surprising when one considers that a collision with a bound nucleon frequently leads to excitation of the residual nucleus, resulting in a loss of energy. One explanation for this apparently exothermal event is that a rare statistical fluctuation has resulted in a spurious increase of the grain density in the track of the

primary K-meson. (At low ionizations the estimation of energy from grain density becomes rather more sensitive to changes in g^*). If the g^* measurements — which have been checked independently by different observers — are not seriously affected by unknown fluctuations then one is forced to consider two other possible explanations of this event. (*a*) The mass estimates of the two K-meson tracks are seriously in error and in both cases one is dealing with a particle about 150 m_e more massive than a τ-meson. This seems unlikely in face of the precision of the measurements on the ending track. (*b*) The incoming heavy meson is about 60 to 100 electron masses heavier than the outgoing K-particle, and has suffered a change in identity at the collision. Should the existence of K-mesons with different masses be established this would appear to be the most satisfactory explanation. At present the question of the occurrence of a variety of K-meson masses remains open.

In the event of the high value of the ionization of the primary being due to a statistical fluctuation and the two K-mesons having the same mass, then it is clear that, apart from the effect of nuclear binding, the collision must have been very nearly elastic and involved a single nucleon.

4. – Remarks.

It is well known that the classification of K-mesons, e.g. τ, $\varkappa$, χ, K_μ, K_β etc., according to their modes of decay, is purely phenomenological and does not imply the existence of a corresponding diversity of intrinsically different elementary particles. On the other hand many K-mesons appear to have closely similar masses, but their different modes of decay may or may not represent alternative methods of transformation of the same particle. It is therefore of interest to consider any points of similarity among the heavy mesons such as might occur in their mode of production or interaction.

DANIEL and LAL [4] have seen two examples of interactions produced by K-mesons from each of which there emerges a τ-meson; in one of them the τ-meson is known to be positively charged. Let us for the moment assume that in the event described in § 2 and in the two Bombay events, the heavy meson does not change its identity upon collision. It then follows that the K-meson and τ-meson have two characteristics in common. Firstly, they produce interactions in flight without self-annihilation. Secondly, as described in § 2 the K-meson was produced in association with a Σ-particle — where $\Sigma^- \to \pi^- + n + \sim 110$ MeV (in the notation of GELL-MANN and PAIS [5]); a similar association in production between such a hyperon and a τ^+-meson

[4] R. R. DANIEL and D. LAL: *Proc. Ind. Acad. Sci.*, in course of publication (1955).
[5] M. GELL-MANN and A. PAIS: *Proc. Int. Nucl. Phys. Conf.* (*Glasgow*), July 1954.

has already been observed ([6]). It is difficult to draw any conclusions at present about those interactions produced by K-mesons in which the emergent K-meson is unclassified, since it stops in the emulsion and decays into a lightly ionizing secondary which cannot be identified ([4,7,8]) and § 3 of this paper.

If on the other hand, a transformation of identity upon collision is admitted to be a possible process then the observation of the K-meson in the event of § 2 is insufficient to establish the association in production of K-mesons and Σ-particles. Moreover, the observed emergence of K- and τ-mesons from K-meson induced disintegrations need not necessarily imply that these particles frequently produce nuclear interactions in flight. As pointed out in § 3, the existence of unlike K-mesons, the heavier transforming into the lighter, provides the simplest explanation for the puzzling energy discrepancy found in the second event.

In addition to these considerations, it is also possible to make a comparison between the available experimental material and the theoretical framework of GELL-MANN and PAIS ([5]). In what follows we shall use the nomenclature of these authors. According to their scheme the following process

$$\pi + \mathcal{N} \rightarrow \mathrm{Y} + \mathrm{K}$$

is a strong reaction. (Statements concerning π-$\mathcal{N}$ collisions also apply to $\mathcal{N}$-$\mathcal{N}$ collisions except for the necessity of conserving nucleons). In the above $\mathcal{N}$ refers to the nucleon, K to K^+ or θ^0, and Y only to the $\Sigma_0^{\pm}$ and Λ^0; for the purposes of discussion we do not consider other hyperons already known (such as $\Xi \rightarrow \Lambda^0 + \pi^- + \sim 60$ MeV) or any new ones which may be postulated.

Whilst the K^+-mesons can be produced in association with the Y-particle, the K (K^-- and $\bar{\theta}^0$-particle) is produced only in association with K. This has the consequence — which has been stated on a number of occasions previously — that in contrast to the K^+, a K^--meson requires a higher threshold energy for production and the number of slow negative particles observed in emulsions may be correspondingly smaller.

In the case of scattering or absorption, however, the isotopic spin assignments lead to the following reactions:

$$\bar{\mathrm{K}} + \mathcal{N} \rightarrow \text{Intermediate state} \begin{cases} \nearrow \mathrm{Y} + \pi & \mathrm{I}(a) \\ \searrow \bar{\mathrm{K}}' + \mathcal{N}' & \mathrm{I}(b) \end{cases}$$

$$\mathrm{K} + \mathcal{N} \rightarrow \text{Intermediate state} \rightarrow \mathrm{K}' + \mathcal{N}' \quad \text{(II)}\,.$$

([6]) D. LAL, YASH PAL and B. PETERS: *Phys. Rev.*, **92**, 438 (1953).

([7]) J. CRUSSARD, M. F. KAPLON, J. KLARMANN and J. H. NOON: *Phys. Rev.*, **95**, 584 (1954).

([8]) G. GOLDHABER: *Proc. Rochester Conference on High Energy Physics* (1955).

Reaction I(a) has been observed experimentally in the case of the nuclear capture of stopped K^--mesons.

Whilst the K^--mesons have two real channels I(a) and I(b), the first of which results in the production of a hyperon and consequent disappearance of the K^-, the K^+ mesons have only one possible channel, that of direct scattering. Both types can presumably suffer charge exchange scattering to give θ^0 and $\bar{\theta}^0$-particles.

Accordingly, when the production of K^+ and K^--mesons occurs in heavy nuclei, where the probability is large for further nuclear interactions before escape, one expects the number of K-mesons to be reduced as a result of reaction I(a) thus leading to a further increase in the relative numbers of slow K^+ to slow K^--mesons observed in emulsions.

An argument of this type would also explain the observations made by FRIEDLANDER *et al.* (9) on the characteristics of nuclear disintegrations giving rise to K^--mesons. All the available experimental data on the scattering of K-mesons in emulsions are consistent with the same general picture. In this connection, it would be important to compare the differences in the scattering properties of K^+ and K^--mesons when high intensity beams of such particles are available from the giant accelerators. Further, it is also of interest to compare the relative intensity of the two reactions I(a) and I(b), for it is likely that I(a) may be more frequent.

A further point raised by a consideration of reaction (II) is that the intermediate state necessary in this process — undoubtedly only virtual — has to be a complex one involving antiparticles etc., if considered only within the framework of the theory of GELL-MANN and PAIS. On the other hand one may ask whether these phenomena are in any way an indication of the existence of a K-meson/nucleon potential which has so far not been directly invoked.

Acknowledgements.

We are grateful to Professor C. F. POWELL, F.R.S. for the hospitality and facilities he has afforded us. Our thanks are also due to Mr. C. J. WADDINGTON and Dr. D. H. PERKINS for measurements they made on the event described in § 3. The K-meson decays were found by Miss A. STRADLING (§ 2) and Miss M. MERRITT (§ 3). Two of us wish to thank the following bodies: National University of Ireland for a Travelling Studentship (D.K.) and the Royal Commission for the Exhibition of 1851 for a Senior Scholarship (M.G.K.M.).

(9) M. W. FRIEDLANDER, D. KEEFE, M. G. K. MENON, R. H. W. JOHNSTON, C. O'CEALLAIGH and A. KERNAN: *Phil. Mag.*, **46**, 144 (1955).

RIASSUNTO (*)

Si descrivono due eventi in cui mesoni pesanti interagiscono con nuclei dell'emulsione fotografica producendo piccole stelle ed emergendo essi stessi dalla collisione. In uno degli eventi una particella relativistica dotata di carica semplice entra nel pacco e produce una stella con sole tre particelle cariche emergenti che sono state identificate con un iperone, un mesone π e un mesone K, rispettivamente. Il mesone K produce due stelle prima di arrestarsi e decade con l'emissione di un mesone μ lento. Nell'altro evento un mesone K penetra nel pacco dall'esterno e, dopo aver interagito, si arresta nell'emulsione e decade con l'emissione di un'unica particella debolmente ionizzante. Si discutono alcuni interessanti particolarità riguardanti le proprietà dello scattering dei mesoni pesanti.

(*) *Traduzione a cura della Redazione.*

IL NUOVO CIMENTO Vol. I, N. 4 1° Aprile 1955

Velocità di ultrasuoni in sistemi di liquidi parzialmente miscibili.

M. Cevolani e S. Petralia

Istituto di Fisica dell'Università - Bologna

(ricevuto il 5 Marzo 1955)

Riassunto. — Con la tecnica della interferometria ultrasonora si è misurata la velocità di propagazione di ultrasuoni a frequenza di 3 MHz in sistemi di liquidi parzialmente miscibili (fenolo-acqua, cicloesano-metanolo, solfuro di carbonio-metanolo, anilina-cicloesano). Mediante misure di densità si è poi determinata la compressibilità delle singole miscele alle varie concentrazioni, la velocità molecolare di Rao e le variazioni di volume che si hanno all'atto della miscelazione. I dati sperimentali vengono discussi alla luce delle recenti vedute sulla propagazione degli ultrasuoni nei liquidi. In generale in queste miscele la compressibilità risulta maggiore di quella prevedibile per miscele ideali: l'energia di coesione molecolare nella miscelazione viene a diminuire. Per il sistema fenolo-acqua si nota pure, per bassa concentrazione molecolare del fenolo, una lieve diminuzione della compressibilità; per il sistema anilina-cicloesano la compressibilità sembra avere andamento rettilineo. I valori sperimentali della velocità di Rao sono molto prossimi a quelli calcolabili teoricamente.

1. – Introduzione.

In una nota precedente [1] abbiamo comunicato i primi risultati di misure di velocità e assorbimento di ultrasuoni in sistemi di liquidi parzialmente miscibili, per valori della temperatura vicini al punto critico di soluzione.

Abbiamo ritenuto opportuno continuare tale studio, onde approfondire di più il comportamento di queste mescolanze. È infatti ben noto come da misure della velocità V di un fascio di ultrasuoni che si propaga in una miscela

[1] S. Petralia e M. Cevolani: *Rend. Acc. Naz. Lincei*, **12**, 674 (1952).

ordinaria di liquidi, a varie concentrazioni dei componenti, si possono trarre conclusioni interessanti per la comprensione delle interazioni molecolari. Le forze intermolecolari influenzano il valore della compressibilità adiabatica β del liquido e questa si può determinare dalla velocità di propagazione del suono e dalla densità ϱ del liquido stesso, essendo $\beta = 1/V^2\varrho$. Ora appunto si è trovato che per la maggior parte delle miscele la compressibilità non varia linearmente con la composizione di queste. Secondo l'interpretazione data da R. PARSHAD [2] nella miscelazione si altera il gioco delle forze intermolecolari, determinandosi in conseguenza delle associazioni nuove o rompendosi quelle già esistenti tra le molecole dei liquidi puri. La rottura di un'associazione, aumentando il numero di molecole interagenti con una molecola data, accresce l'energia di coesione e quindi riduce il valore della compressibilità.

Ci siamo allora proposti di esaminare come varia la compressibilità delle nostre miscele, tenute a temperatura di poco superiore a quella critica di soluzione, al variare della concentrazione dei componenti, allo scopo di vedere se, malgrado la loro caratteristica della non miscibilità a temperatura ordinaria, il loro comportamento è analogo a quello delle miscele ordinarie, oppure se ne discosta. Perciò abbiamo tenuto in qualche caso la temperatura molto vicina alla temperatura critica di soluzione, e in qualche caso abbiamo ripetuto le misure anche a temperatura notevolmente superiore.

2. – Metodo di misura.

Le misure di velocità sono state eseguite mediante un interferometro ultrasonoro. Gli ultrasuoni vi erano prodotti da una piastrina di quarzo oscillante su 3 MHz, alimentata da un sistema oscillatore-amplificatore. I picchi della reazione acustica erano rivelati da un voltmetro elettronico. La frequenza dell'oscillatore era regolata in guisa che il quarzo fosse eccitato in corrispondenza del minimo della sua curva di risonanza; la costanza della frequenza era controllata mediante un frequenziometro BC 221.

La densità delle miscele, alle varie concentrazioni, necessaria per ricavare la compressibilità, è stata misurata col metodo della bilancia idrostatica. Per vero la precisione qui raggiunta non si spinge al disopra di 1 ‰, come sarebbe stato desiderabile, soprattutto in vista di risalire, dai valori della densità, a una determinazione accurata delle variazioni di volume, che hanno luogo nella miscelazione. Tali variazioni sono in rapporto con le interazioni molecolari tra i componenti della miscela e la loro misura può portare, come è noto, un valido contributo alla conoscenza di queste. Notiamo tuttavia che i valori della densità da noi determinati per la miscela fenolo-acqua, alla temperatura di 70 °C

[2] R. PARSHAD: *Journ. Acoust. Soc. Amer.*, **21**, 175 (1949).

si accordano abbastanza bene con quelli che sono riportati da O. R. Howell [3].

La precisione raggiunta nella misura della velocità ultrasonora si può ritenere dell'ordine di 1‰. A raggiungere tale precisione ha contribuito anche la costanza della temperatura, a cui è stato di volta in volta portato l'interferometro. Il sistema termostatico difatti non permetteva oscillazioni di temperatura superiori a 0,03 °C.

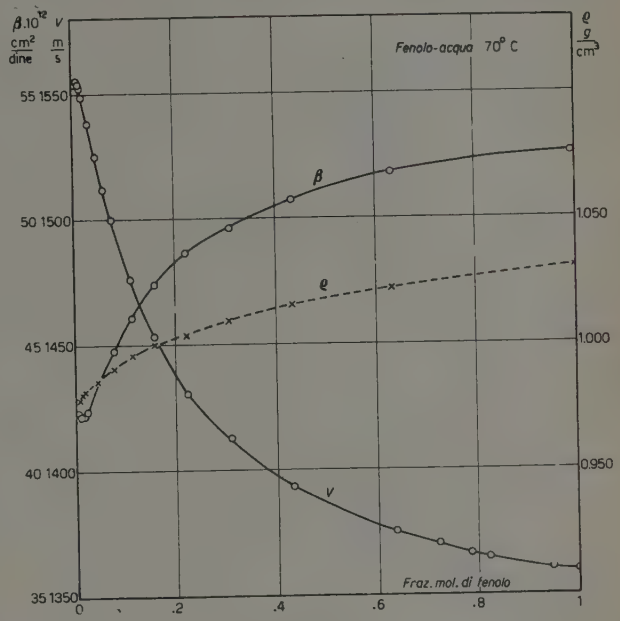

Fig. 1.

3. – Risultati sperimentali.

Le tabelle I-III e le figure 1-8 raccolgono i risultati delle misure per le quattro miscele fenolo-acqua, cicloesano-metanolo, solfuro di carbonio-metanolo, anilina-cicloesano. Precisamente nella tabella I sono riportati per le quattro miscele, in funzione della concentrazione molecolare del primo componente, la densità, la velocità di propagazione, la compressibilità, la variazione di volume molecolare Δv che ha luogo all'atto del mescolamento e la velocità sonora molecolare R di M. R. Rao [4]. Il valore di Δv è definito dall'equazione

$$\Delta v = \frac{M_1\gamma + M_2(1-\gamma)}{\varrho} - \left(\frac{M_1}{\varrho_1}\gamma + \frac{M_2}{\varrho_2}(1-\gamma)\right)$$

essendo M_1 e M_2 i pesi molecolari dei due componenti, di cui il primo entra nel miscuglio con la concentrazione γ e ϱ_1, ϱ_2 sono le rispettive densità. La R è una grandezza empirica definita dall'equazione

$$R = \frac{M}{\varrho}\sqrt[3]{V},$$

essendo M il peso molecolare del liquido di densità ϱ; essa è analoga al para-

[3] O. R. Howell: *Proc. Roy. Soc.*, A **137**, 418 (1932).
[4] M. R. Rao: *Journ. Chem. Phys.*, **9**, 682 (1941).

coro, a cui risulta proporzionale, e gode delle proprietà additive di quest'ultima grandezza.

Le fig. 1, 2, 4, 5 e 6 raccolgono i diagrammi relativi a V, ϱ e β; per tutte le miscele le curve di velocità mostrano una più o meno marcata concavità

Tabella I.

Miscela	Concentrazione molecolare del 1° componente	ϱ g/cm³	V m/s	$\beta \cdot 10^{12}$ cm²/dine	R	Δv cm³
Fenolo-	0,0	0,978	1554,5	42,4	215,8	0,00
-acqua	0,4	0,979	1555,0	42,24	216,9	0,00
70 °C	0,8	0,980	1555,7	42,16	220,3	0,00
	1,2	0,981	1554,6	42,18	223,7	0,00
	2,1	0,983	1549,2	42,4	230,9	0,00
	7,6	0,991	1500,5	44,8	274,8	0,05
	16,1	1,000	1453,9	47,4	343,0	0,11
	22,3	1,004	1430,4	48,7	392,7	0,18
	30,9	1,010	1413,2	49,6	461,5	0,18
	43,4	1,016	1393,2	50,8	560,6	0,19
	63,3	1,022	1375,0	51,8	719,9	0,21
	100,0	1,031	1359,0	52,6	1010,8	0,00
Cicloesano-	0,0	0,763	1020,0	125,9	422,5	0,00
metanolo	6,3	—	1014,2	—	—	—
50 °C	8,7	0,754	1013,0	129,2	486,9	0,37
	11,3	0,752	1014,3	129,3	506,4	0,48
	14,0	0,751	1015,0	129,2	525,9	0,52
	27,6	0,747	1031,6	125,8	628,0	0,70
	47,0	0,745	1058,2	120,0	773,4	0,76
	60,4	0,746	1076,7	115,6	867,7	0,68
	77,4	0,746	1096,3	111,5	999,2	0,45
	87,8	0,746	1110,0	108,8	1080,7	0,38
	95,0	—	1121,2	—	—	—
	100,0	0,748	1132,3	104,9	1173,2	0,00
Solfuro di	0,0	0,776	1065,0	113,6	421,5	0,00
carbonio-	4,5	0,804	1050,7	112,7	430,4	0,15
-Metanolo	9,5	0,832	1038,0	111,6	441,0	0,34
36,5 °C	15,3	0,866	1029,7	108,9	452,4	0,42
	21,9	0,903	1022,0	106,2	465,7	0,49
	29,6	0,943	1018,0	102,4	481,0	0,56
	38,7	0,988	1019,0	97,6	500,1	0,61
	49,5	1,039	1023,0	92,0	520,9	0,58
	79,1	1,164	1051,6	77,6	584,4	0,21
	88,8	1,199	1067,3	73,2	606,0	0,20
	100,0	1,238	1103,7	66,3	635,8	0,00

segue TABELLA I.

Miscela	Concentrazione molecolare del 1° componente	ϱ g/cm³	V m/s	$\beta \cdot 10^{12}$ cm²/dine	R	Δv cm³
Anilina-Cicloesano 50 °C	0,0	0,749	1132,3	104,2	1173,2	0,00
	9,1	0,766	1149,0	98,8	1162,9	0,22
	18,4	0,785	1169,6	93,1	1152,4	0,34
	27,9	0,806	1190,8	87,5	1141,0	0,39
	37,6	0,829	1220,2	81,0	1130,0	0,32
	47,5	0,853	1254,5	74,5	1119,8	0,23
	57,5	0,879	1298,7	67,4	1108,9	0,03
	67,8	0,906	1344,4	61,1	1099,7	— 0,01
	78,3	0,935	1406,8	54,1	1093,5	— 0,11
	89,1	0,964	1470,9	47,9	1088,6	— 0,04
	100,0	0,995	1539,6	42,4	1081,9	0,00
Anilina-Cicloesano 35 °C	0,0	0,763	1203,4	90,5	1174,5	—
	18,4	0,799	1235,2	82,0	1152,3	—
	37,6	0,844	1284,0	71,8	1128,3	—
	57,5	0,895	1356,0	60,8	1094,5	—
	78,3	0,949	1467,2	48,9	1091,4	—
	100,0	1,009	1598,9	38,9	1080,1	—

TABELLA II.

Temperatura °C	Metanolo V (m/s)	Cicloesano V (m/s)	Temperatura °C	Fase omogenea V (m/s)
18,5	—	1243,3	47,2	1071,1
21,0	1121,3	—	47,9	1069,8
23,9	1111,7	1216,2	48,9	1064,4
31,6	1089,1	1181,1	50,0	1059,0
34,0	1081,6	1166,7	51,3	1053,7
37,0	1076,7	1157,8	51,9	1051,3
39,5	1067,2	1142,2	53,1	1048,5
43,1	1057,8	1124,3	54,2	1041,2
45,0	1060,5	1110,5	—	—
46,1	1064,0	1095,8	—	—
46,3	—	1099,8	—	—
47,1	1074,4	1085,3	—	—
47,5	—	1078,9	—	—

verso l'alto. Nella fig. 4, relativa al sistema solfuro di carbonio-metanolo i tratti punteggiati corrispondono a una lacuna di miscibilità. Nella fig. 3 è segnato l'andamento, in funzione della temperatura, della velocità ultrasonora

Tabella III.

Temperatura °C	Metanolo (puro) V (m/s)	Temperatura °C	Cicloesano (puro) V (m/s)
20,4	1118,7	25,4	1251,5
30,5	1085,0	35,6	1201,3
40,0	1053,0	45,8	1152,0
50,8	1017,2	49,7	1133,5
55,6	1001,6	55,1	1106,5

nel cicloesano e nel metanolo puri, come anche nella miscela cicloesano-metanolo nell'intorno del punto critico di miscibilità (che per le nostre sostanze, fornite da Merck, cade a 47,2 °C), per una concentrazione corrispondente alla critica (71% in peso di cicloesano); le tabelle II e III raccolgono i valori numerici. Curve analoghe per le altre miscele sono state già da noi riportate nel precedente lavoro.

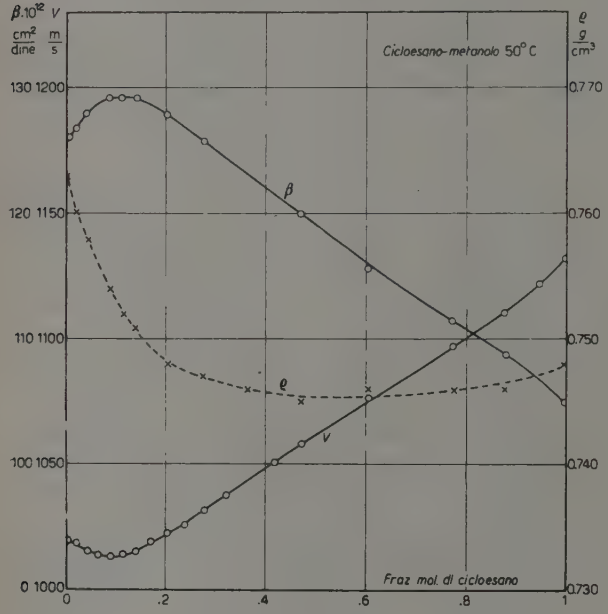

Fig. 2.

Per la velocità molecolare R nella fig. 8 sono stati segnati i punti dedotti dalle nostre misure e inoltre le rette, che rappresentano, in funzione della concentrazione, la stessa velocità, calcolata in base al numero dei legami chimici, che compaiono nelle molecole dei componenti di ogni singola miscela, secondo i criteri stabiliti da R. T. Lagemann e W. S. Dunbar (5). La fig. 7 infine dà l'andamento dei Δv.

Sono stati anche calcolati per ogni miscela i valori di un *raggio molecolare* r, facendo uso di un'espressione stabilita da W. Schaaffs (6) per liquidi puri. Nella formula di Schaaffs viene espresso il covolume di van der Waals in funzione della velocità del

(5) R. T. Lagemann e W. S. Dunbar: *Journ. Phys. Chem.*, **49**, 428 (1945).
(6) W. Schaaffs: *Zeits f. Phys.*, **114**, 110 (1939).

suono, della temperatura assoluta, della massa molecolare e della densità del liquido. Supponendo lecita l'estensione di tale formula al caso di una miscela, la grandezza r così ottenuta dovrebbe rappresentare un valor medio del raggio per una delle specie molecolari componenti la miscela, il cui campo di azione viene alterato dall'aggiunta dell'altro componente. Nella maggior parte delle miscele qui studiate, al variare della concentrazione molecolare, r ha un andamento pressocchè rettilineo, dal valore che compete ad uno dei componenti fino al valore relativo all'altro componente da solo.

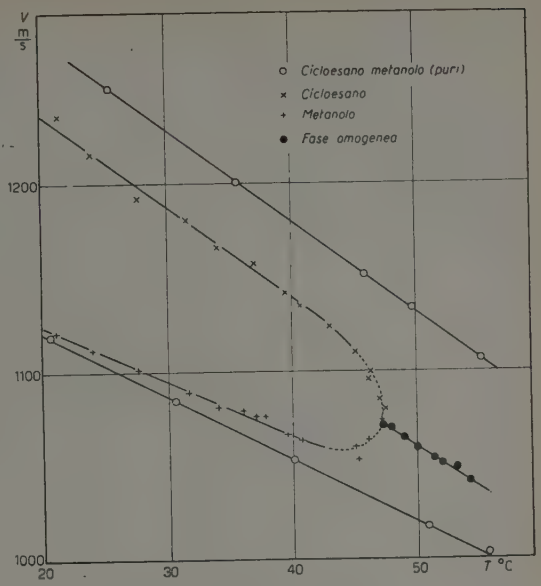

Fig. 3.

Nel caso della miscela fenolo-acqua l'andamento è alquanto diverso dalla linea retta, mostrando una concavità verso il basso. Tuttavia, non essendo riusciti a dare un significato più preciso a tale grandezza, abbiamo preferito non riportare qui i valori di essa.

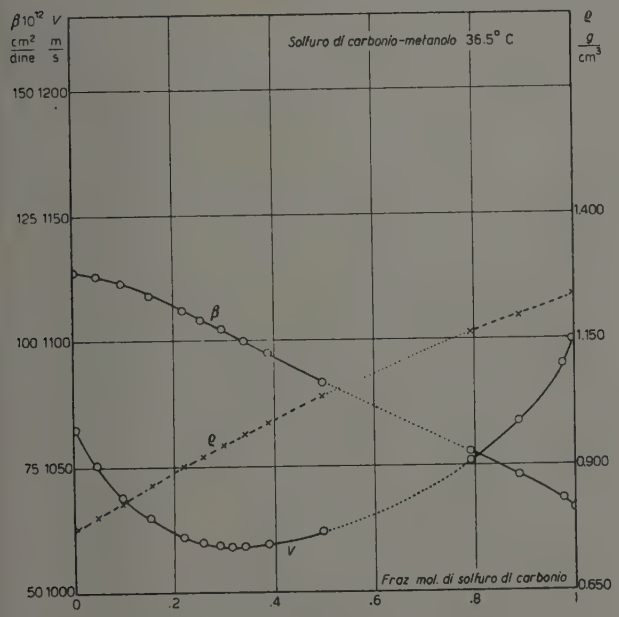

Fig. 4.

4. – Discussione dei risultati.

Dalle figure appare evidente che il comportamento generale delle nostre miscele è analogo a quello delle miscele comuni studiate da altri autori, e ormai ben noto.

Facendo ricorso ai dati forniti dalle *International Critical Tables* (1928), abbiamo ricostruito le curve della temperatura di ebullizione delle miscele ciclo-

esano-metanolo, solfuro di carbonio-metanolo e anilina-cicloesano; per la miscela fenolo-acqua una curva completa della temperatura di ebullizione, alle varie concentrazioni, è stata di recente determinata da H. BRUSSET e Y. GAYNES ([7]). Ora tutte e quattro le curve si mantengono al di sotto della retta che congiunge i punti di ebullizione dei liquidi puri. Ciò sta a indicare che certamente l'energia di interazione molecolare subisce in media una diminuzione nella miscela. Nell'approssimazione da noi raggiunta nella misura delle densità, le variazioni di volume Δv, che si può calcolare debbano aver luogo all'atto della miscelazione, sono, per i sistemi fenolo-acqua, cicloesano-metanolo, solfuro di carbonio-metanolo, positive. Per la miscela fenolo-acqua abbiamo ottenuto una conferma del segno di Δv mediante determinazioni dirette con un volumenometro. Qualche Autore ([7]) per questo sistema riferisce l'esistenza di una contrazione di volume. La massima variazione (positiva) di volume si ha per il sistema cicloesano-metanolo; segue poi, in tal senso, l'altro sistema contenente ancora questo alcool. Nel caso della miscela anilina-cicloesano sembra ci sia una dilatazione di volume per piccolo contenuto in anilina, cui segue una contrazione a forte tenore di anilina. Tale comportamento, e cioè l'inversione nel segno di Δv, è stato notato per altre miscele da H. HARMS ([8]) e si può giustificare in base a considerazioni fatte da I. PRIGOGINE e V. MATHOT ([9]). Le variazioni di volume nel mescolamento comprendono, secondo H. G. MARKGRAF e A. NIKURADSE ([10]) e P. MEARES ([11]), un termine geometrico, dovuto all'assembramento delle molecole, e un termine dovuto alle forze di attrazione

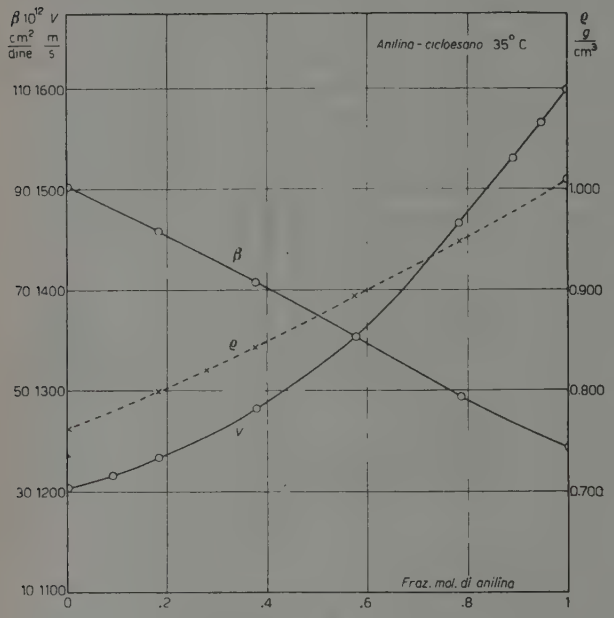

Fig. 5.

([7]) H. BRUSSET e J. GAYNÉS: *Compt. Rend.*, **236**, 1563 (1953).
([8]) H. HARMS: *Dissertation Würzburg* (1937).
([9]) I. PRIGOGINE e V. MATHOT: *Journ. Chem. Phys.*, **20**, 49 (1952).
([10]) H. G. MARKGRAF e A. NIKURADSE: *Zeits. Naturfor.*, **9a**, 27 (1954).
([11]) P. MEARES: *Journ. Chem. Phys.*, **22**, 955 (1954).

molecolare. Secondo i primi due autori nei miscugli di particelle di diversa struttura, ma con dimensioni non molto differenti e senza interazione molecolare specifica, è da attendersi in generale un aumento di volume. Così si comportano parecchie miscele, aventi come uno dei componenti il cicloesano o il solfuro di carbonio.

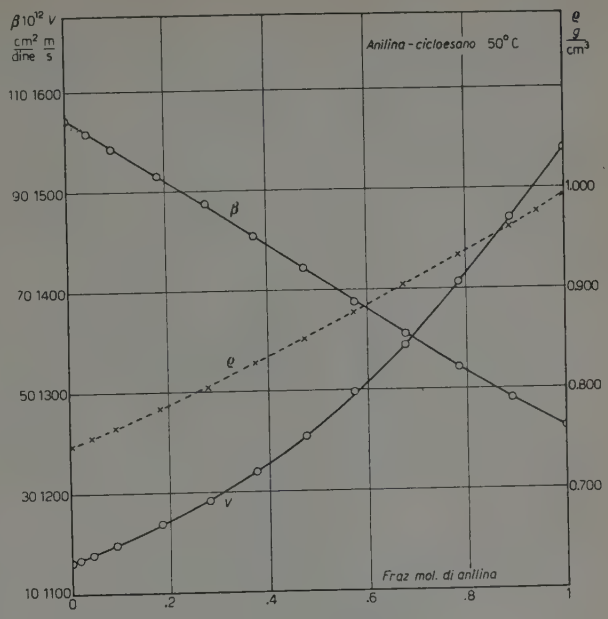

Fig. 6.

Abbiamo fatto pure delle determinazioni qualitative del calore di mescolamento; esso risulta in ogni caso negativo (miscele endotermiche), d'accordo, per alcune miscele, con i risultati che si possono trovare nella letteratura: risulta pertanto di segno opposto a quello di Δv. È questa una regola che sembra verificarsi per molte miscele [11].

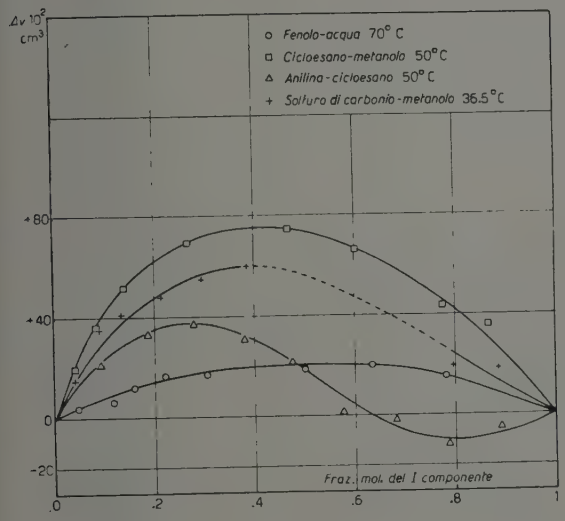

Fig. 7.

Nella curva di compressibilità del sistema fenolo-acqua, determinata alla temperatura di 70 °C, possiamo distinguere due regioni. Al crescere del contenuto in fenolo della miscela e per piccoli valori di questo, la compressibilità diminuisce dal valore che compete all'acqua pura e passa per un minimo a una concentrazione molecolare di fenolo di circa 0,8 %. La diminuzione di compressibilità sta a indicare manifestamente un aumento dell'energia di coesione molecolare. Ora tanto l'acqua che il fenolo sono liquidi associati attraverso legami idrogeno; sembra poi che l'intensità di tale legame sia più rilevante nel fenolo che non nell'acqua.

È probabile perciò che aggiungendo fenolo, questo provveda a rompere le associazioni dell'acqua, che ancora devono esistere alla temperatura di 70 °C, e ciò secondo PARSHAD conduce a una diminuzione di β. Anche la temperatura di ebullizione, per piccole concentrazioni in fenolo, passa per un minimo, che si raggiunge a una concentrazione molecolare di 1,9%, alquanto superiore a quella per cui si ha il minimo di β, secondo le nostre misure. È stato pure constatato (7) che con miscele contenenti meno di 1,9% di fenolo il vapore è più ricco di fenolo che non il liquido da cui deriva, mentre per miscele più ricche di fenolo il vapore contiene più acqua della miscela. Tale comportamento può appoggiare l'ipotesi della rottura delle associazioni dell'acqua operata dal fenolo, in quanto nelle associazioni le molecole di acqua sono più legate e l'energia richiesta per liberarle è maggiore che non per le molecole già distaccate dalle associazioni.

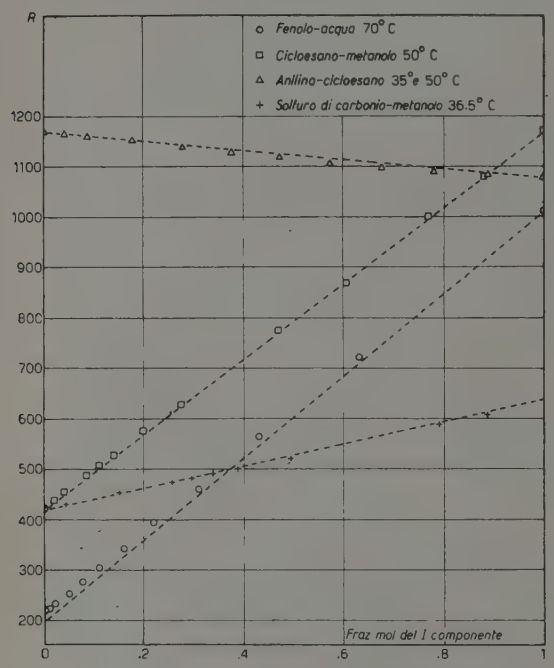

Fig. 8.

Conviene qui ricordare come in un'altra miscela, tetracloruro di carbonio-fenolo, studiata da W. MAIER e A. MEZ (12) e da A. F. CHHAPGAR (13), la presenza di fenolo determini un estremante nell'assorbimento e nella velocità, per piccole concentrazioni di tale sostanza.

Quando la concentrazione molecolare di fenolo nella soluzione aumenta, la compressibilità cresce dapprima rapidamente, poi più lentamente mostrando un'ampia concavità rivolta verso il basso. La maggior parte della curva di compressibilità si svolge al disopra della retta congiungente i valori estremi relativi ai liquidi puri, si ha cioè una compressibilità maggiore di quella che dovrebbe competere a una miscela ideale. Ciò sta a indicare che l'energia di coesione molecolare nella miscela va diminuendo col crescere del contenuto di fenolo; le molecole di questo si associano fra di loro, mentre la proporzione di esse nella fase di vapore diminuisce.

(12) W. MAIER e A. MEZ: *Zeits. Naturfor.*, **7a**, 300 (1952).
(13) A. F. CHHAPGAR: *Journ. Acoust. Soc. Amer.*, **25**, 794 (1953).

Nella curva che rappresenta il Δv per questo sistema, non si nota alcuna variazione per le basse concentrazioni di fenolo, a parte piccolissime oscillazioni, ora positive ora negative, che si possono calcolare sia con i nostri valori per la densità, sia con i valori di ϱ forniti da HOWELL. D'altra parte il segno positivo di Δv è d'accordo con l'aumento che in generale ha luogo per la compressibilità.

Le altre tre miscele, cicloesano-metanolo, solfuro di carbonio-metanolo e anilina-cicloesano, contengono un componente completamente inerte come è il cicloesano, oppure uno quasi inerte quale è il solfuro di carbonio, entrambi con momento di dipolo nullo. Per le prime due miscele le curve di compressibilità stanno al disopra delle rette riunenti i punti estremi (compressibilità dei componenti puri) con un massimo netto per la miscela cicloesano-metanolo, massimo che si ha per una concentrazione molecolare di cicloesano di 11,3%. Nella miscelazione si ha una diminuzione dell'energia di coesione; le molecole del composto inerte non sono capaci di rompere o alterare le intense associazioni esistenti nelle molecole di metanolo, provocheranno solo un allontanamento di queste, determinando l'aumento di compressibilità. Il comportamento è in sostanza analogo a quello di miscele contenenti cicloesano studiate da altri autori [14]. La variazione di volume che si ha all'atto del mescolamento è conforme ai criteri sopra ricordati, è cioè di origine geometrica. La composizione delle miscele per la quale si ha il valore massimo di Δv non coincide però con quella, per la quale si verificano le deviazioni maggiori di β dall'andamento rettilineo, il che potrebbe far pensare che i fattori strutturali, che intervengono a determinare le variazioni di volume, possono esser diversi da quelli che determinano la velocità ultrasonora nella miscela [15].

Per la miscela anilina-cicloesano, la curva di compressibilità (fig. 5 e 6) ha un andamento quasi rettilineo, sia alla temperatura di 35 °C, poco discosta dal punto critico, come alla temperatura superiore di 50 °C. Forse si può scorgere, in entrambe le fig. 5 e 6, una lieve concavità, rivolta verso l'alto, per concentrazioni di anilina superiori al 60%, dove sembra esserci un cambiamento nel segno di Δv. Essa starebbe a indicare una lieve interazione tra le due specie molecolari. Comunque si tenga presente che uno dei componenti è bensì un liquido inerte, ma con discreta polarizzabilità, mentre l'anilina è dotata di momento dipolare e può comportarsi, alle grandi concentrazioni, come liquido associato, per quanto lievemente [16,17].

Infine nella fig. 8 sono riportati i valori di R per le quattro miscele, così

[14] I. GABRIELLI e G. POIANI: *Ric. Scient.*, **22**, 1426 (1952).
[15] F. DANUSSO: *Rend. Acc. Naz. Lincei*, **17**, 234 (1954).
[16] K. HIGASI: *Scient. Pap. I.P.C.R. Tokio*, **28**, 284 (1936).
[17] N. FUSAN, M. L. JOSIEN, R. L. POWELL e E. UTTERBACK: *Journ. Chem. Phys.*, **20**, 145 (1952).

come risultano dall'esperienza e i valori calcolati secondo la legge di additività valida per tale grandezza (rette a tratti). L'estensione di questa grandezza, introdotta inizialmente per liquidi puri, anche alle miscele è stata fatta da O. NOMOTO ([18]). NOMOTO ha ricavato alcune regole, che governerebbero l'andamento di R per le varie miscele. Osserviamo anzitutto che per le miscele qui studiate i valori sperimentali di R cadono abbastanza vicini alle curve teoriche. Per le miscele solfuro di carbonio-metanolo e anilina-cicloesano, costituite da liquidi a densità notevolmente diverse, i punti sperimentali si adagiano su una curva, che ha una lieve concavità rivolta verso l'alto, conforme ai criteri di NOMOTO. Le miscele fenolo-acqua, cicloesano-metanolo contengono invece coppie di liquidi a densità molto vicine e le R corrispondenti hanno andamento rettilineo.

Queste ricerche sono state compiute con l'ausilio finanziario del C.N.R., che qui teniamo a ringraziare.

([18]) O. NOMOTO: *Journ. Phys. Soc. Japan*, **8**, 553 (1953).

SUMMARY (*)

Using ultrasonic interferometry measures have been performed of the propagation velocity of ultrasonics of 3 MHz frequency in systems of partially mixable liquids (phenol-water, cyclohexane-methanol, carbon sulfide-methanol, anylin-cyclohexane). With density measures the compressibility of the mixtures has been determined at different concentrations as well as the molecular velocity of Rao and the changes in volume which happen on performing the mixture. The experimental results are discussed in the light of the modern ideas on the propagation of ultrasonics in liquids. Generally in these mixtures compressibility results to be higher than the one one could foresee for ideal mixtures, the molecular cohesion energy reducing itself in the mixture. For the system phenol-water one notices also, by low molecular concentration of phenol a slight decrease of compressibility; for the system anilyn-cyclohexane the compressibility seems to change rectilinearly. Experimental values of the Rao velocity are very near those theoretically calculated.

(*) *Editor's translations.*

LETTERE ALLA REDAZIONE

(La responsabilità scientifica degli scritti inseriti in questa rubrica è completamente lasciata dalla Direzione del periodico ai singoli autori)

Revision of the β-Ray Spectrum of $^{214}_{83}$Bi(RaC).

R. A. Ricci and G. Trivero

Istituto di Fisica Sperimentale del Politecnico - Torino

(ricevuto il 27 Dicembre 1954)

1. – Several authors have tried to interpret the decay scheme $^{214}_{83}$Bi-(β)-$^{214}_{84}$Po, which presents difficulties due to the complexity of the emitted β and γ ray spectra (1).

In order to test the validity of the different schemes suggested, we have tried to analyze the β spectrum of $^{214}_{83}$Bi with an absorption method, at the same time, using the β-γ coincidences technique (2).

The investigations concern the experimental determination of the absorption curve of $^{226}_{88}$Ra β-spectrum and the absorption curve of the β-γ coincidences.

2. – Fig. 1 shows the experimental apparatus. S is a $^{226}_{88}$Ra sample (about 16 microcurie) in equilibrium with its decay products up to RaD (half-life $T = 22$ years).

F_β is a scintillation counter for β-rays consisting of naphtalene crystal (diameter 1 cm; thickness 0,3 cm) and RCA 1P21 photomultiplier.

F_γ is a scintillation counter for γ-rays (NaI crystal activated with thallium and RCA 913A photomultiplier).

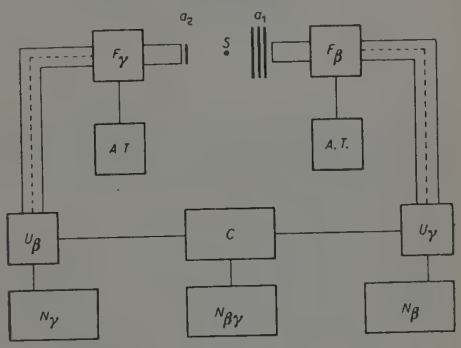

Fig. 1.

The d.c. voltages for the photomultipliers are stabilized to 0.2%.

The voltage pulses at the output of the photomultipliers are amplified and shaped, and then applied to a coincidence circuit C which has a resolving time of 0.23 ± 0.01 μs.

The scalers N_β, N_γ, $N_{\beta\gamma}$ record the total number n_β of pulses β and n_γ of pulses γ respectively, and the total

(1) E. Rutherford, W. B. Lewis and B. V. Bowden: *Proc. Roy. Soc.*, A, **142**, 347 (1933); J. Surugue: *Journ. de Phys. et Rad.*, **8**, 7, 145 (1946); G. D. Latyshev: *Rev. Mod. Phys.*, **19**, 132 (1947); A. H. Wapstra: *Int. Conf. β and γ radioactivity* (September 1952), 1247; F. Demichelis and R. Malvano: *Nuovo Cimento*, **10**, 405 (1953).

(2) A. C. G. Mitchell: *Rev. Mod. Phys.*, **20**, 296 (1948).

number $n_{\beta\gamma}$ of coincidences at the output of the pulse shapers U_β, U_γ, and of the coincidence circuit C.

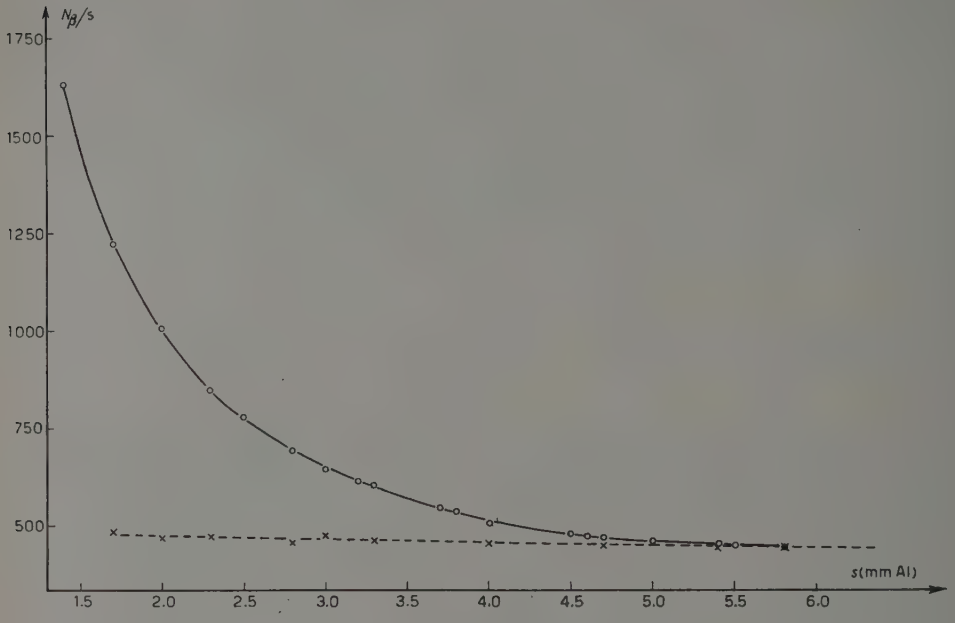

Fig. 2.

The absorbers a_1 consist of a series of aluminium sheets of various thicknesses, calibrated and measured with an accuracy of 0.5%.

a_2 is a lead absorber (1 mm) placed in front of the NaI crystal in order to make it completely insensitive to β-rays.

The background due to dark pulses and spurious events (some γ detection from the β counter and the γ-γ coincidences in the β-γ apparatus) was measured, as frequently as necessary, by covering the source with 9 mm of berillium; this stops completely all β-rays, while it does not lower appreciably the intensity of the γ-rays, owing to its very small cross section for our γ-rays [3].

We have taken into account the accidental fluctuations of the apparatus in order to get normalised experimental data.

The results obtained agreed within the statistical errors in the case of the coincidences and within 2% in the case of β counting rates.

The β-rays which may be detected by this apparatus, are emitted from the nuclides: $^{214}_{82}$Pb(RaB), $^{214}_{83}$Bi(RaC), and $^{210}_{81}$Tl(RaC″). We may eliminate the β-rays of RaB, with a convenient absorber, owing to its relatively low energy (0.65 MeV). The β-rays of RaC″, which have an energy of 1.8 MeV, are harmless owing to the very small probability of the transition RaC-(α)-RaC″ (0.04%).

Thus we may detect only the β-rays of $^{214}_{83}$Bi(RaC) with energy greater than 0.65 MeV.

The γ-rays are emitted from $^{226}_{88}$Ra, $^{214}_{83}$Bi(RaC) and $^{214}_{83}$Po(RaC′).

The γ-rays of $^{226}_{88}$Ra, are not detected owing to their very low energy (0.19 MeV).

[3] A. H. WAPSTRA: *Academisch Proeschrift* (Amsterdam, 1953), 37.

those of $^{214}_{83}$Bi give rise to spurious events and those of $^{214}_{84}$Po are of interest in our measurements.

counting rate n_β (counts per second) as a function of Al thickness s.

Fig. 3 shows the curve of the β-γ co-

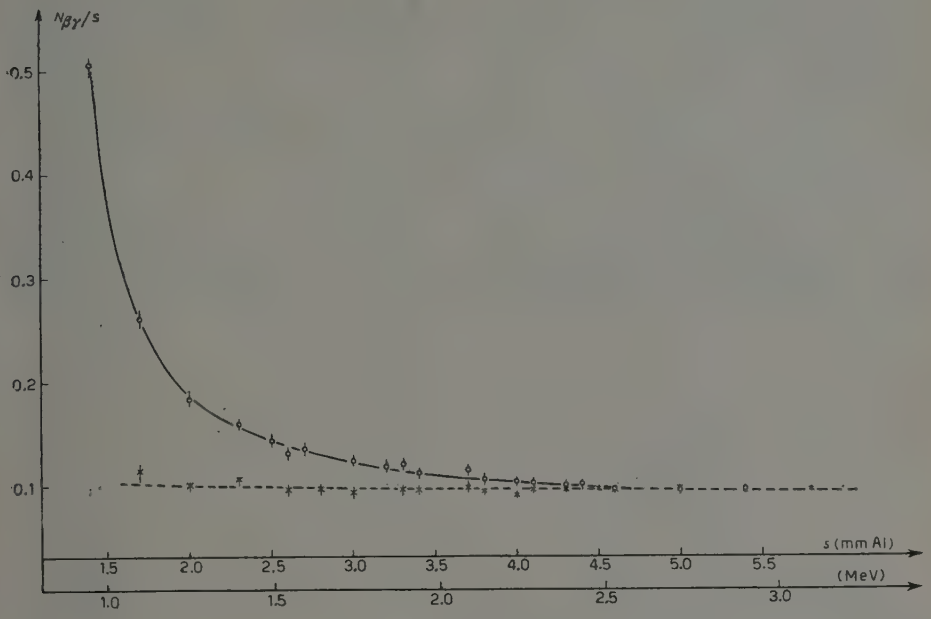

Fig. 3.

3. – We have made β absorption measurements in order to determine:

a) the maximum energy of $^{214}_{83}$Bi β-decay corresponding to the end-point of the electrons absorption curve, obtained by plotting the counting rate given at the β scaler against Al absorber thickness.

b) the coincidences between $^{214}_{83}$Bi β-rays and $^{214}_{84}$Po rays, corresponding to β transitions of $^{214}_{83}$Bi to excited states of $^{214}_{84}$Po.

The end-point of the β-γ coincidences should give the energy upper limit of the β branches, which are followed by emission of γ-rays.

Fig. 2 shows the β-rays absorption curve: the full line curve gives the incidences: the full line curve gives the counting rate $n_{\beta\gamma}$ (counts per second) as a function of Al thickness.

Both Figs. 2, 3, give in the dotted curve the background line; in fig. 3 (*) the scale below the absorber thickness gives the corresponding energies of the upper limit of various β spectra.

The end point of the electron absorption curve can be fixed at $5.8 \pm \pm 0.35$ mm of Al and agrees within a good approximation with the maximum energy (3.17 MeV) of the extreme

(*) The counting rates of the total β-γ coincidences as well as the background coincidences, are corrected from the accidental concidences.

(4) C. D. Ellis: *Proc. Roy. Soc.*, A. **143**, 350 (1935); G. Scharff-Goldhaber: *Phys. Rev.*, **90**, 587 (1953); see also E. Rutherford and cow. (1), and F. Demichelis and R. Malvano (1).

β branch, as found by LATYSHEV and by WAPSTRA.

For the β-γ coincidences (Fig. 3), we find the end point at an aluminium thickness quite higer than the thickness found by WAPSTRA [3]; our thickness corresponds to an energy 2.56 ± 0.25 MeV.

The energy found by WAPSTRA for the first partial β spectrum, using the β-γ coincidences technique, is 1.56 MeV; the same quantity is given by LATYSHEV as 1.65 MeV [1].

We have compared ours and WAPSTRA's results; this comparison is easier than in the case of LATYSHEV's researches.

At 880 mg/cm² (3.25 mm Al) WAPSTRA found a ratio:

$$n_{\beta\gamma}/n_{\beta} = (4 \pm 52) \cdot 10^{-6}$$

Under the same conditions, we find a ratio:

$$n_{\beta\gamma}/n_{\beta} = (5.0 \pm 2.5) \cdot 10^{-4} .$$

Other values, for absorbers thicker than 2.6 mm Al (wich is the thickness corresponding to an energy 1.56 MeV), are collected in Table I.

of a β-γ coincidence with the following energies: 2.56 MeV for the β-ray and 0.61 MeV for the γ-ray.

This conclusion is consistent with the experimental results of several authors about the γ spectrum of $^{214}_{84}$Po, who agree on the existence of an excited and very intense level of 0.61 MeV, whose intensity should not be exausted by the γ-γ cascades connected with this level [5].

Our results allow the establishment of a partial β decay scheme of $^{214}_{83}$Bi relatively to the β branches of higher energy, consisting of two β branches of 3.17 MeV and 2.56 MeV respectively.

This scheme however requires a knowledge of the intensity of each component branch, which we were not able to determine, with our apparatus, with satisfying accuracy.

We notice anyway that A. H. WAPSTRA, by estimating the errors of his measurements, draws a maximum intensity for the supposed β branch of 2.56 MeV, of less than 10%; that is less than $\frac{1}{2}$ of the intensity of the 3.17 MeV transition to the ground state, given by him as 19%.

TABLE I.

mm Al	n_{β}/s	$n_{\beta\gamma}/s$	$n_{\beta\gamma}/n_{\beta}$
2.6	273	$(1.47 \pm 0.35) \cdot 10^{-1}$	$(5.4 \pm 1.4) \cdot 10^{-4}$
3.0	176	(1.20 ± 0.45) »	(6.8 ± 2.5) »
3.7	100	(0.53 ± 0.40) »	(5.3 ± 4.0) »
4.3	41	(0.35 ± 0.32) »	(8.5 ± 7.8) »
5.0	26	(0.16 ± 0.23) »	(6.2 ± 8.8) »

4. – From our experimental data we may conclude that the β branch of 3.17 MeV energy corresponds to a transition of $^{214}_{83}$Bi to the ground state of $^{2\,14}_{84}$Po; this agrees with LATYSHEV's and WAPSTRA's results.

The same data confirm the existence

The examination of our experimental coincidence rate leads us to estimate that the ratio between the intensity of

(5) F. DEMICHELIS and R. MALVANO: *Nuovo Cimento*, **12**, 358 (1954).

the 2.56 MeV branch and that of the 3.17 MeV branch should be greater than $\frac{1}{2}$.

At the moment we are carrying on a new experiment in order to obtain better confirmation of these results and more information about the β spectrum of $^{214}_{83}$Bi.

We want to express our gratitude to Prof. E. PERUCCA for his advice and encouragement; to Proff. F. DEMICHELIS and R. MALVANO for stimulating discussions. Our thanks also to Prof. G. VENTURELLO, who provided us the berillium necessary for the research.

P.S. – A concise report on our results (the statement of the β branch of 2.56 MeV energy in the β decay of $^{214}_{83}$Bi) was already published in *Rend. Acc. Lincei*, **17**, 44 (1954). It was yet a support for the scheme of γ levels in $^{214}_{84}$Po recently proposed by F. DEMICHELIS and R. MALVANO (*Nuovo Cimento*, **12**, 358 (1954)).

But some corrispondence with A. H. WAPSTRA stopped the publication of this paper. We are glad to inform now that also this Author could experimentally confirm the exsistence of the new β branch, and we are indebted to him for his kind control of our conclusions.

Ionospheric Self-Interaction of Radio Waves at Vertical Incidence.

G. J. Aitchison and G. L. Goodwin
Physics Department, The University of Adelaide, Australia

(ricevuto il 1° Gennaio 1955)

An investigation has been carried out to determine whether self-interaction of radio-waves occurs in the ionosphere at a frequency of 1550 kHz, which is close to the local gyro-frequency (approximately 100 kHz at 1600 km altitude). Transmissions were made from the University of Adelaide on twenty-five nights between 0.00 and 05.30 hours local time, from May to October 1954, using a 5 kW transmitter, amplitude modulated with pure audio frequencies in the range 160 Hz to 4000 Hz.

The receiving station was 5.6 km south of the transmitter, so that the sky-wave was reflected from the ionosphere at almost vertical incidence. The receiving equipment included an Eddystone « 680 » receiver with input either from a tuned loop-aerial which supplied sky-wave signals, or from a short simple aerial which supplied ground-wave signals of strengths comparable with those of the sky-wave from the loop-aerial. The amplitude of the ground-wave received by the loop was reduced to a very small value by means of a phased signal from a vertical aerial connected across the loop's output via a split condenser. The signal received by the loop had an average sky-wave amplitude of about 15 times its ground-wave amplitude.

A vacuum-tube-volt-meter and a « Marconi » wave analyser of band width 4 Hz were both connected to the final I.F. stage of the receiver, to measure the R.F. and A.F. levels respectively. To calibrate the receiving equipment to read modulation depth percentage, readings were taken on the ground wave of R.F. and A.F. levels (using arbitrary scales on the two measuring instruments) for signals of known modulation depths as measured at the transmitter. From these calibration each pair of readings of R.F. and A.F. levels, measured for the sky-wave, could be converted to percentage modulation. Measurements of percentage modulation on the sky-wave were made during intervals of less than two minutes, and after each interval the calibration was checked by a few measurements on the ground-wave.

Frequently, reflected signals from the E- and F-layers of the ionosphere were received simultaneously. At such times, « selective fading » caused by the interference of these two sky waves produced

spurious variations in modulation depth of the received signal. To guard against errors due to « selective fading », the following procedures were adopted:

1) Each 15 minutes of modulation with pure audio frequencies was followed by three minutes of modulation with pulses. This enabled the relative amplitudes of ground-wave, *E*-reflected wave and *F*-reflected wave, as received by the loop-aerial, to be measured on a cathode-ray display at the receiving station. Readings were taken only when the R.F. amplitude of one of the two reflected waves was at least three times as great as the sum of the amplitudes of the ground wave and the other reflected wave. Reliable readings were seldom possible for more than one-third of the transmission time, and at times very few readings could be taken for a whole night, due to « selective fading » between the two sky waves.

2) Variations in received signal amplitude cause the R.F. and A.F. levels to fluctuate almost in unison, bur readings were taken only at instants when the A.F. level was a maximum. This ensured that if any errors occurred due to « selective fading », the measured readings of modulation percentage would be slightly larger than the true value. Since the measured modulation percentages were less than those transmitted, this method of measurement reduced rather than enhanced the observed effect. Results of transmission (frequency 1.55 kHz; transmitted modulation depth 20%) are summarized in the table.

On the nights of 9-10th and 10-11th November, 1954, similar tests were made on transmissions from broadcast station 5CL, Adelaide (frequency 730 kHz, power 5 kW) between 23.00 and 03.00 hours local time. Pulse modulation was not used in these tests, as it was assumed that the sky-wave at this frequency was a pure *E*-reflection. No measurable reduction in modulation depth was observed on these transmissions.

The results show that:

1) Near the gyro-frequency, the modulation depths of both an *E*-reflected and an *F*-reflected wave were significantly less than that of the ground wave.

2) The reduction in modulation depth was greater for reflection from the *F*-layer than from the *E*-layer.

3) Within the limits of measurement, no reduction in modulation depth occurred at a frequency of 730 kHz, which is remote from gyro-frequency.

4) A comparison of the values in columns (4) and (6) of the table indicates that there is a greater reduction in modulation depth for larger proportions of *F*-reflection in the received signal.

The results also suggest that the effect is greatest for modulation frequencies of the order of 800 to 1500 Hz. This matter is being further investigated.

In qualitative explanation of these results, it is tentatively suggested that at a frequency near gyro-frequency the extraordinary component of the sky-wave is strongly absorbed in the *E*-layer, while the ordinary component is reflected either from a higher level in the *E*-layer, or from the *F*-layer. In the region where the extraordinary component is absorbed, the absorption coefficient of the ionosphere varies at the modulation frequency, causing a change in the modulation percentage of the ordinary component as it passes through this region.

CUTOLO [1] has observed considerable reductions in the modulation depths of waves reflected from the ionosphere, and has attributed this effect to radio self-

[1] M. CUTOLO: *Nuovo Cimento*, **9**, 687 (1952).

Date	Modulation frequency (Hz)	*F*-layer reflection				*E*-layer reflection			
		F exceeds $3(E+G)$		*F* exceeds $5(E+G)$		*E* exceeds $3(F+G)$		*E* exceeds $5(F+G)$	
		No. of readings	Average modulation depth (%)	No. of readings	Average modulation depth (%)	No. of readings	Average modulation depth (%)	No. of readings	Average modulation depth (%)
(1)	(2)	(3)	(4)	(5)	(6)	(7)	(8)	(9)	10)
31- 5-54	150	6	16.5 ± 1.9	—	—	—	—	—	—
	400	5	17.5 ± 1.4	—	—	—	—	—	—
2- 6-54	120	22	17.0 ± 2.2	—	—	—	—	—	—
	400	14	13.9 ± 4.7	—	—	—	—	—	—
	1 000	1	8.5	—	—	—	—	—	—
	1 500	1	16.0	—	—	—	—	—	—
4- 6-54	150	4	15.6 ± 1.4	—	—	—	—	—	—
	400	2	11.6 ± 1.0	—	—	—	—	—	—
	1 500	6	14.4 ± 2.1	3	12.8 ± 0.6	—	—	—	—
17- 8-54	160	18	12.7 ± 1.8	1	10.7	—	—	—	—
24- 8-54	160	12	14.2 ± 2.1	—	—	—	—	—	—
29- 8-54	160	45	16.3 ± 3.6	35	16.0 ± 3.2	—	—	—	—
20- 9-54	160	51	12.1 ± 2.3	25	12.1 ± 1.4	11	16.1 ± 1.5	5	16.3 ± 1.0
8- 9-54	250	19	15.7 ± 3.7	2	11.6 ± 2.0	—	—	—	—
10- 6-54	300	—	—	—	—	11	16.0 ± 3.0	1	15.1
28- 5-54	400	11	11.7 ± 2.9	—	—	—	—	—	—
11- 7-54	400	10	13.4 ± 2.5	—	—	18	14.1 ± 1.7	1	15.0
4- 8-54	400	5	17.6 ± 1.6	—	—	—	—	—	—
5- 8-54	400	5	11.5 ± 1.3	2	11.3 ± 0.2	22	16.5 ± 2.4	7	17.9 ± 1.2
16- 8-54	400	23	14.3 ± 2.2	15	13.4 ± 1.6	21	17.2 ± 1.9	5	16.5 ± 1.1
16- 9-54	400	41	13.8 ± 2.4	13	11.9 ± 1.9	—	—	—	—
26- 6-54	500	14	12.4 ± 1.7	2	12.2	—	—	—	—
18- 6-54	500	8	15.9 ± 3.4	—	—	—	—	—	—
30- 8-54	800	6	13.8 ± 3.6	—	—	—	—	—	—
7- 9-54	800	11	11.3 ± 3.8	—	—	—	—	—	—
13- 9-54	1 000	71	12.1 ± 5.1	32	10.8 ± 4.3	15	15.3 ± 2.5	6	15.8 ± 3.2
28-10-54	1 250	39	14.6 ± 3.1	6	11.4 ± 1.8	—	—	—	—
26- 9-54	1 500	12	8.1 ± 2.5	1	6.5	15	17.4 ± 1.8	—	—
4-10-54	2 000	59	15.4 ± 3.1	17	13.6 ± 2.9	14	16.9 ± 2.1	2	14.1 ± 1.3
18-10-54	3 000	32	15.7 ± 2.4	1	14.6	—	—	—	—
27-10-54	4 000	34	14.0 ± 2.1	10	12.5 ± 1.9	—			—

Transmission from University of Adelaide; Frequency 1 550 kHz, transmitted modulation depth 20 %.

F exceeds $3(E+G)$ and *F* excess $5(E+G)$ indicate that readings in columns (4) and (6) were taken when the amplitude of the *F*-reflected wave exceeded the sum of the amplitudes of the ground-wave and the *E*-reflected wave by more than 3 times and 5 times respectively. Similarly, inter-

interaction. The effect has been recently confirmed by MITRA (2).

The authors wish to thank Professor L. G. H. HUXLEY for his constant interest and encouragement in the work, and the officers of the Postmaster-General's Department of the Commonwealth of Australia who made the 5CL transmitter available on the nigths mentioned.

(2) S. N. MITRA: *Conference on the Physics of the Ionosphere*, Cavendish Laboratory, Cambridge (1954), pag. 7.

A proposito delle esperienze sull'interazione delle radioonde nella ionosfera.

M. Cutolo

Istituto di Fisica Tecnica dell'Università, Centro Studi di Radiopropagazione - Napoli

(ricevuto il 20 Febbraio 1955)

Nel numero di Luglio dell'anno passato di questo giornale (1), il prof. Boella ha pubblicato una lettera con lo stesso titolo, nella quale egli muove a due miei precedenti lavori (2) alcune critiche relative alla misura (ottenuta mediante lo studio della girointerazione e della autogirodemodulazione) del campo magnetico terrestre nella ionosfera e al fenomeno della autodemodulazione.

1. – Circa la prima questione, dai miei lavori risulta chiaro che non ho affatto preteso di *aver raggiunto* la 3ª e 4ª cifra decimale nella determinazione del campo; ma che ho cercato di dimostrare come il metodo della girointerazione possa permettere di « risolvere il problema del campo magnetico nello strato E, e come tale metodo sia idoneo, *qualora si adoperi una girostazione funzionante in regime impulsivo*, di fare misure precise, *con incertezza soltanto sulla 4ª cifra decimale* » (3). « Se invece si cerca di limitare, *il che è possibile*, l'errore soltanto a 1 sol cm per ciascun massimo, e cioè di 2 cm per la lunghezza d'onda media, si ha una variazione sulla 4ª cifra decimale soltanto di 1 unità, per cui l'errore in H è 1 decimillesimo » (4). Soggiungevo anche (5) che questa precisione *si potrebbe ottenere se si adoperasse* una stazione funzionante in regime impulsivo, *con una quarantina di kW* di cresta, capace, in una decina di minuti, di variare con continuità la frequenza portante intorno alla girofrequenza locale. Non abbiamo noi, invece, adoperato una stazione a onde continue di soli 3,3 kW, che variava la sua lunghezza d'onda di 5 in 5 metri, salvo intorno ai massimi dove si è cercato di variarla di metro in metro o anche meno?

Il prof. Boella, stimando che i metodi da me proposti possano raggiungere la precisione solo nella 2ª cifra decimale, conclude che « rientrano quindi nell'incertezza [per i valori di H] le differenze tra i valori calcolati con la formula di Schmidt, in base a quelli calcolati sulla superficie terrestre, e i valori dedotti dall'esperienze di girointerazione; cosicchè queste non sembra riescano a portare

(1) M. Boella: *Nuovo Cimento*, **12**, 140 (1954).

(2) M. Cutolo: *Nuovo Cimento*, **9**, 687 (1952); **10**, 915 (1953).

(3) M. Cutolo: *Nuovo Cimento*, **10**, 915 (1953).

(4) M. Cutolo: *Nuovo Cimento*, **10**, 918 (1953).

(5) M. Cutolo: *Nuovo Cimento*, **10**, 915 (1953).

TABELLA I. – *Esempi di misure di H nella ionosfera (strato E).*

Data	Valore di H_0 sulla Terra (oersted)	Valore teorico di N nella ionosfera ottenuto mediante la formula di Schmidt (oersted)	Valore sperimentale di H nella ionosfera (oersted)
3 Luglio 1949	$0{,}44770 \pm 3 \cdot 10^{-5}$	0,428	0,434
6 Luglio 1949	$0{,}44770 \pm 15 \cdot 10^{-5}$	0,428	0,431
13 Luglio 1949	$0{,}44770 \pm 55 \cdot 10^{-5}$	0,428	0,423
23 Luglio 1950	$0{,}44770 \pm 0 \cdot 10^{-5}$	0,428	0,430
17 Giugno 1950	0,4477 (*)	0,428	0,458
Febbraio 1954 (India)	0,474	0,450	0,360

(*) Non è nota l'incertezza nella 4ª e 5ª decimale.

per ora un maggior affinamento nella determinazione di H ad alta quota » (6).

Questa considerazione sarebbe giusta se non esistesse la ionosfera. Nella realtà il problema della determinazione di H, nello strato E non consiste tanto in un maggior affinamento delle misure, cioè nel raggiungere la 3ª o 4ª cifra decimale; quanto nel valutare la 2ª, se non addirittura la 1ª cifra, in quanto il valore di H in quella regione dell'atmosfera è influenzato dalle forti correnti elettriche generate dall'azione meccanica delle maree sugli elettroni e sugli ioni dello strato ionizzato che a sua volta risente dell'attività solare.

Pertanto la formula di Schmidt può tutto al più esser valida al limite inferiore della ionosfera, e non nell'interno di questa, dove le correnti producono una diminuzione del campo magnetico nel quale sono immerse; e dove quindi tutto al più essa può servire, come noi abbiamo fatto (7), per avere un primo dato *orientativo* della frequenza giromagnetica e ricavare la banda di frequenza che occorre esplorare.

La fig. 1 mette a confronto l'andamento che H ha in quota secondo la formula di Schmidt e secondo le determinazioni sperimentali eseguite mediante razzi (8). Ora, mentre nelle notti, di assoluta tranquillità ionosferica, in cui fu osservato in Italia il fenomeno di giro-interazione, le variazioni di H sulla terra erano addirittura di alcuni gamma, cioè interessavano la 5ª cifra decimale e più raramente la 4ª cifra decimale (9); nella ionosfera si avevano variazioni nette nella 2ª cifra decimale. Se poi la ionosfera non è tranquilla si hanno addirittura variazioni nella 1ª cifra decimale.

Ora potrebbe la formula di Schmidt dare variazioni nella seconda e nella prima cifra decimale se le variazioni di H sulla terra avvengono nella 5ª e più raramente nella 4ª cifra decimale?

Queste circostanze mostrano che solo

(6) M. BOELLA: *Nuovo Cimento*, **12**, 140 (1954).

(7) M. CUTOLO: *Nuovo Cimento*, **10**, 915 (1953).

(8) S. F. SINGER, E. MAPLE e W. A. BOWEN: *Nature*, **170**, 1093 (1953).

(9) Vedi i dati dell'Osservatorio Magnetico di Chambon-la-Forêt.

da fenomeni *in loco* si può ricavare il valore di H nella ionosfera: *pertanto i nostri metodi possono effettivamente recare un notevole contributo allo studio del campo magnetico terrestre nella ionosfera.* Ricor-

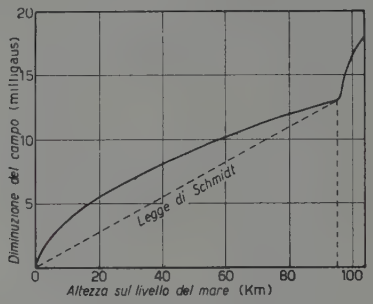

Fig. 1. – La curva piena dà l'andamento del C.M.T. secondo le teorie moderne e le misure con i razzi.

diamo che a tale proposito V. A. Bailey scrive: « Gyrointeraction may be used for measuring the magnetic field in the E-layer with sufficient precision to reveal the presence of those electric currents in the ionosphere which are postulated to account for certain terrestrial magnetic variations » ([10]).

2. – Circa poi il fenomeno dell'autodemodulazione, è facile rendere ragione del perchè la curva di risonanza possa presentarsi con due massimi simmetrici rispetto alla frequenza giromagnetica.

Il Bailey ha dimostrato infatti ([11]) che quando la frequenza di un'onda varia intorno alla girofrequenza locale, l'« indice d'interazione » (ossia l'energia ceduta agli elettroni) varia secondo una curva che può avere un massimo sulla frequenza giromagnetica oppure due massimi simmetrici rispetto ad essa. Il tipo di curva dipende dalla penetrazione dell'onda nello strato: *se la penetrazione è notevole (superiore ai* 4 km), come nel caso delle onde le cui frequenze sono comprese nella banda tra 1 000 e 1 500 Hz, l'indice d'interazione, alla quota dove ha sede il fenomeno, per l'onda la cui frequenza è uguale alla girofrequenza è piccolo, perchè l'onda di tale frequenza essendo penetrata notevolmente nello strato, ha ceduto durante il percorso gran parte della propria energia; invece per le frequenze diverse dalla girofrequenza, l'assorbimento essendo minore a parità di penetrazione, l'indice di interazione è più grande.

M. Carlevaro ha dimostrato ([12]) che sulla girofrequenza l'onda, essendo più assorbita che nelle due frequenze simmetriche, è più demodulata di queste ultime due.

I due fenomeni (girointerazione e autogirodemodulazione) sono dunque opposti, nel senso che al *minimo* relativo all'indice d'interazione sulla girofrequenza (per penetrazioni superiori ai 4 km), corrisponde un minimo della modulazione residua dell'onda e quindi un *massimo* della demodulazione, e ai *massimi* relativi dell'indice d'interazione per frequenze ugualmente discoste dalla girofrequenza, corrispondono due massimi relativi della modulazione residua e cioè *due minimi* relativi della demodulazione.

Per poter costruire una teoria dell'autogirodemodulazione occorrerebbe conoscere l'assorbimento subìto dall'onda nello strato. Ora, dall'esame dei vari diagrammi si vede che la demodulazione si aggira intorno al 40%. Una demodulazione così notevole non deve affatto sorprendere, se consideriamo che, con la stessa potenza emessa (3,3 kW) e con l'identica profondità di modulazione, radio Firenze ha impresso in precedenti esperienze dal 3 al 10% di modulazione parassita sull'onda di radio Taranto (630 m). Se si pensa che la modulazione trasferita in un'altra onda dipende dalla

([10]) V. A. Bailey, R. A. Smith, K. Landecker, A. J. Higgs e F. H. Hibberd: *Nature*, **169**, 911 (1952).

([11]) V. A. Bailey: *Phil. Mag.*, **23**, 929 (1937); **26**, 426 (1938).

([12]) M. Carlevaro: *La Ricerca*, **3-4**, 55 (1951).

frazione di energia perduta dalla seconda onda per assorbimento da parte della regione della ionosfera disturbata, si comprende che la modulazione impressa, di cui risulta affetto l'assorbimento della ionosfera, corrisponde a perdite di energia e a demodulazioni molto più importanti.

Non è escluso che l'espressione poco felice « autogirointerazione » abbia avuto qualche parte nel generare dubbi in proposito. Noi adesso preferiamo il termine di « autogirodemodulazione » appunto per sottolineare il fatto che il fenomeno non è localizzato nella regione della cross-modulation (regione di Bailey), ma interessa tutto il percorso ionosferico dell'onda, e che esso si deve al meccanismo di propagazione di un'onda media nello strato e *non al processo d'interazione propriamente detto*. Infatti le curve di risonanza dell'indice di interazione *si riferiscono all'onda disturbatrice* e *non all'onda ricercata*.

3. – A proposito dell'autodemodulazione su frequenze lontane dalla girofrequenza il prof. Boella ci muove alcune osservazioni che mi pare possano essere ridotte a questi dubbi:

a) si può escludere ogni influenza del ricevitore?

b) perchè l'autodemodulazione cresce con la frequenza di modulazione, mentre nell'interazione la modulazione parassita diminuisce con la frequenza di modulazione?

c) si possono giustificare teoricamente demodulazioni superiori al 10%?

d) la presenza del fading selettivo, specie nelle alte frequenze di modulazione, non sarebbe tanto importante da mascherare in ogni caso l'effetto di autodemodulazione?

A queste domande possiamo così rispondere.

a) Il ricevitore BC314 è stato usato soltanto due volte e solo per ricavare la curva di risonanza di fig. 1 del lavoro dell'Agosto 1952 ([13]). In quel caso la frequenza di modulazione (la medesima per tutte le frequenze portanti) era bassa (230 Hz), e pertanto la linearità del ricevitore era certamente assicurata. I diagrammi di fig. 2 dello stesso lavoro *non* sono stati ottenuti col BC314, ma con altro ricevitore, che era lineare fino a 1000 Hz ([14]). Comunque, anche per eliminare la perplessità circa l'influenza degli apparati sulle misure del campo elettromagnetico proveniente dalla ionosfera, al posto di una supereterodina abbiamo adoperato, in occasione del ciclo di esperimenti, eseguito nel Marzo 1953, su piano internazionale sotto l'egida dell'U.R.S.I. ([15]), un ricevitore del tutto lineare a circuiti accordati. Il diagramma di fig. 2, che raccoglie le misure eseguite in questa occasione, è analogo a quello di fig. 2 dell'Agosto 1952 ([16]) (salvo una maggiore estensione del campo della frequenza sperimentale).

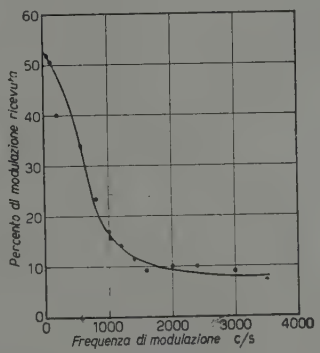

Fig. 2. – Andamento della modulazione residua in funzione della frequenza di modulazione (trasmittente Radio Parigi: 863 kHz, 60% di modulazione, 150 kW; ricezione a Napoli).

([13]) M. Cutolo: *Nuovo Cimento*, **9**, 687 (1952).

([14]) M. Cutolo: *Nuovo Cimento*, **9**, 695 (1952).

([15]) U.R.S.I.: *Bulletin d'information*, Mai-Juin, 16 (1953).

([16]) M. Cutolo: *Nuovo Cimento*, **9**, 692 (1952).

b) Nelle nostre curve, già sin dalle più basse frequenze di modulazione, la demodulazione è sensibile. Le ragioni teoriche per le quali la demodulazione aumenta con la frequenza di modulazione non sono ancora ben chiare. Comunque i nostri risultati sono confermati da quelli ottenuti in altri laboratori (come l'Istituto di Fisica Industriale di Algeri durante il ciclo internazionale ricordato [17]) e, in particolare, da S. N. Mitra in India nel Febbraio 1954 [18]) e dai fisici australiani qualche mese fa [19]).

c) Sembra assai verosimile che per l'autodemodulazione si possa raggiungere una diminuzione della profondità di modulazione maggiore del 10%. Il fatto che la modulazione parassita, impressa su di un'onda da un'altra della potenza di 150 kW (come nel nostro caso di radio Parigi), abbia raggiunto valori superiori al 10%, testimonia infatti una perdita notevole di energia, certamente maggiore di quella che ha provocato il cambiamento del coefficiente di assorbimento, dato che una parte di tutta l'energia è stata acquistata anche dagli ioni ed elettroni presenti nello strato. Inoltre ai fini della demodulazione bisogna tener conto dell'intero percorso ionosferico, laddove nel caso dell'interazione solo una parte del percorso partecipa al fenomeno. Di più, quando la ricezione è effettuata a notevole distanza dal trasmettitore, il fenomeno della demodulazione è incrementato dalle successive riflessioni tra ionosfera e terra. In conclusione il fenomeno di autodemodulazione sembra dover essere necessariamente più cospicuo della semplice interazione.

d) Non posso tacere che mi sembra assolutamente sorprendente come un fenomeno transitorio nel tempo, quale è l'evanescenza selettiva, possa essere responsabile dell'andamento della demodulazione in modo d'avere una curva tanto regolare come quella di fig. 2. Se la demodulazione fosse dovuta all'evanescenza selettiva noi dovremmo avere una curva del tutto irregolare. È evidente infatti che cotesta evanescenza, dipendendo da interferenza di fasci che hanno percorso cammini molto diversi, è necessariamente accompagnata da distorsione della forma dell'onda, causa i continui mutamenti di fase che hanno luogo per variazioni di densità elettronica della ionosfera e deformazioni dello strato riflettente (o degli strati riflettenti, se, come sembra, la riflessione avviene anche nello strato *F*). *Ora le nostre misure sono sempre state eseguite quando l'inviluppo d'onda era visibilmente sinusoidale e perciò in assenza di fading.* Infine altri recenti esperimenti, che presto pubblicheremo, nei quali sono state prese le fotografie delle curve inviluppo d'onda, ci confermano nella convinzione di poter escludere il fading selettivo come responsabile della riscontrata demodulazione.

Come noto, nell'interazione il fading si manifesta nel senso che la sua influenza aumenta, più che diminuire, il percento di modulazione parassita. Ora se la curva della fig. 2 fosse la conseguenza del fading selettivo, non vediamo ragione perchè questo non dovrebbe influenzare anche l'andamento dell'effetto Tellegen, considerato in funzione della frequenza di modulazione. Al contrario la modulazione parassita decresce con la frequenza di modulazione ed ha un andamento che è giustificato qualitativamente e quantitativamente dalla teoria dell'effetto Tellegen.

Ad accentuare la nostra diffidenza circa una marcata influenza del fading selettivo sulla demodulazione, stanno anche gli esperimenti compiuti da S. R. Khastgir e P. M. Das dal 1948 al

[17]) U.R.S.I.: *Bulletin d'information*, Mai-Juin, 16 (1953).

[18]) S. N. Mitra: *Riassunti della Conferenza sulla fisica della ionosfera*, Physical Society (6-9 Settembre 1954).

[19]) G. J. Aitchison e G. L. Goodwin: *Nuovo Cimento*, 1, 722 (1955).

1949 ([20]). Durante alcune trasmissioni effettuate nelle prime ore della notte da Calcutta su 4 840 kHz e ricevute a Dacca (240 km di distanza) con la sola portante, con una frequenza di modulazione fissa *e con il consueto programma radiofonico*, fu notato infatti che le fluttuazioni del campo ricevute presentavano nei tre casi quasi lo stesso andamento sia per quello che riguarda l'ampiezza sia per il periodo. Ciò dimostra che almeno in quel caso il fading *non aveva caratteristiche di selettività*. Durante la seduta del 17 Febbraio 1954 a Torino della Commissione 3-*b* dell'U.R.S.I., feci rilevare che in condizioni di ionosfera tranquilla il fenomeno di autodemodulazione non è affatto mascherato dal fading selettivo, perchè questo si presenta solo ad intervalli di tempo. In conclusione, mentre le notevoli variazioni del percento di modulazione (sopramodulazione o quasi scomparsa della modulazione) sono da attribuirsi forse al fading selettivo e si presentano spesso solo a tratti, le piccole fluttuazioni intorno al valore medio del per cento di modulazione (fig. 3) sono da attribuirsi al maggiore o minore assorbimento dei picchi di modulazione in funzione della variazione della densità elettronica. Queste piccole fluttuazioni continue del grado di modulazione dell'onda sono pertanto un'altra conferma dell'esistenza dell'effetto di autodemodulazione.

Se il fading selettivo fosse continuamente presente, tutte le misure ionosferiche dovrebbero essere inficiate in quanto da esso continuamente influenzate o mascherate.

Ora dall'esame delle grafiche di fig. 3 e di altre analoghe costruite a Napoli e ad Algeri si vede chiaramente come sia possibile, specialmente nelle notti in cui la ionosfera non è agitata, fare le medie dei valori osservati per ciascuna frequenza di modulazione, perchè nella maggior parte dei casi i valori differiscono assai poco tra loro. Ciò si osserva anche nelle registrazioni effettuate a Milano dove è stato possibile, alle volte, fare addirittura 300 misure per ciascuna fre-

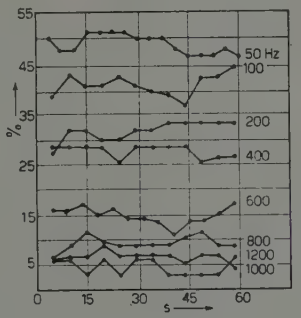

Fig. 3. – Il diagramma dà i percento di modulazione ricevuti a Napoli con segnali provenienti da Radio Parigi (863 kHz, 60 % di modulazione, 150 kW) alle diverse frequenze di modulazione indicate a fianco di ciascuna curva in funzione del tempo di osservazione (in secondi). Risulta evidente che per ciascuna frequenza di modulazione le fluttuazioni della modulazione residua si mantengono piccole ed inoltre le curve non si sovrappongono. Il calcolo della media per ciascuna auto-frequenza appare pertanto giustificato.

quenza di modulazione. L'osservazione dei diagrammi in fig. 2 mostra che la forma della curva è la stessa di quella della modulazione parassita-frequenza di modulazione dell'effetto Lussemburgo, ma l'andamento del fenomeno è l'opposto. Questo fatto concorderebbe con quanto abbiamo visto sopra e cioè che l'andamento dell'autogirodemodulazione si presenta in qualche modo opposto a quello della girointerazione. Prendendo lo spunto proprio da questa osservazione non sarà difficile trovare il bandolo della matassa e comprendere il meccanismo del fenomeno.

4. – A convalidare ulteriormente i risultati da me ottenuti e comunicati nelle note precedenti mi piace ricordare anche quanto segue.

a) Durante la conferenza di Cambridge in Inghilterra, sulla Fisica della

([20]) S. R. Kastgir e P. M. Das: *Proc. Roy. Soc.*, (B) 1° novembre, 924 e 928, fig. 2 e 3 (1950).

ionosfera (6-9 Settembre 1954), S. N. MITRA ha comunicato di aver eseguito in India una serie di esperienze che gli hanno permesso di confermare l'effetto di autogirodemodulazione: « 14 trasmettitori coprenti la banda di frequenze da 590 a 1490 kHz irradiarono un tono di 1000 Hz con un percento fisso dell'80%. Il percento di modulazione del segnale ricevuto proveniente da tutti i trasmettitori fu misurato a Dehli. La curva del percento di modulazione ricevuta in funzione della frequenza dell'onda mostra un significativo abbassamento a 1020 kHz, dove la modulazione era del 48%. La girofrequenza nello strato E è pertanto di 1020 kHz, per cui il valore di H nello strato E è di 0,36 Γ essendo il corrispondente valore sulla superficie terrestre di 0,474 Γ'' ([21]). Le esperienze di MITRA, oltre a confermare l'effetto di risonanza dovuto al campo magnetico terrestre mostrano: primo, che il percento della demodulazione è identico a quello da me misurato nel 1950 e 1951 ([22]); secondo, che esso è molto superiore all'1%, e che infine il fenomeno non scompare affatto per frequenze intorno a 1000 Hz. E poichè i cammini dei fasci elettromagnetici erano differenti causa la diversa ubicazione dei trasmettitori, e la curva di demodulazione è regolare, si conclude anche che *il fenomeno non dipende affatto dal fading selettivo.*

b) Molti mesi prima della pubblicazione della lettera del prof. BOELLA, il fisico russo I. M. VILENSKII ha pubblicato una memoria con la quale ha dimostrato matematicamente come « la considerazione della non linearità permette di prevedere non solo cambiamenti dell'ampiezza e della fase dell'onda, ma anche cambiamenti della profondità di modulazione di ampiezza, la produzione di armoniche superiori 2ω e 3ω della modulazione di ampiezza ω e l'apparizione di una modulazione di fase. Come mostrano le valutazioni numeriche, il cambiamento della profondità di modulazione del tono fondamentale e la grandezza delle armoniche della modulazione di ampiezza possono essere importanti » ([23]).

Ora le formule del Vilenskii dicono che *alle bassissime frequenze di modulazione e per frequenze portanti lontane dalla girofrequenza locale, il percento di demodulazione può arrivare persino al* 23%. Pertanto i nostri risultati sperimentali, che danno alle basse frequenze demodulazioni del 10%, possono giustificarsi teoricamente partendo dalla considerazione della non linearità della ionosfera, laddove per queste frequenze nessuna influenza del fading selettivo può essere chiamata in causa.

c) Un metodo escogitato recentemente dai fisici australiani ([19]) ha permesso di eliminare completamente l'influenza del fading selettivo per cui gli autori hanno potuto chiaramente dimostrare come il fenomeno dell'autodemodulazione effettivamente esiste ed è notevole, ovvero non è prodotto dal fading selettivo.

* * *

Da quanto sopra ho riferito mi sembra scaturire come le critiche e le osservazioni del prof. BOELLA non risultino giustificate, almeno per quel che riguarda le nostre esperienze.

([21]) S. N. MITRA: vedi ([18]).

([22]) M. CUTOLO: *Nature*, 24 Febbraio (1951); *Nuovo Cimento*, **9**, 687 (1952).

([23]) I. M. VILENKII: *Dokl. Akad. Nauk SSSR*, **92**, 515-528 (1953).

A Search for Angular Correlations in τ-Meson Decay.

M. Teucher, W. Thirring and H. Winzeler

Berne

(ricevuto il 27 Febbraio 1955)

A determination of the spin of the τ-meson has been attempted by looking at the energy-distribution of the unlike π-meson, emitted in the disintegration of τ's [1-3].

However, if the τ-meson has a spin > 0, the τ can be polarized, the kind of polarization being determined by the process of emission [4]. The slowing down of the τ does not remove this polarization unless the τ has a high anomalous magnetic moment [4,5]. This suggests looking at the distribution of the angles between the plane of decay of the τ's and the direction of emission of the τ's from the parent stars. If such a distribution is not isotropic, this would prove simultaneously that the τ's have spin > 0 and that a certain kind of polarization is preferred in the process of emission. On the other hand an isotropic distribution will leave in doubt whether the spin is zero or the τ is unpolarized.

Till now we have investigated 9 τ-mesons in nuclear emulsions. 6 of them were produced in a nuclear interaction inside a stack of stripped emulsions. For these 6 we could measure with good accuracy the angle γ between the direction of emission and the normal n to the plane of decay, naturally corrected for the shrinkage of the emulsions. For the other 3 τ's we measured γ taking the direction of entrance into the stack as the direction of emission. This should be a good approximation for events τ_5 and τ_6 which had a long residual range at the point of entrance. τ_4, however, was observed in ordinary photographic plates and had a small energy. In this case the angle measured can be quite different from the true γ. Table I gives the ranges and the energies of the 9 τ's, calculated with Gottsteins table [6].

Fig. 1 gives the histogram in terms of γ for the 9 events. If the distribution were isotropic, one half of the events should have a $\gamma > 60^\circ$. If the distribution is $\sim \sin^2 \gamma \mathrm{d}(\cos \gamma)$ one should ob-

(1) R. H. Dalitz: *Phil. Mag.*, **44**, 1068 (1953).
(2) E. Fabri: *Nuovo Cimento*, **11**, 479 (1954).
(3) E. Amaldi, G. Baroni, G. Cortini, C. Franzinetti and A. Manfredini: *Suppl. Nuovo Cimento*, **12**, 186 (1954).
(4) G. Wentzel: *Helv. Phys. Acta*, **22**, 101 (1949).
(5) E. Heiberg, U. Kruse, J. Marshall, L. Marshall and F. Solmitz: *Phys. Rev.*, **97**, 52 (1955).
(6) H. Fay, K. Gottstein and K. Hain: *Suppl. Nuovo Cimento*, **11**, 234 (1954).

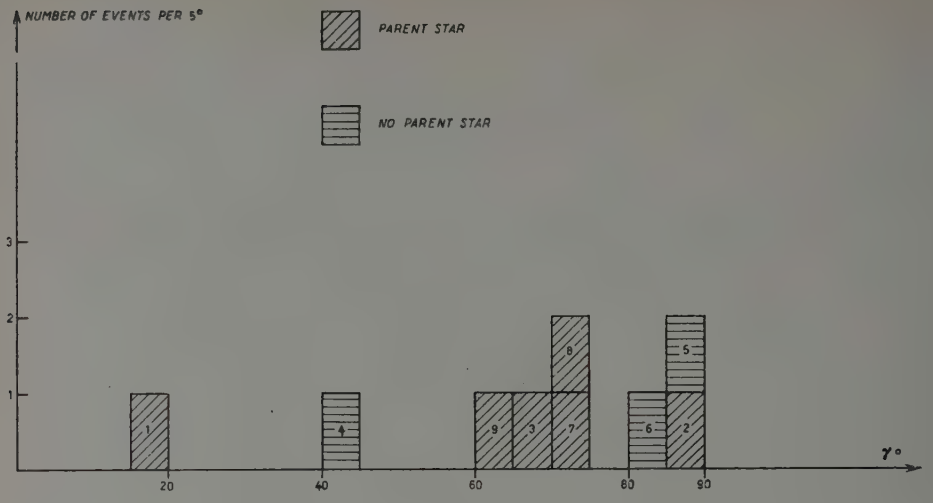

Fig. 1.

TABLE I.

Event	Range (mm)	Energy (MeV)	γ^0
Be_1	22,39	62.8	17,5
Be_2	7.61	34.0	88.5
Be_3	8.80	36.9	66.5
Be_4	$\geqslant$ 0,78	$\geqslant$ 9.3	42
Be_5	$\geqslant$ 16.03	$\geqslant$ 52.0	90
Be_6	$\geqslant$ 19,08	$\geqslant$ 57.4	81
Be_7	0.93	10.3	70.5
Be_8	3.66	22.4	75
Be_9	13.29	46.7	64.5

serve 68.7% above 60°. We have 7 events amongst 9 with $\gamma > 60°$. The agreement with a $\sin^2\gamma$-distribution is better than with an isotropic one. However we can not exclude in this poor statistics that the distribution is isotropic.

It should be possible to get a more significant information about the distribution of the angle γ with all the τ-mesons actually known, but till now this information is not generally included in the data published on τ-mesons. It could also be useful to look at the angle between the emission of the τ and the unlike π.

We must not forget that in the scanning may be a tendency to miss τ-events with small γ. The importance of such a bias could be checked in analysing the distribution of directions of flight and orientation of planes of decay respectively versus the plane of the emulsion.

A detailed description of all our τ-mesons will be given later in *Helvetica Physica Acta*.

All these τ's were found in plates flown by the Sardinia Expedition 1953.

We thank Professors F. G. HOUTERMANS and CH. PEYROU for their helpful interest in this investigation. Six of the τ's were found by Mrs. B. ALBRECHT. The others by Mrss. MÜLLER, RIESEN and THIRRING. This work was supported by the « Schweizer Nationalfonds ».

IL NUOVO CIMENTO Vol. I, N. 4 1° Aprile 1955

Least Squares Curvature in Non-Uniform Magnetic Field.

R. W. Thompson

Department of Physics, Indiana University - Bloomington, Indiana

(ricevuto il 28 Febbraio 1955)

The determination of momentum by measurement of curvature in the magnetic cloud chamber is often carried out in magnetic fields which are appreciably non-uniform. In practice, the momentum is calculated from a relation of form $p = 300 H_a \varrho_a$, where H_a is some average value of the field along the track and ϱ_a is some average value of the radius of curvature. It is clear that the averaging process

$$H_a = \int w(x) H(x) \, \mathrm{d}x ,$$

of which H_a is the result will be expected to depend on the method by which ϱ_a is evaluated. The object of this note is to derive the appropriate weight function $w(x)$ when the curvatures are reduced by the method of least squares. The use and advantages of the least squares method in the reduction of curvatures have been discussed by Thompson *et al.* [1], and the method has also been used by the Manchester group [2] and the Berkeley group [3].

Let y_i be measured at various points x_i along the track. We define the least squares radius of curvature ϱ_a by the equation

$$\varrho_a = \frac{1}{2c} ,$$

where c is derived from least squares adjustment of a parabola

$$y = a + bx + cx^2 , \tag{1}$$

(*) Assisted by the Office of Ordnance Research and by grant of the Frederick Gardner Cottrell Fund of the Research Corporation.

(1) R. W. Thompson, A. V. Buskirk, H. O. Cohn and C. J. Karzmark: *Proceedings of the Bagnères Congress*, Paper No. A. 3, (1953).

(2) K. H. Barker: *Suppl. Nuovo Cimento*, 11, 309 (1954).

(3) W. B. Fretter: private communication.

to the measured points (x_i, y_i). Thus,

$$c = \frac{1}{\Delta}\begin{vmatrix} n & \sum x_i & \sum y_i \\ \sum x_i & \sum x_i^2 & \sum y_i x_i \\ \sum x_i^2 & \sum x_i^3 & \sum y_i x_i^2 \end{vmatrix}, \tag{2}$$

where

$$\Delta = \begin{vmatrix} n & \sum x_i & \sum x_i^2 \\ \sum x_i & \sum x_i^2 & \sum x_i^3 \\ \sum x_i^2 & \sum x_i^3 & \sum x_i^4 \end{vmatrix}.$$

In view of the amount of computation involved, the use of least squares would certainly not appear to be justified in this application. Fortunately, the labor is reduced to negligible proportions if the values of x_i are equally spaced and odd in number: $x_i = i$ (an integer) $= -m, \ldots, 0, \ldots, +m$. In this case, $\sum x_i = \sum x_i^3 = 0$. If $y_0 = 0$, eq. (2) thus reduces to

$$c = \frac{(2m+1)}{\delta_{33}} \sum_{1}^{m} \left(i^2 - \frac{m(m+1)}{3} \right) (y_{+i} + y_{-i}), \tag{3}$$

where

$$\delta_{33} = (2m+1) \sum_{-m}^{+m} i^4 - \left(\sum_{-m}^{+m} i^2 \right)^2.$$

The values of δ_{33} and $\sum i^2$ for m up to 20 are tabulated in Table I.

TABLE I. — δ_{33} *and* $\sum i^2$.

m	$\sum_{-m}^{+m} i^2$	δ_{33}	m	$\sum_{-m}^{+m} i^2$	δ_{33}
1	2	2	11	1 012	814 660
2	10	70	12	1 300	1 345 500
3	28	588	13	1 638	2 137 590
4	60	2 772	14	2 030	3 284 946
5	110	9 438	15	2 480	4 904 944
6	182	26 026	16	2 992	7 141 904
7	280	61 880	17	3 570	10 170 930
8	408	131 784	18	4 218	14 202 006
9	570	257 754	19	4 940	19 484 348
10	770	471 086	20	5 740	26 311 012

If the curvature is small, as implied by eq. (1), the trajectory of the particle can be represented by the equation

$$\frac{d^2y}{dx^2} = \frac{300}{p} H(x),$$

where p is the momentum and $H(x)$ is the magnetic field along the track. Integration to obtain the displacement y_i at the various measured points i gives ($y_0' = 0$)

$$(4) \qquad (y_{+i} + y_{-i}) = \frac{300}{p} \int_{\xi'=0}^{i} \mathrm{d}\xi' \int_{\xi=0}^{\xi'} \left[H(\xi) + H(-\xi) \right] \mathrm{d}\xi \, .$$

Denote

$$(5) \qquad \begin{cases} 2\overline{H}_j \equiv \int_{j-1}^{j} \left[H(\xi) + H(-\xi) \right] \mathrm{d}\xi \, , \\ 2\overline{H}_j \overline{\xi}_j \equiv \int_{j-1}^{j} \left[H(\xi) + H(-\xi) \right] \xi \, \mathrm{d}\xi \, , \end{cases}$$

where $\overline{H}_j$ is the mean value and $\overline{\xi}_j$ is the centroid of the field in the j-th interval. Then, if the momentum p is to be calculated from the equation $p = 300 H_a \varrho_a$, it follows from eqs. (3), (4) and (5), that

$$H_a = \frac{4(2m+1)}{\delta_{33}} \sum_{i=1}^{m} \sum_{j=1}^{i} \left(i^2 - \frac{m(m+1)}{3} \right) (i - \overline{\xi}_j) \overline{H}_j \, .$$

On summation over i we find

$$(6) \qquad H_a = \frac{15m(m+1)}{(2m-1)(2m+1)(2m+3)} \sum_{j=1}^{m} \left[1 - \frac{j(j-1)}{m(m+1)} \right] \cdot \left[1 - \frac{j(j-1) + 1 + 2(2j-1)(\overline{\xi}_j - j + \frac{1}{2})}{m(m+1)} \right] \overline{H}_j \, .$$

If the variation of the field over the j-th interval is small, we can take $\overline{\xi}_j \simeq j - \frac{1}{2}$, in which approximation eq. (6) can be written

$$H_a = \sum_{j=1}^{m} w(m, j) \overline{H}_j \, ,$$

where

$$(7) \qquad w(m, j) = \frac{15m(m+1)}{(2m-1)(2m+1)(2m+3)} \left[1 - \frac{j(j-1)}{m(m+1)} \right] \left[1 - \frac{j(j-1) + 1}{m(m+1)} \right] .$$

It is readily verified that

$$\sum_{j=1}^{m} w(m, j) = 1 \, .$$

In order to show that the error resulting from the approximation $\overline{\xi}_j \simeq j - \frac{1}{2}$ is small, assume that $[H(\xi) + H(-\xi)]$ increases linearly by 10% from $(j-1)$ to j,

For $m = 1$, eq. (7) gives $H_a = \overline{H}_1$; whereas eq. (6) gives $H_a = (62/63)H_1$. For $m = 2$, eq. (7) gives

$$H_a = \frac{1}{441}(315\overline{H}_1 + 126H_2),$$

whereas eq. (6) gives

$$H_a = \frac{1}{441}(314H_1 + 124\overline{H}_2). \tag{8}$$

For larger m, or less variation per interval, the error is even less. Note that the sum of the coefficients in eq. (8) is not equal to unity.

TABLE II. – *The Normalized Weights* $w(m, j)$.

j	m									
	1	2	3	4	5	6	7	8	9	10
1	1.00	0.71	0.52	0.41	0.34	0.29	0.25	0.22	0.20	0.18
2	—	0.29	0.36	0.33	0.29	0.26	0.23	0.21	0.19	0.17
3	—	—	0.12	0.20	0.21	0.21	0.20	0.19	0.17	0.16
4	—	—	—	0.06	0.12	0.14	0.15	0.15	0.15	0.14
5	—	—	—	—	0.04	0.08	0.10	0.11	0.12	0.12
6	—	—	—	—	—	0.02	0.05	0.07	0.09	0.09
7	—	—	—	—	—	—	0.02	0.04	0.05	0.07
8	—	—	—	—	—	—	—	0.01	0.02	0.04
9	—	—	—	—	—	—	—	—	0.01	0.02
10	—	—	—	—	—	—	—	—	—	0.01

The normalized weights $w(m, j)$ from eq. (7) are given to two decimal places for m up to 10 in Table II. In practice, it may often suffice to derive the relative weights from the relation $w(x) \sim [1 - (x/m)^2]^2$, where m is the half-track length.

IL NUOVO CIMENTO Vol. I, N. 4 1° Aprile 1955

S and P Wave Analysis of Proton-Proton Scattering Experiments.

L. Beretta, E. Clementel and C. Villi

Istituti di Fisica dell'Università di Padova e di Trieste
Istituto Nazionale di Fisica Nucleare - Sezione di Padova

(ricevuto il 5 Marzo 1955)

Recently, using consistently the hypothesis of charge independence of nuclear forces, high energy p-p and n-p scattering data have been satisfactorily fitted without D-waves [1]. The method employed allows the determination of certain combinations of the triplet P state phase shifts $\delta_J (J=0, 1, 2)$, whereas the singlet S state phase shift is evaluated in first Born approximation assuming a meson potential well.

However, detailed information either on the phase ${}^1K_0$ or δ_J can be obtained entirely from experimental data taking into account Coulomb interference at small angles and without any preconceived nuclear potential.

In the following we shall outline a way of approach which gives a clear insight in the phase shift mechanism in fitting the experimental data, and which was found suitable also for scattering analysis at intermediate energies, where the angular dependence of the nuclear term in the proton-proton cross-section cannot be neglected.

While this work was in progress, the idea of using Coulomb interference to get nuclear phase shifts has been suggested also by Garren [2], but the procedure he employes is somewhat different and so far applied to high energies, where the analysis in terms of S and P waves only is questionable [3].

We call $z_1(k)$ and $z_2(k)$ the phase shift combinations indicated by α and β in reference [1], $z_3(k) = \sin({}^1K_0)\cos({}^1K_0)$ and $z_4(k) = f(\delta_0, \delta_1, \delta_2)$ the coefficient of $P_2(\cos\vartheta)$. Unless otherwise stated, all other symbols correspond to those used in the above quoted paper.

The Breit-Kittel-Thaxton formula of the proton-proton cross-section, valid for a non central potential, gives at $\vartheta = \pi/2$

$$(1) \quad \sin^2({}^1K_0) = [1 - 2\eta \sin(\eta \log 2)]^{-1}\left[\mathbf{A}P(\pi/2) - z_1(k) + 2\eta \cos(\eta \log 2)\, z_3(k) + \tfrac{1}{2} z_4(k)\right]$$

[1] R. M. Thaler and J. Bengston: *Phys. Rev.*, **94**, 679 (1954).
[2] A. Garren: *Phys. Rev.*, **96**, 1709 (1954).
[3] B. D. Fried: *Phys. Rev.*, **95**, 851 (1954).

where

$$\Delta \boldsymbol{P}(\vartheta) = k^2[\boldsymbol{P}(\vartheta) - P_M(\vartheta)] . \tag{2}$$

From the p-p cross-section, separating the terms independent from $z_i(k)$, we get

$$\Phi_{pp}(k, \vartheta) \equiv \Delta \boldsymbol{P}(\vartheta) - \Delta \boldsymbol{P}(\pi/2)[1+(\eta/2)\boldsymbol{Y}_0(\vartheta)][1 - 2\eta \sin(\eta \log 2)]^{-1} = \sum_{i=1}^{4} a_i(k, \vartheta) z_i(k) , \tag{3}$$

where

$$a_1(k, \vartheta) = 1+(\eta/2)\boldsymbol{Y}_1(\vartheta)P_1(\cos\vartheta) - [1+(\eta/2)\boldsymbol{Y}_0(\vartheta)][1 - 2\eta \sin(\eta \log 2)]^{-1} , \tag{4}$$

$$a_2(k, \vartheta) = 2\eta \cos(\eta \log 2)[1+(\eta/2)\boldsymbol{Y}_0(\vartheta)][1 - 2\eta \sin(\eta \log 2)]^{-1} - (\eta/2)\boldsymbol{X}_0(\vartheta) , \tag{5}$$

$$a_3(k, \vartheta) = -(\eta/2)\boldsymbol{X}_1(\vartheta)P_1(\cos\vartheta) , \tag{6}$$

$$a_4(k, \vartheta) = P_2(\cos\vartheta) + \tfrac{1}{2}[1+(\eta/2)\boldsymbol{Y}_0(\vartheta)][1 - 2\eta \sin(\eta \log 2)]^{-1} . \tag{7}$$

Since to the approximation of 0.1% $a_2(k, \vartheta) \simeq a_3(k, \vartheta)$, the determination of the unknown quantities $z_i(k)$ directly from Eq. (3) by fitting the experimental data at small angles, where the Coulomb interference is sensible, becomes difficult. In particular, for intermediate energies ($\eta \gtrsim 0.015$), this procedure would lead to unreliable results, unless the experimental cross-sections were known with exceedingly high accuracy.

To overcome this difficulty we determine from Eq. (1) the quantity $(\frac{1}{2})z_4(k) - z_1(k)$ as a function of ${}^1K_0$. Then we write down Eq. (3) for two angles ϑ_1 and ϑ_2, and we determine all $z_i(k)$ as functions of ${}^1K_0$. It follows that the proton-proton cross-section, for a given energy and at a given angle, *depends on* ${}^1K_0$ *only*. Finally, by choosing a third angle ϑ_3, the S-wave phase shift ${}^1K_0$ is determined by solving the equation $\boldsymbol{P}({}^1K_0, \vartheta_3) = \boldsymbol{P}_{\exp}(\vartheta_3)$. Once ${}^1K_0$ is known, all $z_i(k)$ are also determined. As a check, the same procedure can be applied to a fourth angle, to esthablish if the value of the cross-section corresponds, within quoted experimental errors, to the previously determined S-wave phase shift. The quantity $(\frac{1}{2})z_4(k) - z_1(k)$ depends on ${}^1K_0$ through a fourth degree equation, and therefore the total number of sets $[{}^1K_0, z_i(k)]$, for a given energy, is four. Selection among these sets is provided by the best fit over all angles with the experimental cross-section. The more accurate the experimental data, the more strict is the discrimination of the set reproducing correctly the essential features of the cross-section. In general, the constructive or destructive interference between nuclear and coulomb terms is decisive in selecting the sign of ${}^1K_0$.

Once the set $[{}^1K_0, z_i(k)]$ is selected, we express $\sin\delta_0 = x$ and $\sin\delta_1 = y$ as a function of δ_2 by means of the following equations

$$x^2_{\pm}(\delta_2) = \frac{\beta^2 - \gamma(2-\alpha) \pm \beta[\beta^2 - \gamma(4+\gamma-2\alpha)]^{\frac{1}{2}}}{2(2-\alpha)^2 + 2\beta^2} , \tag{8}$$

$$y^2_{\pm}(\delta_2) = \tfrac{1}{3}(\alpha - x^2_{\pm}) , \tag{9}$$

where

$$\alpha(\delta_2) = z_1(k) - 5\sin^2\delta_2 , \quad \beta(\delta_2) = z_2(k) - 5\sin\delta_2\cos\delta_2 , \quad \gamma(\delta_2) = \alpha^2 + \beta^2 - 3\alpha . \tag{10}$$

The pairs $x_{\pm}(\delta_2)$ and $y_{\pm}(\delta_2)$ are then selected taking account of the equation $z_4(k) = f(\delta_0, \delta_1, \delta_2)$.

As an example of more extensive calculations which will be published later, we discuss p-p scattering at 18 MeV. The following partial analysis is based on the experimental data of YNTEMA and WHITE (4).

The variation of the S-wave phase shift ${}^1K_0$ is limited within the interval $19^\circ \leqslant {}^1K_0 \leqslant 52.5^\circ$. Correspondingly it is found $-0.2148 \leqslant z_1 \leqslant 0.3431$, $0.0224 \leqslant z_2 \leqslant 0.5464$ and $0.1717 \leqslant z_4 \leqslant 0.3926$. These figures have been obtained assuming $\vartheta_1 = 30^\circ$ [$\boldsymbol{P}(30^\circ) = 25$ mb] and $\vartheta_2 = 40^\circ$ [$\boldsymbol{P}(40^\circ) = 26.60$ mb]. Taking now the angle $\vartheta_3 = 60^\circ$, we find that the p-p cross-section as a function of ${}^1K_0$ varies in the interval $22.22 \text{ mb} \leqslant \boldsymbol{P}({}^1K_0, 60^\circ) \leqslant 36{,}69$ mb, and the equation $\boldsymbol{P}({}^1K_0; 60^\circ) = \boldsymbol{P}_{\text{exp}}(60^\circ) = 27.37$ mb is satisfied for ${}^1K_0 = 43.7^\circ$. It follows that $z_1 = 0.0378$, $z_2 = 0.1678$ and $z_4 = 0.1697$. Since $\alpha(\delta_2) > 0$, the phase shift δ_2 is defined within the interval $-10.7^\circ \leqslant \delta_2 \leqslant 10.7^\circ$. A further reduction of this interval is provided by the condition $\beta^2 \leqslant \gamma(4 + \gamma - 2\alpha)$, which insures that the phase shifts are all real. It is found that the possible solutions correspond to δ_2 varying within the interval $-5.7^\circ \leqslant \delta_2 \leqslant 8.3^\circ$.

Incompatible with the equation $z_4(k) = f(\delta_0, \delta_1, \delta_2)$ were found the following sets: $[\delta_2 < 0,\ x_{\pm} < 0,\ y_{\pm} > 0]$, $[\delta_2 < 0,\ x_+ \lesssim 0,\ y_+ \lesssim 0]$, $[\delta_2 > 0,\ x_- < 0,\ y_- < 0]$ and $[\delta_2 < 0,\ x_- > 0,\ y_- > 0]$.

Taking mean values of solutions which differ from each other by less than 1% for ${}^1K_0 = 43.7^\circ$, we find the following values for the phase shifts δ_J:

(a) $\delta_0 = 19.4^\circ$, $\delta_1 = -7.4^\circ$, $\delta_2 = 2{,}75^\circ$;

(b) $\delta_0 = -14.6^\circ$, $\delta_1 = 10.5^\circ$, $\delta_2 = -1.5^\circ$;

(c) $\delta_0 = 24.1^\circ$, $\delta_1 = -4.3^\circ$, $\delta_2 = -1.1^\circ$.

The cross-section at $\vartheta = 90^\circ$ has the value 27.37 mb, the plateau is reached at $\vartheta = 60^\circ$, the dip occurs at $\vartheta = 27^\circ$ [$\boldsymbol{P}(27^\circ) = 24.95$ mb]. The value of the cross-section at $\vartheta = 20^\circ$, where at the present no experimental data are available, appears to be 28.3 mb.

According to this analysis it is seen that the nuclear term of the p-p cross-section shows a sensible angular dependence, which was found essential to determine the plateau. An attempt has also been made to consider $\boldsymbol{P}_{\text{NUC}}$ angle independent, i.e. $z_4 = 0$. In this case we found ${}^1K_0 = 50.5^\circ$, $z_1 = 0.0257$ and $z_2 = -0.0447$. Correspondingly, the following sets were determined:

(a) $\delta_0 = 3.3^\circ$, $\delta_1 = -4.3^\circ$, $\delta_2 = 1.5^\circ$;

(b) $\delta_0 = -4.8^\circ$, $\delta_1 = 3.6^\circ$, $\delta_2 = 1.9^\circ$;

(c) $\delta_0 = 6.3^\circ$, $\delta_1 = -3.2^\circ$, $\delta_2 = 0.25^\circ$.

As a consequence of the assumption $z_4 = 0$, the calculated cross-section was not found flat definite, within quoted experimental errors, between $\vartheta = 60^\circ$ and $\vartheta = 90^\circ$.

(4) J. L. YNTEMA and M. G. WHITE: *Phys. Rev.*, **95**, 1226 (1954).

Sull'introduzione di un intervallo di tempo fondamentale nella teoria dell'elettrone.

P. Caldirola

Istituto di Scienze Fisiche dell'Università - Milano
Istituto Nazionale di Fisica Nucleare - Sezione di Milano

(ricevuto il 5 Marzo 1955)

Nella teoria classica dell'elettrone da noi proposta [1] l'equazione del moto

$$\frac{m_0}{\tau_0}\left[u_\alpha(\tau)-u_\alpha(\tau-\tau_0)+\frac{u_\alpha(\tau)\,u_\beta(\tau)}{c^2}\,u_\beta(\tau-\tau_0)\right]=\frac{e}{c}\,F_{\alpha\beta}u_\beta(\tau)$$

viene stabilita partendo dall'assunzione che il moto « macroscopico » dell'elettrone può essere definito solo in una successione discreta di istanti separati l'un l'altro da un intervallo fondamentale τ_0 di valore

$$\tau_0=\frac{4}{3}\,\frac{e^2}{m_0c^3}\,. \tag{1}$$

Vogliamo ora mostrare, per mezzo del principio di indeterminazione di Heisenberg, come la considerazione di un siffatto intervallo abbia un significato notevole anche in campo quantistico.

Ricordiamo che se si vuol determinare a un istante τ l'energia E di una particella di massa m_0; le grandezze τ e E sono conoscibili solo con la limitazione imposta dalla relazione di indeterminazione

$$\Delta\tau\cdot\Delta E\geqslant\hbar\,. \tag{2}$$

In particolare la conoscenza sempre più esatta della grandezza τ (onde $\Delta\tau\to 0$) comporta un'incertezza sempre maggiore sul valore della grandezza E (onde $\Delta E\to\infty$). Ciò vuol dire che il procedimento di misura attribuisce alla particella un moto incontrollabile di fluttuazione cui compete un'energia tanto più elevata quanto più rapida è l'operazione di misura.

Se si suppone che possano esistere stati interni « eccitati » della particella caratterizzati da valori della massa più elevati di quella m_0 che compete alla particella ordinaria (vale a dire nel suo stato interno fondamentale), avremo che la locuzione « particella di massa m_0 » avrà un significato abbastanza preciso solo finchè ΔE è minore della differenza fra l'energia intrinseca μ_0c^2 che compete al primo stato eccitato della particella e quella m_0c^2 del suo stato fondamentale; vale a dire finchè $\Delta E\leqslant(\mu_0-m_0)c^2$ [2].

[1] P. Caldirola: *Nuovo Cimento*, **10**, 1747 (1953); P. Caldirola e F. Duimio: *Nuovo Cimento*, **12**, 699 (1954); R. Cirelli: *Nuovo Cimento*, **1**, 260 (1955); P. Caldirola: *Nuovo Cimento*, **1**, 269 (1955); **1**, 347 (1955).

[2] La legittimità di applicare le relazioni di indeterminazione nel modo qui seguito dovrebbe a tutto rigore essere giustificata da una preci-

Dalla (2) deriva allora che l'istante di osservazione della particella dovrà soffrire di una incertezza:

$$\Delta\tau \geqslant \frac{\hbar}{(\mu_0 - m_0)c^2} . \tag{3}$$

Supponendo, come da qualcuno [3] è stato suggerito, che il mesone μ possa considerarsi come il primo stato eccitato dell'elettrone e osservando che per la sua massa si ha:

$$(\mu_0 - m_0)c^2 \cong 206 m_0 c^2 \simeq \frac{3}{2}\frac{\hbar c}{e^2} m_0 c^2 ,$$

sostituendo nella (3) si ottiene:

$$\Delta\tau \geqslant \frac{2}{3}\frac{e^2}{m_0 c^3} . \tag{4}$$

In altri termini, il valore della massa a riposo m_0 di un elettrone non può essere dato ad un istante esatto ma solo entro un intervallo temporale

$$\Delta\tau \cong \frac{2}{3}\frac{e^2}{m_0 c^3} .$$

È interessante notare come questa limitazione, pur essendo stata dedotta dalla relazione di indeterminazione di Heisenberg fondamentale della teoria quantistica, non contenga la costante di Planck [4].

Osserviamo ancora che, volendo seguire un elettrone (di massa definita m_0) nel suo moto, come conseguenza di quanto precede avrà significato solo la considerazione di due istanti successivi τ_1 e τ_2, ciascuno assegnabile con l'incertezza (4) e quindi tali che:

$$\tau_2 - \tau_1 \cong 2\,\Delta\tau \simeq \frac{4}{3}\frac{e^2}{m_0 c^3} .$$

Orbene la quantità $\frac{4}{3}(e^2/m_0 c^3)$ coincide con l'intervallo di tempo elementare (I) che separa, nella teoria da noi proposta, due istanti successivi in cui è definito il moto « macroscopico » classico dell'elettrone.

È ovvio che la dimostrazione precedente può essere invertita: ammessa cioè un'indeterminazione $\Delta\tau \simeq \tau_0/2$ nella misura del tempo τ, si può risalire all'esistenza di uno stato eccitato dell'elettrone cui compete unà massa pari a quella del mesone μ.

Ringrazio il dott. LOINGER per alcune sue apprezzate osservazioni.

sazione matematica del concetto di stato interno eccitato di una particella.

(3) Ad esempio: D. BOHM e M. WEINSTEIN: *Phys. Rev.*, **74**, 1784 (1948): M. SUYAWARA: *Prog. Theor. Phys.*, **7**, 599 (1952); T. HAMADA e M. SUYAWARA: *Prog. Theor. Phys.*, **8**, 363. (1952).

(4) Naturalmente ciò è vero se si suppone che la relazione $206 \simeq \frac{3}{2}\frac{\hbar c}{e^2}$ non sia una mera coincidenza numerica ma abbia un effettivo fondamento teorico connesso al modello stesso del mesone μ. Tale relazione, suggerita da tempo da Y. NAMBU: *Prog. Teor. Phys.*, **7**, 595 (1952), è oggi accettata da diversi autori.

Esempio di una probabile particella Λ_0 di alta energia.

A. De Marco, A. Milone e M. Reinharz

Istituto di Fisica dell'Università - Genova
Istituto Nazionale di Fisica Nucleare - Sezione aggregata di Genova

(ricevuto il 9 Marzo 1955)

1. – Avviene frequentemente di trovare nell'esplorazione di lastre nucleari eventi costituiti da una traccia con ionizzazione doppia del minimo che si risolve poi in due tracce al minimo di ionizzazione. Tali eventi sono di solito attribuiti a coppie di elettroni.

Riteniamo utile descrivere uno di tali eventi da noi studiato, che sembra poter essere interpretato come la disintegrazione in volo di una particella Λ_0 di una energia di $\sim 5 \pm 1$ GeV.

L'evento è stato trovato durante l'esplorazione di lastre nucleari G5 esposte per $6^h\ 40^m$ ad una altezza media di 24000 m (spedizione Sardegna 1953), esplorazione eseguita per la ricerca di elettroni d'urto. L'evento, mostrato in figura, è costituito da una coppia di particelle al minimo di ionizzazione, formanti tra loro un angolo talmente piccolo che le due tracce restano inseparate per un tratto di 5000 μ. In questo tratto e precisamente a 4700 μ dal vertice della coppia, ha origine un'altra traccia al minimo di ionizzazione, facilmente identificabile dal suo scattering per un elettrone.

Data la natura dell'evento è ragionevole assumere che detto elettrone sia stato generato in un urto elastico di una delle due particelle costituenti la coppia con un elettrone dell'emulsione. Ci è sembrato quindi opportuno approfittare di questa circostanza per vedere se era possibile identificare il processo che aveva dato origine alla coppia.

2. – I risultati delle misure eseguite su ciascuna traccia sono riportati nella seguente tabella:

traccia	lunghezza μ	$N/100\ \mu$	$(\bar{\alpha}/100\mu)^\circ \cdot 10^3$
a	5000	$56{,}6 \pm 1{,}6$	—
s	20000	$26{,}8 \pm 0{,}9$	$16 \pm 3{,}6$
d	20000	$26{,}6 \pm 0{,}9$	$8 \pm 1{,}6$
e	2000	$24{,}0 \pm 1{,}0$	1000 ± 150

$\omega = \widehat{ae} = 7°57' \pm 0°48'$

Le misure di ionizzazione sono state fatte con ingrandimento $1600\times$, risolvendo i singoli grani, mentre quelle di $\bar{\alpha}$ sono state eseguite per le tracce s e d

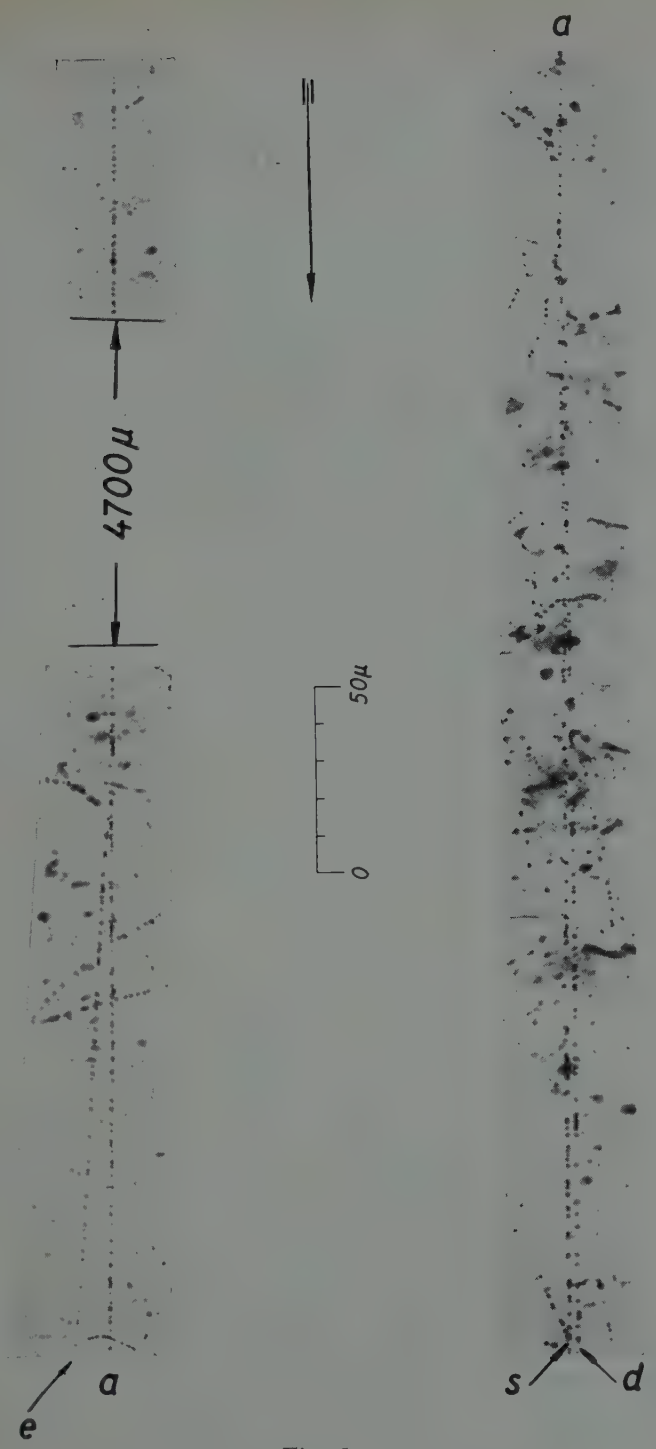

Fig. 1.

con il metodo delle saggitte e per la traccia *e* con il metodo angolare. Le misure sono state corrette dalla distorsione, determinata col metodo di Mayor [1] e che è risultata circa un ventesimo del valore della saggitta media relativa alle celle di misure. Gli errori su $\bar{\alpha}$ sono stati calcolati seguendo le indicazioni consigliate nel *Suppl. Nuovo Cimento*, **12**, 228 (1954).

Per la misura degli angoli θ e ω, per il calcolo dei relativi errori e per la determinazione dell'energia cinetica E della particella urtante, ottenuta dalle misure fatte sull'elettrone urtato, sono stati seguiti i criteri esposti in un articolo in corso di pubblicazione sul *Nuovo Cimento*.

3. – Se la particella responsabile dell'elettrone d'urto fosse un elettrone, dovrebbe avere un'energia cinetica $E = (83{,}4^{+8{,}56}_{-2{,}84})$ MeV e di conseguenza un angolo di scattering $\bar{\alpha} = (0{,}38^{+0{,}2}_{-0{,}19})^\circ$ che non è compatibile con nessuno dei valori trovati sperimentalmente su ciascuna delle due tracce. D'altra parte un elettrone con un'energia cinetica di 83,4 MeV non può produrre un elettrone d'urto di 32 MeV senza subire una deviazione apprezzabile (5°) dalla sua direzione iniziale. Possiamo quindi concludere che entro i limiti di precisione delle misure, la particella responsabile dell'elettrone d'urto non può essere un elettrone (*). Siccome non vi è alcuna evidenza di particelle di massa intermedia fra l'elettrone e il mesone, si può calcolare la massa della particella urtante per mezzo della formula (5) dell'articolo su citato. Si ottengono, tenendo conto dei valori di $\bar{\alpha}$ riportati nella tabella, i seguenti valori per le masse delle particelle costituenti il ramo di destra e il ramo di sinistra della coppia:

ramo di destra: $m = (440 \pm 145)$ MeV (traccia *d*)

ramo di sinistra: $m = (220 \pm 75)$ MeV (traccia *s*)

È quindi plausibile che la particella responsabile dell'elettrone d'urto sia quella relativa al ramo di sinistra della coppia, la cui massa è compatibile con quella di un mesone leggero.

Escluso che si tratti di una coppia di elettroni, si possono fare le seguenti ipotesi:

1) l'evento è una particella θ_0: in tal caso le due particelle, costituenti i due rami della coppia, sono entrambe dei mesoni leggeri, e l'energia di legame risulta $Q = (16{,}4^{+26{,}7}_{-13{,}8})$ MeV.

2) l'evento è una particella Λ_0: in tal caso le due particelle sono un mesone leggero ed un protone. Se il mesone è il ramo di sinistra si ha $Q = (94{,}41^{+86{,}6}_{-57{,}7})$ MeV, se invece è il ramo di destra si ha $Q = (474{,}7^{+228{,}8}_{-147{,}7})$ MeV.

Confrontando i valori di Q così trovati con quelli delle energie di legame relativi alle particelle θ_0 e Λ_0, si vede che la seconda ipotesi, nel caso che il mesone sia il ramo di sinistra, è la più ragionevole, per cui l'evento può essere considerato, con molta probabilità, come una particella Λ_0 di alta energia.

Desideriamo ringraziare il gruppo lastre dell'Istituto di Fisica della Università di Roma per aver concesso di utilizzare i loro microscopi per le nostre misure, ed i proff. E. Pancini e A. Borsellino per l'incoraggiamento e le utili discussioni.

(1) J. V. Mayor: *Brit. Journ. Appl. Phys.*, **3**, 309 (1952).

(*) Ciò quando si trascuri il fatto che, nell'8% dei casi, la misura dell'energia dell'elettrone può essere errata, per difetto, a causa della perdita di energia per radiazione.

On the Decay of ^{134}Cs.

G. Bertolini, M. Bettoni and E. Lazzarini
Istituto di Fisica Sperimentale del Politecnico - Milano

(ricevuto il 10 Marzo 1955)

^{134}Cs is known to decay by β emission on excited states of ^{134}Ba. Several measurements have been made on the energy of the γ-rays and on the β-rays spectrum with scintillation and magnetic spectrometers ([1-6]).

The continous spectrum shows a low energy component (~ 90 keV) and two high energy components (~ 650 keV) the end points of which differ by 30÷40 keV. However the evaluation of the higher component is only informative since the end of the spectrum is disturbed by the internal conversion lines of 560 and 600 keV γ-rays.

We have investigated the β-decays in coincidence with γ-rays of different energies with an intermediate image β-ray spectrometer and a NaI(Tl) crystal, fig. 1. The γ-ray spectrum detected by the NaI crystal is shown in fig. 2.

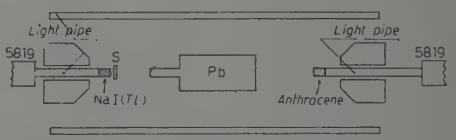

Fig. 1. – Schematic diagram of magnetic spectrometer.

In fig. 3 (*a*, *b*, *c*) are shown the Fermi plots of the β-spectrum in coincidence with γ-rays of energy higher than D_1, D_2 and D_3 respectively. In fig. 3*a* the β-spectrum going to 1.395 MeV level is predominant and in fig. 3*c* a β-spectrum of allowed shape with end point of approximatively 335 keV shows up. On the other hand in fig. 3*b* the three β-spectra going to 1.700, 1.395 and 1.361 MeV levels are present. In this way the straight lines of figs. 3*a* and 3*c* and the convex line of fig. 3*b* can be understood.

([1]) T. Siegbhan M. Deutsch: *Phys. Rev.*, **71**, 483 (1947); **73**, 410 (1948).

([2]) M. A. Waggoner. M. L. Moon and A. Roberts: *Phys. Rev.*, **80**, 420 (1950).

([3]) L. G. Elliot and R. E. Bell: *Phys. Rev.*, **72**, 979 (1947).

([4]) F. H. Schmidt and G. L. Keister: *Phys. Rev.*, **86**. 632 (1952).

([5]) J. M. Cork, J. M. Le Blanc, W. G. Nester, D. W. Martin and M. K. Brice: *Phys. Rev.*, **90**, 444 (1953).

([6]) M. C. Joshi and B. V. Thosar: *Phys. Rev.*, **96**, 1022 (1954).

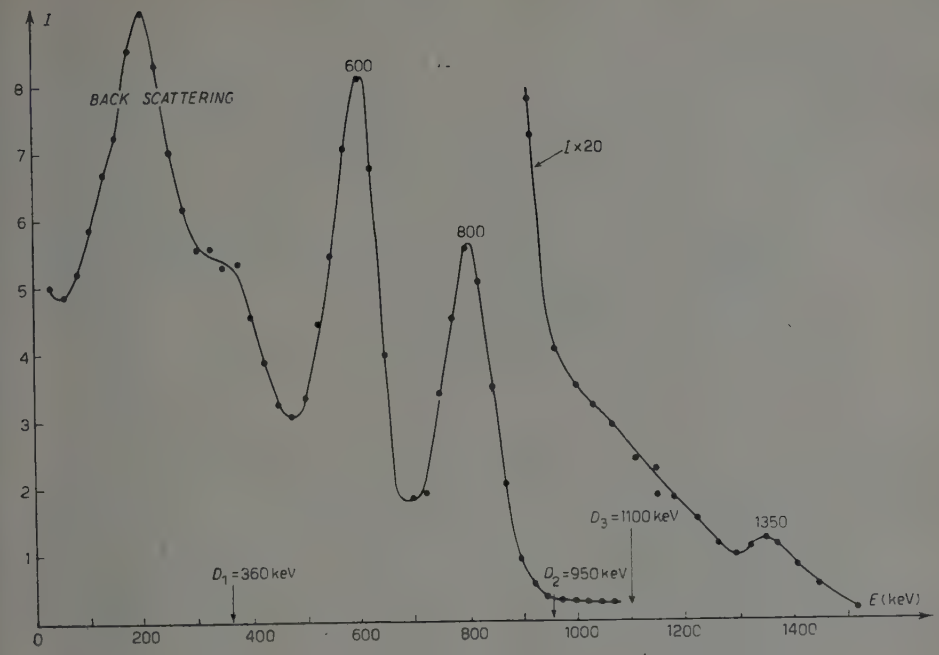

Fig. 2. – γ-ray spectrum detected by the NaI(Tl) crystal.

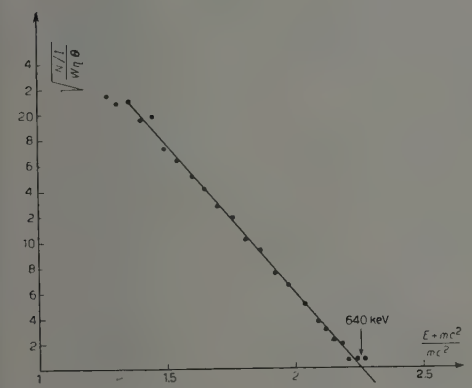

Fig. 3*a*. – Fermi plot of β-spectrum in coincidence with γ-rays of energy higher than D_1 (360 keV).

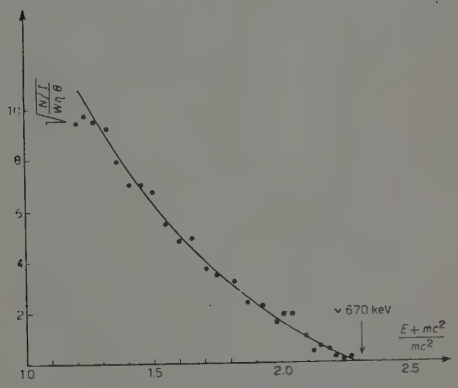

Fig. 3*b*. – Fermi plot of β-spectrum in coincidence with γ-rays of energy higher than D_2 (950 keV).

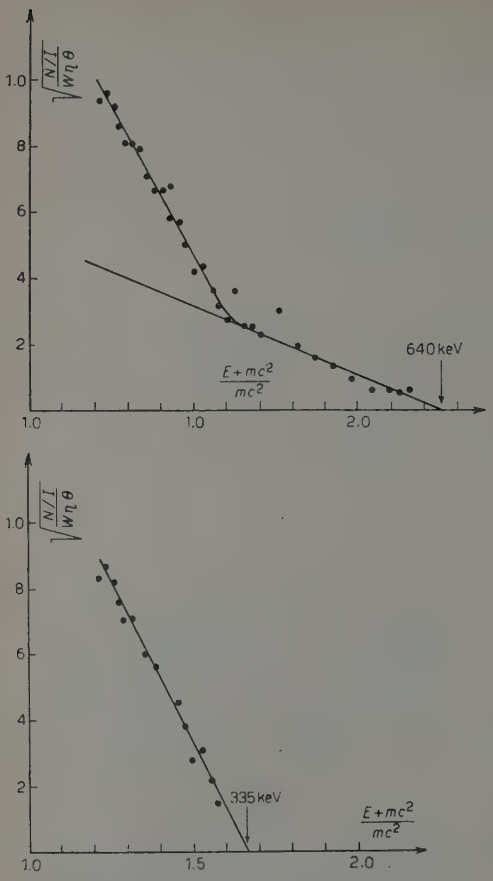

Fig. 3c. – Fermi plot of β-spectrum in coincidence with γ-rays of energy higher than D_c (1100 keV). The figure below shows the Fermi plot of the 335 keV β-spectrum.

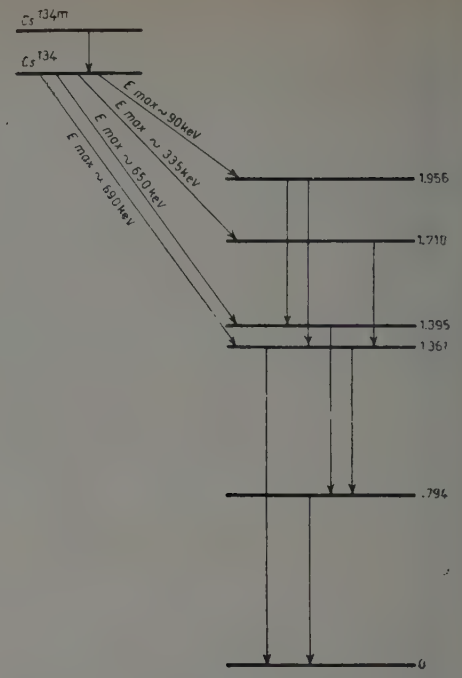

Fig. 4. – Proposed decay scheme of ^{134}Cs.

With these results and with preliminary measurements on the γ-γ coincidences a quite reasonable decay scheme of ^{134}Cs can be that shown in fig. 4.

A complete description of β-γ and γ-γ coincidence is going to be published soon.

IL NUOVO CIMENTO Vol. I, N. 4 1° Aprile 1955

The Optical Model and the Nucleon-Nucleus Scattering.

A. Kind and C. Villi

Istituti di Fisica dell'Università di Padova e di Trieste
Istituto Nazionale di Fisica Nucleare - Sezione di Padova

(ricevuto il 10 Marzo 1955)

Recently the optical model of the nucleus has been re-examined on the basis of recent measurements of the total neutron cross sections for neutron energies ranging from 0 to 3 MeV [1] and from 40 to 300 MeV [2]. The attempt to fit the measured cross sections by adjusting the values of the inverse mean free path for absorption of neutrons in nuclear matter K and the average potential V, encountered by a nucleon inside a nucleus, has given evidence that not only K but also V varies with neutron energy. In particular, agreement, within quoted experimental errors, between the calculated cross sections and the observed ones in the energy range $60 \div 300$ MeV is obtained provided the potential V behaves as a monotonically decreasing function of the neutron energy E from a maximum value of $V \approx 30$ MeV for $E \approx 60$ MeV to $V \approx 10$ MeV for $E \approx 300$ MeV.

In this note we attempt to give a first rough theoretical justification of the empirical results concerning V on the basis of the independent particle model.

Consider a neutron of energy E and wave number k, outside the nucleus, colliding with a nucleus made up of A nucleons filling up all states of lower energy. In the limiting case of low neutron energies, the independent particle model, according to which the incoherent part of the nuclear interaction is negligible compared with the coherent one, allows the calculation of the mean potential energy of the neutron within the nucleus in terms of perturbation theory. With reference to the elastic part of the nuclear interaction, the same can also be assumed valid for high neutron energies and the mean potential energy can still be calculated by means of perturbation methods. It follows that in both cases, in order to calculate V, one may assume as a zero approximation that the nuclear matter remains unperturbed by the passage of the neutron through it.

The consequences of this approximation in the optical picture are the following. Let ΔL be the work done by the interaction forces exerted between the incident neutron and the nuclear matter. Then, the kinetic energy of

(1) H. Feshbach, C. E. Porter and V. F. Weisskopf: *Phys. Rev.*, **96**, 448 (1954).

(2) T. B. Taylor: *Nuclear Scattering of high energy neutrons and optical model of the nucleus*, to be published in the *Physical Review*.

the neutron will increase from the value E, outside the nucleus, to a certain value E', inside the nucleus, and the mean kinetic energy of the nuclear matter itself will also undergo an elastic increase ΔU_A. Since the energy conservation requires that

$$E' + \Delta U_A = E + \Delta L, \tag{1}$$

the variation of the magnitude of the propagation vector inside the nucleus is given by

$$k_1 = k\left\{\left(1 + \frac{\Delta L - \Delta U_A}{E}\right)^{\frac{1}{2}} - 1\right\}. \tag{2}$$

Assuming in eq. (2) $\Delta L - \Delta U_A = V$, one gets the standard definition of the refractive index of nuclear matter according to the optical model, provided V is assumed dependent on the magnitude $k' = k + k_1$ of the propagation vector of the neutron inside the nucleus. The zero approximation $\Delta U_A = 0$ means, therefore, that the whole of the interaction energy is spent in increasing the kinetic energy of the neutron and, consequently, one has to expect that the momentum of the nucleon within the nucleus is in this way overestimated. Although only the consideration of a higher approximation will put the picture in correct terms by sharing the available interaction energy between the incident neutron and the nuclear matter, it was thought of interest to develop the consequences of the approximation $\Delta U_A = 0$ and compare the calculated anomalous dispersive properties of nuclear matter for neutron waves with those revealed by the above quoted analyses ([1,2]).

We describe the interaction of the incident neutron with the individual nucleons of the nucleus in terms of a central potential having a Yukawa behavior and exchange properties expressed by the operator

$$\boldsymbol{O} = \boldsymbol{\tau}_i\boldsymbol{\tau}_j[g^2 + f^2(\boldsymbol{\sigma}_i\boldsymbol{\sigma}_j)]\,. \tag{3}$$

The range of the nuclear forces a_0^{-1} and the two interaction parameters g^2 and f^2 will be determined from experiments. The wave function of the system nucleus + nucleon is totally antisymmetrized and written as a Slater determinant. Following the usual procedure, one gets, after summation over spin and isotopic spin and integration over space coordinates:

$$V(k') = -\frac{48\hbar^2 a_0^2}{M\Omega}\cdot \cdot(g^2 + 3f^2)\sum_{j=1}^{A}\frac{1}{1 + (\boldsymbol{k}'-\boldsymbol{k}_j)^2}, \tag{4}$$

where Ω is the nuclear volume, M the nucleon mass, $\boldsymbol{k}'$ and $\boldsymbol{k}_j$ the momentum vectors of the guest neutron and of an individual nucleon of the nucleus. To perform the summation over nucleons we introduce polar coordinates in momentum space and integrate over $\boldsymbol{k}_j$. It is found

$$V(k') = -\frac{12\hbar^2 a_0^2}{\pi M}(g^2 + 3f^2)G(k_0, k'), \tag{5}$$

where

$$G(k_0, k') = k_0 + + \frac{1 + k_0^2 - k'^2}{4k'}\log\frac{1 + (k' + k_0)^2}{1 + (k' - k_0)^2} - - \mathrm{tg}^{-1}(k' + k_0) + \mathrm{tg}^{-1}(k' - k_0), \tag{6}$$

k_0 being the Fermi sphere in units a_0. Finally, from Eq. (2), with $\Delta U_A = 0$, we have

$$E\{(k'/k)^2 - 1\} = V(k'), \tag{7}$$

which is solved taking into account Eq. (5) to get V as a function of the kinetic energy E of the neutron outside the nucleus.

The result of this calculation is given in the figure, where the Taylor's curve (dotted curve) and the zero energy

data [1] (+) are compared with Eq. (5) (full line curve). We have assumed a nuclear radius $R = r_0 A^{\frac{1}{3}}$ with $r_0 = 1{,}43 \cdot 10^{-13}$ cm and for the range of nuclear forces $a_0^{-1} = 1{,}76 \cdot 10^{-13}$ cm. With

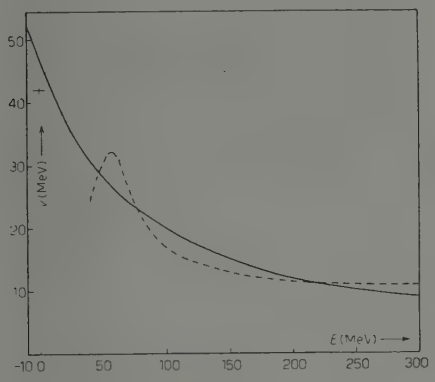

Fig. 1.

these values the best fit with experimental data on total neutron cross sections is obtained provided $g^2 + 3f^2 = 2$. Although we have no possibility to determine the values of g^2 and f^2 separately, we may point out that the value 2 for the combination $g^2 + 3f^2$ is consistent with the values $g^2 = 0.258$ and $f^2 = 0.595$ considered by Fröhlich to fit the two lowest energy levels of the neutron-proton system and the ground state of ^{3}H.

As can be seen, there is a large discrepancy between the theoretical and the empirical curve in the energy range between 40 and 60 MeV, which cannot be eliminated along the lines of the present calculation. However, we point out that the behavior of the Taylor's curve in this energy region is strongly dependent on the assumption concerning the constant density of the nuclear matter and it seems hard to think, on the basis of the optical model, that in the very steep maximum there is much physical meaning.

We thank Professor N. Dallaporta for very helpful discussions and Dr. T. B. Taylor, who made his paper available to us before publication.

Measurement of the Cross-Section and the Energy Spectrum in the Double Compton Effect.

A. Bracci, C. Coceva, L. Colli and R. Dugnani Lonati
Laboratori CISE - Milano

(ricevuto il 12 Marzo 1955)

The double Compton effect is a third order process in which a γ quantum interacts with a free electron and as a consequence one electron and two γ are diffused.

The order of magnitude of the cross-section of such process was calculated in 1934 by Heitler and Nordheim [1] in rather restrictive conditions, unfavourable for experimental verification.

Lately Mandl and Skyrme [2] have taken up again the question of calculation with the quantum electrodinamics methods of Dyson and Feynman, obtaining the general expression for differential cross-section of this process. A first experimental indication of the double Compton effect was obtained by Cavanagh [3].

In the present work the cross-section and the energy distribution of the two γ quanta diffused in the double Compton effect is measured for energy of incident γ of about 1 MeV and in the particular case of the emission at 90° of the two diffused γ, with respect to the incident γ and between themselves. This condition was chosen in view of the notable simplification, it has, of the formulae to be compared with the experimental results.

The experimental set up is shown in Fig. 1.

The source of γ is ~ 200 mC of ^{60}Co which emits γ-rays of 1.17 and 1.33 MeV energy. The γ beam, collimated within a solid angle of 0.34% of a sphere, invests a thin target of berillium. Measurements have been taken with targets 1 and 2.5 mm thick.

The berillium was chosen because of its low atomic number. There might be some events in which two γ are diffused simultaneously in the target, one γ due to a normal Compton scattering and the other to bremsstrahlung emission in the target by the scattered electron; since the bremsstrahlung emission depends on Z^2, where Z is the atomic number of the target element, the probability of these events is strongly reduced taking as a target a light element.

The γ are revealed by two scintillation spectrographs with cubic sodium

---

(1) W. Heitler and L. Nordheim: *Physica*, **1**, 1059 (1934).

(2) F. Mandl and T. H. R. Skyrme: *Proc. Royal Soc.*, **215**, 497 (1952).

(3) P. E. Cavanagh: *Phys. Rev.*, **87**, 1131 (1952).

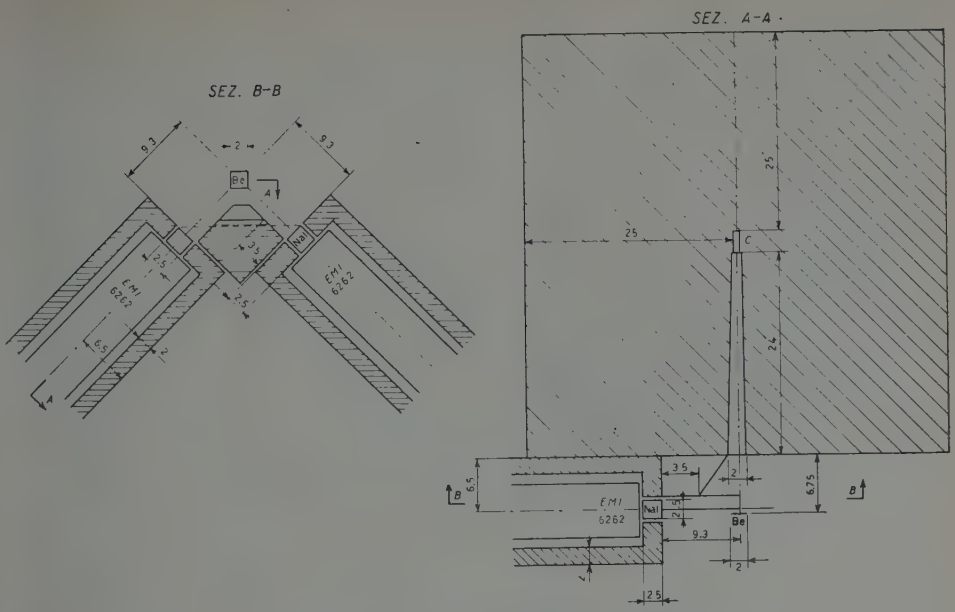

Fig. 1. – Experimental set-up. $C = \gamma$ rays of ^{60}Co. Be = berillium target. ▒ Screening material: lead. NaI = Sodium Iodide Crystals.

iodide crystals of 1 inch and photomultipliers EMI 6262 of 14 stages. The crystals are screened with a layer of polystyrene 0.2 g/cm² thick, to avoid the detection of Compton electrons diffused by the target. Such layer does not practically absorb γ up to 20 keV energy; the γ diffused by the berillium target are revealed when they form with the incident beam an angle between $\sim 80°$ and $100°$.

In Fig. 2 the electronic scheme is outlined. The photomultipliers work at a rather high voltage in such a way that the output pulse at the anode can trigger directly without the need of further amplification a coincidence with resolving time of $3.3 \cdot 10^{-8}$ s.

Under these conditions the output pulses at the anode are no more proportional to the energy released in the crystal by γ-rays. For this reason two pulses proportional to the energy of the γ absorbed by the crystal are taken from the twelfth dynode of the photomultipliers and are sent after due amplification to the vertical plates (one to the upper, the other to the lower

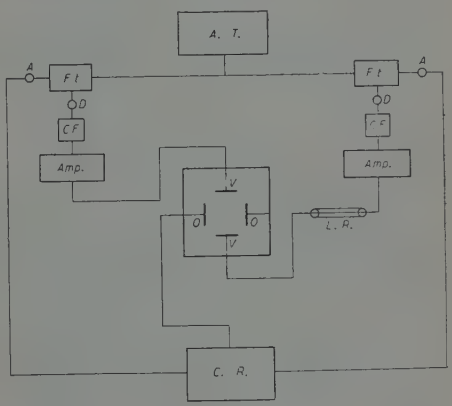

Fig. 2. – Electronic scheme.

A.T. = High voltage supply.
F.T. = Photomultipliers.
A = Anode output.
D = Dynode output.
CF = Cathode Follower.
Amp = Amplifier.
L.R. = Delay line.
C.R. = Coincidence circuit.
V = Vertical plate of the oscillograph.
O = Horizontal plate of the oscillograph.

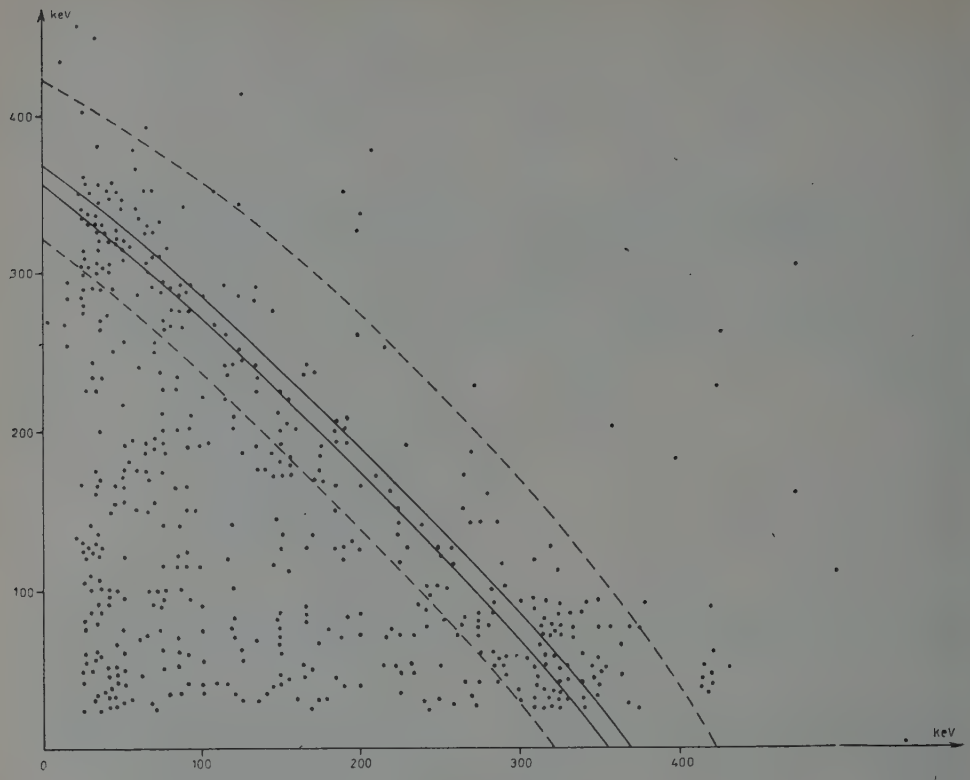

Fig. 3. – Map showing double Compton Effect. Coordinates are the energies of the two Υ forming a couple as photographed on the oscillograph. Each point represents a couple of γ scattered by the target, which gave rise to a coincidence. This map was taken with 2,5 mm berillium thickness.

plate) of the oscillograph, one of these pulses with $\sim 6 \cdot 10^{-6}$ s delay.

The oscillograph sweep is started by the output pulse of the coincidence. It is thus possible to photograph couples of proportional pulses which correspond to coincidence events. From the analysis of the photographs a diagram is constructed where a pair of pulses in coincidence is represented by a point, the coordinates of which correspond respectively to the height of the two pulses. In such diagram it is possible to distinguish easily background points due to events which are independent of the target or due to casual coincidences. This is due to the fact that points corresponding to different processes fall in rather separated areas of such a map. In addition these events can be measured independently and deduced from the diagram.

Fig. 3 represents one of the diagrams obtained after such deduction has been made. The continouos curves trace the points representing the energies of a couple of γ scattered by double Compton effect, obtained on the basis of conservation laws in the case where the two γ are diffused at an angle of 90° with incident γ and between themselves, and where the energy of the incident γ is 1.17 and 1.33 MeV. The dotted curves correspond to the extreme angles of diffusion that the experimental set up allows.

In the area contained between the two dotted curves are found the expe-

rimental points representing double Compton events in which the two scattered γ release all their energy in the crystals. On the other hand the points in the lower area correspond to the detection in the crystals by single Compton effect.

In this lower area are also found the points corresponding to those γ diffused from the target through double Compton effect, which have undergone a process of diffusion in the lead of the screen surrounding the crystals themselves.

For the comparison of experimental results with the theoretical calculations of the cross-section and the energy distribution of the diffused γ, it is convenient to consider only the points between the two dotted curves. In this area, points due to background without berillium target are found to be about 2.5% of the total events detected and events due to casual coincidences are found to be 20%.

With points in such area, corrected as said above, it is possible to construct a spectrum of energy in the form of an histogram with channels of 25 keV; this spectrum must be corrected for the detection yield versus the energy. The yield was calculated on the basis of the data obtained by MAEDER MÜLLER and WINTERSTEIGER (1) which were adapted to our geometrical conditions; it has been experimentally controlled for energies of 500 keV and 1.2 MeV.

Fig. 4 shows the energy spectra, corrected as said above, given by the histograms n. 1 and n. 2. The histogram n. 3 represents the energy distribution calculated according to MANDL and SKYRME (2) in the particular case applicable to our experimental set up. As the figure shows, the agreement between the theory and the experimental values is good.

From the integral of the experimental

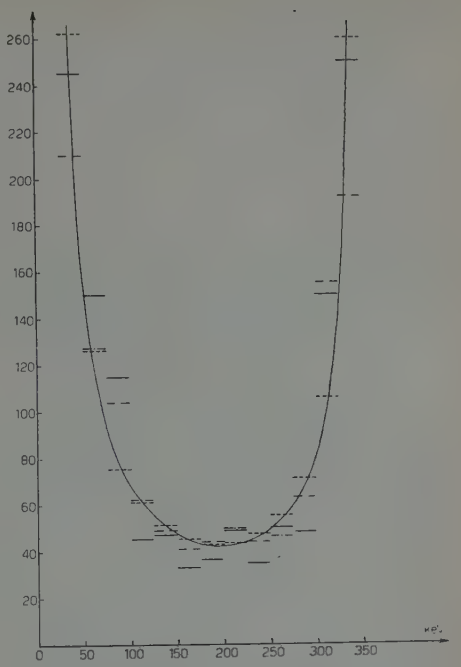

Fig. 4. – Energy spectrum of γ diffused by double Compton effect in our experimental conditions, given in an arbitrary scale.

—— histogram n. 1, taken with 2,5 mm berillium thickness.

–·– histogram n. 2, taken with 1 mm berillium thickness.

- - - histogram n. 3, as calculated from the continuous curve, which represents the theoretical spectrum. The histograms are normalized to the same area.

histogram it is possible to deduce the cross-section of the process. We made only an approximate calculation for this cross-section, which gives $4 \cdot 10^{-30}$ cm^2 per unit solid angle.

Measurements and calculations are in progress for a better estimate of this value.

The results obtained with different berillium thickness, are in good agreement between themselves.

The authors wish to express their appreciation for the many valuable suggestions and discussions to Proff. G. BOLLA, B. FERRETTI, P. CALDIROLA and U. FACCHINI.

(1) D. MAEDER R. MÜLLER and V. WINTERSTEIGER: *Helv. Phys. Acta*, **27** 1 (1954).

LIBRI RICEVUTI E RECENSIONI

Reports on Progress in Physica; Volume XVII (1954) a cura di A. C. Stickland. Ed. The Phusical Society, London, pag. 280; 50 s.

È uscito quest'anno il 17° volume dei *Reports on Progress in Physics* della Società di Fisica di Londra. Questo volume, che prosegue una ben nota raccolta, contiene otto articoli, tutti con il carattere di rassegna critica gli Autori sono noti specialisti della materiape-l'esposizione è in generale piuttosto a profondita, ma sempre accompagnata da parti introduttive e da spiegazioni tendenti a rendere il testo comprensibile di per se stesso. Ogni articolo reca una raccolta di riferimenti bibliografici, talvolta molto estesi.

Il primo di questi lavori, scritto da M. H. L. Pryce di Oxford, espone le ragioni per cui è stato proposto un modello « a shell » per la struttura del nucleo e ne dimostra i vantaggi e le limitazioni, confrontandolo con i modelli di tipo « collettivo ».

Il secondo articolo è una rassegna critica dei più recenti progressi nella teoria classica della diffrazione, ad opere di C. J. Bouwkamp, dei laboratori di ricerca Philips di Endhoven, basata su di una bibliografia molto estesa.

J. A. Chalmers tratta poi numerosi problemi sulla elettricità atmosferica, scegliendo quelli su cui negli ultimi anni si sono avuti progressi significativi.

Sulle condizioni fisiche della corona solare, le conoscenze si sono estese e approfondite notevolmente da una decina d'anni a questa parte, dopo i lavori di Edlén (1942), ma alcuni problemi non sono ancora completamente risolti. Ne riferisce C. W. Allen dell'Osservatorio Astronomico della Università di Londra in un breve articolo recante anche dati numerici e fotografie.

E. Teller della Università di California tratta invece delle teoria sull'origine dei raggi cosmici, concludendo in favore del meccanismo di accelerazione proposto da Fermi, completato dalla localizzazione dei campi acceleratori suggerita da Unsold.

Il problema della struttura elettronica delle molecole e della natura de legami chimici viene discusso da W. Moffitt della Harvard University, che presenta una teoria generale degli stati di valenza corredata da esempi illustrativi. Seguono un articolo di A. B. Lidiard sull'antiferromagnetismo, ed una rassegna delle notizie sin ora raccolte su movimenti orizzontali della ionosfera, a cura di B. H. Briggs e di M. Spencer del Cavendish Laboratory di Cambridge, che raccoglie i risultati di osservazioni compiute in ogni parte del mondo.

F. A. Levi

I. A. D. Lewis e F. H. Wells – *Millimicrosecond Pulse Techniques*; Pergamon Press, 1954, 309 pag.; 50 s.

Lo scopo di questa opera è quello di fornire al lettore una trattazione monografica sui circuiti destinati ad operare in una banda di frequenze intermedie tra quella delle onde corte e quella delle

microonde, ed in particolare studiati per il funzionamento ad impulsi. In questa zona, nella quale si ha a che fare con intervalli di tempo dell'ordine del millimicrosecondo, ci si trova al confine tra il regno dei circuiti a costanti concentrate, per i quali le dimensioni geometriche degli elementi componenti non hanno grande importanza essendo sempre assai più piccole della lunghezza d'onda, e quello dei circuiti a costanti distribuite, adatti per altissime frequenze.

La tecnica descritta nel volume, ha quindi due aspetti fondamentali: da un lato si cerca di perfezionare i circuiti classici a costanti concentrate per adattarli a frequenze più alte, dall'altro si ricorre alle costanti distribuite che devono essere studiate dal punto di vista della propagazione delle onde. Importanti applicazioni si hanno nella fisica nucleare come pure in molti altri campi di ricerca e per tali ragioni il libro presenta notevole interesse per i fisici oltre che per gli ingegneri specializzati in elettronica e microonde.

Una breve introduzione teorica richiama le leggi fondamentali ed i procedimenti matematici necessari per la comprensione del testo e serve come premessa alla parte più estesa del volume, costituita da cinque capitoli nei quali sono presi in considerazione i singoli elementi dei circuiti e le apparecchiature fondamentali; essi trattano nell'ordine: linee di trasmissione, trasformatori, generatori di impulsi, amplificatori e oscillografi a raggi catodici.

Un esteso capitolo, derivato in gran parte dalla personale esperienza degli Autori, illustra le applicazioni alla fisica nucleare, mentre altre apparecchiature sono brevemente elencate alla fine del volume. La trattazione è caratterizzata da una equilibrata fusione tra le considerazioni teoriche ed i dati pratici; essa si presenta però piuttosto sintetica e richiede al lettore una adeguata preparazione specializzata. La documentazione è ampia ed accurata ed il volume è arricchito oltre che da numerosi schemi e diagrammi anche da disegni costruttivi e fotografie di parti di circuiti.

F. A. Levi

G. Ludwig – *Die Grundlagen der Quantenmechanik*; Ed. Springer-Verlag (Berlin – Göttingen – Heidelberg, 1954), pag. 460 (fig. 52).

Questo trattato si differenzia fra i numerosi sullo stesso argomento che sono stati pubblicati in questi ultimi decenni per l'intento di presentare la teoria quantistica nei suoi fondamenti matematici e di dare una visione unitaria e coerente dei concetti che stanno alla base della sua interpretazione fisica. Ed effettivamente il pregio maggiore dell'opera del Ludwig consiste nell'aver saputo realizzare un'innegabile armonia fra l'apparato matematico e la struttura fisica della teoria.

Naturalmente questo risultato è stato conseguito non senza sacrifizi: senza dubbio la lettura del libro risulta talvolta un po' pesante, specialmente per chi l'affronta senza essere dotato di una adeguata preparazione matematica.

Per questa ragione noi ne consigliamo lo studio, onde trarne un utile profitto, solo a chi ha già seguito un buon corso universitario di fisica teorica.

La materia, distribuita in dodici capitoli, comprende l'ordinaria meccanica quantistica (esclusa la teoria dei campi), presentata dal punto di vista della teoria delle trasformazioni, seguendo un procedimento assiomatico. Le rappresentazioni di Heisenberg, di Schrödinger di interazione sono illustrate come applicazioni della teoria generale precedente.

Particolarmente interessanti, per la densità di concetti di cui sono permeati, i capitoli V e VI relativi all'esame dei processi di misura e del modello di universo che scaturisce dalla teoria quantica:

consigliamo lo studio di detti capitoli anche ai cultori più seri e più preparati di filosofia della Scienza.

Vogliamo però osservare come, nonostante la preoccupazione dell'Autore di fare un'opera rivolta a presentare in modo critico i fondamenti della teoria dei quanti, numerose siano tuttavia le applicazioni a problemi pratici (spettri di atomi a uno o più elettroni, intensità e regole di selezione per le righe spettrali, problemi d'urto, spettri molecolari e legame chimico, ecc.).

In due appendici matematiche sono infine presentati, in modo succinto ma scevro di qualsiasi faciloneria, i fondamenti dello spazio hilbertiano e della teoria dei gruppi con particolare riguardo alle loro rappresentazioni.

Perfetta si può dire la veste tipografica, come è tradizione del resto della casa Springer.

Concludiamo consigliando la lettura accurata del libro del Ludwig in modo particolare a tutti i nostri giovani laureati che intendono dedicarsi allo studio della fisica teorica col desiderio di comprenderne i fondamenti logici e non soltanto di farne applicazioni più o meno interessanti a problemi di attualità.

P. Caldirola

K. Bechert – *Theorie des Atombaus*; (1ª e 2ª parte, 2 volumir formato piccolo), Walter de Gruiter & Co., Berlino, 1954.

Questi due volumetti di 148 e 170 pagine fanno parte (III e IV tomo) del trattato *Atomphysik* di K. Bechert e Chr. Gerthsen (3ª edizione rifatta) edito dalla Walter de Gruyter (Berlino 1954) nella collezione tascabile Sammlung Göschen.

Malgrado il piccolo formato e la minutezza del carattere tipografico, si può propriamente parlare di « trattato » per la scelta degli argomenti, la completezza e la chiarezza dell'esposizione.

La prima parte, che può considerarsi una introduzione alla meccanica quantistica, comprende i seguenti capitoli.

Le Relazioni di Indeterminazione - la Teoria di Bohr - il Principio di Corrispondenza - la Meccanica Quantistica - l'Analogia Ottica - Meccanica - Semplici Esempi di Meccanica Ondulatoria - Relazione tra Calcolo degli Operatori, Meccanica Quantistica e Meccanica Ondulatoria - l'Atomo di Idrogeno.

Gli argomenti di carattere generali esposti nei primi capitoli sono illustrate da numerosi esempi di applicazione della teoria dell'atomo, talchè il lettore, a giustificazione del titolo del volume, è ragguagliato oltre che sui fondamenti ed i metodi della meccanica quantistica, anche sullo spettro dell'atomo di idrogeno, sulla struttura a « shell » dell'atomo, sui potenziali di ionizzazione, sullo spettro dei metalli alcalini, sugli spettri Röntgen caratteristici, sull'effetto Auger, sull'effetto Zeeman, ecc.

Il secondo volumetto della *Theorie des Atombaus* tratta dei seguenti argomenti:

Atomi con 2 Elettroni - Perturbazioni indipendenti dal Tempo - Teoria dell'Urto - Momento Angolare delle Particelle atomiche - lo Spin dell'Elettrone nella Meccanica Ondulatoria - Molecole - Perturbazioni dipendenti dal Tempo, Diffusione della Luce, Effetto Fotoelettrico - Teoria dell'Elettrone di Dirac.

Il lettore troverà anche in questa parte dell'esposizione numerose applicazioni della teoria al calcolo dettagliato di specifici effetti.

Oltre ai pregi già menzionati, che giustificherebbero ampiamente una edizione più costosa dell'opera, va lodato il proposito di mettere nuovamente alla portata di numerosi lettori, tramite questi economici manualetti, i metodi e le applicazioni della meccanica atomica.

S. Gallone

K. M. CASE, F. DE HOFFMANN e G. PLACZEK – *Introduction to the theory of neutron diffusion*; vol. I, pag. VIII+174, Los Alamos, Giugno 1953.

La teoria elementare della diffusione dei neutroni è trattata in varie pubblicazioni recenti, in connessione con il problema della costruzione dei reattori nucleari. La letteratura sulla teoria non elementare di diffusione dei neutroni è invece sparsa ed ha carattere altamente specializzato.

Si sentiva così la necessità di un libro che servisse di base per un più approfondito esame della letteratura esistente. Questo è lo scopo che si prefiggono gli autori del presente libro, basato su una serie di lezioni tenute da G. PLACZEK nell'estate del 1949 all'Università di California a Los Angeles. Per accorgersi come l'intento sia riuscito basta dare una scorsa al piano della monografia. Nel capitolo I e II si cerca di familiarizzare il lettore con i problemi della diffusione trattando il caso molto semplice di sorgenti nel vuoto e quello un po' più complicato di un mezzo semplicemente assorbente. Nel cap. III viene introdotta e discussa l'equazione del trasporto per neutroni monocinetici senza fare la restrizione usuale di mezzo non moltiplicante. L'abbandono di questa restrizione, rende anche più interessante nel cap. IV la dettagliata risoluzione di problemi standard come quello del mezzo infinito senza sorgente, o con sorgente puntiforme o piana, isotropa e non. Nel cap. V infine vengono introdotti dei teoremi che riconducono la soluzione di problemi in mezzi finiti a quella di mezzo infinito. In particolare viene risolto il problema di Milne generalizzato a un semispazio con proprietà moltiplicanti.

La rimanente parte del capitolo, di notevole interesse perchè dovrebbe affrontare in particolare il problema della criticità di mezzi finiti, è rimandata al volume II.

Al pregio di rigore matematico e chiarezza con cui è esposta tutta la materia del volume, va aggiunto il fatto che di ogni problema è presentata la risoluzione numerica riassunta in moltissime tabelle e grafici, che rendono il libro di notevole utilità per le applicazioni pratiche.

U. L. BUSINARO

Direttore responsabile: G. POLVANI Tipografia Compositori - Bologna

Questo fascicolo è stato licenziato dai torchi il 23-III-1955